DURABILITY OF POLYIMIDE ADHESIVES AND THEIR BONDED JOINTS FOR HIGH TEMPERATURE APPLICATIONS

Hari Parvatareddy

Dissertation submitted to the Faculty of the
Virginia Polytechnic Institute and State University
in partial fulfillment of the requirements for the degree of

Doctor of Philosophy
in
Materials Engineering Science (MESc)

David A. Dillard, Chair
John G. Dillard
Norman E. Dowling
Ronald G. Kander
Tom C. Ward
Garth L. Wilkes

November, 1997
Blacksburg, Virginia

Keywords: Durability, Physical Aging, Chemical Aging, Strain Energy Release Rate, Fracture Toughness, Solvent Sensitivity, Mode-Mix, Adhesive Bond, Titanium Bonds, Wedge Test, Double Cantilever Beam, FM-5 Adhesive

Copyright © 1997, Hari Parvatareddy

DURABILITY OF POLYIMIDE ADHESIVES AND THEIR BONDED JOINTS FOR HIGH TEMPERATURE APPLICATIONS

by

Hari Parvatareddy

Chairman: David A. Dillard

Materials Engineering Science Department

(Abstract)

The objective of this study was to evaluate and develop an understanding of durability of an adhesive bonded system, for application in a future high speed civil transport (HSCT) aircraft structure. The system under study was comprised of Ti-6Al-4V metal adherends and a thermosetting polyimide adhesive, designated as FM-5, supplied by Cytec Engineered Materials, Inc.

An approach based on fracture mechanics was employed to assess Ti-6Al-4V/FM-5 bond durability. Initially, wedge tests were utilized to find a durable surface pretreatment for the titanium adherends. Based on an extensive screening study, chromic acid anodization (CAA) was chosen as the standard pretreament for this research project. Double cantilever beam specimens (DCB) were then made and aged at 150°C, 177°C, and 204°C in three different environments; ambient atmospheric air (14.7 psia), and reduced air pressures of 2 psi air (13.8 KPa) and 0.2 psi air (1.38 KPa). Joints were aged for up to 18 months (including several intermediate aging times) in the above environments. The strain energy release rate (G) of the adhesive joints was monitored as a function of exposure time in the different environments. A 40% drop in fracture toughness was noted over the 18 month period, with the greatest degradation observed in samples aged at 204°C in ambient atmospheric air pressure. The loss in adhesive bond

performance with time was attibutable to a combination of physical and chemical aging phenomena in the FM-5 resin, and possible degradation of the metal-adhesive interface(s). Several mechanical and material tests, performed on the bonded joints and neat FM-5 resin specimens, confirmed the above statement. It was also noted that physical aging could be "erased" by thermal rejuvenation, partially restoring the toughness of the FM-5 adhesive material.

The FM-5 adhesive material displayed good chemical resistance towards organic solvents and other aircraft fluids such as jet fuel and hydraulic fluid. The results from the FM-5 adhesive and its bonded joints were compared and contrasted with VT Ultem and REGULUS^{TM} polyimide adhesives. The FM-5 adhesive showed the best performance among the three adhesive systems.

The effect of mode-mixity on the fracture toughness of the Ti-6Al-4V/FM-5 adhesive bonded system was also evaluated. DCB tests in conjunction with end-notched flexure (ENF) and mixed-mode flexure (MMF) tests, were used to fracture the bonded joints under pure mode I, pure mode II, and a combination of mode I and II loadings. The results showed that the mode I fracture toughness was twice as large as the mode II toughness. This was a rather surprising find, in sharp contrast to what several researchers have observed in the past. Our current understanding is that the crack path selection during the failure process plays a significant role in explaining this anomalous behavior. Finally, failure envelopes were generated for the titanium/FM-5 bonded system, both prior to and following thermal aging. These envelopes could serve as useful tools for engineers designing with Ti-6Al-4V/FM-5 bonds.

Acknowledgements

I owe sincere appreciation to Prof. David A. Dillard for his valuable time, advice, and guidance throughout this project. He was a constant source of encouragement and extremely understanding at all times. I thank you "sir" for all your help and guidance, and for helping me realize one of my biggest goals in life.

I owe sincere appreciation to Prof. John G. Dillard for teaching me several aspects of surface chemistry, for numerous brain-storming sessions that have helped me tremendously with my research, for his excellent handling of the Virginia Tech-Boeing-NASA Langley HSCT effort, and above all, for his constant source of encouragement. Prof. Dillard, I will always remember your infectious enthusiasm towards work, research, and life in general. I will truly miss driving with you in the CASS van to the ASC meetings.

I owe sincere appreciation to Prof. James E. McGrath for all the useful suggestions and comments he provided towards my research over the past 3-4 years. Prof. McGrath was always encouraging and appreciative of my research at both the Boeing meetings and the NSF activities, for which I am very thankful.

I owe sincere appreciation to Prof. Garth L. Wilkes for several valuable ideas and discussions, for helping me greatly with my communication skills, and also for serving on my advisory committee. Prof. Wilkes I thank you for your advice and encouragement, and for running an outstanding Materials Engineering Science (MESc) program.

I owe sincere appreciation to Prof. Tom. C. Ward for serving on my advisory committee, for several valuable ideas and discussion, and for being an outstanding teacher of polymer science. Prof. Ward, I thank you for taking time to accomodate me in your busy schedule at short notice on several occasions, and for running an outstanding NSF-SURP program, that I have greatly benefitted from over the last 4 years.

I owe sincere thanks to Prof. Ronald G. Kander for serving on my advisory committee, as well as, for several useful discussions regarding my research work.

I owe sincere thanks to Prof. Norman E. Dowling for serving on my advisory committee and for several useful comments about my research.

I am also grateful to Profs. James P. Wightman and Kenneth L. Reifsnider for several useful discussions during the course of this “interdisciplinary” project.

A Special thanks to Prof. John J. Lesko (Jack) for always being a constant source of encouragement and help in times of need.

I owe special thanks to Brenda Jackson for all her help with the surface treatment and spectroscopy work.

I owe thanks to several undergraduates both from Virginia Tech (Brian Williams, William Haile) and from other universities affiliated to the NSF-SURP program (John Montgomery) that have helped with my research.

A special mention of thanks to Mr. Bob Simmonds, Mr. George Lough, Mr. Frank Cromer, and Mr. Mac McCord for their technical assistance through the length of the project.

Thanks are also due to the secretaries in Patton Hall (Ms. Shelia Collins, Ms. Paula Lee, and Ms. Beverly Williams), Norris Hall (Ms. Cindy Hopkins, Ms. Pat Baker, and Ms. Wanda Robertson), Randolph Hall (Ms. Sandy Simpkins), Davidson Hall (Ms. Linda Haney, Ms. Katy Hatfield, Ms. Kim Mills, and Ms. Tammy Hiner), Hancock Hall (Ms. Neta Byerly and Ms. Kathy Black), and Hahn Hall (Ms. Joyce Moser, Ms. Esther Brann, and Ms. Laurie Good) for all their help over the years.

Friendships developed with colleagues contribute significantly to intangible aspects of any major professional undertaking. I wish to thank friends and colleagues (both present and past) in the Materials Response Group, Adhesion Mechanics Laboratory, Prof. John Dillard’s Lab, Prof. Tom Ward’s Lab, Prof. Ron Kander’s Lab, and Prof. Jim McGrath’s Lab, and others who have made my stay in Blacksburg a memorable one. All of you will be greatly missed.

I personally wish to acknowledge the financial support from Boeing Commercial Airplane Group over the duration of this project. I wish to thank the Boeing Company for providing me with several Titanium/FM-5 bonds and neat FM-5 resin samples for testing. I wish to thank Cytec Engineered Materials, Inc. and Dr. Richard Mayhew for providing the supported FM-5

adhesive for this study. I also owe special thanks to Mr. Kevin Pate (project monitor-Boeing Company), Mr. Tuan Cao (Boeing Company), and Mr. Paul Hergenrother (project monitor-NASA Langley) for several suggestions and useful discussions.

I owe my sincere appreciation to my family, friends, relatives, and other well-wishers, who have supported and encouraged me over the years. I want to thank my sister for her love, affection and support over the years. I want to thank my wife, Padma, for her love, support, and understanding over the last year. Her company over the last year has made my stay in Blacksburg a more enjoyable and pleasant experience.

Finally, I dedicate this work to my beloved parents Mrs. P. Vijayalakshmi and Dr. P. Ramachandra Reddy whose love, affection, encouragement, and blessings have always been with me.

Table of Contents

List of Tables

List of Figures

1.0 Introduction

The potential number of applications for adhesives in bonding structural components is rising rapidly. Interest is particularly high in aerospace, automotive, infrastructure, biomedical, and marine communities where many new applications require bond integrity over long periods of time [1,2]. Structural adhesive joints offer many advantages over conventional fasteners such as rivets and bolts, including lower weight, ability to bond dissimilar materials, greater fatigue resistance, damping characteristics, electrical and thermal insulation, and lower fabrication/manufacturing costs [3-5]. The word "structural" is applied to a wide range of adhesives, typically epoxy-based phenolics or acrylics, which are usually thermosetting with high modulus and enhanced load bearing abilities [4]. More recently, thermoplastic and thermosetting polyimides have been synthesized which offer useful properties such as high toughness and thermo-oxidative stability for long term structural applications at elevated temperature [6-11]. Also, recent advances made with surface pretreatments for the adherend surfaces have spurred an increased interest in utilizing adhesive joints for aircraft and automotive structures [12]. The purpose of the current study was to evaluate the durability of structural adhesive joints for application in the proposed Mach 2.4 high speed civil transport (HSCT) aircraft.

In general adhesive joints fail by progressive crack growth and the initiation and propagation of cracks in a bonded joint are directly related to the service conditions to which the joint is exposed [13]. Static loads, fatigue loads, elevated temperature, and humidity are some of the principal conditions which cause the formation and propagation of cracks in an adhesive bond [14]. Therefore, any study involving adhesive joints should include a detailed assessment of the durability of the bond system in the service conditions of that particular application. A durability study of bonded joints should involve among other things, an approach based on fracture mechanics.

In the present study a fracture mechanics-based approach utilizing wedge, double cantilever beam (DCB), end-notched flexure (ENF) and mixed-mode flexure (MMF) specimens

was used to study adhesive bond durability. The DCB fracture test specimen is one of the most well defined specimens for evaluation of material properties of adhesives, and it is one of the few adhesive bond fracture tests which has been incorporated into an ASTM standard (D3433-75) [15]. In the recent past several researchers have used this bond geometry to study adhesive joint properties under both mechanical loading and environmental exposure [16-22].

Cracks in adhesive joints propagate in a variety of ways depending on the remote loading condition, local stress state, size and location of pre-existing flaws, integrity of interfacial bonding, adhesive type, adherend type, and the environmental conditions to which the joints are exposed [23]. The crack path and the nature of this path influences among other things, joint strength and fracture toughness of the system [24]. Cracks can propagate within the adhesive layer, at the adhesive-adherend interface, or alternate between the two adhesive-adherend interfaces. It has been shown by several researchers that in evaluating long term durability of adhesive joints, *interfacial properties* become increasingly important in addition to the *bulk adhesive properties.* This is because failures tend to occur at the interface, due to the degradation of the interfacial region, when joints are subjected to harsh environmental conditions [25-28].

In the present study, Ti-6Al-4V alloy was used for the adherends, while the adhesive was a high temperature thermosetting polyimide designated as FM-5. The anticipated life of the HSCT structure is in excess of 60,000 flying hours, and typical temperatures encountered by the aircraft during flight are around 177^{o}C. In order to simulate HSCT conditions, the Ti-6Al-4V/FM-5 bonds and neat resin samples were aged at 177^{o}C and 204^{o}C in one of three different environments; atmospheric air, and reduced air pressures of 2 psi air (13.8 KPa) and 0.2 psi air (1.38 KPa). The 2 psi air environment corresponds to the air pressure at service altitude for the HSCT aircraft. Samples were aged for periods up to 18+ months, with specimens being tested at several intermediate times.

1.1 Research Objectives

An adhesive bonded "system" is comprised of an adhesive, adherends, appropriate surface pretreatment to the adherends, and the interphase/interface regions resulting between the first three components. To assess the durability of a bonded joint, it is essential to gain a fundamental understanding of how each of the above components react to external applied loads, either mechanical or environmental. The objectives of this research are four-fold as listed below and elucidated in the following paragraphs.

i) Select a durable surface pretreatment for titanium metal, for the long-term aging study of bonded joints.

ii) Gain an understanding of physical and chemical aging in the FM-5 resin, and study how these phenomena affect bond durability.

iii) Study the chemical resistance of titanium/FM-5 bonded joints towards common organic solvents and aircraft fluids.

iv) Study the effect of mixed-mode loading on the durability of the titanium/FM-5 bonded system.

The first objective of this study deals with trying to optimize the bond toughness by screening several surface pretreatments for the Ti-6Al-4V adherends. A durable surface pretreatment chosen from the screening tests would then be used as a control standard for the duration of the present study. Studies dealing with the selection of a durable surface pretreatment for titanium metal were conducted in collaboration with Professor John Dillard and his students of the Chemistry Department at Virginia Tech. The adherend-adhesive interphase region has been shown to be the area that most influences the long term performance of bonded joints [25-28]. This interphase is affected by many things including the properties of the bulk adhesive and adherend. However, most importantly this interphase is affected by the interaction of the surfaces of the adhesive and adherend. Surface pretreatments are the most accessible manner in which to optimize this interactive region. Several studies in the past have shown that

appropriate surface pretreatments have considerably enhanced bond strength as well as bond durability [29-35].

The second objective of this study addresses the combined effects of both physical and chemical aging on the long term durability of the Ti-6Al-4V/FM-5 adhesively bonded system. Physical aging is the slow evolution of a polymer to thermodynamic equilibrium by time-dependent changes in volume, enthalpy, and entropy, as well as mechanical properties [36-39]. Physical aging is a thermo-reversible process. Unlike physical aging, chemical aging is, in general, not thermo-reversible and is often referred to as chemical degradation. The chemical changes occurring during oxidation of a polymer can be characterized by the breaking of chemical bonds, reduction in molecular weight, loss in weight associated with the outgassing of lower molecular weight species, and in some cases, additional cross-linking of the polymer chains [40]. It is important to address both physical and chemical aging in bonded systems because these phenomena act simultaneously, with one usually dominating the other at longer aging times. This study aims at gaining a basic understanding of bond durability by studying the combined effect of physical and chemical aging on the bonded system, accomplished by monitoring material and mechanical properties on a *macro* as well as *micro* level. Some of the questions to be answered in this research are:

i) Is physical aging detected before chemical aging or vice versa?

ii) Which of the two phenomena is more dominant after longer aging times?

iii) Which of the two phenomena is more detrimental to long term adhesive bond durability?

iv) Can the effects of both physical and chemical aging be separated to establish the individual impact of each type of aging on bond integrity?

v) What diagnostic tools and tests are most definitive and efficient in detecting both kinds of aging at a very early stage?

vi) How can information collected on the Ti-6Al-4V/FM-5 system impact future durability studies on other adhesive bonded systems?

A third objective for this study, is to assess the solvent resistance of the FM-5 polyimide resin. It has been observed that several thermoplastic adhesives and polymers are sensitive to

organic solvents, that is they exhibit a phenomena called environmental stress cracking (ESC) [41-45]. A recent study conducted by Dillard et al [46] showed that even high performance polyimides may be susceptible to solvent induced stress cracking. The problem of ESC may have significant implications to the aircraft industry (several common organic solvents are used as degreasers and paint strippers in the aircraft industry) as designers begin to focus on polyimides.

The final objective of this study, is to investigate the effect of mode-mix on the bonded toughness of Ti-6Al-4V/FM-5 bonds. In the present study, a fracture mechanics approach was chosen as the framework for specimen design, testing and analysis, because fracture tests display a more controlled failure mode than maximum strength based tests which usually fail catastrophically (eg: single lap shear specimen). As a result, these fracture based tests should permit obtaining a more fundamental understanding of the failure mechanisms of the adhesive system being studied. Fracture tests apply the concept of strain energy release rate (SERR) to analyze and describe crack growth phenomena. In adhesive systems, the critical SERR can be a function of variables such as adherend materials, surface pretreatment, adhesive layer thickness, etc. The total energy released via crack propagation in a bonded joint can be decomposed into three major components corresponding to the modes by which debonding can occur: opening (mode I), shearing (mode II), and tearing (mode III). Opening and shearing are the predominant modes of failure in most testing geometries [47]. Pure mode I, pure mode II, and mixed mode (combination of mode I and mode II) tests were conducted on the bonded joints, prior to and following aging, and failure/fracture envelopes developed for the adhesive system. The failure envelopes could serve as useful tools for engineers designing with the Ti-6Al-4V/FM-5 bonded system.

1.2 Overview of the Study

This study is divided into six sections. Chapter 1 includes a general introduction and the objectives for the present research. Chapter 2 deals with a literature review covering topics such as theories of adhesion, titanium adherends and surface pretreatments, polyimide adhesives,

physical aging, chemical aging, solvent stress cracking, fracture mechanics and fracture based tests, and finally, a review of some durability studies involving adhesively bonded joints. Chapters 3 through 5 are essentially written as technical papers dealing with various aspects of Ti-6Al-4V/FM-5 bond durability. Chapter 6 titled "Closure" summarizes the key findings of chapters 3 through 5, and suggests some possibilities and directions for future work in this area.

Chapter 3 is entitled "Environmental Aging of Ti-6Al-4V/FM-5 Adhesive Bonded System: Implications of Physical and Chemical Aging on Durability". This chapter deals with the study of physical and chemical aging in the FM-5 adhesive and Ti-6Al-4V/FM-5 bonds, and their effects on long term mechanical and material properties. The approach taken in this chapter required the utilization of fracture tests, in conjunction with characterization techniques such as dynamic mechanical analysis (DMA), differential scanning calorimetry (DSC), thermo-mechanical analysis (TMA), Soxhlet extraction, x-ray photoelectron spectroscopy (XPS), and infra-red spectroscopy (FT-IR). The subject matter of this chapter is the basis for two journal papers, the first one entitled "High Temperature and Environmental Effects on the Durability of Ti-6Al-4V/FM-5 Adhesive Bonded System" has been accepted to appear in ASTM STP 1302. The authors of this paper are H. Parvatareddy, A. Pasricha, B. Holmes, J. G. Dillard and D. A. Dillard. The second paper entitled "Durability of Ti-6Al-4V/FM-5 Adhesive Bonded System: Implications of Physical and Chemical Aging on Durability" has been accepted to appear in the Jounal of Adhesion Science and Technology. The authors of this paper are H. Parvatareddy, J. G. Dillard, J. E. McGrath, and D. A. Dillard.

Chapter 4 is entitled "Solvent Effects on High Temperature Polyimides and Their Bonded Joints". This chapter deals with the evaluation of environmental stress cracking (ESC) behavior in neat FM-5 adhesive resin as well as Ti-6Al-4V/FM-5 bonded joints. Wedge and tensile tests were used as a part of this study. Results from the FM-5 adhesive resin system were compared and contrasted to those obtained on VT Ultem polyimide, developed by the Chemistry Synthesis Laboratory at Virginia Tech under the direction of Prof. J. E. McGrath, and REGULUS^{TM} thermoplastic polyimide, developed by The Mitsui Toatsu Company in Japan. Results from

this chapter are the basis for a paper submitted to the Journal of Adhesion. The authors of this paper are H. Parvatareddy, J.G. Dillard, J. E. McGrath, and D. A. Dillard.

Chapter 5 is entitled “Effect of Mode Mix on Fracture Toughness of Ti-6Al-4V/FM-5 Adhesive Joints”. This chapter deals with mode I, mode II, and mixed mode (modes I and II) fracture testing of the Ti-6Al-4V/FM-5 adhesive bonds with a view of gaining a fundamental understanding of i) the effects of mode mix on fracture toughness of bonds and ii) crack path selection in adhesive joints under mixed mode loadings. Fracture envelopes were developed for the Ti-6Al-4V/FM-5 bonds as a function of time following elevated temperature aging. Results from this chapter are the basis for a paper submitted to the International Journal of Fracture. The authors of this paper are H. Parvatareddy, J. K. Montgomery, and D. A. Dillard.

1.3 References

1. R. Joseph, J. P. Bell, A. J. McEvily, and J. L. Liang, *J. Adhesion* **41**, 163-187 (1993)

2. S. Mall and G. Rammamurthy, *Intl. J. Adhesion Adhesives* **9**, 33-40 (1989)

3. B. Dattaguru, R. A. Everett, Jr., J. D. Whitcomb, and W. S. Johnson, *J. Eng. Mater. Technol.* **106**, 59-65 (1984)

4. A. J. Kinloch and S. J. Shaw, in: *Developments in Adhesives-2*, A. J. Kinloch (Ed.), Applied Science Publishers, New York (1983)

5. A. Stevenson and E. H. Andrews, in: *Adhesion 3*, K. W. Allen (Ed.), Applied Science Publishers, Essex, England (1982)

6. T. L. St. Clair and D. J. Progar, *J. Adhesion* **47**, 67-82 (1984)

7. J. G. Smith, and P. M. Hergenrother, *Polymer Pre-prints.* **35**, 353-355 (1994)

8. A. Falcone, K. D. Pate, T. Q. Cao, G. F. Hsu, and M. E. Rogalski, *Proc. 41st Intl. SAMPE Symp*., Anaheim, California, 1035-1046 (1996)

9. M. R. Allen, *NASA-CR-198193* (1995)

10. C. L. Hendricks and S. G. Hill, in: *Polyimides: Synthesis, Characterization, and Applications*, Vol. 2, 1103-1115. Plenum Press, New York (1984)

11. R. D. Rossi, *Engineered Materials Handbook, Volume 3, Adhesives and Sealants,* H. F. Brinson (Ed.), ASM International, Materials Park, Ohio, 151-162 (1990)

12. H. M. Clearfield, D. K. Shaffer, S. L. Vandoren, and J. S. Ahearn, *J. Adhesion* **29**, 81-90 (1989)

13. W. S. Johnson and S. Mall, *ASTM STP 876*, 189-199 (1985)

14. D. Broek, *Elementary Engineering Fracture Mechanics*, 3rd Ed., Ch. 2, Martinus Nijhoff Publishers, Netherlands, 38-60 (1982)

15. ASTM D3433-93, *Annual Book of ASTM Standards*, **15.06** Adhesives, 218 (1994)

16. H. Parvatareddy, A. Pasricha, D. A. Dillard, B. Holmes, and J. G. Dillard, *ASTM STP 1302*, 149-174 (1997)

17. M. D. Rakestraw, M. A. Vrana, D. A. Dillard, J. G. Dillard, and T. C. Ward, *Durability and Damage Tolerance*, AD-Vol. **43**, *ASME WAM*, 65-77 (1994)

18. M. D. Rakestraw, M. W. Taylor, D. A. Dillard, and T. Chang, *J. Adhesion* **55**, 123-138 (1995)

19. A. J. Kinloch and S. O. Osiyemi, *J. Adhesion* **43**, 79-90 (1993)

20. G. K. A. Kodokian and A. J. Kinloch, *J. Adhesion* **29**, 193-218 (1989)

21. B. Blackman, J. P. Dear, A. J. Kinloch, S. Osiyemi, *J. Mater. Sci. Lett.* **10**, 253-256 (1991)

22. D. R. Lefebvre, D. A. Dillard, and H. F. Brinson, *Expt. Mech.* **28** (4), 38-44 (1988)

23. H. R. Daghyani, L. Ye, and Y. W. Mai, *J. Mater. Sci.* **31**, 2523-2529 (1996)

24. N. A. Fleck, J. W. Hutchinson, and Z. Suo, *Intl. J. Solids and Structures* **27** (13), 1683-1703 (1991)

25. P. A. Fay and A. Maddison, *Intl. J. Adhesion Adhesives* **10**, 179-186 (1990)

26. J. F. Watts, J. E. Castle, and T. J. Hall, *J. Mater. Sci. Lett.* **7**, 176-178 (1988)

27. A. J. Kinloch, *J. Adhesion* **10**, 193-219 (1979)

28. A. J. Kinloch, S. J. Shaw, and D. L. Hunston, *Polymer.* **24**, 1355-1363 (1983)

29. F. Bouquet, J. M. Cuntz, and C. Coddet, *J. Adhesion Sci. Technol.* **6** (2), 233-242 (1992)

30. H. S. Schwartz, *SAMPE J.* **13** (2), 2-13 (1977)

31. O. D. Hennemann, *Proc. 8th Ann. Mtg.*, The Adhesion Society, Savannah, Georgia, 26a-26c (1985)

32. H. M. Clearfield, D. K. McNamara, and G. Davis, *Engineered Materials Handbook, Volume 3, Adhesives and Sealants*, H. F. Brinson (Ed.), ASM International, Materials Park, Ohio, 259 (1990)

33. G. W. Critchlow and D. M. Brewis, *Intl. J. Adhesion Adhesives* **15** (3), 161-172 (1995)

34. B. L. Holmes, M. S. Thesis, Virginia Polytechnic Institute and State University, Blacksburg, VA (1994)

35. J. A. Filbey, Ph. D. Dissertation, Virginia Polytechnic Institute and State University, Blacksburg, VA (1987)

36. L. C. E. Struik, *Physical Aging in Amorphous Polymers and other Materials*, Elsevier, Amsterdam (1978)

37. L. C. E. Struik, *Internal Stress, Dimensional Instabilities and Molecular Orientations in Plastics*, John Wiley and Sons, New York (1990)

38. J. L. Sullivan, E. J. Blais, and D. Houston, *Composite Sci. Technol.* **47**, 389-403 (1993)

39. J. Z. Wang, H. Parvatareddy, T. Chang, N. Iyengar, D. A. Dillard, and K. L. Reifsnider, *Composite Sci. Technol.* **54**, 405-415 (1995)

40. N. M. Emanuel and A. L. Buchachenko, *Chemical Physics of Polymer Degradation and Stability*, VNU Science Press, Netherlands (1987)

41. J. B. Howard, *Engineering Design for Plastics*, Reinhold, New York (1964)

42. R. P. Kambour, *J. Polym. Sci.: Macromolecular Review*. **7**, 1-154 (1973)

43. A. N. Gent, *J. Mater. Sci.* **5**, 925-932 (1970)

44. A. J. Kinloch and R. J. Young, *Fracture Behavior of Polymers*, Ch. 7, Applied Science, London, 236-238 (1983)

45. E. J. Stober, J. C. Seferis, and J. D. Keenan, *Polymer.* **25**, 1845-1852 (1984)

46. D. A. Dillard, P. R. McDaniels, and J. A. Hinkley, *J. Mater. Sci. Lett.* **12**, 1258 (1993)

47. A. J. Kinloch, *Adhesion and Adhesives-Science and Technology*, Chapman and Hall, London, 311-313 (1987)

2.0 Literature Review

2.1 Adhesives and Adhesion

An adhesive is described as a material which when applied to the surfaces of materials (adherends) can join them together and resist separation [1]. Adhesives have existed for thousands of years but have become much more important in the past few decades. This popularity in utilizing adhesives has primarily increased because of the growing availability of new and improved adhesives and the significant advances in bonding technology [2]. Modern applications for adhesives are very diverse, ranging from aircraft, automobile and civil structures to pressure sensitive films and tapes. Some of the attributes an adhesive should possess include: the ability to distribute external loads within the bonded joint, the ability to carry static and fatigue loads throughout the service life of the bonded joint, and the ability to adequately wet and bond to the adherend surfaces and make for a durable bond over the service life of the intended application. Adhesives are classified in many different ways, and some of the most common ways of classification depends on i) their physical appearance or state, ii) chemical composition or functionality, iii) curing or processing conditions and iv) end use or final application.

Adhesion refers to the attraction between an adhesive and substrate(s) [1]. When an adhesive and adherend are brought into contact it results in an adhesively bonded "system". The system is comprised of an adhesive, adherends, appropriate surface pretreatment to the adherends, and the interphase/interface regions resulting between the first three components. To assess the durability of a bonded joint, it is essential to gain a fundamental understanding of how each of the above components reacts to external applied loads, either mechanical or environmental. The performance/durability of an adhesively bonded system depends on other criteria as well, such as material properties of the adhesive and adherends, the physical-chemical interactions between the adhesive and the substrates, bonding conditions, bonding geometry, residual stresses in the bond, and imperfections in the bondline. In order to obtain good adhesion and optimal bond performance for a specific application, it is of utmost importance to evaluate

all the above factors for a given adhesive-adherend combination, and then proceed to design a bonded joint.

2.2 Mechanisms of Adhesion

Over the years the scientific community has put forth several theories/mechanisms, in an attempt to provide an explanation for the phenomenon of adhesion. The theories are based on concepts at molecular, microscopic, and macroscopic levels. None of the theories (described below) can individually explain all aspects of adhesion; however, for the case of an individual joint, one or more of the theories of adhesion may be applicable.

2.2.1 Electrostatic

Deryaguin [3] proposed that a transfer of electrons between the adhesive and the adherends can generate an attractive charge between the two, resulting in adhesion. He interpreted the bond between the adhesive and the adherend as a capacitor, the separation of whose plates resulted in a separation of charge, creating a potential which is increased until a discharge occurs. This is one of the more controversial theories, as many reserachers are in disagreement over the magnitude of the forces involved in the mechanism. Skinner, et. al., [4] compared the calculated electrostatic forces with the van der Waals contribution and the experimentally measured work of adhesion in metal/adhesive joints. They concluded that the electrostatic contribution to adhesion was very small compared to the van der Waals forces, and that the measured work of adhesion was larger than both the electrostatic and van der Waals forces combined.

2.2.2 Mechanical Interlocking

McBain and Hopkins [5] stated that mechanical interlocking and hence good adhesion occurs when a liquid adhesive can flow into the pores on the surface of a solid substrate and solidify. This mechanical anchoring would prevent the adhesive from being pulled off the surface of the adherend. Venables et al [6] have shown that some pretreatments of aluminum result in the formation of a very porous surface region, which promotes adhesion by mechanical interlocking of the adhesive. In general, roughening the surface of the adherends and removal of contaminants from the surface region, results in a increased surface area, and enhanced spreading of the adhesive [7]. It should be noted, however, that good adhesion can also be obtained using smooth adherend surfaces as shown in studies by Mittal [8]. The conclusion therefore is that mechanical interlocking is an important ingredient, that contributes to "adhesion".

2.2.3 Diffusion

The Diffusion theory is somewhat similar to mechanical interlocking only it takes place on the molecular level. The diffusion theory was developed by Voyutskii [9], who stated that the phenomenon of adhesion could be explained by the diffusion of chains of one polymer into a second polymer and vice versa. This mechanism can only occur when the adhesive is significantly soluble in the substrate and the kinetics of diffusion allow enough flow before the adhesive solidifies. Some of the parameters that promoted adhesion according to this theory were increasing contact time and temperature, and mild polarity of the side chains. An excess of polar side groups, however, caused adhesion strength to the substrate to decrease due to steric effects and intramolecular attractions. Voyutskii also found that this interpenetration of diffusing species was greatest between similar materials (polar-polar, non-polar-non-polar), resulting in the strongest bonds. He also concluded from his study with mutually soluble polymers, that the factors which promoted adhesion were the same factors which promoted diffusion.

2.2.4 Adsorption

The adsorption theory of adhesion is based on the concept that adhesion occurs due to the establishment of interatomic and intermolecular forces at the interface, provided that intimate contact between adhesive and adherend is established. This theory is currently regarded as the most widely applicable theory in adhesion science, and is credited to Sharpe and Schonhorn [10]. The forces at the adhesive-adherend interface may be generally grouped into two categories: i) primary forces, meaning ionic, covalent and metallic bonds, and ii) secondary forces, including van der Waals forces, dipole-dipole, induced dipole-dipole, hydrogen bonds, and acid-base interactions [11]. While primary forces have bond energies ranging from 60-1050 KJ/mol, secondary forces have energies ranging from 0.08-40 KJ/mol. The force of attraction between two solid surfaces separated by one nanometer has been calculated to be approximately 100 MPa, which is considerably higher than the measured strength of adhesive joints [11]. The above discrepancy has been attributed to voids and other defects present in a bonded joint. Despite the vast differences in the theoretical and experimental values in bond strength, the reason given, however, for a high joint strength, is secondary bonding forces. According to Kinloch [11], the contribution of primary bonding forces to adhesive bond strength has been difficult to assess, although, surface analysis techniques have shown evidence for interfacial bonding in some instances.

Kemball [12] noted that the equations for physisorption and chemisorption onto a surface, contained a dependence on intermolecular distance. This dependence on intermolecular distance serves to explain the discrepancy between predicted and experimental joint strengths based on secondary forces. Huntsberger [13] explained that poor adhesive performance is associated with poor wetting of the surface by the adhesive, since good intermolecular contact requires that the adhesive wet the surface.

The work of adhesion (W_A) also requires wetting of the liquid on the solid surface as given by the Young-Dupre equation [14]:

$$W_A = \gamma\ (1 + \cos\theta) + \pi_e \qquad 2.1$$

where,

γ = surface tension of liquid

θ = wetting angle of liquid on solid

π_e = equilibrium spreading pressure

Fowkes [15] assumed that the equilibrium spreading pressure is zero for high energy liquids on low energy surfaces, so that the Young-Dupre equation becomes:

$$W_A = \gamma\ (1 + \cos\theta) \qquad 2.2$$

The work of adhesion, according to Fowkes [15] is the sum of all the forces of interaction. For example:

$$W_A = W_A^d + W_A^h + W_A^p + W_A^i + W_A^{ab} \qquad 2.3$$

where,

W_A^d = dispersive component

W_A^h = hydrogen bond component

W_A^p = dipole-dipole component

W_A^i = dipole-induced dipole component

W_A^{ab} = acid-base component

Fowkes assumed that W_A^p and W_A^i are negligible compared to W_A^h and W_A^{ab}, and since hydrogen bond forces are a type of acid-base interaction, the work of adhesion may be written as:

$$W_A = W_A^d + W_A^{ab} \qquad 2.4$$

2.3 Titanium Adherends

Titanium metal has a high strength to weight ratio, a high melting point of 1668^{o}C, and excellent corrosion resistance [16]. Titanium possesses two phases, an α-phase which has a hexagonal close-packed structure, and a β-phase which has a body-centered cubic structure and forms above 882.5^{o}C. The α-phase alloys possess high strength and toughness and are resistant to oxygen degradation, but show poor forming characteristics. β-phase alloys on the other hand

are more easily formed, show good hot and cold strength, but are more susceptible to atmospheric contamination and possess a lower strength to weight ratio due to their higher density [16].

Ti-6Al-4V is an $\alpha-\beta$ alloy. The aluminum stabilizes the α-phase and raises the α to β transition temperature. On the other hand, vanadium stabilizes the β-phase and raises the β to α transition temperature. $\alpha-\beta$ alloys show good formability and good cold and hot strength [17] making them excellent materials for high performance structures.

2.3.1 Surface Pretreatment for Titanium Adherends

Surface preparation of adherends for adhesive bonding has been realized by the adhesion community to be the dominant factor in the performance and reliability of adhesively bonded components. Surface pretreatments are used to develop an adherend surface that optimizes the bonding at the adhesive-adherend interface. For metals, surface preparation involves the removal of weak oxide and contamination boundary layers which can reduce the bond strength. In their place, a stable oxide layer is produced. Surface pretreatments may also modify the topography of the adherend which may increase the mechanical interaction between the adhesive and adherend. More specifically, it may allow an interlocking of the adhesive into the grooves and pores on the adherend surface. Lastly, pretreatment may generate changes in the chemical nature of the surface to improve interactions at the adhesive-adherend interface.

Surface pretreatments for titanium metal can be categorized into mechanical, chemical, and anodization treatments. The mechanical treatments serve to remove residual contaminants and roughen the surface, both of which can be accomplished by grit blasting with metal oxide, wire brushing, or scouring with Scotch-Brite™ [18]. Chemical treatments include a phosphate-flouride coating process, the results of which are notably published in the works of Allen and Allen [19] and Wegman and Bodnar [20]. Another chemical treatment for titanium, which is commercially available is called Turco 5578™ (an alkaline etchant), described in the study by Filbey [21], Ditchek et al [22] and Brown [23]. A commercial treatment which combines

mechanical abrasion and chemical treatment in one step is the Vought Abrasive Surface Treatment (VAST)^{TM} developed by Vought Systems [18]. The VAST^{TM} treatment showed poor durability in samples that were exposed to aggressive environments as seen from the study by Brown [23]. Yet another commercial chemical pretreatment for titanium is the Pasa-Jell^{TM} treatment, which is available either in a liquid form or as a paste [18]. Etching of titanium metal in a sodium hydroxide/hydrogen peroxide solution has proven to be a good pretreatment, and this process was developed by the Royal Aircraft Establishment and referred to as the RAE etch [18].

Filbey [21], in her study of Ti-6Al-4V/epoxy bonds, states that anodization of titanium adherends produces the strongest, most durable bonds. The porous nature, and therefore increased surface area, of oxides resulting from anodization enhance the durability of the bonds. The most common anodization for titanium metal is chromic acid anodization (CAA) developed by Boeing [18]. One of the drawbacks of the above process is that the anodizing of the metal results in toxic chromate (Cr VI) waste material, which is environmentally hazardous and expensive to dispose. Another less commonly used anodizing process for titanium is the sodium hydroxide anodization (SHA) described in detail in the study by Filbey [21].

In the present study, several surface pretreatments were screened using wedge test specimens and a three day water boil to assess the durability of the Ti-6Al-4V/FM-5 bonds [24]. Pretreatments included grit blasting, acid/base etching, silane treatments, and CAA. Currently, a treatment involving plasma spraying of the adhesive polymer onto the metal surface following grit blasting of the substrate is also being investigated [25].

2.4 Polyimide Adhesives

Ever since polymeric materials were introduced to join metal adherends in environmentally harsh structural applications, there has been an ever-growing demand on synthetic chemists to develop newer, more durable, high performance adhesive systems to meet the above challenges. Aromatic polyimides are among the most studied family of adhesives for applications requiring resistance to high temperature or aggressive environments [26]. This group

of materials was first synthesized commercially in the 1960s and have since found a wide range of applications [26]. Some advantageous features of polyimides that make them very attractive for aircraft applications are thermo-oxidative stability, radiation and solvent resistance, and excellent mechanical performance.

Polyimides are generally divided into two groups, thermoplastics and thermosets. Thermoplastic polyimides are mostly formed by a step-growth condensation reaction, between an aromatic diamine and an aromatic dianhydride. This reaction may be a one-step or a two-step process, with the intermediate formation of the polyamic acid in the two step process [26]. Unlike thermoplastic polyimides, thermosetting polyimides experience a chemical transformation during cure that renders the material thermally nonprocessible. The crosslinking reaction that occurs in the formation of thermosetting polyimides is often a chain growth mechanism, or addition polymerization between an aromatic diamine and an aromatic dianhydride. These polyimides offer certain advantages over thermoplastic polyimides in that they possess better solvent resistance, higher glass transition temperatures, and less creep [26].

A thermosetting polyimide, FM-5, was utilized in the present study, details of which are provided in section 3.3.1. The FM-5 adhesive was supplied by Cytec Industries Inc., Havre de Grace, MD. The FM-5 adhesive is a modified version of LaRC PETI-5 (which was originally synthesized at NASA Langley Research Center [27]).

2.5 Physical Aging

A polymer, quenched from the rubbery state above the glass transition temperature, T_g, to a temperature below T_g, does not immediately achieve thermodynamic equilibrium [28]. A characteristic of the polymer in the quenched state, is that an excess of entrapped free volume exists in the structure. Struik [29,30] referred to the gradual loss in the excess free volume and thereby the approaching of volume and enthalpy equilibrium as physical aging (see Figure 2.1). During the physical aging process many mechanical properties of the material change. These

include modulus [31], yield stress [32], density [33], and creep rate [33]. Struik [30] also showed that physical aging causes embrittlement in a polymeric material.

Mechanical studies of physical aging include a wide variety of tests including creep, stress relaxation, dynamic, tensile, impact, etc. In the present study creep tests were utilized for studying the relaxation phenomena of the FM-5 adhesive, the material's characterization being based on Struik's physical aging model [32]. This model is a modification of Leaderman's work on time-temperature superposition (TTSP) [34]. Struik [32] showed that short-term/momentary creep compliance curves formed by conducting creep tests of very small durations compared to the total aging time, could be shifted along the horizontal (time) axis to form master curves. The shift rate, μ, which is an index of the kinetics of the physical aging process, could then be calculated from this curve shifting procedure.

The Williams-Landel-Ferry (WLF) model discussed in reference 35 shows that shifts in time caused by a change in temperature maintained the shape of the creep curves. Thus, the effect of temperature on relaxation can be described as a shift function $\log a_T(T)$. Physical aging in a polymer is said to start upon cooling it below the T_g. Therefore, the shift parameter can be said to be a function of both aging time (t_e) and temperature (T), and is generally written in its log form as:

$$\log a_{TP}(T, t_e) = \log a_T(T) + \log a_P(t_e) \qquad 2.5$$

where P designates physical aging.

The linear viscoelastic momentary creep compliance for glassy polymers at any arbitrary temperature, time and aging time is given by [32]:

$$D(t, T, t_e) = B(T)\, D(t/a_{TP}, T_r, t_{er}) \qquad 2.6$$

where the subscript r refers to the reference time and temperature.

In the above equation, the term B(T) can be physically interpreted as a vertical shift. The interpretation of the horizontal shift factor a_{TP} is that all retardation and relaxation times for the molecular processes, for viscoelastic behavior, are affected to the same degree by a change in T and t_e [32]:

$$a_{TP}(T,\ t_e) = \frac{\tau_i(T,\ t_e)}{\tau_i(T_r,\ t_{er})} \qquad 2.7$$

Writing $a_{TP}(T, t_e)$ as a product of aging and temperature shift factors, and taking the logarithm, the total shift factor can be represented in the form:

$$\log\ a_{TP}(T,\ t_e) = \log\left[\gamma t_e^{\mu}\right] + \log a_T \qquad 2.8$$

where log g is the shift factor at unit aging time, m is the shift rate, and log a_T is the shift factor due to temperature only. Thus to predict long term viscoelastic behavior it is necessary to characterize the shift parameters, μ, and log a_T as functions of T and t_e [32].

The shift rate, μ, is given by the expression:

$$\mu = \frac{-d\log a}{d\log t_e} \qquad 2.9$$

Calorimetric studies involving the measurement of physical aging utilize differential scanning calorimetry (DSC). Experimentally, DSC is one of the easier methods used for determination of changes in enthalpy by measurement of the specific heat function [36]. During a DSC test enhalpy relaxes in a very similar fashion as does volume during physical aging. In the present study the enthalpic changes in the FM-5 resin were monitored as a function of aging time to gain an understanding of the physical aging phenomenon in the adhesive. Studies by Berens and Hodge [37], Echeverria [38], and Petrie [39] are examples of works where the researchers utilized DSC measurements to study physical aging in polymers.

Dilatometric studies are a means of measuring changes in the free volume and hence the physical aging phenomena. Two common dilatometric techniques are linear and volumetric dilatometry described in detail in the studies by Struik [29] and Matsuoka [40]. In this research, a thermo-mechanical analyzer (TMA), which acts as a linear dilatometer, was used to study changes in the T_g and coefficient of thermal expansion (CTE) of the resin, and thereby monitor physical aging in FM-5 adhesive resin.

2.6 Chemical Aging

Unlike physical aging, chemical aging is a thermally irreversible phenomena. Therefore, chemical aging, such as oxidation, is often called chemical degradation. The chemical changes occurring during oxidation of a polymer can be characterized by the breaking of chemical bonds in the main and side chains, reduction in molecular weight (for thermoplastics), and loss in weight associated with the outgassing of low molecular weight species. Decomposition of linear polymers at very high temperatures is also called depolymerization [41]. These degradations in the fundamental chemistry of the polymers will cause a reduction in the mechanical properties such as modulus and ultimate strength.

In polymers, the oxidation reaction propagates through a free radical mechanism [41-43]. This is referred to as auto-oxidation [44]. The free radicals may be initiated by several external stimuli such as light, heat, trace metals, and react most readily with molecular oxygen making auto-oxidation a general phenomenon. The initiation of free radicals is caused by the rupture of chemical bonds when absorbed energies exceed the bond energy in macromolecules. During auto-oxidation, molecular chain scissions occur, changing molecular weight and molecular weight distributions for thermoplastics and the crosslinking density for thermosets. These changes due to auto-oxidation depend on the conversion of oxygen. It can be argued that the amount of conversion and, therefore, the degree of degradation depend on both the oxygen partial pressure and the reacting temperature [42].

Besides these environmental factors, the variation in the structure of polymers also affects the degradation. Branched polymer chains are usually less stable to oxidation than backbone chains because the branch points have lower dissociation energy associated with them. The level of crystallinity in a polymer also greatly affects the amount of degradation. If the crystalline structure is very dense then it greatly restricts the oxygen diffusion into the polymer. Auto-oxidation in semicrystalline polymers is limited to the amorphous region, except for a minor surface reaction of the crystallites [43].

Degradation via auto-oxidation depends on two sequential processes, that is, oxygen diffusion and chemical reaction. The degradation kinetics depends on the rates of the two processes. Apparently, if one of the two processes is much slower than the other one, then the slower process will be the controlling process in determining the degradation kinetics. On the other hand, if the two rates are comparable, one needs to consider both in determining the degradation kinetics [45].

The effect of degradation due to thermal oxidation on the molecular and rheological characteristics of filled thermoplastics was studied by Paharenko et al [46]. They were studying the characteristics of polyethylene and polyamide. They characterized the amount of degradation by the trend of changes seen in the molecular mass distribution curves, melt fluidity index, tensile strength, and percent elongation of the polymer specimens. They noted that thermo-oxidative degradation resulted in a decrease in the tensile strength, the melt fluidity index, percent elongation, flexural strength, and toughness.

Scheirs, Bigger, and Delatycki [47] studied the effect of thermal oxidation on the spherulitic morphology of high density polyethylene (HDPE) using polarized optical microscopy and small-angle x-ray scattering (SAXS). Their data indicated that the average lamellar thickness decreases concomitantly with thermal treatment and that oxidative scissions occur preferentially at the chain folds where the polymer molecules are strained. They related the morphological changes in the polymer to chemical degradation by monitoring polymer melt flow index, molecular weight distribution, crystallinity, and peak melting temperature.

Lin and Pearce [48] studied the degradation of an isothermally aged epoxy resin system via a vacuum Thermo-Gravimertic Analysis (TGA) technique. The chemical decomposition kinetics were obtained from weight loss measurements of the polymer. Weight loss in this case occurred due to the outward diffusion of decomposition by-products from the specimens. A parallel study was conducted on PMR-15 polyimide resin system [49]. In this case too, weight losses and dimensional changes of the specimens were monitored for the exposure time. Physical changes were observed by optical and electron microscopy. As a result of this study, it was found that polyimide polymer degradation occurs within a thin surface layer of the sample and

this grew during thermal aging. Similarly, the thermo-oxidative weight losses of additive-cured polyimide resins and their graphite fiber composites were studied by Alston [50]. He found an excellent correlation between the thermo-oxidative stability of all graphite fiber polyimide composites and their corresponding polyimide resins.

Crissman and McKenna [51] studied the effects of physical and chemical aging in poly methyl methacrylate (PMMA), and its impact on the creep and creep rupture behavior of the polymer. They reported that following longer aging times at elevated temperatures, PMMA failed at much lower strains as a result of chemical degradation.

2.7 Solvent Sensitivity and Environmental Stress Cracking

Since the 1970s several researchers [52-57] found that many thermoplastic polymers, loaded mechanically and immersed in certain kinds of fluids, undergo failures by crazing or cracking. The loads required for failure of specimens exposed to solvents are significantly less than those required for failure in air. Failures like these are called environmental stress cracking (ESC).

The mechanisms of ESC are not fully understood. One suggestion is that the presence of the liquid lowers the surface energy of the polymer and makes the formation of new surface easier during crazing [57]. One other suggestion is that the organic liquid plasticizes and swells the polymer matrix, resulting in a lowering of the T_g, allowing deformations and crazing to take place at lower stresses and strains [54]. An example of this is apparent in the catastrophic failure of polycarbonate on exposure to acetone under stress. The solubility parameters (δ) of the polycarbonate and acetone are very close [58]. Acetone enters the polycarbonate which is under a state of stress and plasticizes the material resulting in crazing, cracking and failure depending on the stress levels. Vincent and Raha [59] indicated that one other possible reason for ESC was the capacity of the solvent to hydrogen bond to the polymer matrix. Their research was conducted with amorphous thermoplastic materials. A more recent study by Hay and Kemmish [60] showed that crystallinity is another factor which affects ESC. They showed that high

crystallinity PEEK resisted ESC more than low crystallinity PEEK. A recent study conducted by Parvatareddy, et. al. [61] showed that a thermoplastic-toughened thermosetting resin system showed susceptibility to ESC on brief exposures to common organic solvents and aircraft fluids. Studies by Dillard, et. al., [62] and Clifton [63] showed that even high performance polyimide adhesives may be sensitive to organic solvents and aircraft fluids. In light of the observations made by Dillard et al [62], it is essential to study the solvent sensitivity of high performance structural adhesives in context to the solvents which may come into contact with the adhesive and/or joint during the service life. In the present study, the FM-5 polyimide is being evaluated as a possible candidate for a future high speed civil transport (HSCT) aircraft structure. Therefore, the adhesive resin must be suitably tested to address the issue of ESC during exposures to common aircraft fluids and solvents.

2.8 Fracture Testing

Testing of an adhesively bonded system is a complex issue as the "system" consists of adherends, adhesive, primers, surface pretreatments, oxide layers, and interphases between the previously mentioned components, making the interpretation of results a very difficult proposition. Even if a perfect test geometry were available in which all stresses were uniform and totally identifiable, the test results from an adhesive joint would still represent system properties and not adhesive material properties [1]. Therefore, any small changes made to one component of the "system" could significantly alter the adhesive performance. This elicits the need for great care and caution to be used in the process of designing, testing and analyzing data that deals with adhesive joints. Another important issue that is to be kept in mind while working with bonded joints is that the use of nonideal testing geometries significantly complicates the analysis of the data. Singular stress fields exist at certain locations along the length of an adhesive joint, making every bonded joint a "structure" [64]. Therefore, it is important to understand that the results obtained from testing a bonded joint possessing a certain geometry will more or less represent the adhesive system performance, when used in a structure possessing an almost

similar geometry. Also, factors such as thickness of the adhesive layer, mode mix ratio, plastic zone size, etc. have to be considered to gain a comprehensive understanding of joint performance.

Reinhart [65] stated that mechanical testing plays a very important role in the assessment of adhesives and adhesively bonded joints. Testing serves as a tool for quality control of adhesives and their bonded joints, besides aiding in other processes such as adhesive formulation, development and selection. Kinloch [1] points out that tests act as "simulations" for practical joint designs in research laboratories. It must be noted though that the testing conditions, testing geometries and testing loads should closely mimic the service environment/conditions to learn anything useful. The American Society for Testing and Materials (ASTM) and the U.S. Military and Federal Adhesive Specifications provide listings of standardized mechanical tests involving adhesives [66,67].

There are basically two different approaches with respect to mechanical testing and analysis of adhesive joints, specifically with respect to joint design and failure prediction. The first approach considers the nature and maginitude of the stresses found in certain type of joint designs and test methods. This approach permits quantitative joint design studies and failure predictions based on parameters such as adhesive properties, joint geometry, test rate, and temperature [1]. An advantage of using the above approach is that it enables many aspects of the mechanical behavior of adhesive joints to be easily understood and predicted. However, a drawback to this method would be that stress states calculated for a particular specimen are indeed very specific to that particular test geometry and to determine failure loads for different loading geometries, additional techniques are required [1]. The second approach for studying adhesive joints is called the study of continuum fracture mechanics and is detailed in the following section.

2.8.1 Review of Fracture Mechanics

Adhesive joints usually fail by the initiation and propagation of flaws. Since the study of fracture mechanics is based entirely on the presence and growth of flaws, this approach has been

widely used to predict crack growth, fracture and failure in adhesive joints [1]. The main aims of the fracture theory are to analyze mathematically the loads at which the flaws propagate and describe the manner in which they grow [1]. The sources of flaws in adhesives are voids, cracks, dirt particles, additive particles and other inhomogeneities that naturally occur during the making of the adhesive material. These flaws are either present in a critical size or develop during the fracture test. In the present study a fracture mechanics approach (joint design, testing, and analysis) is utilized to study the durability of Ti-6Al-4V/FM-5 adhesive bonds.

There are two main approaches for the study of fracture mechanics, the first one is based on the works of Griffith [68] and Orowan [69] and supposes that fracture occurs when sufficient energy is released by the growth of the crack to supply the energy required for the formation of new surfaces. This approach, provides for a measure of the energy required to extend a crack over a unit surface area, and this energy is referred to as the fracture energy or the critical strain energy release rate (SERR), G_c. The second approach called the stress intensity factor approach, based on the work of Irwin [70] states that the stress field around a crack could be uniquely described by a parameter called the stress intensity factor, K, and that fracture occurs when the value of K exceeds a critical value, K_c. While K is a stress field parameter independent of the material, K_c, is a material property usually referred to as the fracture toughness.

Griffith's hypothesis [68] describes quasi-static crack propagation in terms of the work done by external forces, W_d, the elastic stored energy in the bulk specimen, U, and the surface free energy, γ_m as:

$$\frac{\partial(W_d - U)}{\partial a} \geq 2\gamma_m \frac{\partial A}{\partial a} \qquad 2.10$$

In the above equation ∂A is the increase in surface area with crack growth of ∂a. For a crack propagating in a lamina of thickness, b, the above equation modifies to:

$$\frac{1}{b}\frac{\partial(W_d - U)}{\partial a} \geq 2\gamma_m \qquad 2.11$$

Orowan [106], Rivlin and Thomas [71], and Berry [72], in their study of metals and cross-linked rubbers found that the energy required for crack propagation was far greater than twice the surface free energy. This discrepancy was due to the fact that the surface energy term only

included energy required for secondary bond rupture, while in a situation where cracks propagated along the material interfaces, primary bonds would have to be broken in some cases. The energy required solely for rupturing intrinsic bonding forces, such as primary and secondary bonds is referred to as the intrinsic fracture energy, G_o. For perfectly elastic systems this would be the term equivalent to the surface energy term in the above equation. However, most fracture processes (even involving brittle adhesive systems) result in localized viscoelastic and/or plastic energy dissipation at regions of high strain within the material. Therefore, if the assumption is made that energy dissipation around the crack tip occurs in a manner independent of applied forces and test geometry, then the $2\gamma_m$ term can be replaced by G_c, the critical strain energy release rate [1]. G_c encompasses all the energy losses incurred around the crack tip and the above equation further modifies to:

$$\frac{1}{b}\frac{\partial(W_d - U)}{\partial a} \geq G_c \qquad 2.12$$

For bonded joints exhibiting bulk linear-elastic behavior (both material as well as geometric), the above equation can be written as [1]:

$$G_c = \frac{F_c^2}{2b}\frac{\partial C}{\partial a} \qquad 2.13$$

where F_c is the load at the onset of crack propagation, and C the compliance of the bonded joint, given by the load over displacement. The above equation is the foundation of G_c calculations for several bonded configurations. In most tests C is usually determined as a function of a, that is either theoretically or experimentally, and the $\partial C/\partial a$ term calculated.

If a sharp crack is present in the bulk material of a uniformly stressed, infinite, homogeneous body, and if Hookean behavior and linear elastic fracture mechanics (LEFM) are assumed, then Westergaard [73], has developed stress function solutions relating the local stress concentration of stresses at the crack tip to applied far field stress, σ_o. For regions close to the crack tip the solution is given by:

$$\sigma_{ij} = \sigma_o\left(\frac{a}{2r}\right)^{1/2} f_{ij}(\theta) \qquad 2.14$$

where σ_{ij} are the components of the stress tensor at a point, and r and θ are the polar coordinates of the point. The length of the crack tip is given by the distance 2a.

Irwin [70] modified the above equation to include the parameter, K, the stress intensity factor, which relates the magnitude of the stress intensity near the crack to the applied load and structure geometry. The modified equation took the form:

$$\sigma_{ij} = \frac{K}{(2\pi r)^{1/2}} f_{ij}(\theta) \qquad 2.15$$

Cracks in general can be loaded in three different modes, mode I or cleavage/tensile-opening mode, mode II or in-plane shear mode, and mode III or antiplane shear/tearing mode. Mode I failures are most common with respect to adhesive joints in service conditions, although failures by the other two modes of loading cannot be discounted. For mode I loading, crack tip stresses are given by the equations below:

$$\begin{Bmatrix} \sigma_{11} \\ \tau_{12} \\ \sigma_{22} \end{Bmatrix} = \frac{K_I}{(2\pi r)^{1/2}} \cos(\theta/2) \begin{Bmatrix} 1 + \sin(\theta/2)\sin(3\theta/2) \\ \sin(\theta/2)\cos(3\theta/2) \\ 1 - \sin(\theta/2)\sin(3\theta/2) \end{Bmatrix} \qquad 2.16$$

$$\sigma_{33} = 0 \quad \text{(plane stress)} \qquad 2.17$$

$$\sigma_{33} = \upsilon(\sigma_{11} + \sigma_{22}) \quad \text{(plane strain)} \qquad 2.18$$

$$\tau_{23} = \tau_{13} = 0 \qquad 2.19$$

Equations similar to those above have been developed for mode II and mode III.

From the above equation one can see that as 'r' tends to zero, the stress σ_{ij}, tends to infinity and hence stress by itself does not make a reasonable local fracture criterion. Since the stress intensity factor, K, uniquely defines the stress field around the crack, Irwin [70] postulated the following fracture condition for mode I loading:

$$K_I \geq K_{Ic} \qquad 2.20$$

The stress intensity factor for mode I can be expressed as:

$$K_I = Q\sigma_o a^{1/2} \qquad 2.21$$

and the critical stress intensity factor given by:

$$K_{Ic} = Q\sigma_c a^{1/2} \qquad 2.22$$

In the above equation σ_c is the applied stress at the onset of crack growth and Q is a geometry constant, which can be determined either experimentally or theoretically.

The preceding several paragraphs dealt with cracks in the bulk adhesive material. In the case of adhesively bonded joints, cracks propagate close to or at the bimaterial interfaces, and the ensuing paragraphs deal with interfacial aspects of crack growth. An interfacial crack, loaded in mode I or mode II, usually induces both tensile and shear stresses at the crack tip. Thus, to describe the stress field around an interfacial crack, both mode I and mode II terms of stress intensity factor are needed. The stress intensity factors K_{Ii}, K_{IIi} (subscript i refers to interface) used here do not have a clearly defined significance as in the case of bulk adhesive material. Researchers such as Williams [74], Erdogan [75], and Rice and Sih [76] have used mathematical modeling to show that the local stresses ahead of the crack tip at a bimaterial interface are given by:

$$\frac{\sigma_{yy}(r,0)}{\sigma_{yy}^{\infty}} = \pm\frac{r}{\sqrt{r^2-a^2}}\left\{\cos\left(\varepsilon\ln\left|\frac{r+a}{r-a}\right|\right)+2\frac{a}{r}\varepsilon\sin\left(\varepsilon\ln\left|\frac{r+a}{r-a}\right|\right)\right\}$$

$$\frac{\sigma_{xy}(r,0)}{\sigma_{yy}^{\infty}} = \pm\frac{r}{\sqrt{r^2-a^2}}\left\{\sin\left(\varepsilon\ln\left|\frac{r+a}{r-a}\right|\right)-2\frac{a}{r}\varepsilon\cos\left(\varepsilon\ln\left|\frac{r+a}{r-a}\right|\right)\right\} \qquad 2.23$$

where ε is a bimaterial constant and is a function of the moduli and Poisson's ratio of the two materials forming the interface. ε is given by:

$$\varepsilon = \frac{1}{2\pi}\ln\left[\left(\frac{\kappa_a}{G_a}+\frac{1}{G_s}\right)\Big/\left(\frac{\kappa_s}{G_s}+\frac{1}{G_a}\right)\right] \qquad 2.24$$

where G_a and G_s are the shear moduli of the adhesive and the substrate, and κ_a and κ_s are functions of the Poisson's ratios of the adhesive, ν_a and substrate ν_s.

$\kappa_j = 3\text{-}4\nu_j$ (plane strain) 2.25

$\kappa_j = (3\text{-}\nu_j)/(1+\nu_j)$ (plane stress) 2.26

j = a or s as required 2.27

For an interfacial crack of length 2a in an infinite sheet under a tensile applied stress, σ_o, the stress intensity factors in mode I and II for an interfacial crack are given by [1]:

$$K_{Ii} = \sigma_o \frac{\left\{(2\pi)^{1/2}\left[\cos(\varepsilon \ln 2a) + 2\varepsilon \sin(\varepsilon \ln 2a)\right]\right\}}{\cosh(\pi\varepsilon)} (a)^{1/2} \quad 2.28$$

or,

$$K_{Ii} = \sigma_o Q_{Ii} a^{1/2} \quad 2.29$$

and

$$K_{IIi} = \sigma_o \frac{\left\{-(2\pi)^{1/2}\left[\sin(\varepsilon \ln 2a) - 2\varepsilon \cos(\varepsilon \ln 2a)\right]\right\}}{\cosh(\pi\varepsilon)} (a)^{1/2} \quad 2.30$$

or,

$$K_{IIi} = \sigma_o Q_{IIi} a^{1/2} \quad 2.31$$

In the above equations, Q_{Ii} and Q_{IIi}, are geometry factors, which may be a function of the bimaterial constant [1]. Also, there is still a logarithmic term of a dimensional parameter, a, in equations 2.28 and 2.30. Since Q and K are dependent upon the units of a, it therefore becomes extremely difficult to evaluate the mode I and mode II contributions independently.

Several researchers have suggested that for cracks at or near the interface, a combined interfacial stress intensity factor can be defined, which is given by the equation below as [1]:

$$K_i = \left(K_{Ii}^2 + K_{IIi}^2\right)^{1/2} \quad 2.32$$

The above expression/approach is useful as it not only combines mode I and mode II contributions, but also eliminates the length term, a. This enables the calculation of K_{Ic} without any ambiguities/complications mentioned in the approach previous to this one.

Using equation 2.32, if the stress intensity factor were to be calculated from tensile stresses alone, then the above equation reduces to:

$$K_{ic} = Q_i \sigma_c a^{1/2} \quad 2.33$$

In conclusion it must be mentioned that, there is very little experimental data available to validate the above fracture criteria, and that these criteria do not adequately predict the fracture behavior of adhesive bonds with cracks at or near an interface [1]. However, if some of the difficulties in using the stress intensity factor approach can be resolved, then it has the potential to become an invaluable tool for designing and predicting life of adhesively bonded structures [1]. It must also

be mentioned that, currently, the energy balance approach is commonly adopted by reseachers when studying crack growth in adhesive joints [1].

Irwin [70] suggested that if a material is elastic up to the uniaxial yield stress, σ_{ay}, and then becomes plastic, then the size of the plastic zone and crack-opening displacements for both plane stress and plane strain conditions can be approximated by the following equations:

$$r_y = \frac{1}{2\pi}\left(\frac{K_I}{\sigma_{ay}}\right)^2 \quad \text{(plane stress)} \tag{2.34}$$

$$r_y = \frac{1}{6\pi}\left(\frac{K_I}{\sigma_{ay}}\right)^2 \quad \text{(plane strain)} \tag{2.35}$$

$$\delta_t = \frac{K_I^2}{E_a \sigma_{ay}} \quad \text{(plane stress)} \tag{2.36}$$

$$\delta_t = \frac{K_I^2}{E_a \sigma_{ay}}\left(1 - \upsilon_a^2\right) \quad \text{(plane strain)} \tag{2.37}$$

where E_a refers modulus of the adhesive and ν_a, the Poisson's ratio of the adhesive material.

It has been reported that the measured value of G_{Ic} or K_{Ic} varies with the width of the specimen over a range of widths, and that this usually arises because the state of stress near the crack tip varies from plane stress in a thin specimen to plane strain near the center of a wide plate [1]. The value for the fracture energy in plane strain conditions is usually less than under plane stress, because the tensile stress at which a material yields is greater in a triaxial stress field (plane strain) than in a biaxial field (plane stress) [1]. For the very same reason, a very limited degree of plasticity develops at the crack tip for plane strain condition. Thus, for most engineering design and life prediction studies, the lower, more conservative plane strain value is used. The width, b, necessary to achieve this condition is usually taken to be [1]:

$$b \geq 2.5\left(\frac{K_{Ic}}{\sigma_{ay}}\right)^2 \tag{2.38}$$

In linear elastic fracture mechanics (LEFM), values of strain energy release rate, G and stress intensity factor, K are related. For a crack in a homogeneous body, under plane strain conditions, G and K are related as:

$$G = \frac{(1-\upsilon^2)}{E} K_I^2 + \frac{(1-\upsilon^2)}{E} K_{II}^2 + \frac{(1+\upsilon)}{E} K_{III}^2 \qquad 2.39$$

or equivalently:

$$G = G_I + G_{II} + G_{III} \qquad 2.40$$

where, for mode I loading we get:

$$G_I = \frac{K_I^2}{E} \quad \text{(plane stress)} \qquad 2.41$$

and

$$G_I = \frac{K_I^2}{E}(1-\upsilon^2) \quad \text{(plane strain)} \qquad 2.42$$

For a crack in the center of an adhesive layer, several researchers [77,78] have shown that the above expressions are still valid. They also reported that by using an appropriate value of the adhesive modulus, E_a, one can correlate G(joint) and K(joint). For plane strain condition the expression is:

$$G_{Ic}(\text{joint}) = \frac{K_{Ic}^2(\text{joint})}{E_a}(1-\upsilon_a^2) \qquad 2.43$$

In the case of a crack at the interface there is no clearly established relationship but researchers such as Malyshev, et. al. [79], and Williams [80] have proposed that the appropriate value of the modulus should be some weighted average of the moduli of the materials forming the interface. According to them, G_{ic} and K_{ic} may be related as:

$$G_{ic} = K_{ic}^2 \frac{1}{2}\left[\frac{1}{E_a} + \frac{1}{E_s}\left(\frac{2\alpha_m - 1}{\alpha_m^2}\right)\right] \qquad 2.44$$

where,

$$\alpha_m = \frac{\xi + 1}{\chi + 1} \qquad 2.45$$

and

$$\xi = E_s / E_a \qquad 2.46$$

$$\chi = 1 + \frac{E_s}{2}\left(\frac{1+\upsilon_a}{E_a} - \frac{1+\upsilon_s}{E_s}\right) \qquad 2.47$$

It must be noted here that the exact form of the above relationships is very important, and that an appropriate modulus term be selected for the calculation [1]. Another noteworthy point is that, currently there are no relationships available for the case of a crack very close to but not at an interface. The correct modulus term to be used in the above case would most likely be an average based on the modulus of the adhesive material and the modulus of the interface [1].

The thickness of the adhesive layer, h_a, does not usually affect the measured value of the adhesive fracture energy for brittle adhesives but for tougher adhesive systems, this value may significantly affect the measured value of G_c of the joint. Kinloch and Shaw [81], have shown that for a rubber toughened adhesive, the relation between G_{Ic} and h_a is complex, with G_{Ic} passing through a maximum value, G_{Icm}, at a certain thickness, h_{am}. This complex behavior with tough adhesives is primarily attributed to the extensive plasticity that occurs in the vicinity of the crack tip. Due to the presence of relatively thin adhesive layers and high yield strength substrates, there are restrictions imposed on the full development of the plastic zone ahead of the crack tip. Since the toughness is largely derived from the dissipated energy, in forming the plastic zone, the fracture energy will steadily decrease as the adhesive thickness is reduced below a certain value [81]. Secondly, Wang et al [77] have found that the constraint imposed upon the adhesive layer by the rigid substrates may increase the level of the local tensile stresses ahead of the crack tip, causing an increase in the length of the plastic zone. This phenomenon was experimentally verified. The degree of constraint is greatest with thinner adhesive layers, giving rise to an expression that relates the maximum adhesive fracture energy versus the adhesive thickness [1]:

$$h_{am} = \frac{1}{\pi}\frac{E_a G_{Ic}(\text{bulk})}{\sigma_{ay}^2} \qquad 2.48$$

It must also be mentioned here that testing rate and testing temperatures have an effect on the measured properties.

Andrews and Kinloch [82] have measured the adhesive fracture energy, G_c, of crosslinked rubber bonded to several plastic substrates as a function of testing rate and temperature. They concluded from their studies that G_c increased as a function of increasing testing rate or decreasing testing temperature. The reason given for the observed behavior by the authors in reference 82 is that there exists a viscoelastic hysteresis in the rubbery adhesive as a result of internal friction or a viscosity mechanism. At testing temperatures above T_g, the WLF equation [35] (referred to in a previous section on physical aging), may be used to relate the fracture energy, testing rate, and testing temperature by the formation of master curves. A master curve is constructed by multiplying the rate by the time-temperature shift factor, a_T. The equation used to model the rate-temperature dependence of the fracture energy is given by [1]:

$$G_c = G_o \varphi_v \left(a, T, \varepsilon \right) \qquad 2.49$$

In the above equation, G_o is the intrinsic fracture energy of the adhesive material, φ_v a constant that takes into account geometry dependent energy dissipative mechanisms, and ε, the strain level. φ_v is dependent on the strain level during a test.

At very low rates of testing when the energy dissipation tends to be negligible, the value of φ_v becomes unity, and G_c becomes equal to G_o. In practice it is very difficult to access this region experimentally since the test rates are very low and oxidative mechanisms may occur during the time-scale of the test. Nevertheless, since φ_v is also a property of the bulk adhesive it controls the bulk fracture energy, and when the value of φ_v is not strongly dependent on strain, then the value of G_o for a joint may be obtained from [1]:

$$G_o(\text{joint}) = G_o(\text{bulk}) \left[\frac{G_c(\text{joint})}{G_c(\text{bulk})} \right]_{\left(a_T \right)} \qquad 2.50$$

2.8.1 Wedge Test

The wedge test is a very simple and useful test to determine adhesive bond properties. References 83-85 are examples of literature describing the wedge test, the analysis of the wedge test, and some data collected on different adhesive systems. This test has been incorporated into a testing standard as ASTM D 3762 [86]. The wedge test permits obtaining a quantitative measure of the fracture energy, G, of an adhesive bond subjected to environmental conditioning [87]. In the wedge test, crack length data can be collected as a function of time and using appropriate equations, this data can be used to calculate fracture energy as a function of crack growth rate. The equation for the strain energy release rate, G, is [83,88]:

$$G = \frac{3E\Delta^2 h^3}{16a^4} \qquad 2.51$$

where,

E: modulus of elasticity of adherend

h: adherend thickness

Δ: thickness of the wedge

a: debond or crack length

The underlying assumptions for applying the above equation are, first, that there is no plastic deformation in the substrate, and secondly, that the specimen compliance is primarily due to beam bending with minimal contributions from beam shear and adhesive deformation. One disadvantage to this test is that the specimen must always be removed from the conditioning environment to make a crack length measurement. This is not easy if the samples are being conditioned in a vigorous environment. There may also be some subjectivity involved in measuring crack length in some samples where the cracks are very difficult to view especially after environmental exposure.

2.8.2 Double Cantilever Beam Test

The double cantilever beam (DCB) specimen, was first introduced for fracture toughness testing by Ripling and Mostovoy [89]. When the load is applied perpendicular to the crack plane, the DCB can be used for the mode I fracture energy calculation, if the adherends are made of the same material and are of the same thickness. In the recent past DCB tests have also been used very extensively to study the effects of static , fatigue, and environmental loads on adhesive bonds and thereby the durability of the bonded joints [90-96]. Rakestraw, et. al. [91,92] utilized the DCB specimen to study steel/epoxy bonds, Kinloch and Osiyemi [97], Kodokian and Kinloch [98], and Blackman, et. al. [99] used this specimen to study graphite epoxy composite/adhesive bonded joints. Lefebvre, et. al. [100] utilized a modified DCB specimen to study rubber/metal bond durability. The fracture energy in the case of the static DCB tests can be determined by using equation 2.52 (given below), which was derived using the compliance method with corrections for the crack length offset and adherend stiffness [91,92,99]. One of the assumptions for using equation 2.51 for calculation of fracture energy is that specimen compliance is primarily due to beam bending; however, in the case of compliant adhesives there may be crack tip deflections and rotations. To account for these factors as well as other factors such as adherend and adhesive properties, bond thickness, etc, which are very system dependent, equation 2.52 was used to calculate G:

$$G = \frac{9\Delta^2 (EI_{eff})}{4B(a + x)^4} \qquad 2.52$$

where,

B: specimen width

C: compliance

a: crack length

x: apparent crack length offset

EI_{eff}: effective flexural rigidity

Δ: specimen's opening displacement at point of load application

The term Δ in the above equation refers to the specimen's opening displacement at the point of load application in the case of the DCB test compared to wedge opening as defined earlier. The parameters EI_{eff} and x are determined from experimental data according to:

$$EI_{eff} = \frac{2}{3m^3} \quad \text{and} \quad x = \frac{b}{m} \qquad 2.53$$

where the experimental coefficients m and b are the slope and y-intercept, respectively, of the cube root of the measured compliance, when plotted as a linear function of the crack length (see Figure 2.2). Compliance, C, is obtained by dividing the specimen's crack opening displacement, Δ by the corresponding load, P, where Δ and P are experimentally measured. Due to the linear relationship of $C^{1/3}$ versus crack length experimental data, a value of the crack length can be obtained for a given crack opening displacement, Δ, and the load, P, and the strain energy release rate G computed.

Fatigue DCB tests are conducted to study the cyclic debonding rate of adhesive bonds or joints as a function of strain energy release rate. The model chosen for this research is the widely used empirical equation of Paris and Erdogan [101], which may be expressed as:

$$\frac{da}{dN} = C(G_{IMAX})^n \qquad 2.54$$

where,

a: crack length

N: number of cycles

G_{IMAX}: maximum applied cyclic strain energy release rate calculated from equation 2.52.

Here, C and n are considered system constants and are determined from the experimental data, by modeling the linear portion of Figure 2.3, labelled as Region II. Higher values of C or n indicate that an adhesive system is more susceptible to fatigue crack growth. A higher value of n is especially dangerous because it means a slight change in loading could cause a significant increase in the fatigue crack growth rate, thus making the system highly unstable if cracking ever begins. A threshold value such as the one depicted in Figure 2.3 may or may not be exhibited by a particular material system. Also, attempting to determine accurately if and where a threshold

value exists on the fatigue crack growth curve may be a time and resource consuming effort. It should be noted that DG is often used in place of G_{IMAX} in equation 2.54. However, recent research suggests that G_{IMAX} is a better parameter for use in characterizing the fatigue behavior of adhesively bonded systems [97,102]. The choice of this convention does not significantly alter the results. It must be mentioned here that the data analysis procedure used for the fatigue DCB test data is almost identical to the static DCB tests. Once the data analysis procedure is carried out, the central difference method is used to calculate the terms da, dN, and G_{IMAX} for the i^{th} time interval of the fatigue test according to:

$$(da)_i = (a)_{i+1} - (a)_{i-1}$$
$$(dN)_i = (N)_{i+1} - (N)_{i-1} \qquad 2.55$$
$$(G_{IMAX})_i = \frac{(G_{IMAX})_{i+1} + (G_{IMAX})_{i-1}}{2}$$

From the above $(da/dN)_i$ is then computed.

2.8.3 End Notched Flexure Test

The laminated DCB test geometry can also be used to determine mode II fracture toughness simply by applying a three point bending load instead of opposing end loads. This concept was first applied to interlaminar delamination of composite materials [103]. This specimen has been dubbed the end notched flexure (ENF) specimen and used by several researchers [104-110] to determine mode II fracture properties of structural adhesives. The fracture energy for an ENF test is determined by using equation given below [103,111]:

$$G = \frac{3(a + x)^2 P^2}{64BEI_{eff}} \qquad 2.56$$

where,

a: crack length

B: specimen width

EI_{eff}: effective flexural rigidity

P: load

2.8.4 Mixed Mode Flexure Test

The mixed mode flexure (MMF) specimen is similar to the pure Mode II ENF specimen except that at one end, the load is applied to the upper arm only, thus providing crack opening as well as shear. The opening mode contribution to the MMF specimen was calculated using beam theory and was found to be 57% [112]. The fracture energy for a MMF test was determined by using equation 2.57 given below, which was also derived using the compliance method [110, 112-114]:

$$G = \frac{7(a + x)^2 P^2}{64BEI_{eff}} \qquad 2.57$$

where,

a: crack length

x: crack length correction

B: specimen width

EI_{eff}: effective flexural rigidity

P: load

2.9 Durability of Bonded Joints

The end use of any adhesively bonded system is dictated by the bonded joint meeting durability requirements of a particular application. Currently, the mechanisms of adhesion are not understood well enough to allow researchers to accurately predict the lifetime of a bonded structure without conducting laboratory tests. In most cases, durability testing is often accelerated by increasing load/stress, humidity, temperature, etc, since some applications may require a lifetime requirement of several thousands of hours. Several factors affect the

performance of an adhesive bond over time, including temperature, stress, humidity, UV exposure, salt water, oxidation, etc.

Adhesive bonds used in the aerospace industry have very rigid guidelines for the purpose of assessing durability. One of the reasons for stringent durability criteria is due to the fact these bonds experience a combined variety of adverse environments during their service lifetime [115]. A simple example is one involving joints that may be subjected to a water soak/freeze/thaw cycle. It is also important to understand that an adhesive bond behaves very differently when subjected to one single environment, than when it is subjected to a combination of environments/exposures.

2.9.1 Review of Durability Studies on Adhesively Bonded Joints

Gosselin [116] studied the durability of steel/adhesive bonds using lap shear tests following accelerated environmental aging. He concluded that moisture ingression into the bonds resulted in the greatest degradation in bond strength. Schwartz [117] used wedge tests to study the long term durability of aluminum/epoxy joints aged at 250^{o}C. Schwartz used two different surface pretreatments for the aluminum adherends, phosphoric acid anodization (PAA), and a Forest Products Laboratory (FPL) etch. Based on the wedge test results, Schwartz concluded that the PAA was the more durable surface pretreatment. Minford [118] studied the long term durability of aluminum/adhesive joints. He correctly pointed out that to assess the long term strength of any bonded metal joint it was important to study both physical and chemical properties of the adhesive-adherend interface, and physical and material properties of the bulk adhesive. Brewis, et. al. [119] studied the effect of humidity on the durability of aluminum/epoxide lap shear joints by aging the lap joints in air at 50^{o}C in a range of humidities for up to 10,800 hours. Brewis, et. al. [120] concluded that there existed a critical relative humidity of 65% above which the lap joints possesed very poor durability. Matz [120] conducted a durability study for 10,000 hours at 70^{o}C in air and at a relative humidity of 95%, to optimize a surface pretreatment for titanium/adhesive joints. Matz reported that the suitable surface pretreatment was a NaTeSi treatment for the metal. A very extensive study was carried

out by Greer [121] on several adhesive bonded systems spanning 11 years. He evaluated the long term thermal aging properties of structural adhesives such as epoxies, phenolics, and acrylics at 177^{o}C. The aluminum/adhesive joints were aged in marine, jungle, and industrial environments. Greer found that the most durable adhesive was a phenolic nitrile resin. A more recent study by Bouguet, et. al. [122] showed that CAA was a very durable surface pretreatment in bonding stainless-steel with epoxy. The steel joints were exposed to moisture for several months and good correlation was found between bond durability, surface mophology, and oxide-film composition.

It is important to note that the "overall" durability of an adhesive bonded system is not necessarily limited to the service aging conditions, but also due to several other factors. The adhesive material in most cases is not one simple entity but a combination of several monomers, reactants, additives, and fillers. Each of these individual components has a specific role with respect to the integrity of the adhesive. Secondly, there could be additional cross-linking in the adhesive resin in conjunction with chemical changes and dergradation mechanisms taking place as a result of aging. Dillingham [123] showed that thermal residual stresses in the bonded joints as a result of cool-down from the bonding process could affect bond durability. Ross, et. al. [124] demonstrated that the surface exposure time (SET) prior to bonding, adherend and adhesive shelf life and storage conditions, and production batches also played significant roles in influencing bond durability. A study by Thuen and Hinrichs [125] showed that rheology and flow characteristics of the adhesive resin, and the development of an optimum curing cycle for bonding joints, played a role in defining the durability of the adhesive bonded system.

2.10 References

1. A. J. Kinloch, *Adhesion and Adhesives-Science and Technology*, Chapman and Hall, London, 311-313 (1987)

2. D. J. Zalucha, *Engineered Materials Handbook, Volume 3, Adhesives and Sealants*, H. F. Brinson (Ed.), ASM International, Materials Park, Ohio, 39-40 (1990)

3. B. V. Deryaguin, *Research* **8**, 70 (1948)

4. S. M. Skinner, R. L. Savage, J. Rutzler, *J. Appl. Phys.* **24**, 439 (1953)

5. J. W. McBain and D. G. Hopkins, *J. Phy. Chem.* **29**, 188 (1925)

6. J. D. Venables, D. K. McNamara, J. M. Chen, T. S. Sun, R. L. Hopping, *Appl. Surf. Sci.* **3**, 88 (1979)

7. C. W. Jennings, *J. Adhesion* **4**, 25 (1972)

8. K. L. Mittal, *J. Vac. Sci. Technol.* **13**, 19 (1976)

9. S. S. Voyutskii, *Autohesion and Adhesion of High Polymers*, Wiley-Interscience, New York (1963)

10. L. H. Sharpe, H. Schonhorn, *Chem. Eng. News* **15**, 67 (1963)

11. A. J. Kinloch, *J. Mater. Sci.* **15**, 2141-2151 (1980)

12. C. Kemball, *Adhesion*, D. D. Eley (Ed.), Oxford University Press, London (1961)

13. J. R. Huntsberger, *Treatise on Adhesion and Adhesives*, Vol. 5, R. L. Patrick (Ed.), Marcel Dekker, Inc., New York (1981)

14. W. Gutowski, *Fundamentals of Adhesion*, L. H. Lee (Ed.), Plenum Press, New York (1991)

15. F. M. Fowkes, *J. Adhesion* **4**, 155 (1972)

16. F. A. Cotton, G. Wilkinson, *Basic Inorganic Chemistry*, John Wiley and Sons, Inc., New York (1976)

17. R. M. Brick, A. W. Pense, R. B. Gordon, *Structure and Properties of Engineering Materials*, 4th Ed., Mc-Graw Hill Book Company, New York (1977)

18. A. Mahoon, *Durability of Structural Adhesives*, A. J. Kinloch (Ed.), Applied Science Publishers, London (1983)

19. D. R. Allen, A. S. Allen, *SAMPE J.*, 64-73 (1967)

20. R. F. Wegman, M. J. Bodnar, *SAMPE Quart.* **5**, 28 (1973)

21. J. A. Filbey, Ph. D. Dissertation, Virginia Polytechnic Institute and State University, Blacksburg, VA (1987)

22. B. M. Ditchek, K. R. Breen, T. S. Sun, J. D. Venables, *25th National SAMPE Symp.*, 13-19 (1980)

23. S. R. Brown, *27th National SAMPE Symp.*, 363-370 (1982)

24. H. Parvatareddy, J. G. Dillard, J. E. McGrath, and D. A. Dillard, B. L. Holmes, *J. Adhesion Sci. Technol*. in press (1997)

25. J. G. Dillard, F. R. Jackson, B. L. Holmes, L. Aartun, H. Parvatareddy, D. A. Dillard, R. Zatorski, *J. Adhesion.* in press (1997)

26. R. D. Rossi, *Engineered Materials Handbook, Volume 3, Adhesives and Sealants,* H. F. Brinson (Ed.), ASM International, Materials Park, Ohio, 151-162 (1990)

27. J. G. Smith, and P. M. Hergenrother, *Polymer Pre-prints.* **35**, 353-355 (1994)

28. A. J. Kovacs, *J. Polym. Sci.* **30**, 131-147 (1958)

29. L. C. E. Struik, *Physical Aging in Amorphous Polymers and other Materials,* Elsevier, Amsterdam (1978)

30. L. C. E. Struik, *Poly. Eng. Sci.* **17**, 165-173 (1977)

31. L. C. E. Struik, *Polymer* **28**, 1521-1533 (1987)

32. L. C. E. Struik, *Polymer* **30**, 799-814 (1989)

33. L. C. E. Struik, *Polymer* **30**, 815-830 (1989)

34. H. Leaderman, *The Textile Foundation,* Washington D. C. (1943)

35. M. L. Williams, R. F. Landel, J. D. Ferry, *J. American Chem. Soc.* **77**, 3701-3706 (1955)

36. J. Mijovic, L. Nicolais, A. D'Amore, J. M. Kenny, *Poly. Eng. Sci.* **34**, 381 (1994)

37. A. R. Berens and I. M. Hodge, *Macromolecules* **15** (3), 756-761 (1982)

38. I. Echeverria, P. C. Su, S. L. Simon, and D. L. Plazek, *J. Polym. Sci.: Part B: Polym. Phy.* **3**3, 2457-2468 (1995)

39. S. E. B. Petrie, *J. Polym. Sci.: A-2.* **10**, 1255-1272 (1972)

40. S. Matsuoka, *J. Rheology* **30**, 869 (1986)

41. N. M. Emanuel and A. L. Buchachenko, *Chemical Physics of Polymer Degradation and Stability*, VNU Science Press, Netherlands (1987)

42. A. David, D. Sims, *Weathering of Polymers,* Applied Science Publishers, London (1983)

43. W. Schnabel, *Polymer Degradation:Principles and Practical Applications*, Hanser International, New York (1981)

44. R. J. Young, P. A. Lovell, *Introduction to Polymers*, 2nd Ed., Chapman and Hall Publishers, New York (1991)

45. J. Szekcky, *Gas-Solid Reactions*, Academic Press, New York (1976)

46. V. A. Paharenko, E. M. Kirienko, I. M. Nosalevich, *Mech. Comp. Materials.* **5**, 869-877 (1981)

47. J. Scheirs, S. W. Bigger, O. Delatycki, *J. Polym. Sci.: Part B, Polym. Phy*. **29**, 795-804 (1991)

48. S. C. Lin, E. M. Pearce, *J. Appl. Poly. Sci.* **23**, 3355-3374 (1979)

49. K. J. Bowles, D. Jayne, T. A. Leonhardt, *SAMPE Quart.* **24** (2), 2-9 (1993)

50. W. B. Alston, *NASA Report No. TM-105553* (1992)

51. J. M. Crissman, G. B. McKenna, *J. Polym. Sci.: part B, Polym. Phy.* **28**, 1463-1473 (1990)

52. R. P. Kambour, *J. Polym. Sci.: Macromolecular Review*. **7**, 1-154 (1973)

53. A. N. Gent, *J. Mater. Sci.* **5**, 925-932 (1970)

54. A. J. Kinloch and R. J. Young, *Fracture Behavior of Polymers*, Ch. 7, Applied Science, London, 236-238 (1983)

55. E. H. Andrews, L. Bevan, *Polymer* **13**, 337-346 (1972)

56. H. R. Brown, *Polymer* **19**, 1186-1188 (1978)

57. E. J. Stober, J. C. Seferis, J. D. Keenan, *Polymer* **25**, 1845-1852 (1984)

58. G. A. Bernier, R. P. Kambour, *Macromolecules* **1**, 393-400 (1968)

59. P. I. Vincent, S. Raha, *Polymer* **13**, 283-292 (1972)

60. J. N. Hay, D. J. Kemmish, *Polymer* **29**, 613-620 (1988)

61. H. Parvatareddy, C. A. Heithoff, A. P. Clifton, D. A. Dillard, R. G. Kander, *ASTM STP 1274*, 56-68 (1996)

62. D. A. Dillard, P. R. McDaniels, and J. A. Hinkley, *J. of Mater. Sci. Lett.* **12**, 1258 (1993)

63. A. P. Clifton, M.S. Thesis, Virginia Polytechnic Institute and State University, Blacksburg, VA (1996)

64. K. M. Leichti, *Engineered Materials Handbook, Volume 3, Adhesives and Sealants,* H. F. Brinson (Ed.), ASM International, Materials Park, Ohio, 335 (1990)

65. T. J. Reinhart, Jr., *Adhesives Age* **16**, 35 (1973)

66. *Annual Book of ASTM Standards*, Part 22, American Society for Testing and Materials, Philadelphia, PA (1982)

67. R. Chait, E. T. Clegg, *Adhesives in Manufacturing*, G. L. Schneberger (Ed.), Marcel Dekker, New York (1983)

68. A. A. Griffith, *Phil. Trans. Roy. Soc.* A221, 163 (1920)

69. E. Orowan, *Rept. Prog. Phy.* **12**, 185 (1948)

70. G. R. Irwin, *Appl. Mater. Res.* **3**, 65 (1973)

71. R. S. Rivlin, A. G. Thomas, *J. Polym. Sci.* **10**, 291 (1953)

72. J. P. Berry, *J. Polym. Sci.* **50**, 107 (1961)

73. H. M. Westergaard, *J. Appl. Mech.* A-June, 46 (1939)

74. M. L. Williams, *Bull. Seism. Soc. Am.* **49**, 199 (1959)

75. F. Erdogan, *J. Appl. Mech.* **30**, 232 (1963)

76. J. R. Rice, G. C. Sih, *J. Appl. Mech.* **31**, 477 (1964)

77. S. S. Wang, J. F. Mandell, F. J. McGarry, *Int. J. Fract.* **14**, 39 (1978)

78. G. G. Trantina, *J. Comp. Matl.* **6**, 192 (1972)

79. B. M. Malyshev, R. L. Salganik, *Int. J. Fract. Mech.* **1**, 114 (1966)

80. J. G. Williams, *Fracture Mechanics of Polymers*, Ellis Horwood, Chichester (1984)

81. A. J. Kinloch, S. J. Shaw, *J. Adhesion.* **12**, 59 (1981)

82. E. H. Andrews, A. J. Kinloch, *Proc. Roy. Soc.* A332, 385 (1973)

83. J. Cognard, *J. Adhesion.* **20**, 1-13 (1986)

84. J. Cognard, *J. Adhesion.* **22**, 97-108 (1987)

85. M. B. Ouezdou, A. Chudnovsky, and A. Moet, *J. Adhesion.* **25**, 169-183 (1988)

86. ASTM Standard D3762, *Annual Book of ASTM Standards, Adhesives*, Vol. **15.06**, 360-364 (1984)

87. J. Cognard, *J. Adhesion.* **26**, 155-169 (1988)

88. J. A. Marceau, Y. Moji, J. C. McMilliam, *Adhesives Age* **28**, (1977)

89. S. Mostovoy and E. J. Ripling, *J. Appl. Polym. Sci.* **10**, 1351-1371 (1966)

90. R. Joseph, J. P. Bell, A. J. McEvily, and J. L. Liang, *J. Adhesion.* **41**, 163-187 (1993)

91. M. D. Rakestraw, M. A. Vrana, D. A. Dillard, J. G. Dillard, and T. C. Ward, *Durability and Damage Tolerance,* AD-Vol. **43**, *ASME WAM,* 65-77 (1994)

92. M. D. Rakestraw, M. W. Taylor, D. A. Dillard, and T. Chang, *J. Adhesion.* **55**, 123-138 (1995)

93. S. Mall and K. T. Yun, *J. Adhesion.* **23**, 2215-2231 (1987)

94. S. Mall, W. S. Johnson, and R. A. Everett, Jr, *Adhesive Joints*, K. L. Mittal (Ed.), Plenum Press, New York, 639-645 (1984)

95. N. B. Rao and A. R. Acharya, *Eng. Fract. Mech.* **51** (2), 317-322 (1995)

96. S. J. Hooper and R. Subramanian, *ASTM STP 1156*, 318-340 (1993)

97. A. J. Kinloch and S. O. Osiyemi, *J. Adhesion.* **43**, 79-90 (1993)

98. G. K. A. Kodokian and A. J. Kinloch, *J. Adhesion.* **29**, 193-218 (1989)

99. B. Blackman, J. P. Dear, A. J. Kinloch, S. Osiyemi, *J. Mater. Sci. Lett.* **10**, 253-256 (1991)

100. D. R. Lefebvre, D. A. Dillard, and H. F. Brinson, *Expt. Mech.* **28** (4), 38-44 (1988)

101. P. C. Paris and F. Erdogan, *ASME Trans*., *J. Basic Eng.* **4**, 528 (1963)

102. R. H. Martin and G. B. Murri, *ASTM STP 1059*, 251-264 (1990)

103. A. J. Russell and K. N. Street, *ASTM STP 876*, 349-370 (1985)

104. E. J. Ripling, S. Mostovoy, and H. T. Corten, *J. Adhesion.* **3**, 107-113 (1971)

105. P. D. Mangalgiri, W. S. Johnston, and R. A. Everett, Jr., *J. Adhesion.* **23**, 263-288 (1987)

106. A. J. Russell and K. N. Street, *ASTM STP 937*, 275-294 (1987)

107. S. Mall and N. K. Kochar, *J. Composite Technol. Res.* **8**, 54-67 (1986)

108. H. Chai and S. Mall, *Int. J. Fracture* **36**, R3 (1988)

109. H. Chai, *ibid.* **37**, 137 (1988)

110. K. M. Leichti and T. Freda, *J. Adhesion.* **28**, 145-169 (1989)

111. Y. wang and J. G. Williams, *Composite Sci. Technol.* **43**, 251-256 (1992)

112. J. R. Reeder and J. H. Crews Jr., *AIAA J.* **28** (7), 1270-1276 (1990)

113. S. Bashyam and B. D. Davidson, *AIAA-96-1419*, 886-896 (1996)

114. A. J. Kinloch, Y. Wang, J. G. Williams, and P. Yayla, *Composite Sci. Technol.* **47**, 225-237 (1993)

115. D. M. Brewis, *Durability of Structural Adhesives,* A. J. Kinloch (Ed.), Applied Science Publishers, London (1983)

116. C. A. Gosselin, *SAE Spl. Publ. SP-612*, Warrendale, Pennsylvania, 15-23 (1984)

117. H. S. Schwartz, *SAMPE J.* **13** (2), 2-13 (1977)

118. J. D. Minford, *Adhesives Age.* **21** (3), 17-23 (1978)

119. D. Brewis, J. Comyn, A. K. Rawal, and A. J. Kinloch, *Int. J. Adhesion Adhesives* **10**, 247-253 (1990)

120. C. Matz, *Int. J. Adhesion Adhesives.* **8** (1), 17-29 (1988)

121. R. H. Greer, *Structural Adhesive and Bonding: Proc. of the Conf.,* El Segundo, California, 174-189 (1979)

122. F. Bouquet, J. M. Cuntz, and C. Coddet, *J. Adhesion Sci. Technol.* **6** (2), 233-242 (1992)

123. R. G. Dillingham, *Proc. of 8th Ann. Mtg*., The Adhesion Society, Savannah, Georgia, 3a-3d (1985)

124. M. C. Ross, E. McAbee, M. J. Bodnar, *SAMPE J.* **25** (6), 15-19 (1975)

125. J. Thuen and R. Hinrichs, *SAMPE J.* **16** (5), 6-17 (1980)

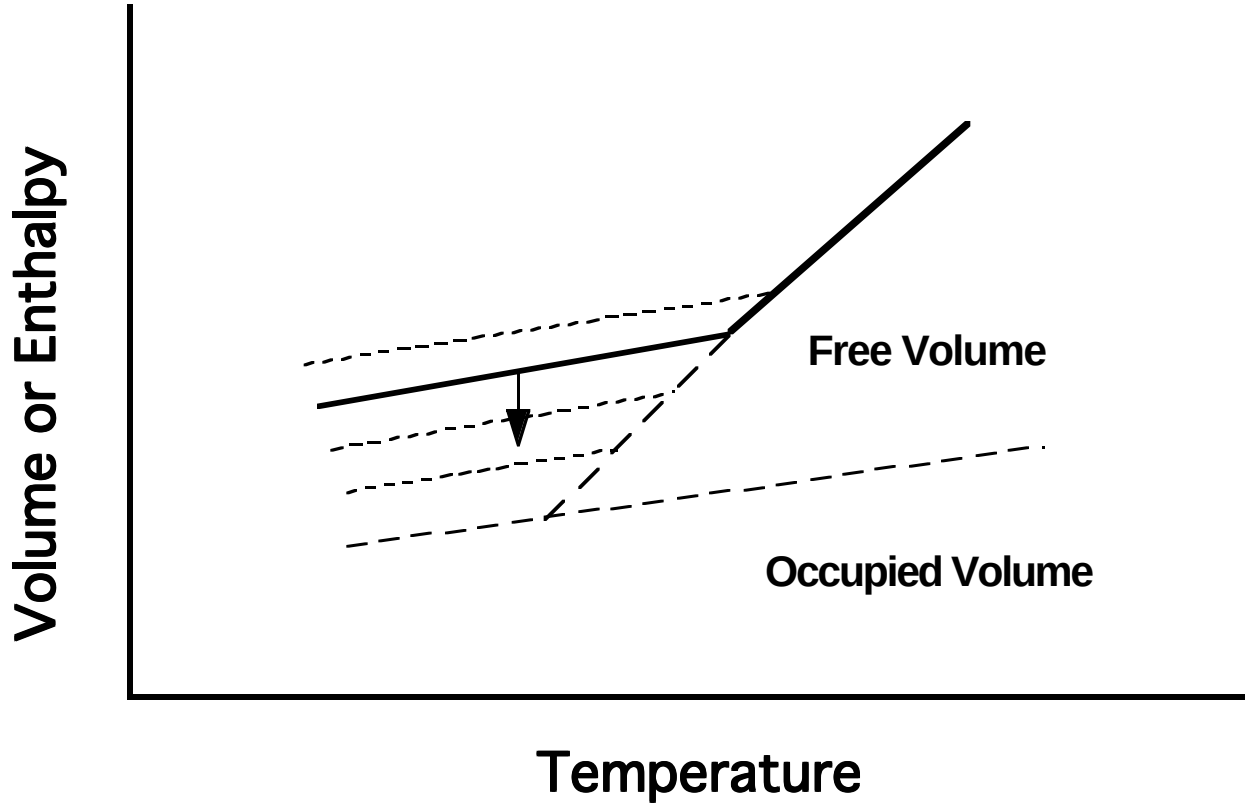

Figure 2.1 Schematic of the physical aging process [29].

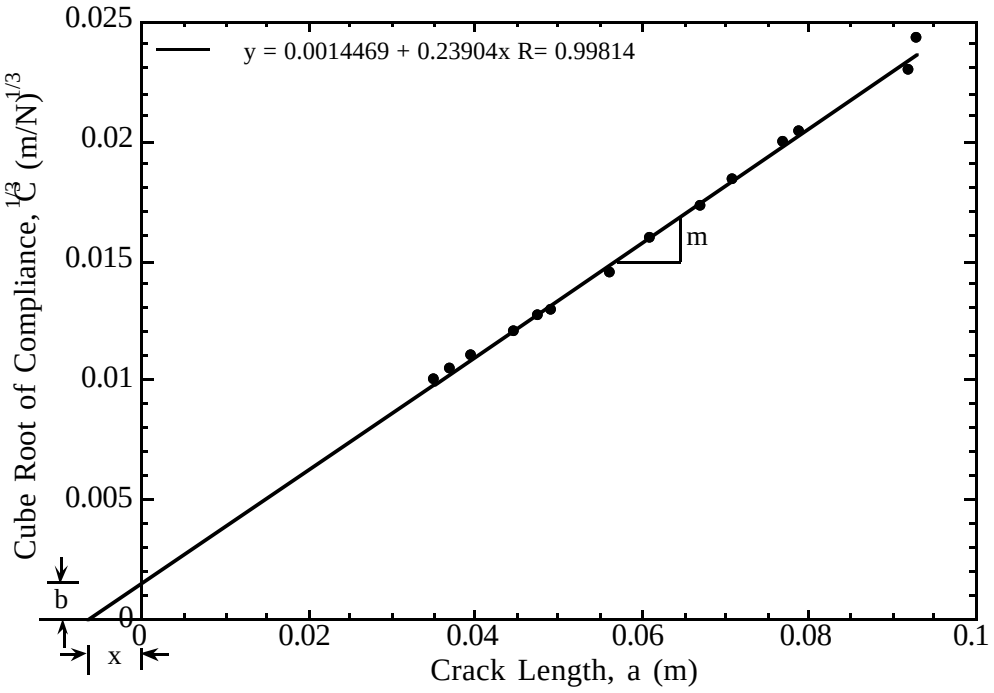

Figure 2.2. Typical complaince versus crack length plot for for determination of EI_{eff} and x.

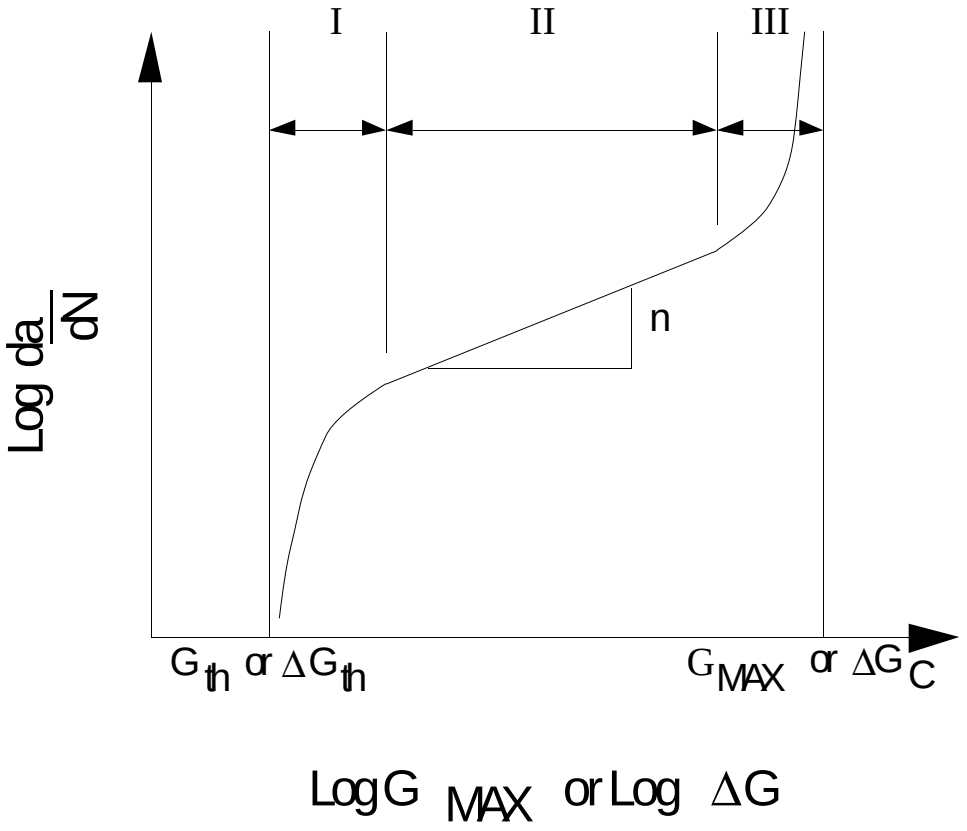

Figure 2.3. Typical fatigue curve showing the three regions of failure.

3.0 Environmental Aging of Ti-6Al-4V/FM-5 Adhesive Bonded System: Implications of Physical and Chemical Aging on Durability

3.1 Abstract

Ti-6Al-4V/FM-5 adhesive bonded wedge and double cantilever beam (DCB) specimens were aged for up to 18+ months (including several intermediate aging times) at elevated temperatures (177°C and 204°C) in one of three different environments, ambient atmospheric air and reduced air pressures of 2 psia (13.8 KPa) and 0.2 psia (1.38KPa), to assess bond durability. The FM-5 adhesive (T_g~250°C) was a polyimide blend developed by Cytec Engineered Materials, Inc., modified from the original LaRC PETI-5 polymer synthesized at the NASA Langley Research Center. Bonds aged for different times were tested to measure the critical strain energy release rate (G_C) as a function of temperature and environment. The greatest loss in bond strength occurred after aging in air at 204°C. Following thermal conditioning of the aged bonds at 300°C for 2 hours, part of the strength loss could be recovered. This strength recovery was attributed to rejuvenation of physical aging effects in the adhesive resin. Further evidence for physical aging, which is a thermo-reversible phenomena, was observed from tests conducted on neat resin specimens using DMA (dymanic mechanical analysis), DSC (differential scanning calorimetry), and TMA (thermo-mechanical analysis). The unrecovered portion of the bond strength following longer term aging was attributed to chemical aging/degradation of the bonded "system". The "system" in this study includes the adherends, the adhesive, the surface pretreatment (chromic acid anodization, CAA), and their respective interphase/interface regions. Evidence for chemical aging was inferred from weight loss, stress-strain, and Soxhlet extraction data on the neat resin specimens, and FT-IR (infra-red spectroscopy), and XPS (x-ray photoelectron spectroscopy), conducted on both the neat resin specimens as well as the bonded joints.

3.2 Introduction

Structural adhesive joints are being widely used and studied as alternatives to conventional fasteners in the automotive, aerospace, and other industries. Adhesive bonding offers advantages such as lower weight and lower manufacturing costs [1]. Furthermore, high performance adhesives which are currently being synthesized (e.g. epoxies, phenolics, acrylics, thermoplastic polyimides) offer other useful properties such as higher modulus, higher toughness, and stability at high temperatures. Also, recent advances made with surface pretreatments for the adherend surfaces have spurred an increased interest in utilizing adhesive joints for aircraft and automotive structures [2].

In general adhesive joints fail by progressive crack growth and the initiation and propagation of cracks in a bonded joint are directly related to the service conditions to which the joint is exposed [3]. Static loads, fatigue loads, elevated temperature, and humidity are some of the principal conditions which cause the formation and propagation of cracks in an adhesive bond [3]. Therefore, any study involving adhesive joints should include a detailed assessment of the durability of the bond system in the service conditions of that particular application. A durability study of bonded joints should involve among other things, an approach based on a fracture mechanics.

In the present study, the durability of the Ti-6Al-4V/FM-5 adhesive bonded system was evaluated utilizing wedge and double cantilever beam (DCB) fracture specimens. The current study was part of a comprehensive study to develop a durable material system for application in the proposed Mach 2.4 high speed civil transport (HSCT) aircraft. According to the design criteria, the material system to be used on the aircraft should be durable for over 60,000 hours of flight encountering temperatures during flight in the range of 150^{o}C to 204^{o}C. Physical aging and chemical aging of the adhesive material are some of the important issues which have to be evaluated and taken into consideration for predicting the bond durability. To simulate the service environment conditions of the HSCT, the Ti-6Al-4V/FM-5 bonds and FM-5 neat resin samples were aged at one of three temperatures; 150, 177, and 204^{o}C, in one of three different

environments; atmospheric air, and reduced air pressures of 2 psi air (13.8 KPa) and 0.2 psi air (1.38 KPa). The 2 psi air environment corresponds to the service altitude air pressure of the HSCT aircraft.

Wedge tests are very popular for evaluating adhesive bond durability. These tests are very simple to conduct and very cost effective. The works of Cognard [4], and Ouezdou, et. al. [5] describe the wedge test in detail, provide the analysis of the test, and discuss data collected on several adhesive systems using the wedge test. In the current study the wedge test has been used extensively as a screening tool to evaluate several surface pretreatments for the titanium adherends. Based on these screening tests, chromic acid anodization (CAA) was chosen to be the standard surface pretreatment for the duration of this study. In addition, wedge tests have been used to conduct long term bench mark studies on the bonded joints following aging at different temperatures and environments of interest.

In the recent past DCB tests have also been used very extensively to study the effects of static, fatigue, and environmental loads on adhesive bonds and thereby the durability of the bonded joints [6-8]. The DCB joint offers several advantages over other test joints which are currently used with regularity to characterize the performance of adhesive bonds, e.g: single lap shear (SLS) joint. The first major advantage in using a DCB specimen is its capability to produce multiple data points from a single test specimen compared to the single data point collected from the catastrophic failure of the SLS specimen. Furthermore, the controlled failure of a DCB specimen makes it possible to obtain a fundamental understanding of the joint's failure process. This also means fewer tests are necessary for confidently characterizing any differences in a bonded system's performance. Another advantage to using the DCB test geometry is that the stress distribution in the specimen remains fairly consistent within the same specimen as debonding occurs [9], making it easier to analyze this kind of specimen without using complicated numerical procedures. However it must be mentioned that during the initial part of the aging study, and the screening tests conducted to find a durable surface pretreatment for the titanium metal, both DCB and wedge test specimens were not very discriminating of the FM-5 bonds. Failure in most cases occured within the adhesive layer. During this period, some insight

into the failure process was gained using the SLS specimen. In light of the above observation, there may still be merit to using the SLS joint as an initial screeing test specimen for adhesive bonds.

3.3 Experimental

3.3.1 Materials

The adhesive used in the study was designated as FM-5, which is based on a polyimide originally developed at NASA Langley Research Center (LaRC PETI-5) [10] and then modified and supplied by Cytec Industries Inc., Havre de Grace, Maryland. The LaRC PETI-5 structure is shown in Figure 3.1. The FM-5 adhesive was supplied in two forms; as polymer film supported on a woven fiberglass cloth and as an unsupported film. The supported film contained 85% polymer by weight, and contained approximately 4% by weight of the solvent N-methyl-2-pyrrolidinone (NMP). The supported film was used to bond titanium adherends to conduct wedge, DCB and differential scanning calorimetry (DSC) tests. The unsupported film had less than 0.5 % by weight of the solvent and was used to conduct the material characterization tests such as dynamic mechanical analysis (DMA), themo-mechanical analysis (TMA), x-ray photoelectron spectroscopy (XPS), infra-red spectroscopy (FT-IR), stress-strain, Soxhlet extraction, thermo-gravimetric analysis (TGA), and weight loss. The adhesive was initially cured at a temperature of 350^{o}C for 60 minutes, while maintaining a curing pressure of 75 psi (0.518 MPa). The above curing procedure was later modified as follows: the samples were first heated up to 250^{o}C under contact pressure at a heating rate of 5^{o}C/min, held there for 30 minutes and then heated up under a pressure of 75 psi (0.518 MPa) to 350^{o}C and maintained there for an additional 60 minutes (see Figure 3.2). The samples were then brought to room temperature at a cooling rate of 15°C/min. This modified cure was used to eliminate air bubbles and voiding which were apparent in the bondline of some earlier bonded specimens. The solvent present in the adhesive, which in this case is NMP, has a boiling point of 202^{o}C. In the original

curing process, the NMP did not have enough time to escape from the bond. By holding the temperature at 250^{o}C for an additional 30 minutes, most of the solvent apparently evaporated from the system. Figures 3.3 and 3.4 are scanning electron photomicrographs (taken on a scanning electron microscope, model SX40, International Scientific Instruments) showing the differences in the fracture surfaces using the two curing processes. As can be seen from these micrographs, the modified cure cycle seems to eliminate most of the air bubbles and voiding noted in the original procedure.

The glass transition temperature, T_g, of the cured adhesive was approximately 250^{o}C using both dynamic mechanical analysis (DMA) and differential scanning calorimetry (DSC) measurements.

The adherends used in the study were cut from Ti-6Al-4V plates, having dimensions of 200 x 25 x 3.175 mm, and supplied by President Titanium Company, Hanson, MA. The adherends were surface pretreated before bonding with the adhesive.

3.3.2 Surface Pretreatment

The titanium surface treatment was chromic acid anodization (CAA). First the titanium adherends were wiped with acetone and cleaned with a 3M Scotch-Brite pad and rinsed in deionized water. Titanium was then soaked in Isoprep 177 (Allied Kelite) for 10-15 minutes, followed by a 5 minute warm water rinse in deionized water at a temperature greater than 43^{o}C. The sample pieces were then soaked in a nitric acid (HNO_3) bath (114 ml H_2O, 151 ml conc HNO_3, 10.9 ml of 50% HF) for 1.5 minutes followed by a cold water rinse in deionized water. The anodization was accomplished at 5 volts and a current of 0.11-0.14 amperes/m^2 for 20 minutes, followed again by a cold water rinse in deionized water. The composition of the bath was 45 gms of CrO_3/L. Ti-6Al-4V was used as the cathode. The samples were then dried in an oven for 1-1.5 hours at 66^{o}C.

3.3.3 Wedge, DCB, and Lap-Shear Specimen Fabrication

Wedge and double cantilever beam specimens were produced by individually bonding 200 x 25.4 x 3.175 mm plates of pretreated Ti-6Al-4V. The supported film was cut to dimensions of 175 x 25.4 mm and placed between the titanium adherends and bonded in a hot press using the modified cure cycle (see below). The initial 25 mm of the specimen was left unbonded and this region was used to attach end blocks in the case of the DCB specimens. The thickness of the adhesive film was measured before and after bonding and was found to be around 0.5 mm before bonding and around 0.125 mm after bonding. The drop in the thickness of the adhesive layer following the bonding procedure resulted from a "squeezing-out" of the adhesive from the specimen edges during the cure-cycle. This "squeeze-out" would have been considerably reduced if larger panels were bonded together, instead of bonding individual specimens. Irrespective of this adhesive flow problem, which was initially viewed with some concern, there were no noticeable differences in properties within different test specimens made in different batches. Typical schematics of the wedge and DCB specimen geometries are shown in Figure 3.5.

For bonding purposes, the samples were first heated to 250^{o}C under contact pressure at a heating rate of 5^{o}C/min, held at 250^{o}C for 30 minutes and then heated under pressure of 75 psi (0.518 MPa) to 350^{o}C, and maintained there for an additional 60 minutes. Following the 60 minute cure, the samples were cooled to room temperature at a cooling rate of 15^{o}C/min, under pressure.

Lap shear specimens were produced by individually bonding 100 x 25 x 2.2 mm adherends of pretreated Ti-6Al-4V. A bond overlap of 12.7 mm (0.5") was used and this is a standard procedure described in ASTM D1002 [11]. The supported film was cut to the dimensions 25.4 x 12.7 mm and placed between the titanium adherends and bonded in a hot press using the cure cycle described above. A schematic of the lap shear specimen is shown in Figure 3.6.

3.3.4 Specimen Conditioning

The bonded specimens and neat resin samples were conditioned in aging ovens for over 18 months (samples continue to be aged at this time), and selected samples were periodically removed and tested at aging times which are logarithmically separated. The two aging ovens are convection type ovens manufactured by Precision Scientific Group, Chicago, Illinois and these were maintained at temperatures of 177^{o}C and 204^{o}C. Samples were also aged in three different environments in each oven. Two steel chambers were placed in each of the ovens. A set of two chambers (one from each of the two ovens) was then interconnected by copper tubing and needle valves and connected to a vacuum pump, which maintained a constant pressure in the chambers at all times. A similar arrangement was constructed with the other set of two chambers. This facilitated the aging of samples in 6 different environments in the 2 ovens. The aging environments included ambient atmospheric air, reduced air pressure of 2 psi air (13.8 KPa) corresponding to the service altitude pressure of the HSCT, and 0.2 psi air (1.38 KPa). These three environments were so chosen to age the specimens in three different oxygen partial pressures, and thereby study the effects of chemical aging in the bonded joints.

3.4 Testing

3.4.1 Single Lap Shear Testing

Single lap shear (SLS) tests were performed on Ti-6Al/4V/FM-5 joints in accordance with ASTM D1002-72 [11]. The dimension of the adherends used in these tests were 100 x 25.4 x 3.175 mm, with the overlap/bonded area of the joint being 12.7 x 25.4 mm. The lap shear testing was performed in an Instron machine Model 4505. The low and high temperature testing was accomplished by using a Thermotron oven, Model F-2-CHM-C02 in conjunction with the Instron machine. At least 4 samples were tested per given testing condition.

3.4.2 Wedge Testing

The fracture energy using a wedge test specimen can be calculated by using equation 2.51. The underlying assumptions for applying equation 2.51 are, first, that there is no plastic deformation in the substrate, and secondly, that the specimen compliance is primarily due to beam bending with minimal contributions from beam shear and adhesive deformation. One disadvantage to this test is that the specimen must always be removed from the conditioning environment to make a crack length measurement. This is not easy if the samples are being conditioned in a vigorous environment. There may also be some subjectivity involved in measuring crack length in some samples where the cracks are very difficult to view especially after environmental exposure. In the current testing program five specimens were tested per environment and the values reported are averages from the five specimens. Crack measurements were taken on both sides of the test specimens.

The wedge tests conducted in this research were modified versions of the ASTM D 3762 [12]. The ASTM D 3762 test uses specimens cut out of plates with the dimensions of 17.8 x 21.5 x 1.5 mm. These dimensions are quite different from the 200 x 25.4 x 3.175 mm plates which were used for making the specimens in the present testing program. The ASTM test recommends the use of a 1.5 mm teflon spacer to control the bond thickness and also for the purpose of initiating a starter crack. Due to the fact that the FM-5 resin was available as a supported film, no teflon spacer was used during bonding as the glass scrim cloth helps maintain a constant bondline thickness. To ensure that a constant starter crack was obtained, wedges were very carefully inserted into the bondline by using a vice in this study. Also, based on the observations made by Cognard [4,13] and the static DCB tests conducted in this study, it was calculated that for the geometry of the specimens and wedges used in the study, (2 mm thick wedges were used in all the tests) a starter crack of at least 25 mm must be initiated to obtain satisfactory fracture energy values.

3.4.3 Static DCB Testing

The fracture energy for the static DCB tests was determined using equation 2.52, which was derived using the compliance method with corrections for the crack length offset and adherend stiffness. Specimens were tested in an Instron machine controlled through its GPIB interface using LabVIEW software developed by National Instruments, Austin, TX. The specimens were loaded at a crosshead speed of 1 mm/minute. As each specimen was loaded, several events took place as elucidated. As the load versus displacement curve deviates from linearity, the crack had begun to grow and the critical fracture energy, G_{IC}, has been reached. Now, due to the rate dependent failure of these adhesive systems, the loading value continued to increase. When the load reached a maximum and began to decrease rapidly, the specimen had achieved a maximum loading level, G_{MAX}. Once the maximum load was detected, the crosshead motion was stopped to allow the crack growth to continue until it approached quasi-static equilibrium conditions. The term, quasi-static equilibrium, is used because the crack was not always allowed to stop completely. The criterion used to establish a reasonable arrest loading level was that the value of strain energy release rate decreased by less than 1 J/m^2 over a minute. This procedure was used to identify the arrest fracture energy, G_{ARR}. Once crack growth slowed sufficiently, the specimen was unloaded to make sure plastic deformation of the adherends had not occurred. If plastic deformation had occurred, the P-Δ curve would not return to the origin, but instead would intersect the deflection-axis to the right of the origin. Finally, this load-hold-unload procedure was repeated until the specimen failed. Typical test data from a Ti-6Al-4V/FM-5 bond are shown in Figure 3.7. In all the DCB bonds reported here, the P-Δ curves did return to the origin indicating that there was no plastic deformation of the adherends. This was also confirmed by visual inspection of the specimens after testing.

3.4.4 Rejuvenation of Static DCB Specimens

Rejuvenation refers to the erasure of previous thermal history of a polymeric material by heating it above the T_g and quenching [14]. Rejuvenation eliminates all prior physical aging in the polymer. In the present study DCB specimens were rejuvenated after specific aging times, to erase all previous physical aging, thereby permitting the study of individual contributions of physical and chemical aging on bond strength reduction. As stated previously, physical aging is a thermo-reversible phenomena , while chemical aging is thermally irreversible. The Ti-6Al-4V/FM-5 bonds were rejuvenated for 2 hours at 300^{o}C. The motivation for selecting 300^{o}C as the rejuvenation temperature came from the DMA test data. Following 12 months of aging at elevated temperatures, the T_g of the neat adhesive increased from approximately 250^{o}C to just above 270^{o}C (details are given in the section on DMA testing and results). Therefore, it was decided that 300^{o}C was an appropriate rejuvenation temperature as it was at least 20^{o}C higher than the T_g of the resin [14,15]. The same test specimen was used to collect data both prior to and following rejuvenation, at a given aging time, temperature, and environment. The aged specimens were tested for some distance along the bond line, then rejuvenated, then continued to be tested until total failure.

3.4.5 Fatigue DCB Testing

Fatigue DCB tests were conducted on a servo-hydraulic MTS 810 testing machine. All tests were conducted using displacement control at a frequency of 5 Hz and the machine was programmed to apply a sinusoidal displacement with an R ratio of 0.1. Data acquisition was made possible by using LabVIEW software. Maximum and minimum loads and the number of loading cycles was periodically computed and written to a data file. Crack length readings were also periodically entered into the data set as with the quasi-static DCB tests. Usually 10-20 crack length readings are sufficient over the duration of a test. The fatigue data were modeled by equation 2.54, which is also referred to as the Paris equation [16].

3.4.6 DMA Testing

To study the effects of thermal aging on the glass transition temperature (T_g) of the FM-5 resin, a TA 983 Dynamic Mechanical Analyzer (DMA) was used in fixed frequency mode. The T_g was taken to be the peak of the loss modulus, E". The specimen sizes in the test were: 40.0 x 10.0 x 1.0 mm. Samples were aged in environmental chambers prior to testing. The same test specimen was used to collect data following aging, as well as after subsequent rejuvenation. Specimens were tested at 1°C/min and a fixed frequency of 1 Hz, between the temperatures of 50°C and 300°C to obtain the glass transition characteristics.

Sequenced creep tests were also conducted on the DMA to measure physical aging in the FM-5 neat resin specimens. The samples tested had nominally the same dimensions as those tested in the fixed frequency tests. The creep tests had five load/unload cycles, with the ratio of unload to load times being 15. The creep times for each loading section were 5, 15, 45, 135, and 405 minutes. During the tests, the initial displacement of the arm position was specified as 0.1 mm, which resulted in a maximum bending stress around 4 MPa. The shift rate, μ, which is an index of the kinetics of the physical aging process, was evaluated at several test temperatures ranging between 50°C and 220°C.

3.4.7 DSC Testing

Differential Scanning Calorimetry (DSC) was utilized to study the changes in the T_g of the resin material as a function of aging time, aging temperature, and aging environment. Measurements were conducted using a TA 912 Differential Scanning Calorimeter at a heating rate of 10°C/min. The T_g of the aged specimens was determined from the first scan. After the first scan was completed the samples were held at 300°C for 2 hours to accomplish rejuvenation, following which they were quenched to room temperature using liquid nitrogen and rescanned. The second scans provided information on the effect of rejuvenation on T_g. In all cases, the T_g values were taken as the midpoint of the change in slope of the baseline. The DSC data were also

used to study physical aging in the neat resin by monitoring the enthalpy recovery as a function of isothermal aging.

3.4.8 TMA Testing

Thermo-mechanical analysis (TMA) was utilized to study the changes in the T_g and coefficient of thermal expansion (CTE) of the resin material as a function of aging time and temperature. In the present study a TA 943 thermo-mechanical analyzer was used at a constant heating rate of 10^oC/min. The TMA, which acts as a linear dilatometer, consists of a quartz probe which rests upon a specimen, and a transducer, which measures the vertical position of the probe as the specimen undergoes volume expansion or contraction upon heating or cooling. Sample dimensions used in the study were approximately 5 x 5 x 1 mm.

3.4.9 Stress-Strain Testing

Tensile dog-bone stress strain specimens of neat FM-5 resin were prepared using a TensilKut unit (ASTM D-638), from neat resin plaques that were supplied by the Boeing Company. Samples were tested in accordance with ASTM D638M-91a [17], follwing aging at 177°C and 204°C, in both air and 2 psia environments for periods up to and including 6 months. At least 5 specimens were tested per aging condition. The testing was performed on a 4505 Instron machine at a cross head displacement rate of 1 mm/min. Utilizing LabVIEW software the load at break and the strain to failure (measured by using an extensometer) were recorded for all the specimens.

3.4.10 Weight Measurements

Three specimens each of the FM-5 neat resin having dimensions of 60 x 10 x 0.5 mm were used to monitor weight loss/change with aging at 177^oC and 204^oC in two different environments.

The two environments were ambient atmospheric air and reduced air pressure of 2 psia air (13.8 KPa). Samples were periodically removed from the aging ovens over several months, weighed, and returned to the ovens. Samples were weighed using an electronic analytical balance from Mettler Inc. Each data point reported in the results is an average value from three specimens weighed separately.

3.4.11 TGA Testing

To investigate the thermal stability of the FM-5 polymer, both prior to and after aging, a TA 951 thermogravimetric analyzer was used. Sample sizes between 20 to 50 mg were used for testing. Samples were tested between 50°C and 600°C at a heating rate of 10°C/min. To investigate the effect of oxygen on the decomposition process, air and nitrogen were used as the testing environments. These gases were introduced into the test furnace at a rate of 60 mL/min.

3.4.12 Soxhlet Extraction Tests

Neat resin samples of the FM-5 resin were extracted with NMP to determine the gel content in the crosslinked polyimide films. Extractions were carried out on samples aged at 177^{o}C and 204^{o}C in atmospheric air and reduced air pressure of 2 psia (13.8 KPa). The procedure for the extraction process is as follows:

The cured films were first placed into dried, pre-weighed cellulose thimbles. The thimbles were previously soaked in NMP for at least 24 hours and then dried at 150^{o}C for 3 days under vacuum. The combined weight of the sample and thimble was recorded and the assembly was placed in a Soxhlet extractor under refluxing NMP for 7 days. Sample weight was determined by subtracting the thimble weight from the combined weight. After the extraction period, the thimble and the sample were removed from the extractor, air dried for 24 hours and vacuum dried at 150^{o}C for 3 days. The gel fraction weight was found by subtracting the thimble weight from the combined weight of the thimble and the sample.

3.4.13 XPS Characterization

To study the changes in the neat resin and DCB fracture samples on an elemental basis (both before and after aging), x-ray photoelectron spectroscopy, XPS, was performed using a Perkin Elmer model 5400. The XPS has a spot size of 1.0 x 3.0 mm and typical surface sampling depths of 40-50 $\mathring{A}$ can be obtained using this instrument.

3.4.14 FT-IR Characterization

Diffuse reflectance spectra were obtained on the adhesive resin using a Nicolet 5DXB FT-IR spectrometer equipped with a DTGS KBr detector and external reflection accessories provided by Harrick Scientific Co. For all spectra, the chamber was purged with dry nitrogen gas and 1000 coadded scans were collected in each case at an angle of incidence equal to 40° and a spectral resolution of 4 cm^{-1}.

3.5 Results and Discussion

3.5.1 Single Lap Shear Results

With a view of understanding the effects of elevated temperature aging on bond strength, CAA treated Ti-6Al-4V/FM-5 samples were aged at 177°C and 204°C in atmospheric air. Following 4 months of aging at 177°C, the average lap shear strength from 5 samples has dropped by approximately 10% from the original value of 7200 psi, while a similar drop in strength was seen after only 4 weeks on samples aged at 204°C. These results, summarized in Table 3.1, show that aging temperature does play a significant role as regards the durability of the Ti-6Al-4V/FM-5 bonded system. This study is currently being conducted by Mr. Rajesh Tiwari [18] in the Chemistry Department at Virginia Tech, working with Prof. John Dillard.

In order to study the effect of test temperature and rate on bond strength, lap shear specimens made with CAA treated Ti-6Al-4V metal plates and bonded with FM-5 resin were tested. To simulate conditions of the HSCT, the testing temperatures chosen for this study included, -54°C, 25°C, and 177°C. The rationale behind selecting these temperatures was as follows; -54°C is the temperature of the service atmospheric environment through which the aeroplane would travel, 25°C corresponds to ambient atmospheric temperature during the time the aircraft is landed, and 177°C are skin friction temperatures experienced by the aeroplane structure during supersonic flight. The testing rates chosen for the study included the ASTM D1002 lap shear testing rate of 1.27 mm/min [11], and two additional rates of one and two orders of magnitude larger, namely, 12.7 mm/min and 127 mm/min.

Figure 3.8 shows the results obtained as a function of testing temperature for specimens pulled at 1.27, 12.7 and 127 mm/min. It is apparent that the LSS decreases with increasing testing temperature. One notable observation from this graph is that even at the highest test temperature of 177°C, the LSS of the bonded system were in the 4000-5000 psi range, which is an acceptable value for aerospace applications [19,20]. Also, this general trend of decreasing LSS with temperature is indicative of the viscoelastic nature of the adhesive, with 177°C being closest to the T_g of the adhesive material, which was determined to be around 250°C. The variation in LSS as a function of the test rate is less straight forward (see Figure 3.9). For the specimens tested at -54°C the strength is about 8500 psi when tested at 1.27 mm/min. The strength decreases to approximately 6300 psi for specimens tested at 12.7 and 127 mm/min. For samples tested at room temperature (25°C) and at 177°C, the maximum strength was measured at the intermediate testing rate of 12.7 mm/min, although the statistical differences in strength are almost within experimental error, and would suggest that the rate of testing has little or no significant influence on the test results. One explanation for the fact that the strength decreased at the higher testing rates is that FM-5 adhesive is a very glassy polymer and at very high testing rates glassy materials generally appear more brittle. One other observation from the testing was that irrespective of the testing conditions, all the samples failed in a cohesive manner, that is

within the adhesive material. The error bars on the graphs correspond to standard deviations at the 95% confidence level.

3.5.2 Wedge Test Results

Wedge tests were primarily used as screening tests to choose suitable and durable surface pretreatments for the titanium substrates. Table 3.2 summarizes the wedge test results on Ti-6Al-4V/FM-5 bonds with several different surface pretreatments. Results indicate averages from five specimens exposed to a 3 day water boil, and the standard deviations included are at the 95% confidence level. From these tests only the chromic acid anodized (CAA) and the chromium oxide grit blasted samples failed cohesively. For the present adhesive bond system, a cohesive failure could be described as failure at the adhesive/glass scrim cloth interface, and not at the titanium-adhesive interface. Based on these results it was decided to incorporate the CAA as a control treatment for the Ti-6Al-4V adherends for the duration of this study. Figure 3.10 compares the crack growth rates of CAA Ti-6Al-4V/FM-5 wedge specimens versus those having phenyl and allyl silane surface treatments. Over a 3 day exposure period to boiling water, the CAA specimens exhibit superior durability (higher arrest fracture energy) compared to the silanes pretreated specimens.

Long term bench mark wedge data were also collected on CAA treated Ti-6Al-4V/FM-5 bonds, following aging at 204^{o}C in three different air pressure environments. Results obtained have been summarized in Figure 3.11. From Figure 3.11 it is seen that for samples aged in standard atmospheric air for 17,280 hours, the fracture energy values have dropped to just below 1500 J/m^2 and the average crack length from 4 specimens is approximately 36.5 mm. Samples aged for 12,960 hours at a reduced air pressure of 2 psia had an average crack length of approximately 34.5 mm, and the fracture energy values have decreased to just below 1800 J/m^2. Crack length in this case were fairly constant over the last 4000 hours of aging. Very similar results were obtained from the wedge specimens aged at 0.2 psia environment. While the locus of failure in the specimens appears to be primarily cohesive for up to 6 months of aging, mixed

mode failures were seen on specimens aged beyond the 6 month period. Figure 3.12 shows the fracture surface of a wedge specimen that was aged for 14,400 hours in air at 204°C. The fracture surface shows mixed mode failure in the sample, with predominant adhesive failure seen at the specimen edges. Also, one can see a darkening of the adhesive material at the bond edges, indicating that the degradation of the bond is starting at the specimen edges and moving inward, pointing to a diffusion controlled degradation mechanism.

3.5.3 Static DCB Test Results

The general trend of decreasing toughness with time for Ti-6Al-4V/FM-5 samples aged at 204°C in ambient atmospheric air is illustrated in Figure 3.13. Following 18 months of aging at 204°C, the G_{MAX} value has decreased to 1700 J/m^2 from an intial value of 2550 J/m^2, a decrease of about 33%, and the G_{ARR} value decreased from 2100 J/m^2 to 1580 J/m^2, a reduction of approximately 25%. The G values for samples aged at 177°C showed a similar decrease in fracture energy, although of a slightly lower magnitude. The static DCB results for the Ti-6Al-4V/FM-5 specimens that were aged at 204°C in different air atmospheres are shown in Figure 3.14. The overall trend is that aging in the reduced pressure atmospheres leads to a less pronounced reduction in bond toughness as measured by the G values. Similar observations were made once again in the samples aged at 177°C. The error bars in Figures 3.13 and 3.14 are standard deviations at the 95% confidence level and are obtained from a single DCB test by conducting several load and unload cycles. The significant conclusions from the above results are that the greatest decrease in bond toughness occurs in atmospheric air at 204°C, and that the lower the concentration of oxygen in the aging environment, the smaller the drop in adhesive toughness. The latter conclusion suggests that there is chemical degradation in the material system. The critical strain energy release rate as a function of time, presented in Figure 3.15, emphasizes the fact that adhesive toughness decreases with time. The samples aged at 204°C for 360 days show a toughness that is only 67% of the initial toughness. It must be mentioned here that, for the most part, failure in the bonded samples is “cohesive” (interfacial failure at scrim

cloth). Following 6 and 12 months of aging, however, the DCB samples showed some areas of "adhesive failure" (visual failure at titanium adherend surface) around the outer edges of the specimens. This is clearly elucidated in photographs included as Figure 3.16 and 3.17. Failure at the exposed outer edges may be due to adhesive degradation or processes related to changes at the anodized titanium surface.

Figure 3.18 shows the effect of rejuvenating the DCB specimens and retesting them, following aging in the three air atmospheres for 6 months at 204^{o}C. Almost 50% of the drop in toughness, compared to the as-received toughness value, can be recovered on all the aged samples following rejuvenation. Rejuvenation apparently erases the physical aging in the test specimen contributing to the recovery of toughness. However, there is an irrecoverable portion to the drop/loss of toughness. This may be attributed to chemical aging, thermal degradation of resin, changes at the titanium interface, etc. Figures 3.19 and 3.20 show similar data collected on the DCB specimens following 12 and 18 months of aging at 204^{o}C, respectively. The notable observation from these figures is that while the samples aged at 2 psia and 0.2 psia can be rejuvenated to recover most of their lost toughness, the specimens aged in air at atmospheric pressure did not show any significant increase in toughness following rejuvenation. This result further strengthens the claim that both physical and chemical aging are taking place simultaneously in the material system, and that chemical aging dominates at longer aging times. Another observation that can be drawn is that degradation is sensitive to the oxygen concentration in the aging environment, and unlike the physical aging, is irreversible. Table 3.3 summarizes the drop in fracture energy of the titanium/FM-5 bonded system following aging at 204°C in the three different air pressure environments. Following rejuvenation, the individual contributions of physical and chemical aging responsible for the decrease in fracture energy are also computed and reported in Table 3.3.

Static DCB fracture test data reported above were collected in all cases by testing one specimen at each aging condition. To replicate some of the above aging studies, specimens were prepared under similar bonding conditions (samples were B-stage cured by holding at 250°C for an additional 30 minutes, and each specimen was individually bonded at Virginia Tech) and were

aged and tested. Figures 3.21 and 3.22 summarize data collected on DCB specimens that were aged for 6 and 12 months respectively, at 177°C, in the three different environments. While the samples from the original aging study were designated as samples #1, the more recently tested specimens were designated as samples #2. It is quite apparent from the examination of the findings that a good correlation exists among the two sets of results. The failure mode for both sets of specimens was cohesive after 6 months of aging, while mixed-mode failure occurred for the 12 month aged samples.

To study the effect of test temperature on the fracture toughness of the adhesive bonds, CAA Ti-6Al-4V/FM-5 bonds were tested at selected temperatures of -54°C, 25°C, and 177°C. The results of this study are summarized in Figure 3.23, and the significant finding is that the difference in maximum and arrest fracture energies is small at the highest test temperature, compared to the results at lower temperatures. The near equivalence of G_{MAX} and G_{ARR} at 177°C (which is closer to the T_g of the adhesive) is due to the viscoelastic nature of the adhesive. On the other hand, the differences in the respective G_{MAX} and G_{ARR} values at the lower test temperatures are explained as a result of the more brittle characteristic (slip-stick failure process) of the polymer at lower temperatures.

3.5.4 Fatigue DCB Test Results

Initial fatigue DCB tests were conducted on phenyl silane treated Ti-6Al-4V/FM-5 bonds, the results of which are summarized in Figures 3.24-3.26. Some of the observations/insights gained from these previous tests are as follows: i) samples were debonding at energy release rates under 100 J/m^2 over a 2-3 day duration of the test, ii) failure mode of the joints was cohesive and very similar to that for the static DCB tests, and iii) the aged samples show a slightly reduced crack growth rate compared to the as-received specimen. Initially, the fact that perceptible debond propagation was occurring at energy release rates as low as 100 J/m^2 was viewed with concern. However, in light of similar results and low threshold energy release rate values reported by other researchers [21-23], the results obtained from the present adhesive

system may be acceptable. Anodized Ti-6Al-4V/FM-5 adhesive bonds were aged at 177°C in air for 6 and 12 months respectively, to study the effect of thermal aging on fatigue performance. The results from this study are shown in Figure 3.27. As can be seen from the figure, the G_{th} (threshold fracture energy) value decreases by a factor of two, going from the as-received specimens to the specimens aged for the longest period of time at temperature. In adhesive joints, a G_{th} can be defined for crack growth slower than 10^{-8}/cycle. From Figure 3.27, it can be seen that a true theshold was not reached for the specimens tested; however, it appears that the results obtained are in the near vicinity of threshold fracture energies. Also, there appears to be an ordering within the specimens as regards the fatigue performance going from the unaged to the intermediate aged to the longest aged samples. One other observation that was made from the failed fatigue specimens was that mixed mode failure was detected on the samples aged for 12 months, while all the other specimens exhibited cohesive failure.

3.5.5 DMA Results

Changes in the glass transition temperature, T_g, of neat FM-5 resin were monitored following air aging of the specimens for periods up to 18 months at 177°C, and 204°C. These results are summarized in Table 3.4. Samples aged for 2, 6, 12, and 18 months at the two aging temperatures were then rejuvenated at 300°C for 2 hours. Following rejuvenation all the samples were retested using the same testing conditions as before. At all the aging times tested, none of the samples could be rejuvenated to obtain a T_g matching that of the as-received specimen. However, it must be mentioned that the difference in T_g between the as-received specimen and those tested after aging and rejuvenation, increased with aging time. In fact, the T_g was around 10°C higher than the as-received values in some cases. This indicates that other competing mechanisms (e.g. additional cross-linking, solvent expulsion) are taking place in the polymer besides physical aging, and that these other phenomena cannot be erased by thermal rejuvenation. Another point to be noted is that the T_g of the resin samples did not increase significantly following additional aging between the 6 month and 18 month period, and this was consistently

observed at the two aging temperatures. Typical DMA traces for specimens aged at 177°C are included as Figures 3.28-3.31.

DMA creep measurements were carried out on neat FM-5 supplied as precured coupons by Cytec Engineered Materials, Inc. Figure 3.32 shows a schematic of a sequenced creep test conducted to measure physical aging. Each of the tests had five load and unload cycles, with the specimen compliance determined during each loading period. The physical aging effects can be characterized by the amount of horizontal shift required to superimpose a creep compliance curve at a specific aging time, on to one at the reference aging time, to form a smooth master curve. This shifting procedure is similar to the principle of time-temperature superposition (TTSP) [24]. During the shifting, the shift factor, or the amount of horizontal shift, was measured. If the shift factor versus the logarithic aging time is plotted, an approximate straight line results, the slope of which is the shift rate, m, which characterizes the physical aging kinetics. Figure 3.33 shows typical creep compliance data measured on the FM-5 resin at 150°C; Figure 3.34 shows the master curve formed after horizontal shifting at the above test temperature. Figure 3.35 shows a plot of the horizontal shift factor versus aging time used for the determination of m at 150°C. Figure 3.36 shows the shift rate versus temperature plot obtained on the FM-5 resin samples between the test temperatures of 50°C and 220°C. As one would expect, the value of m decreases at temperatures approaching the T_g (a-transition) and also at temperatures approaching room temperature. This phenomenon has been observed in other polymeric materials [25-28].

Figure 3.37 shows the creep data obtained at 177°C on an as-received specimen. Figure 3.38 shows the data obtained on a specimen that was aged in air at 177°C for 6 months. Prior to testing, the aged specimen was rejuvenated at 300°C for 2 hours. On comparison of Figures 3.37 and 3.38, the aged and rejuvenated sample appears at least 10% more compliant than the as-received specimen. Similar observations were made at the 150°C and 204°C test temperatures. Figure 3.39 compares shift rate data between the as-received coupons versus the aged and rejuvenated samples, at test temperatures of 150°C, 177°C, and 204°C. From the figure, one can see that at all the above 3 temperatures, the shift rates obtained following aging and rejuvenation

were consistently higher than those obtained on as-received samples at the same study temperatures. This observation is consistent with a chemical degradation phenomenon in the adhesive resin; chain scissioning resulting in lower molecular weight species, leading to greater mobility and higher compliance.

As stated in the principle of time-temperature superposition, temperature plays a significant role on the creep behavior of a polymer [24]. In order to compare the effect of aging time with temperature, the aging times and temperatures that produce the same shift factors were calculated for the FM-5 resin system and plotted in Figure 3.40. From this aging time-temperature equivalency curve, an increase in a decade of aging time is approximately equivalent to a reduction of 7 to 8°C in temperature. Phrased in other words, aging the FM-5 adhesive resin for one year is equivalent to testing it at a 50°C colder temperature. It must however be mentioned here that this data be viewed cautiously as it only assumes a viscoelastic behavior of the adhesive material, and fails to take into account factors such as embrittlement, loss in fatigue properties, and other characteristics that become important with elevated temperature aging over extended periods of time.

3.5.6 DSC Results

DSC tests were conducted on scrimmed FM-5 resin samples as a function of aging time, temperature, and environment. The changes in the T_g of the resin at 177^{o}C and 204^{o}C, using DSC measurements are summarized in Table 3.5. All the measurements were made at a constant heating rate of 10^{o}C/min. In addition to T_g measurements, enthalpic relaxation, DH, of the FM-5 resin was also monitored. These data are summarized in Table 3.6. As the isothermal aging time increases, the height, area, and temperature of the endothermic annealing peak increases. This is quite evident from the DSC traces obtained from the FM-5 resin at 204^{o}C, as summarized in Figure 3.41. These observations are general for polymeric materials and have been noted by many researchers [29-31]. Figure 3.42 shows the DSC traces of the samples aged for 6 and 12 months at 204^{o}C in air, both before and after rejuvenation. The rejuvenated samples show trace

characteristics that are similar to those for the as-received sample, indicating once again that the samples are undergoing physical aging, and that this aging can be thermally erased. In the present study, the enthalpy increased from 1.212 J/g to 7.344 J/g for samples aged in air at 177^{o}C for periods up to 12 months, while in a similar time frame the samples aged in air at 204^{o}C showed an increase in ΔH, from 1.267 J/g to 8.879 J/g. It must be mentioned here that the enthalpy numbers shown in Figure 3.41, were calculated by subtracting the first run scan data from the baseline data. The second run data is reported only for the specimens that were rejuvenated and rescanned following aging for 6 and 12 months respectively at 204°C (see Figure 3.42). It is seen from the rejuvenated specimen scans, that there still exists a small enthalpic relaxation peak. This peak could be a result of thermally irreversible processes that have taken place in the adhesive resin. In hindsight, it is felt that it may have been more appropriate to report enthalpic relaxation numbers attributable to physical aging (in Figure 3.41), by subtracting first run scan data from the second run data. Samples were also aged in the two reduced pressure environments and the changes in ΔH monitored with aging time. Figure 3.43 shows a plot of the enthalpic relaxation as a function of aging time on a log-log scale. Data collected up to and including the 12 month aging period, at the two aging temperatures, and the three aging environments are shown in this plot. A number of observations can be made from this plot. All of the data collected at the 204^{o}C aging temperature are shifted upward, compared to the data collected at 177^{o}C. Another observation is that at the longer aging times, the curves seem to level off in all the three aging environments and there is a certain ordering to the data at both aging temperatures. The data obtained on the air aged samples appear to have the greatest enthalpic relaxation with aging time, the 0.2 psi air aged samples the least, and the 2 psi air aged samples intermediate. Some possible explanations for the leveling off in the data at the longer aging times are as follows; i) “free volume” is created in the samples at longer aging times due to the onset of chemical degradation , which creates more free chain ends, thereby contributing to the total volume of the system. The data in the preceding paragraphs quite conclusively showed that both physical and chemical aging were taking place simultaneously in the resin system, and that at longer aging times, chemical aging dominates over physical aging. ii) the levelling off in the data can result from the lowering in the molecular weight

of the samples following long term aging. There is evidence of weight loss in the neat resin samples, on the order of 3-4 wt% over a 12 month period. Further, there is also a drop of 6-7% in gel fraction following Soxhlet extraction in the 12 month aged samples. iii) it is also possible that the diffusion of gases like oxygen in and out of the samples, can also play a role in the interpretation of the observed experimental data. Echeverria [30] in his study with polyetherimide noted that at aging temperatures near T_g, equilibrium is reached within the time scale of the experiment, and this manifests itself by the levelling off of ΔH. At this point there is no definitive explanation with respect to the ordering of the data collected at the three different aging environments at a given temperature. It is however important to note that oxygen does exist in the reduced air pressure environments; however, the concentration of oxygen is much less than that in ambient air at atmospheric pressure. It is also possible that the as-received samples had some oxygen trapped in them, even before the aging was initiated. Figure 3.44 shows DSC traces obtained on samples that were aged for 6 months in air at 150°C, 177°C, and 204°C. It is apparent from this figure that enthalpic relaxation, ΔH, increases from 6.126 J/g to 8.147 J/g going from an aging temperature of 150°C to 204°C, for the same aging time. This indicates that physical aging is more rapid at the higher aging temperature of 204°C.

3.5.7 TMA Results

Figure 3.45 summarizes the TMA results obtained on FM-5 neat resin samples that were aged in air at 204°C for up to 12 months. During the testing, samples were thermally scanned between the temperatures of 50-325°C at a heating rate of 10°C/min. Dimensional changes of the samples were monitored throughout the above mentioned temperature range. Figure 3.45 shows that the T_g of the samples increased from 248°C to 273°C over a 12 month aging period. One other observation from the figure is that the coefficient of thermal expansion of the glassy phase (α_g) decreased by a factor of two over a 12 month aging period. There are no ready explanations for the above behavior.

3.5.8 Stress-Strain Test Results

The results from aging studies on neat resin samples at both 177°C (in air and 2psi air), and 204°C (in air) for periods up to 6 months are summarized in Table 3.7. The results show a decrease in the load to failure (as much as 20% in some cases) and in the strain to failure (as much as 40% in some cases) as aging time increases. The greatest drop in material properties occurred for the samples aged at 204°C compared to the as-received specimens, (see Figure 3.46). A reasonable explanation for the observed findings is that degradation of the adhesive resin and embrittlement are occurring as a result of thermal aging.

3.5.9 Weight Measurements

Three specimens of FM-5 neat resin were aged at 204^{o}C and 177^{o}C in air at 14.7 psi air and reduced air pressure of 2 psi (13.8 KPa) and were weighed periodically to monitor weight loss. These results are summarized in Figure 3.47, with two standard deviations indicated on the curves. It is noted, that irrespective of the aging temperature, there appears to be a significantly higher weight loss in the 14.7 psi air aged specimens compared to the specimens aged at 2 psi air. This is indicative of a chemical degradation process which is more vigorous in the specimens aged in the environment having a greater oxygen concentration. This is further confirmed from the Soxhlet extraction studies performed on the FM-5 resin. The average weight loss at the greatest aging time is between 2-3%. The FM-5 neat resin samples contained around 0.5% by weight of solvent (NMP). Therefore, some of the very initial weight loss could be due to solvent removal from the material as well as moisture losses.

3.5.10 TGA Results

TGA plots are presented in Figure 3.48 for as-received and aged FM-5 neat resin specimens. A general expected result is that weight loss is less for samples tested in nitrogen

when comparing as-received and aged specimens, respectively. The most prominent loss occurs for the as-received sample tested in air. Some of the initial losses from the as-received samples could be attributed to the residual NMP solvent and moisture present in the adhesive films, and these are mostly eliminated in aged films. In comparing the weight losses (in either atmosphere) for as-received and aged samples (6 months at 177°C), it is apparent that the aged samples exhibit a smaller weight loss. The identity of the components lost during the measurements has not been determined. However, in separate experiments conducted on cured FM-5 films (by Prof. John Dillard's group in the Chemistry Department), the mass spectrum as a function of temperature, revealed peaks at 250°C and 350°C that were assigned to NMP solvent.

3.5.11 Soxhlet Extraction Test Results

Table 3.8 summarizes the results obtained from Soxhlet extraction studies conducted on FM-5 neat resin samples aged for periods of up to 12 months in 14.7 psia air and 2 psi air (13.8 KPa) at 177^{o}C and 204^{o}C. The percent gel fraction dropped from 98.1% to 90.6% in samples aged in air for 12 months at 204^{o}C, while over a corresponding aging time the percent gel fraction in 2 psia air aged samples dropped to 95%. In the samples aged at 177^{o}C, the percent gel fraction dropped from 98.1% to 94% following air aging for 12 months, while for a corresponding aging time, the drop in 2 psi air environment was 96.5% from an initial value of 98.1%. These results substantiate the claim that chemical aging is taking place in the resin material following long term aging, and that this degradation is sensitive to the oxygen concentration in the aging environment. It can also be inferred from the extraction tests that the degradation mechanism appears to be of an oxidative chain scissioning type, judging by the fact that more sol fraction% is extacted from the resin following longer aging times and greater periods of exposure to the environment possessing the higher oxygen concentration. Table 3.9 summarizes extraction results that were repeated on films that were aged under similar conditions as in the experiment above, the only difference being that the extractions in this case were all conducted using room temperature NMP solvent. The results from this study show similar trends as regards the gel fraction%, when

compared to the first experiment. However, it is apparent from the second study that the gel fraction decrease is less severe for all environmental aging conditions. This difference could be attributed to the fact that the refluxing solvent used in the initial study was at an elevated temperature, thereby inducing some additional degradation in the adhesive material.

3.5.12 XPS Results

XPS analysis was performed on Ti-6Al-4V/FM-5 wedge test specimens that were aged for over 10,000 hours in the three different air pressures (atmospheric air, 2 psia, and 0.2 psia) at 204°C. These specimens were part of a long-term bench mark aging study involving CAA adhesive bonds. The wedge specimens were removed from the aging ovens and "force failed" by driving the wedge into the bonded portion of the sample until total fracture. The above procedure served a dual purpose of determination of the failure mode in the samples, and investigation of potential changes in the adhesive chemistry. Three failure regions were of interest for surface characterization: 1) the initial failure region-initial crack region, before the wedge exposure tests were initiated; 2) the region which failed during the test and was exposed for some period of time to the test environments; and 3) the region which did not fail during the test but which was force failed after the specimen was removed from the test atmosphere. It should be recognized that the "force failed" region was anaerobically aged during the test in that the final failure surface was not exposed directly to the environment-thus alterations in the adhesive material would be due to thermal effects, rather than effects as a result of thermal and environmental exposure conditions. Some results from the initial failure region will be discussed, but no analyses will be discussed for the region that failed during the test. Visual analysis of the initial failure region indicates that all samples failed cohesively, while the features noted from the force failed regions show a mixed mode failure, that is a combination of adhesive and cohesive failure. This change in the mode of failure when comparing the initial and the force failed regions was supported by the XPS analysis. Table 3.10 presents the atomic concentrations for metal (mfs) and adhesive failure surfaces (afs) for both regions and fully cured scrimmed FM-5

adhesive. The XPS results for the metal failure surface (arbitrary designation, since adhesive was found on both failure surfaces in this initial failure region) reveal no aluminum or titanium on this failed surface. Further, the concentrations for carbon, oxygen, nitrogen, and silicon (from the scrim cloth) on the metal failure surface are equivalent to the values determined for the cured FM-5 adhesive. The XPS results for the adhesive failure surface for the initial failure region are also equivalent to the findings for the metal failure surface and the cured adhesive, except that traces of titanium and aluminum are detected. Nevertheless, the near equivalence of the results for both failure surfaces and for the cured adhesive indicates failure within the adhesive and specifically at the scrim cloth-adhesive interface.

The surface analysis results for the metal failure side from the "forced failure" region show 4% titanium and 1% aluminum. The elements detected on the adhesive failure surface include carbon, oxygen, nitrogen, and silicon, with traces of titanium and aluminum. The concentration of silicon on this adhesive surface is less than that noted for the cured adhesive or for the adhesive failure surface from the initial failure region. The respective concentrations of carbon, oxygen, nitrogen, and silicon when compared to the percentages for the other adhesive failure surfaces suggest that failure occurs within the adhesive bit in a region that is less characteristic of the scrim cloth-adhesive interface. That titanium and aluminum as well as significant concentrations of "adhesive" elements are detected on the metal failure surface support the idea that debonding in the forced failure region occurs via a mixed mode process. Thus the effect of long-term exposure at elevated temperature, 204°C, is to change the failure mode from one that is cohesive to one that is mixed mode, with a significant exposure of the metal oxide surface.

The XPS results for the adhesive failure surfaces for surfaces obtained by forced failure after having been maintained at 204°C at different air pressures are given in Table 3.11. The principal finding is that the quantity of silicon varies, and greater silicon is detected for specimens aged at reduced pressures compared to that detected on the sample aged at atmospheric pressure. Also the concentration of the oxygen for the specimen maintained at 0.2 psia is less than that for the sample aged for the same time and temperature at 2 psia. Analysis of the metal failure

surfaces for each of the samples exposed to different air pressures reveals titanium and "adhesive" element signals. The detection of titanium and adhesive component elements suggests mixed mode failure for the forced failure region for these specimens.

DCB specimens prepared by bonding CAA Ti-6Al-4V with scrimmed FM-5 adhesive, were aged for 12 months at 177°C and 204°C in air, and XPS analysis was performed on the failed specimen surfaces. The fracture energy values for these samples have been reported in a previous section dealing with results on static DCB testing. These samples failed primarily cohesively, although a 2-3 mm strip around the edge of each sample appeared to fail interfacially according to visual inspection. XPS analysis was performed on this narrow strip of adhesive failure region and the atomic concentration data for the metal and adhesive failure surfaces reported in Table 3.12. The atomic concentrations for both the adhesive failure surfaces correspond to those detected for fully cured scrimmed FM-5 adhesive. The absence of detectable titanium on these surfaces indicates that failure did not occur in the metal oxide layer. Although some titanium is detected on the metal failure surfaces, the concentration is not as high as expected for an anodized, non-bonded titanium surface. The percent titanium on a non-bonded anodized surface is approximately 10-15%. The silicon and chlorine that are detected from the analysis arise due to contamination from handling or the seal (silicone) in the aging ovens. These results indicate that the edge of the sample failed in the same cohesive manner as the "bulk" of the sample, although the failure is very close to the oxide layer and leaves a very thin film of adhesive on the metal surface.

XPS analysis was also performed on the residual material that was left after driving away the NMP solvent from the Soxhlet extraction solution. The Soxhlet extraction solution used in this study was from the adhesive film that was aged for 12 months in air at 204°C. Following the extraction process the clear NMP solvent became turbid. A few drops of this solution were placed on a gold foil and dried in an oven, leaving behind a "residue". It must be mentioned here that the extraction solution from the as-received adhesive film remained perfectly clear and there was no evidence of turbidity as seen from the aged films. XPS results from this "residue" are compared with those obtained on a cohesively failed DCB specimen, and shown in Table 3.13.

The results show very good correlation in the atomic concentrations of carbon, oxygen and nitrogen between the "residue" and the cohesively failed DCB specimen. This confirms that we have indeed extracted polyimide material from the aged adhesive film using the Soxhlet procedure. Therefore, one conclusion that can be drawn from this study is that there is a degradation (possibly chain scissioning) of the FM-5 adhesive material, following aging at elevated temperature. One other siginificant observation from the XPS analysis of the "residue" material was the presence of around 3% silicon. Since the extractions were performed on unscrimmed adhesive material, it is inferred that the silicon was probably used as a filler material in the adhesive, and therefore manifests in the extraction solution.

3.5.13 FT-IR Results

Diffuse reflectance infra-red spectroscopy was performed on the residual material that was dried out from the Soxhlet extraction solution, the XPS analysis for which was discussed in the above section. Figure 3.49 shows the spectrum for the "residue" material from the Soxhlet extraction process, with the different spectral assigments of the major peaks indicated on the figure. There is excellent agreement of these spectral peaks with those obtained for LaRC PETI-5 powder and summarized in Table 3.14 [32]. The PETI-5 spectral assignments were made by comparison with the spectral assignments for polyimides in literature [33,34]. The infra-red data serve as another piece of conclusive evidence that polyimide entities have been indeed extracted from the aged FM-5 adhesive during the solvent extraction process, and that there is chemical degradation of the adhesive material taking place following elevated temperature aging.

3.6 Summary and Conclusions

This research was initiated to evaluate the durability of Ti-6Al-4V/FM-5 adhesive bonded system for application in the proposed HSCT aircraft structure. In the present study, the criteria for material selection is based on the bonded system showing sufficient durability for over 60,000 flying hours, when exposed to elevated temperatures and an environment (corresponding to the service altitude of the HSCT aircraft) having a reduced air pressure of 2 psi air (13.8 Kpa). Several factors affect the durability of an adhesively bonded joint which is subjected to long-term environmental aging. Two important factors are physical and chemical aging of the adhesive resin. This paper addresses the combined effects of both types of aging on the durability of Ti-6Al-4V/FM-5 bonds, via measurement of mechanical and material properties.

Several questions were posed by the author in the introduction part of this paper (section 1.2) to be answered as part of this research. To date, there are no complete answers to all these questions, due to the very complex nature of the problem being addressed. The adhesive system in this study comprises the adherends, adhesive, surface pretreatment (CAA), and their respective interphase/interface regions. The interaction of all these components with the applied mechanical loads and environmental exposures, is not a straight-forward one. Besides the physical and chemical aging phenomena, the study is further complicated by other factors taking place in the adhesive resin such as volatile expulsion, additional cross-linking, etc. One other significant factor that has limited the author's understanding of the long-term aging behavior of the Ti-6Al-4V/FM-5 bonded system, is the chemical nature of the FM-5 resin. FM-5 is a proprietary polymer, manufactured and supplied by Cytec Engineered Materials, Inc. after suitable alteration of the original LaRC PETI-5 adhesive. Since the fillers, modifiers, and additives in the FM-5 resin were unknown, it was difficult to pin-point exactly the source or location of chemical degradation in the adhesive material/bonded joints following long-term thermal aging. However, several indirect measurements made using Soxhlet extractions and spectroscopic analysis techniques, pointed clearly towards a degradation of the resin material following aging. Currently, there are two possible theories that could contribute towards the

chemical aging phenomena in the adhesive. The first one is chain-scissioning in the polymer following thermal aging in an environment containing oxygen. The weight loss, solvent extraction, XPS, and FT-IR data definitely support this claim. Also, the aged DCB specimens showed a "picture-frame" type failure pattern with interfacial failures around the edges. This failure was indicative of a degradation mechanism that was diffusion controlled, for eg: diffusion controlled oxidation. The second theory for chemical degradation is a hydrolysis of the adhesive material, resulting in a breakdown of the imidized polymer network into its amic acid precursor. There is no conclusive evidence to support this claim. It must be mentioned, however, that it is quite possible for a combination of the above two factors to be responsible for the degradation of the bonded system.

Physical aging, which begins right after an adhesive is formulated, has no time delay. Therefore, it can be detected much earlier than chemical aging. The DMA, DSC, TMA, stress-strain, and static DCB test results showed that this was indeed the case with the FM-5 adhesive. The above tests also showed that chemical aging became more dominant following longer aging times. However, it is not possible to conclude as to which of the two aging phenomena is more detrimental to long term bond durability. This study has also shown that there is reasonable potential in using DCB fracture tests with respect to sorting out the effects of physical and chemical aging phenomena in bonded joints. Both types of aging were detected in the Ti-6Al-4V/FM-5 bonds, and it was further shown that suitable thermal rejuvenation techniques can be used to "de-couple" their effects on bond toughness.

3.7 References

1. R. Joseph, J. P. Bell, A. J. McEvily, and J. L. Liang, *J. Adhesion.* **41**, 163-187 (1993)

2. S. Mall, W. S. Johnson, and R. A. Everett, Jr, *Adhesive Joints*, K. L. Mittal (Ed.), Plenum Press, New York (1984)

3. A. J. Kinloch and S. J. Shaw, in: *Developments in Adhesives-2*, A. J. Kinloch (Ed.), Ch. 3, Applied Science Publishers, New York (1983)

4. J. Cognard, *J. Adhesion.* **20**, 1-13 (1986)

5. M. B. Ouezdou, A. Chudnovsky, and A. Moet, *J. Adhesion.* **25**, 169-183 (1988)

6. M. D. Rakestraw, M. A. Vrana, D. A. Dillard, J. G. Dillard, and T. C. Ward, *Durability and Damage Tolerance*, AD-Vol. **43**, *ASME WAM*, 65-77 (1994)

7. M. D. Rakestraw, M. W. Taylor, D. A. Dillard, and T. Chang, *J. Adhesion.* **55**, 123-138 (1995)

8. B. Blackman, J. P. Dear, A. J. Kinloch, S. Osiyemi, *J. Mater. Sci. Lett.* **10**, 253-256 (1991)

9. J. H. Crews Jr., K. N. Shivakumar, I. S. Raju, *AIAA J.* **29**, 1686-1691 (1991)

10. J. G. Smith, and P. M. Hergenrother, *Polymer Pre-prints.* **35**, 353-355 (1994)

11. ASTM Standard D1002-72, *Annual Book of ASTM Standards, Adhesives*, Vol. **15.06** (1992)

12. ASTM Standard D3762, *Annual Book of ASTM Standards, Adhesives*, Vol. **15.06**, 360-364 (1984)

13. J. Cognard, *J. Adhesion.* **22**, 97-108 (1987)

14. L. C. E. Struik, *Polymer* **30**, 799-814 (1989)

15. T. S. Gates and M. Feldman, *NASA Tech. Memo. 109047* (1993)

16. P. C. Paris and F. Erdogan, *ASME Trans., J. Basic Eng.* **4**, 528 (1963)

17. ASTM Standard D638M-91a, *Annual Book of ASTM Standards,* Vol. **10.01**, 172-180 (1992)

18. R. Tiwari, *Personal Communication,* February (1997)

19. T. L. St. Clair and D. J. Progar, *J. Adhesion.* **47**, 67-82 (1984)

20. R. D. Rossi, *Engineered Materials Handbook, Volume 3, Adhesives and Sealants*, H. F. Brinson (Ed.), ASM International, Materials park, Ohio, 151-162 (1990)

21. B. Dattaguru, R. A. Everett, Jr., J. D. Whitcomb, and W. S. Johnson, *J. Eng Mater. Technol.* **106**, 59-65 (1984)

22. M. R. Allen, *NASA-CR-198193* (1995)

23. C. L. Hendricks and S. G. Hill, in: *Polyimides: Synthesis, Characterization, and Applications*, Vol. 2, Plenum Press, New York (1984)

24. H. Leaderman, *The Textile Foundation*, Washington D. C. (1943)

25. L. C. E. Struik, *Polym. Eng. Sci.* **17**, 165-173 (1977)

26. L. C. E. Struik, *Polymer* **28**, 1521-1533 (1987)

27. L. C. E. Struik, *Polymer* **30**, 799-814 (1989)

28. L. C. E. Struik, *Polymer* **30**, 815-830 (1989)

29. A. R. Berens and I. M. Hodge, *Macromolecules* **15** (3), 756-761 (1982)

30. I. Echeverria, P. C. Su, S. L. Simon, and D. L. Plazek, *J. of Poly. Sci.: Part B: Polymer Phy.* **33**, 2457-2468 (1995)

31. S. E. B. Petrie, *J. Polym. Sci.: A-2.* **10**, 1255-1272 (1972)

32. J. G. Dillard, F. R. Jackson, B. L. Holmes, L. Aartun, H. Parvatareddy, D. A. Dillard, and R. Zatorski, *J. Adhesion.* in press (1997)

33. H. Ishida and M. T. Huang, *Spectrochimica Acta.* **51A**, 319 (1995)

34. H. Ishida, S. T. Wellinghoff, E. Baer, and J. L. Koenig, *Macromolecules.* **13**, 826-840 (1980)

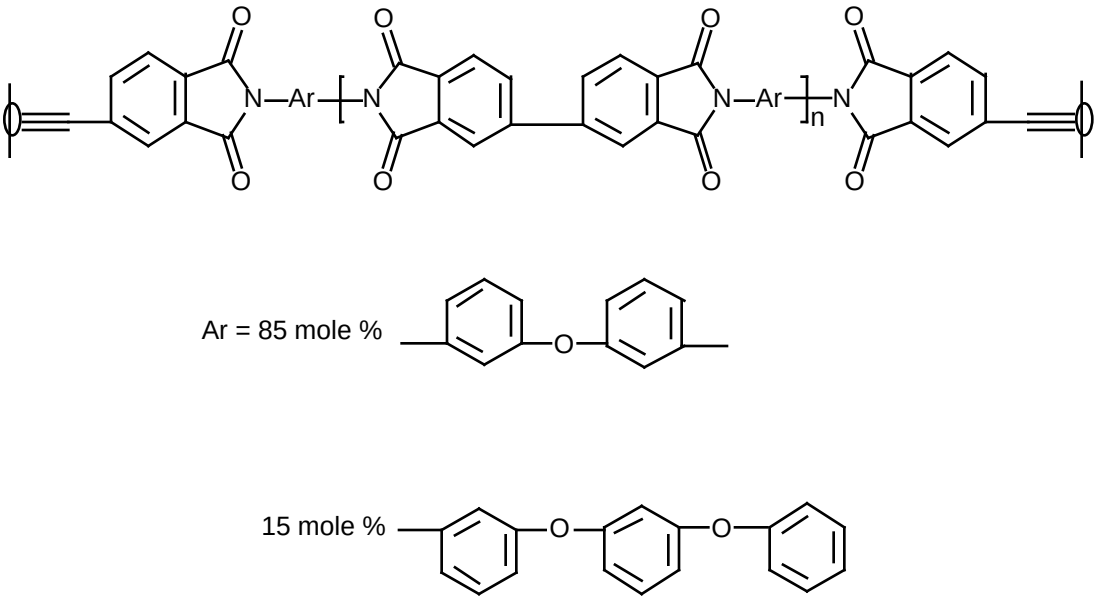

Figure 3.1. Chemical structure of LaRC PETI-5 adhesive [10].

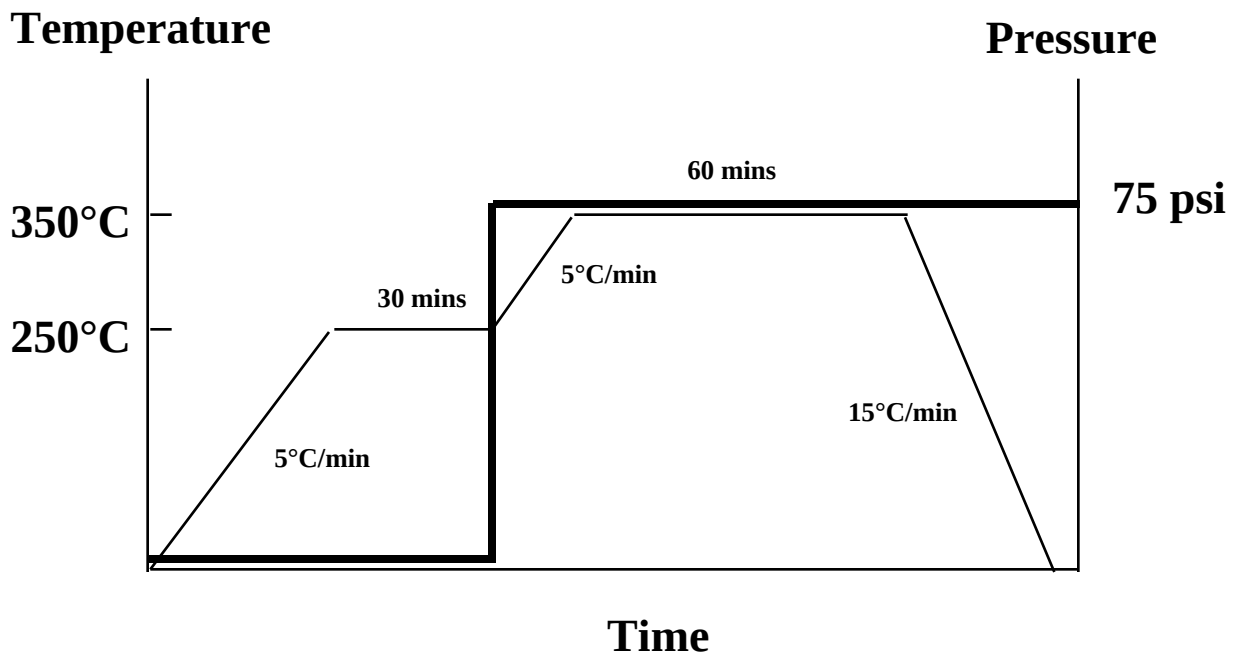

Figure 3.2. Cure cycle for the FM-5 adhesive material.

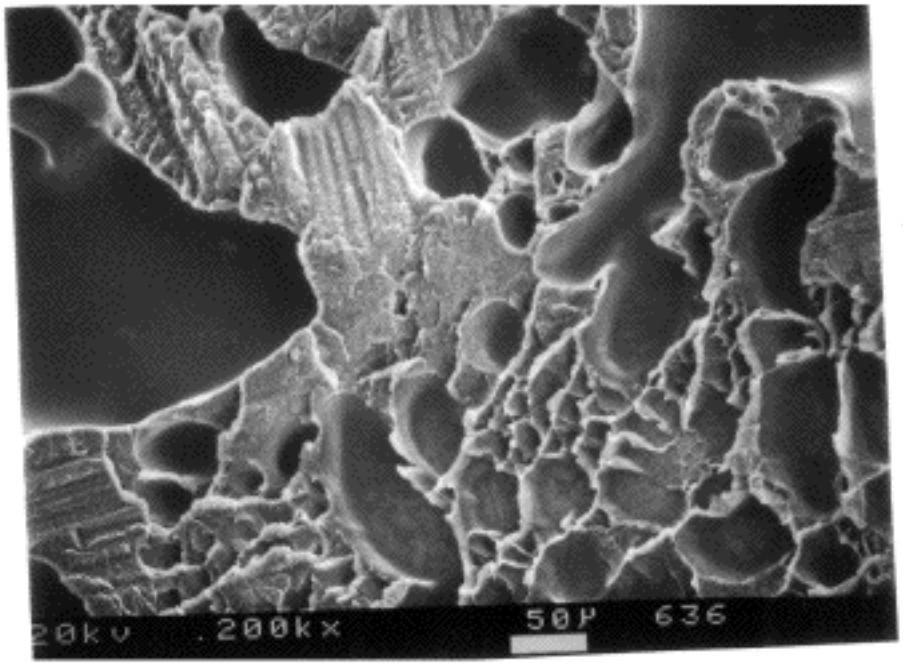

Figure 3.3. Micrograph of a Ti-6Al-4V/FM-5 fracture surface showing extensive voiding. This specimen was bonded using the original cure cycle.

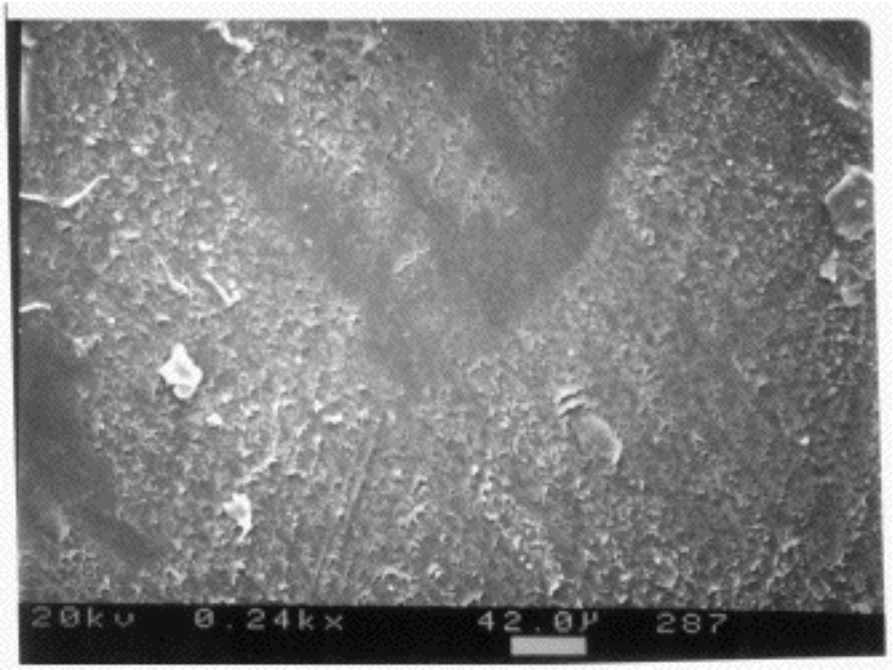

Figure 3.4. Micrograph of a Ti-6Al-4V/FM-5 fracture surface showing no voids and solvent pockets. This specimen was bonded using the modified B-staged cure cycle.

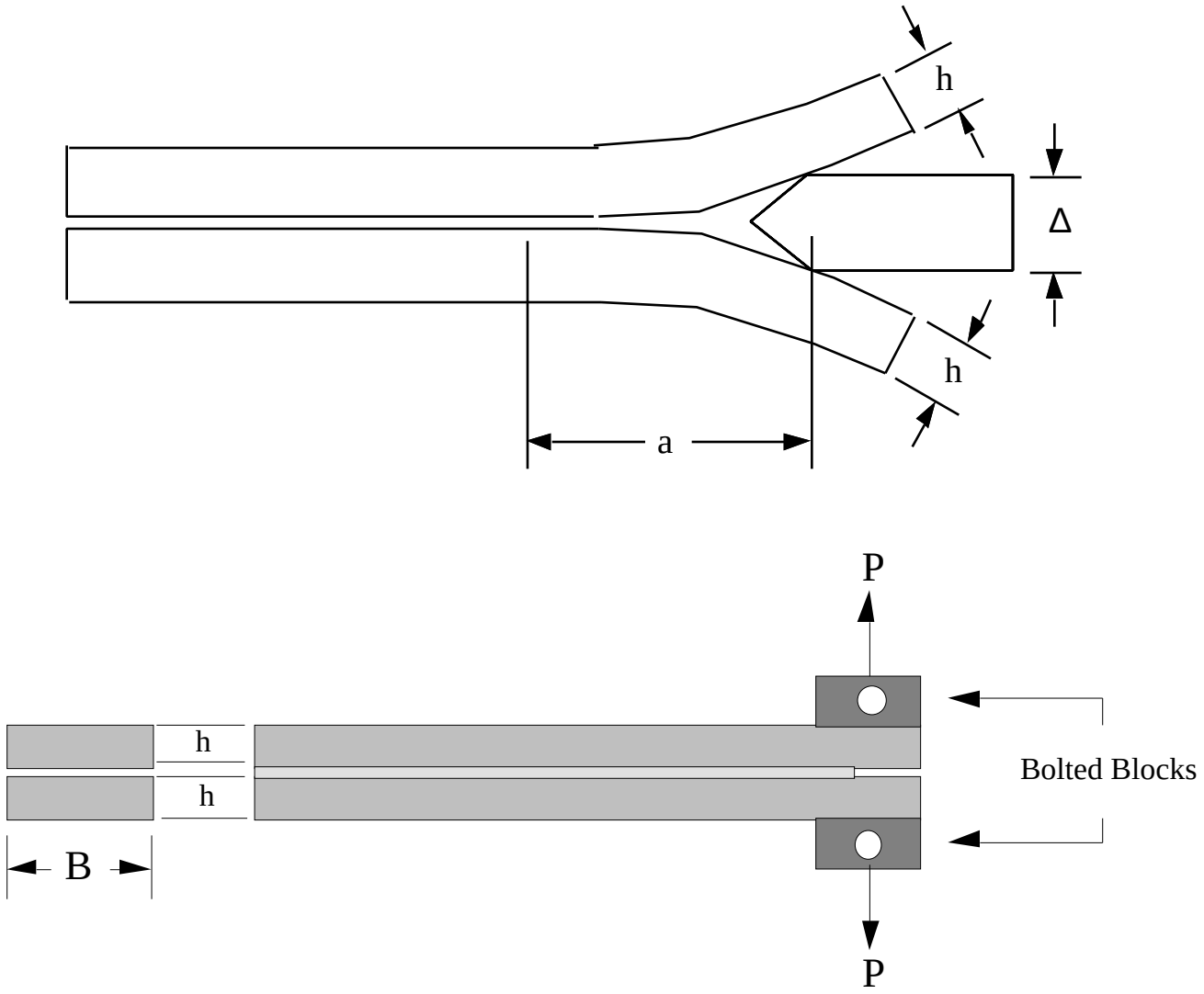

Figure 3.5. Typical schematics of wedge and DCB specimens.

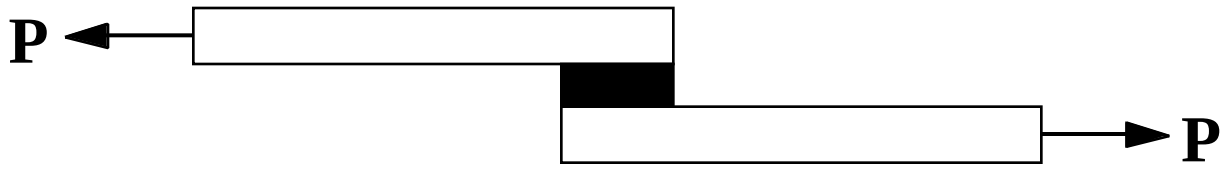

Figure 3.6. Schematic of a lap shear specimen. (Not to scale)

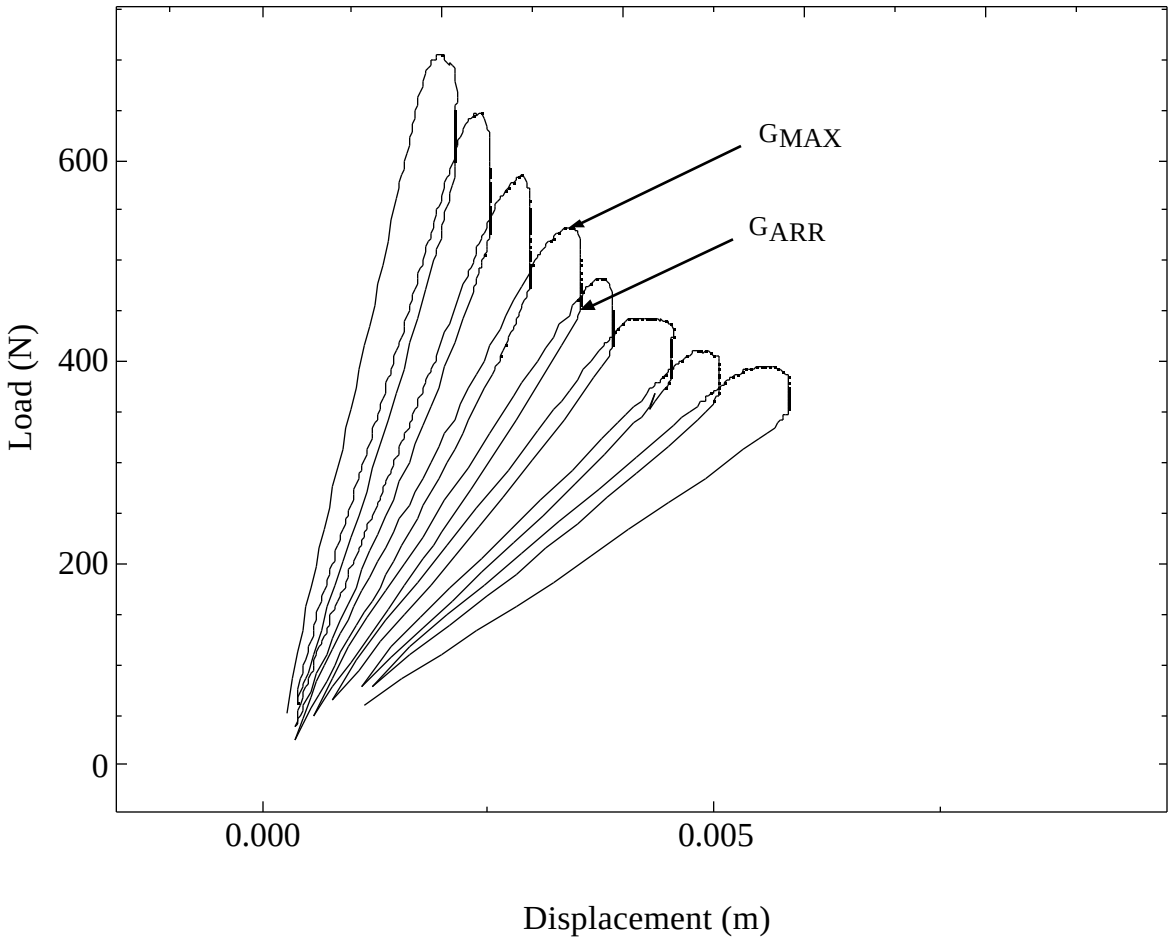

Figure 3.7. Typical load versus displacement plot from a static DCB test conducted on a Ti-6Al-4V/FM-5 bond.

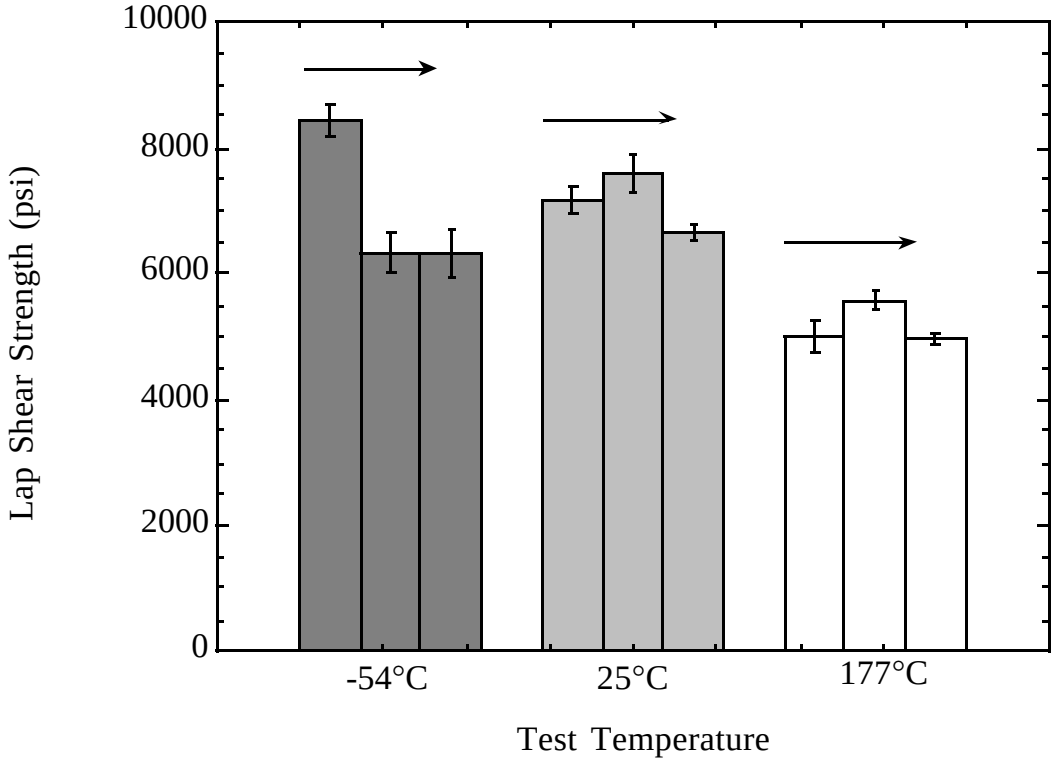

Figure 3.8. Lap shear test data obtained as a function of test temperature for specimens pulled at 1.27, 12.7, and 127 mm/min. Arrows are pointing in the direction of increasing testing rate.

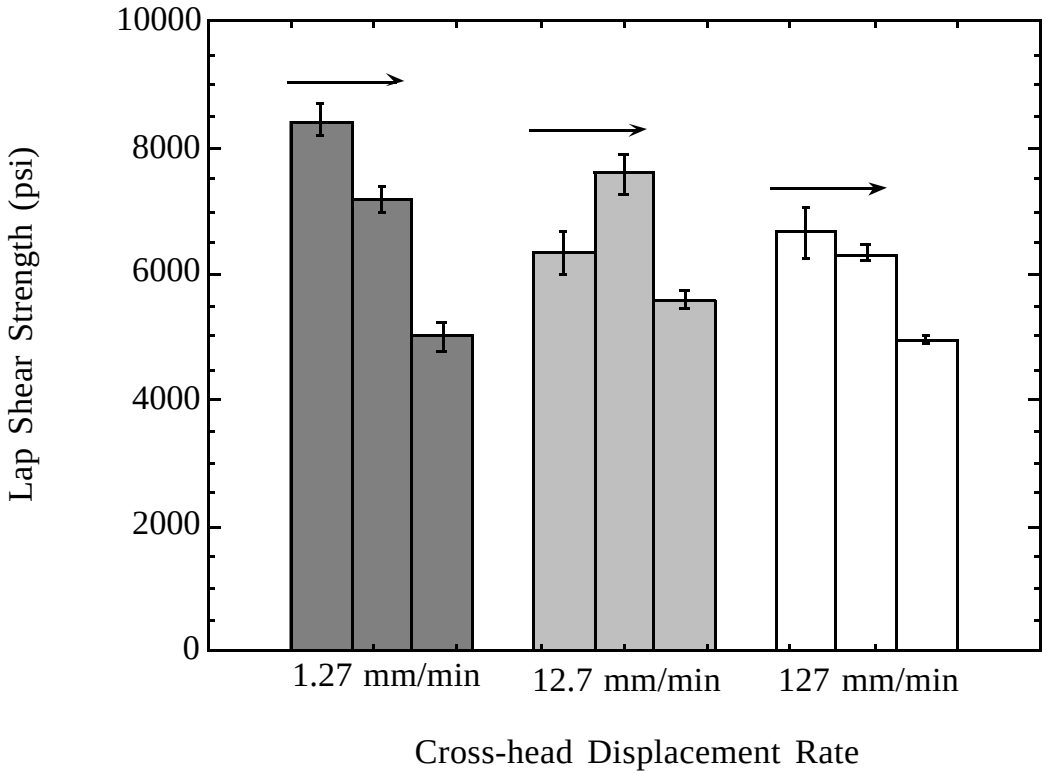

Figure 3.9. Lap shear test data as a function of testing rate for the temperatures of -54°C, 25°C, and 177°C. Arrows are pointing in the direction of increasing temperature.

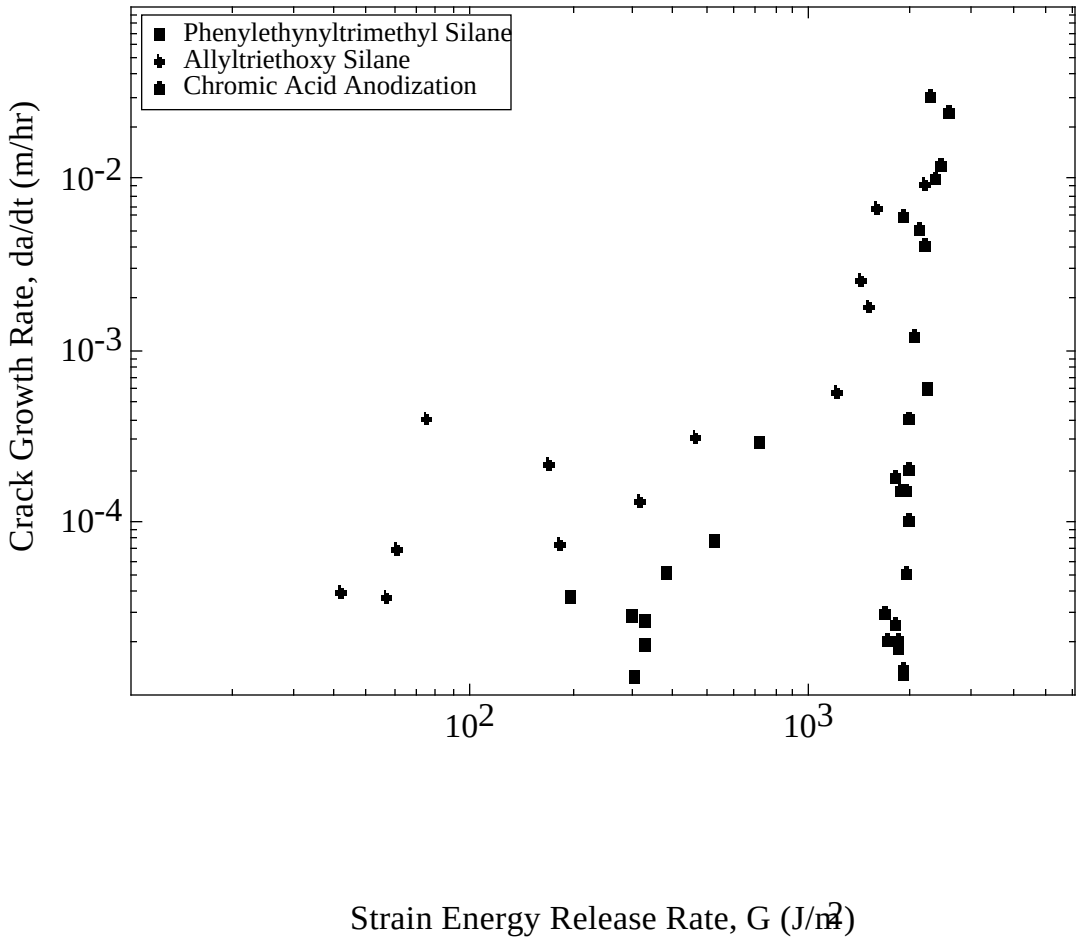

Figure 3.10. Comparison of wedge crack growth rates of Ti-6Al-4V/FM-5 bonds for CAA, phenyl silane and allyl silane surface pretreatments.

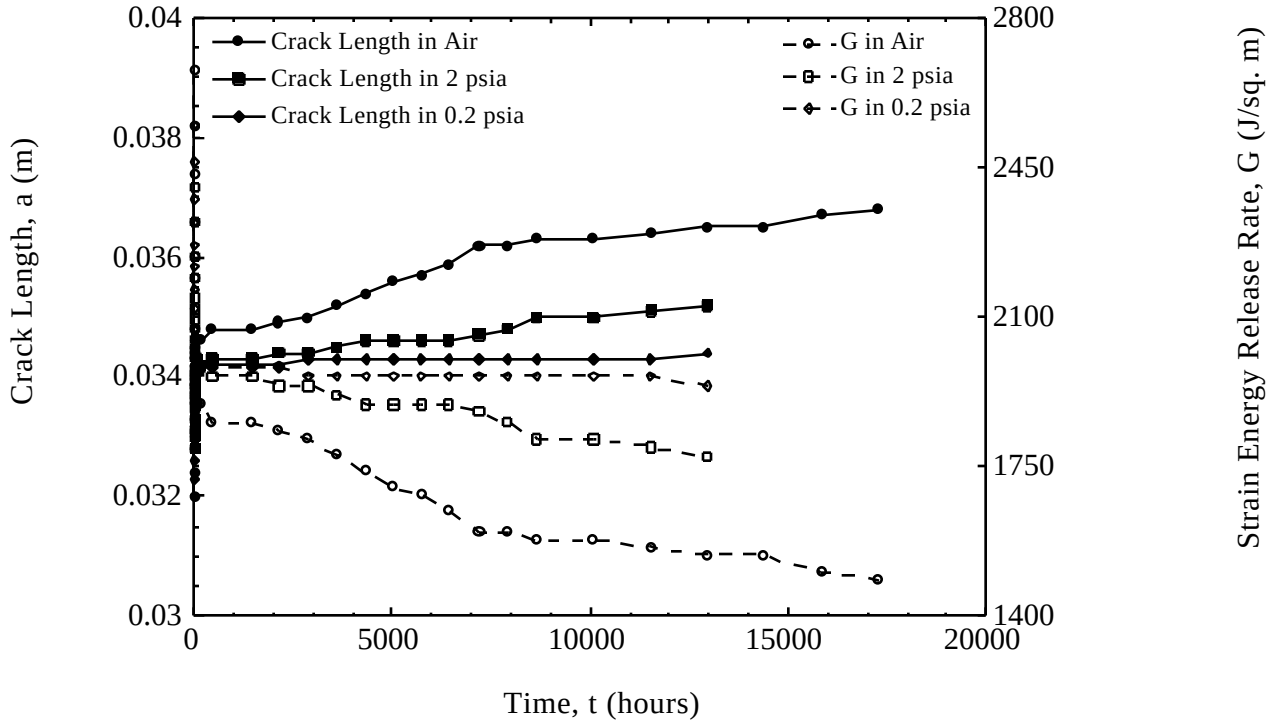

Figure 3.11. Long term wedge test data collected on CAA Ti-6Al-4V/FM-5 bonds aged in different air pressures at 204°C. Data are average of 5 specimens per aging condition.

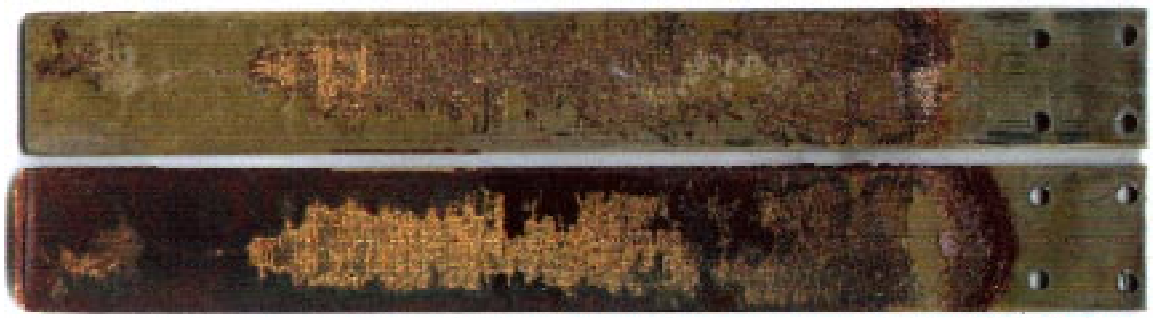

Figure 3.12. Fracture surface of a wedge specimen aged for 14,400 hours in air at 204°C.

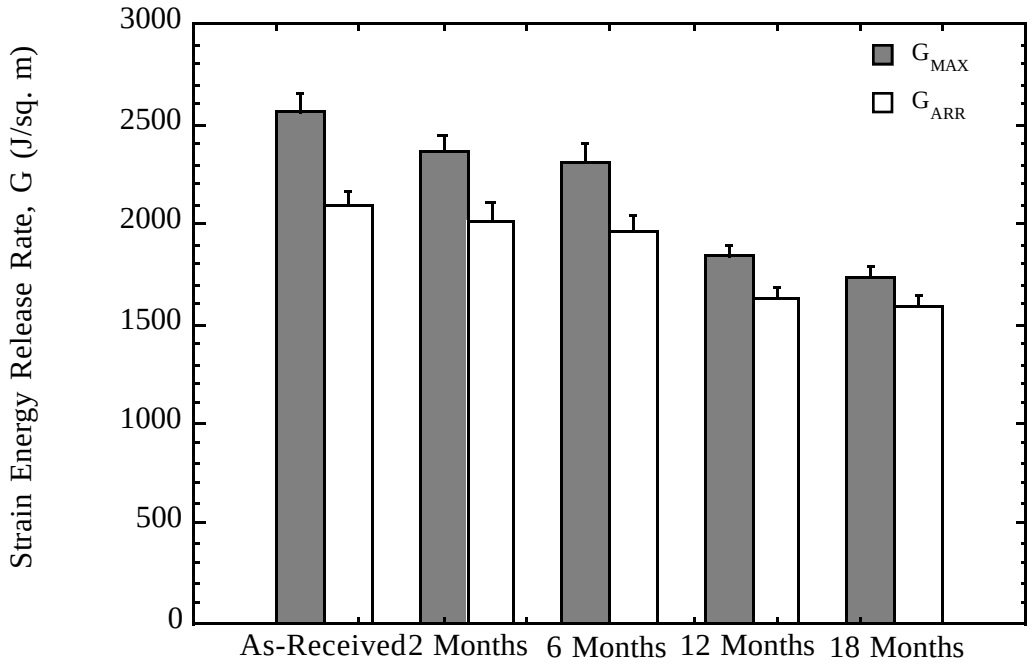

Figure 3.13. Static DCB test data showing strain energy release rate as a function of aging time for Ti-6Al-4V/FM-5 bonds aged at 204°C in ambient atmospheric air.

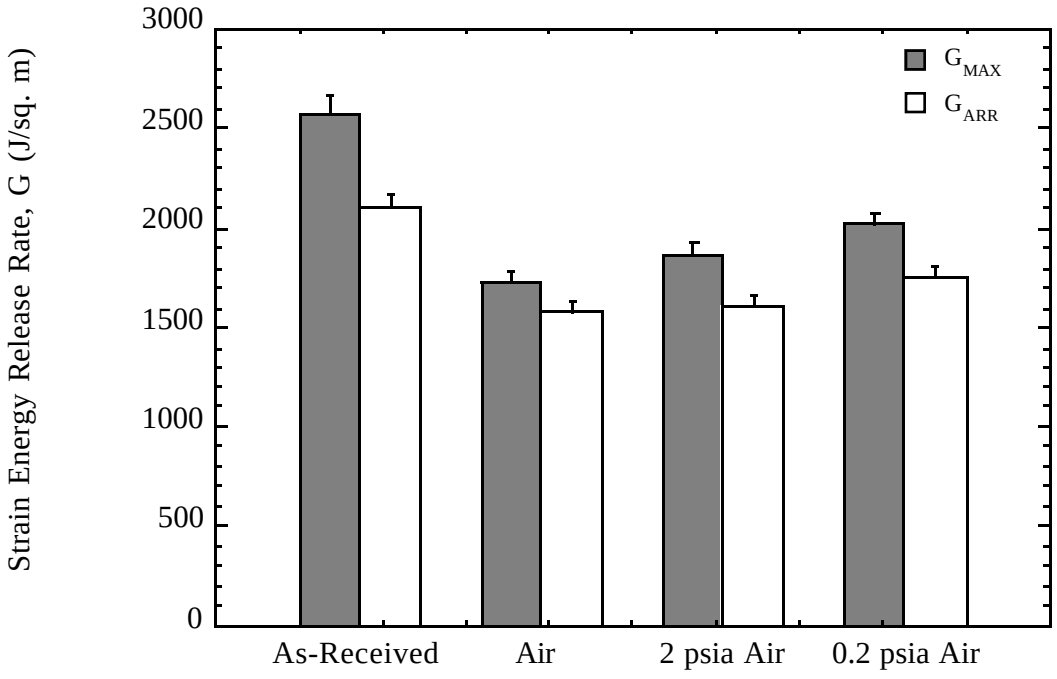

Figure 3.14. Static DCB test data showing strain energy release rate as a function of aging environment for Ti-6Al-4V/FM-5 bonds aged at 204°C.

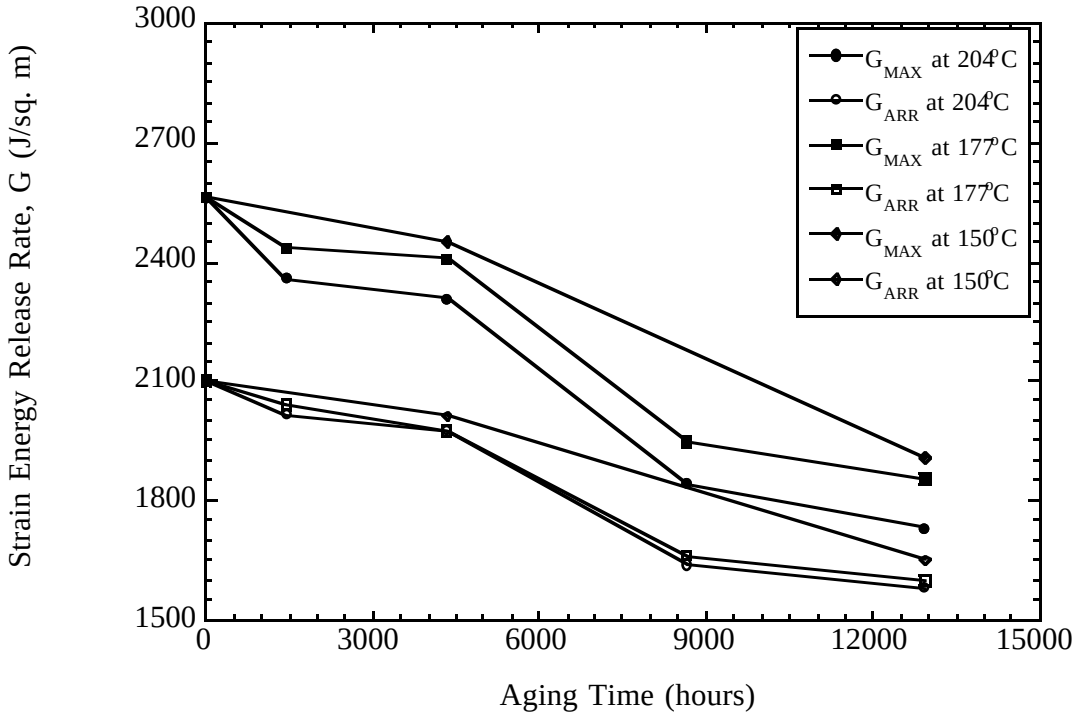

Figure 3.15. Maximum and arrest strain energy release rates as a function of aging time and temperature for Ti-6Al-4V/FM-5 bonds.

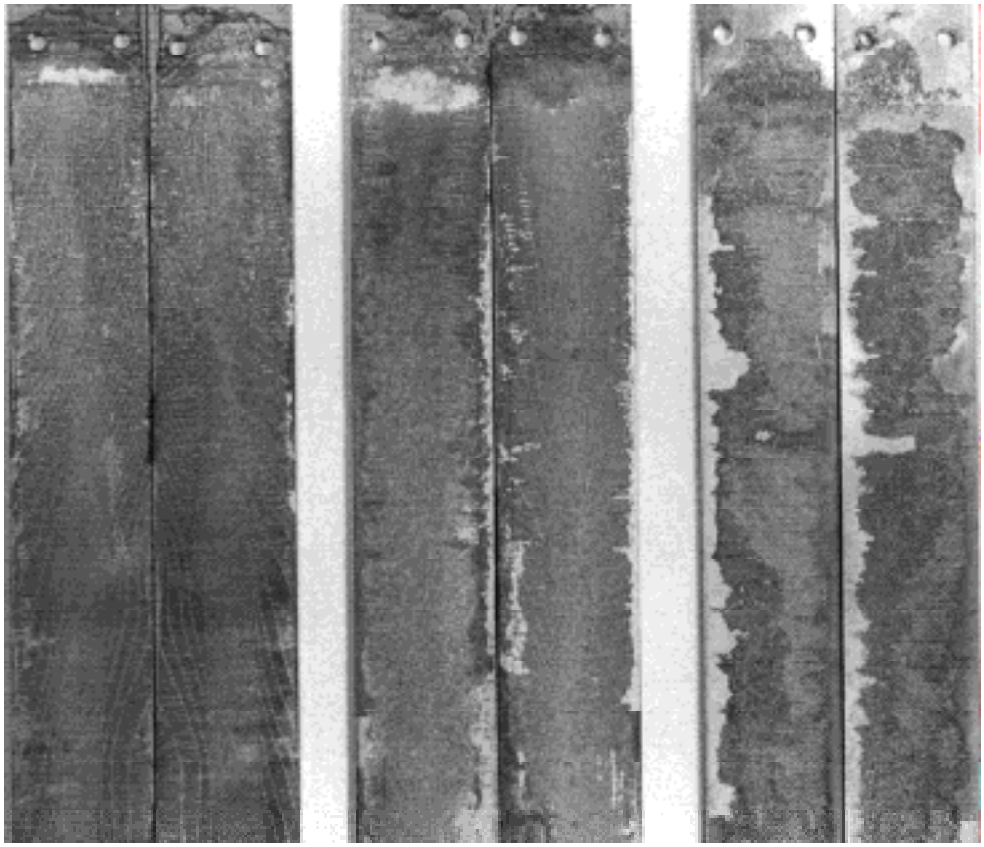

As-Received 177°C 204°C

Figure 3.16. Photograph showing the fracture surfaces of Ti-6Al-4V/FM-5 bonds, both as-received, and following aging at 177°C and 204°C for 12 months.

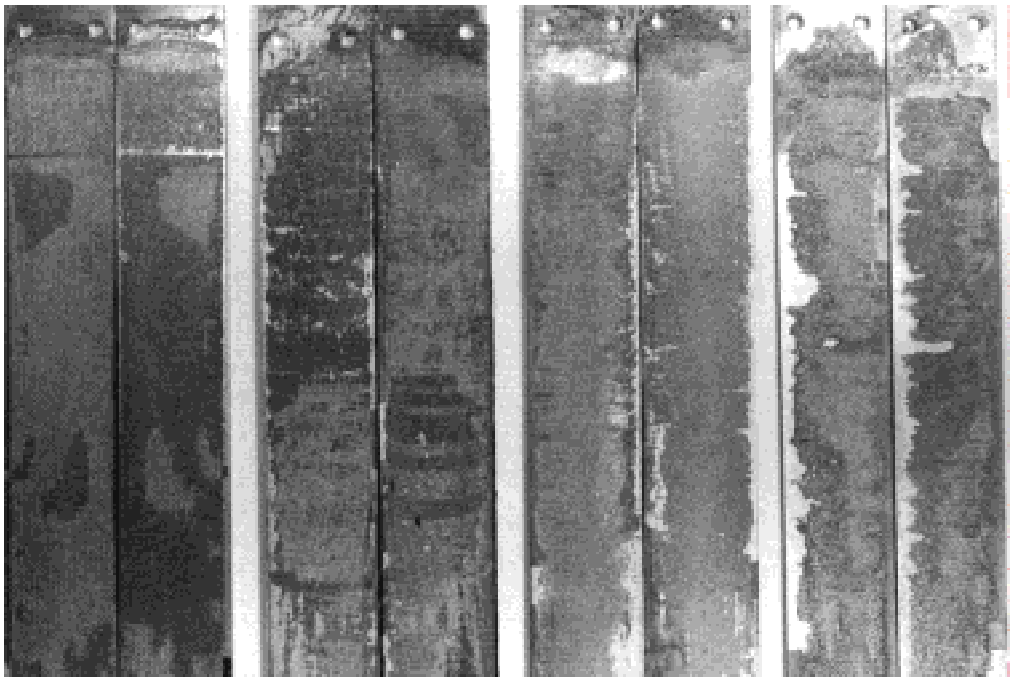

Figure 3.17. Photograph showing the fracture surfaces of Ti-6Al-4V/FM-5 bonds following aging up to 12 months at 204°C.

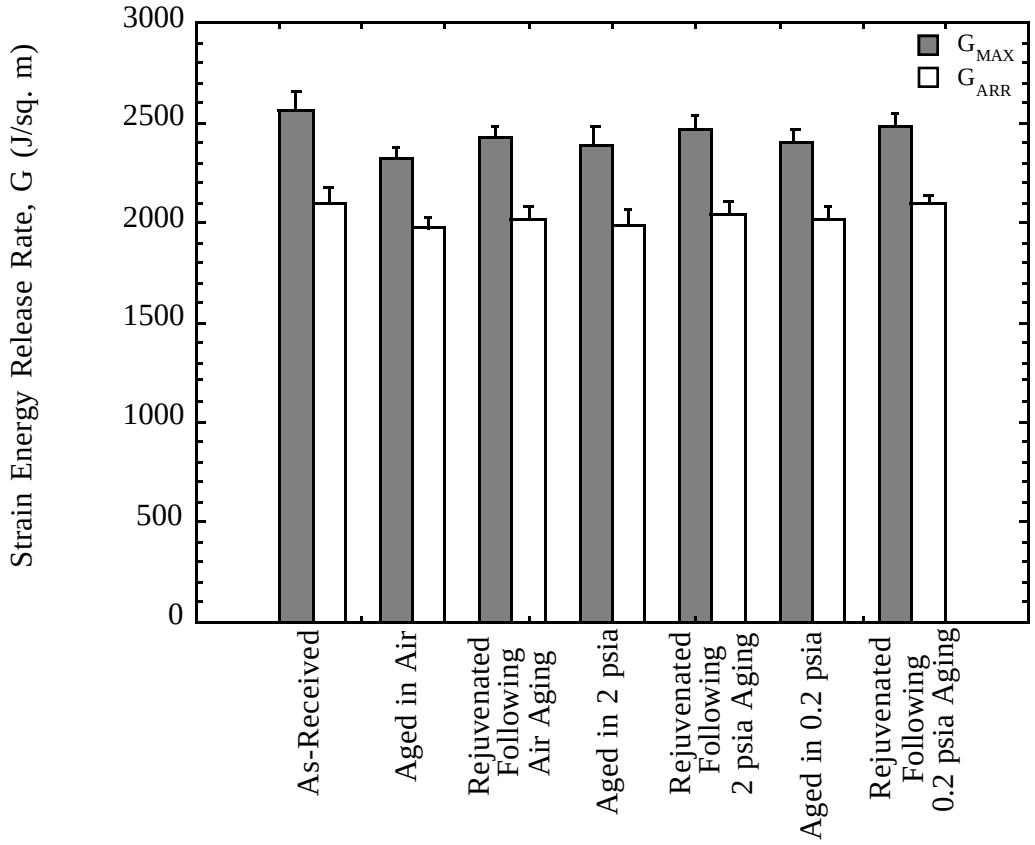

Figure 3.18. Static DCB test data on Ti-6Al-4V/FM-5 bonds to study the effects of bond toughness degradation and subsequent rejuvenation as a function of environmental aging. Samples were aged for 6 months at 204°C.

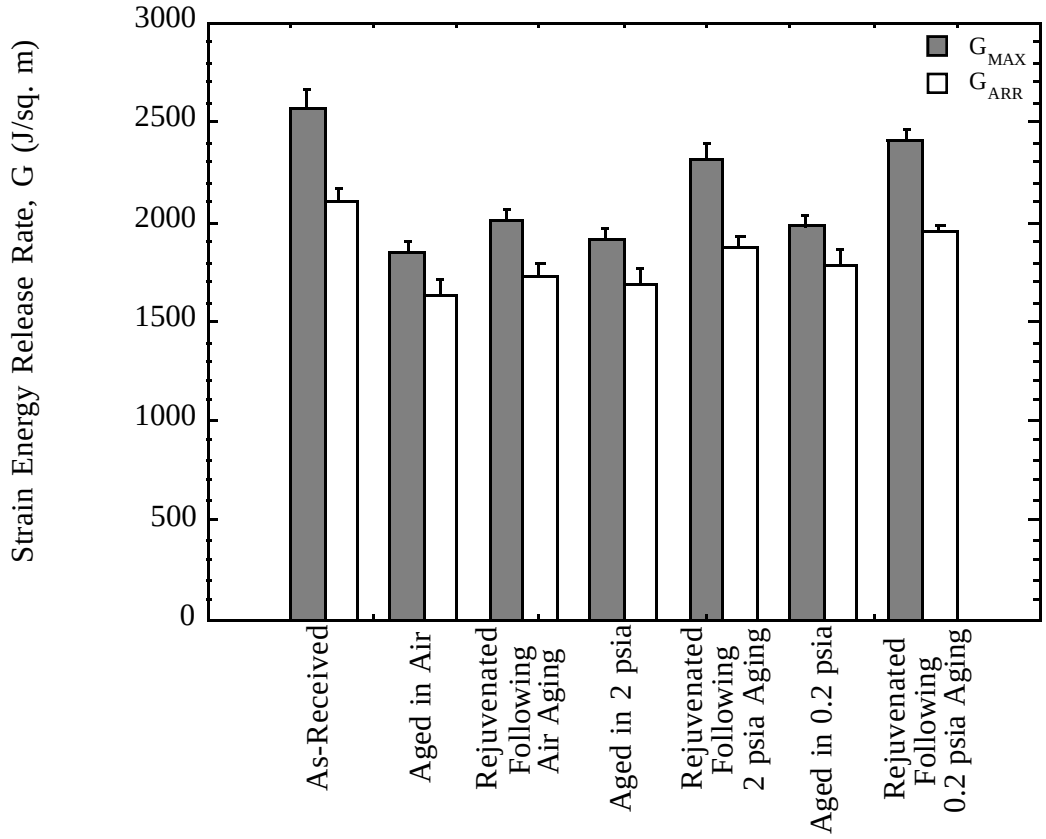

Figure 3.19. Static DCB test data on Ti-6Al-4V/FM-5 bonds to study the effects of bond toughness degradation and subsequent rejuvenation as a function of environmental aging. Samples were aged for 12 months at 204°C.

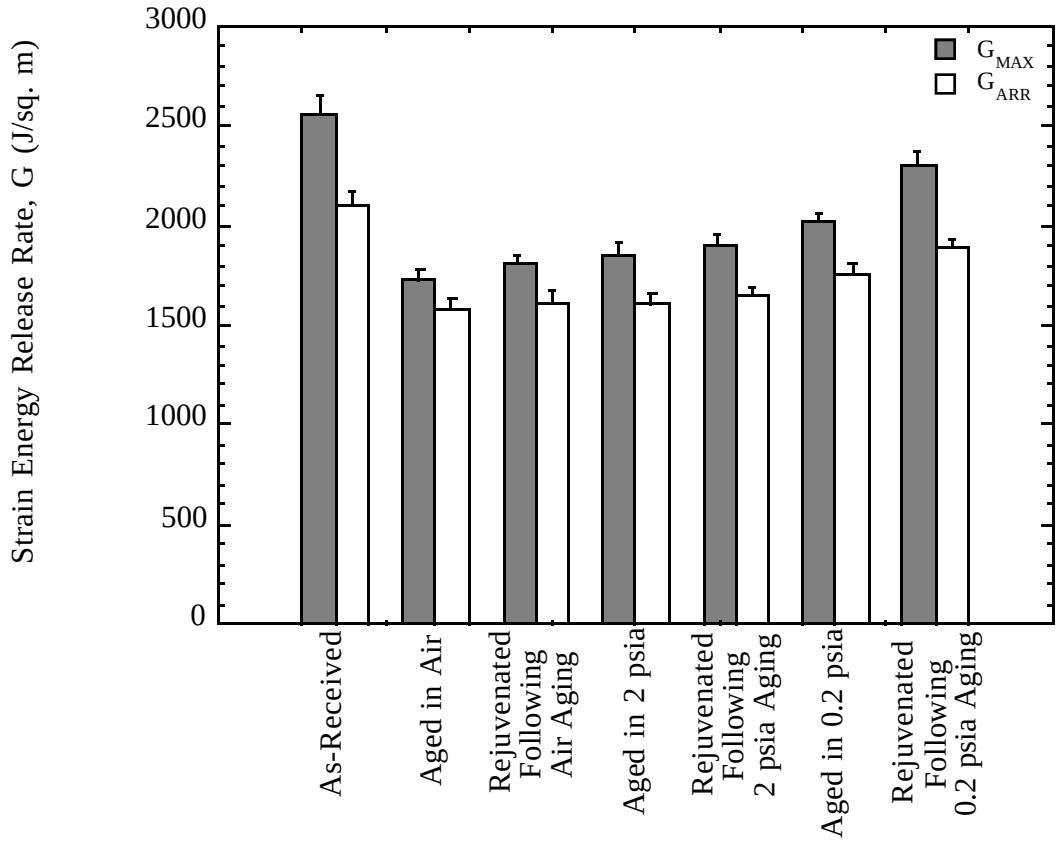

Figure 3.20. Static DCB test data on Ti-6Al-4V/FM-5 bonds to study the effects of bond toughness degradation and subsequent rejuvenation as a function of environmental aging. Samples were aged for 18 months at 204°C.

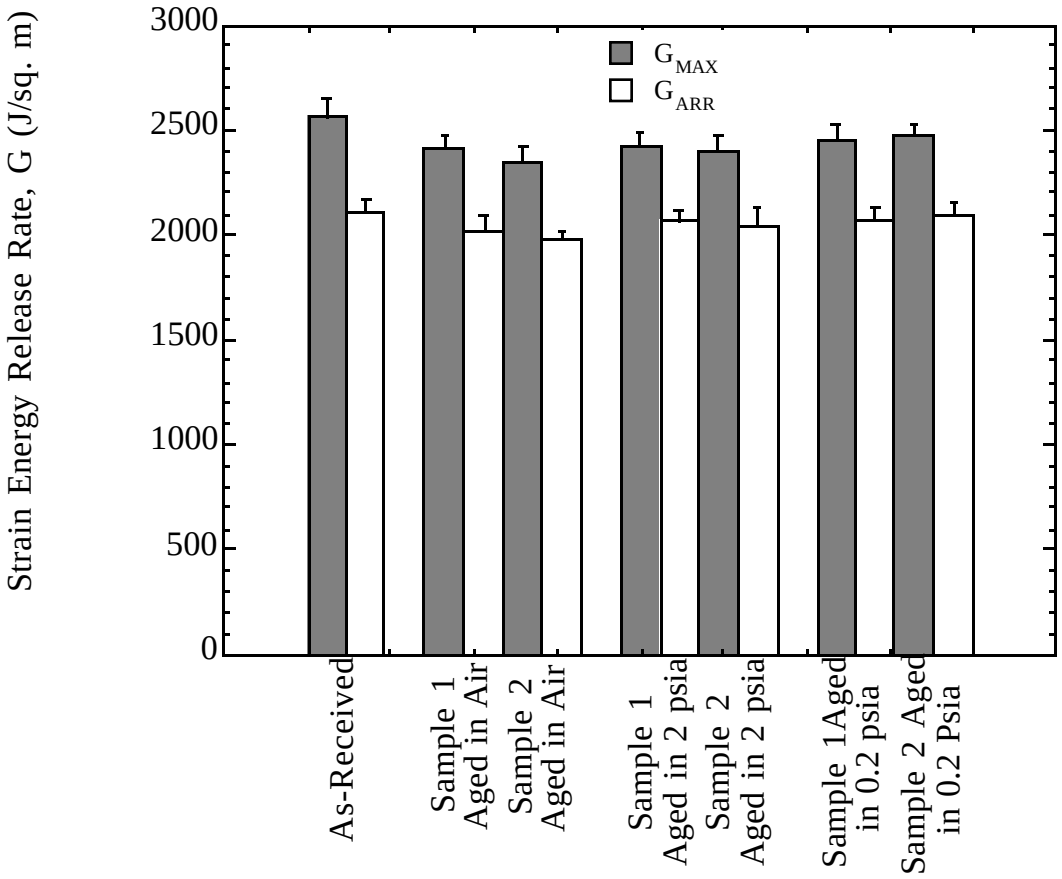

Figure 3.21. Replication of static DCB test data on CAA Titanium/FM-5 bonds aged for 6 months in different environments at 177°C. Samples #1 refers to the original test data and samples #2 refer to replicated data.

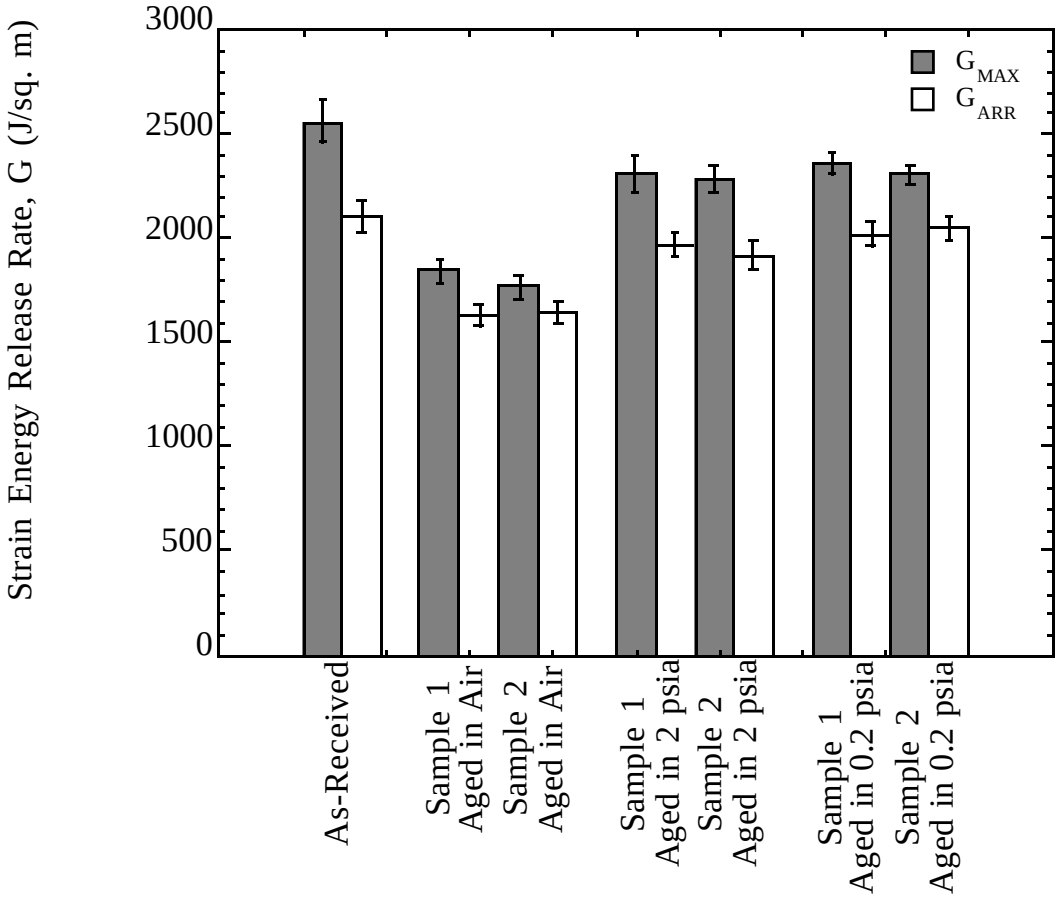

Figure 3.22. Replication of static DCB test data on CAA Titanium/FM-5 bonds aged for 12 months in different environments at 177°C. Samples #1 refers to the original test data and samples #2 refer to replicated data.

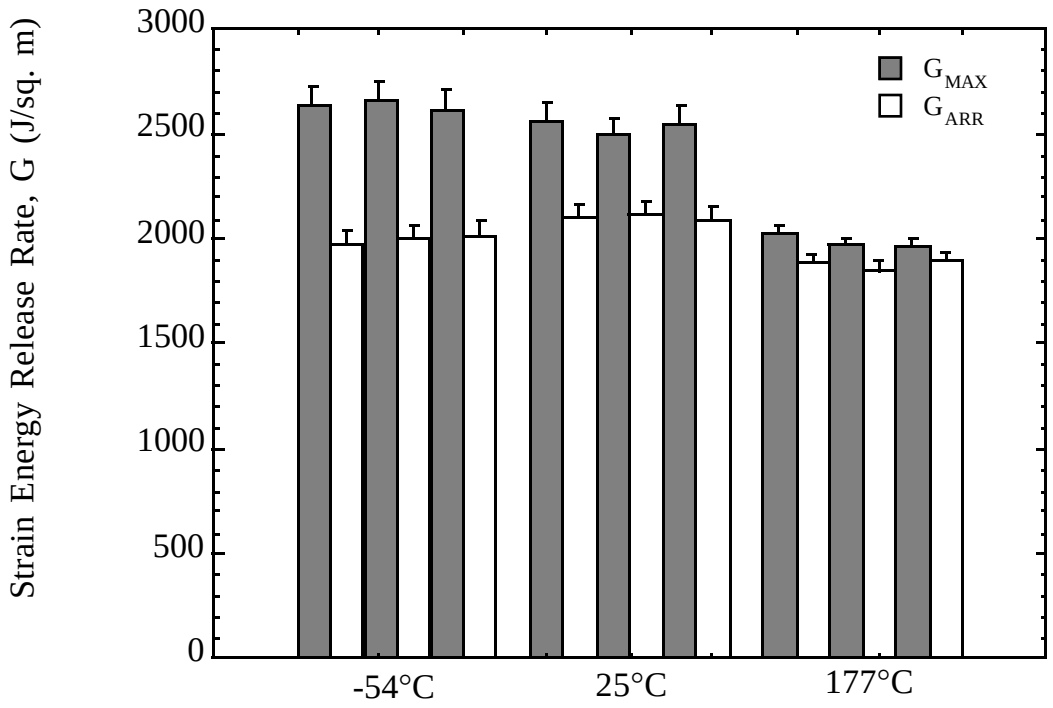

Figure 3.23. Fracture toughness as a function of test temperature for CAA Titanium/FM-5 bonds. Three specimens were tested at each condition.

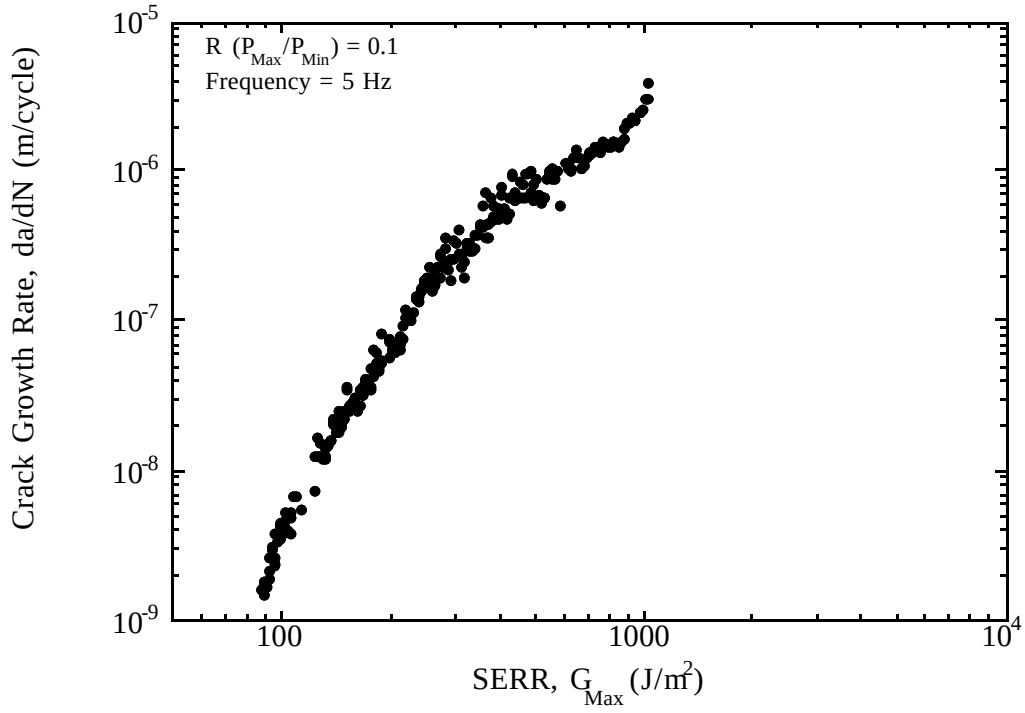

Figure 3.24. Fatigue DCB data on a phenyl silane treated Ti-6Al-4V/FM-5 as-bonded specimen.

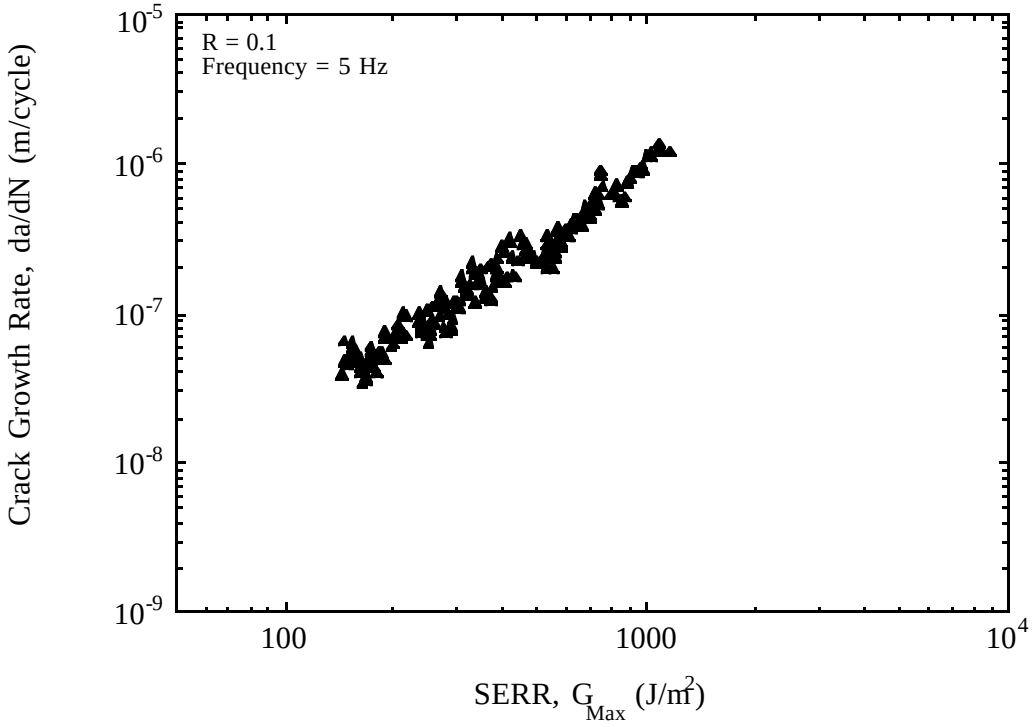

Figure 3.25. Fatigue DCB data on an aged phenyl silane treated Ti-6Al-4V/FM-5 specimen. Sample was aged for 1 month in air at 204°C.

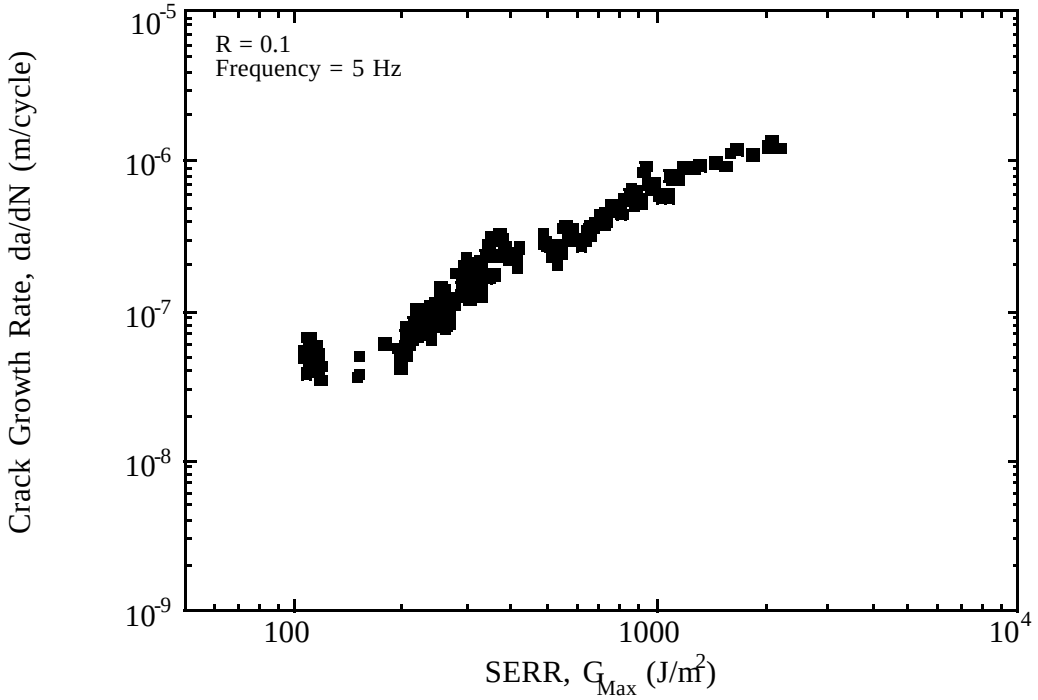

Figure 3.26. Fatigue DCB data on an aged phenyl silane treated Ti-6Al-4V/FM-5 specimen. Sample was aged for 4 months in air at 204°C.

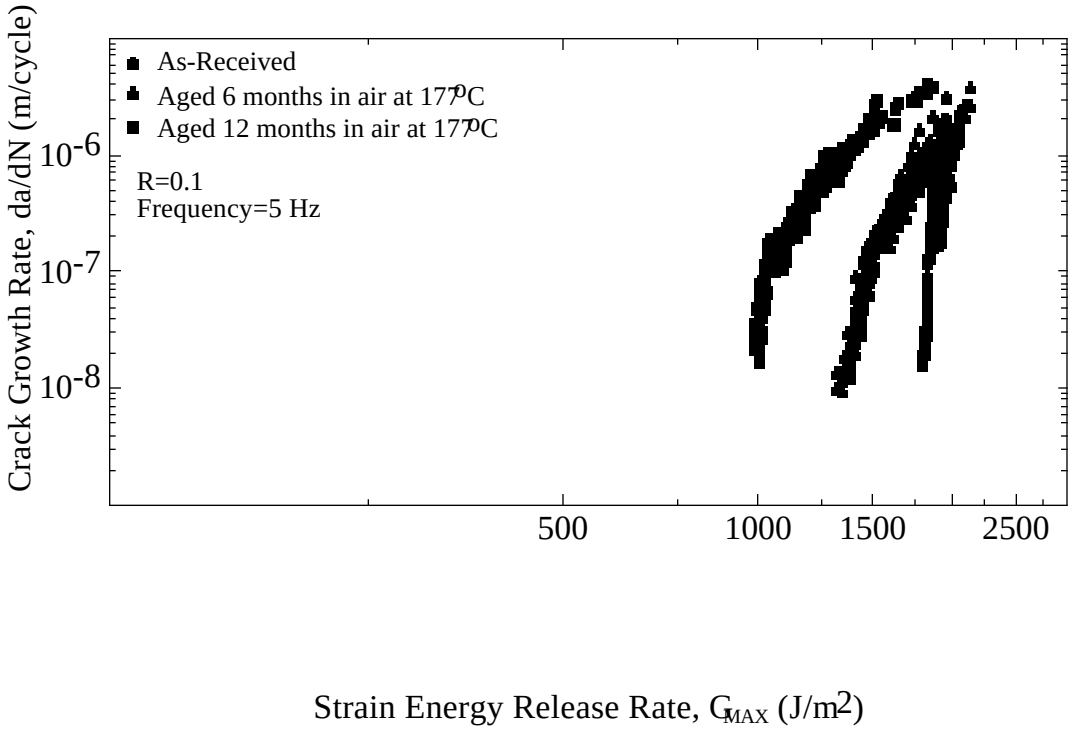

Figure 3.27. Fatigue test results on CAA Ti-6Al-4V/FM-5 bonded specimens. Samples were aged for up to 12 months in air at 204°C.

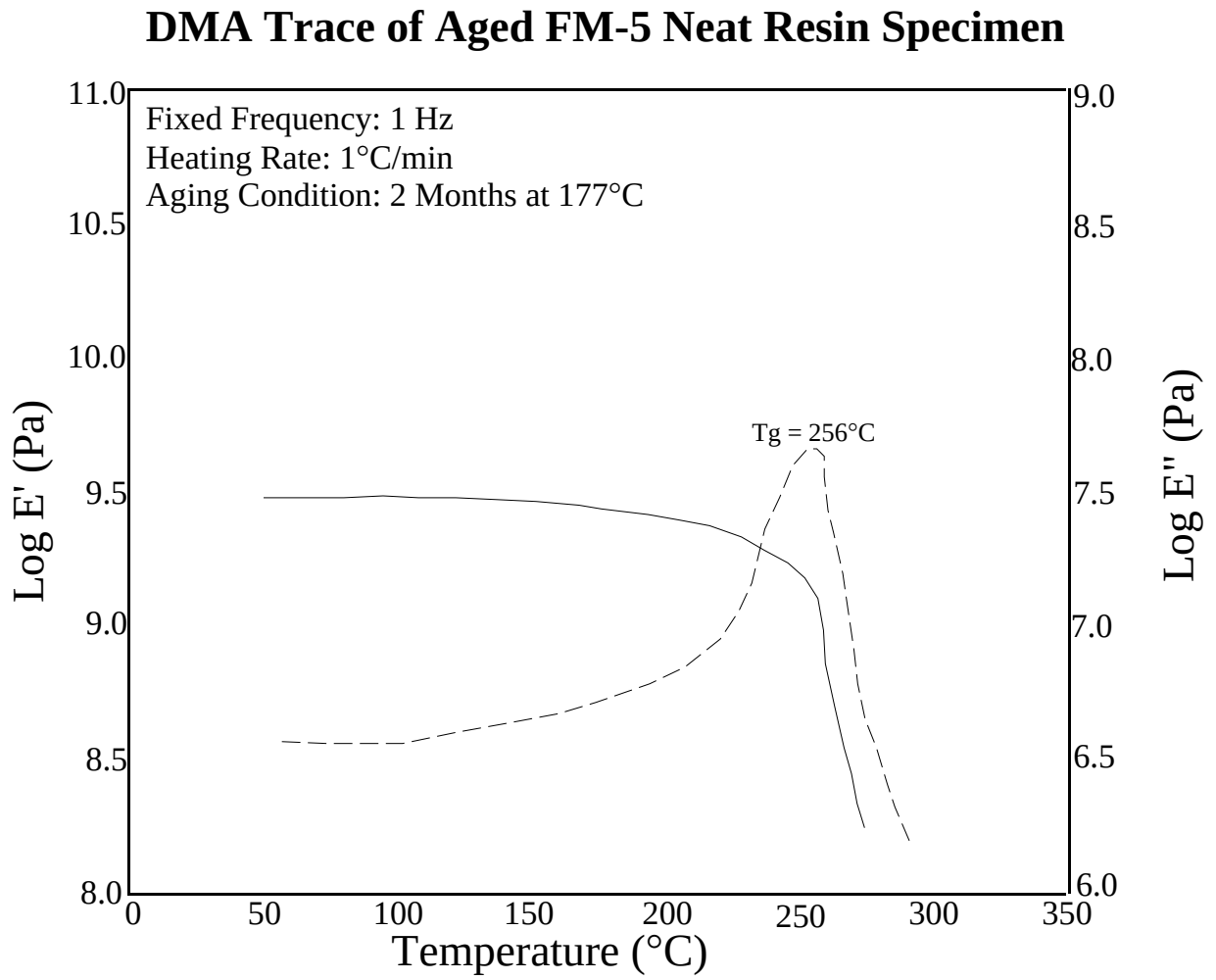

Figure 3.28. DMA characteristics of a FM-5 neat resin specimen aged for 2 months in air at 177°C.

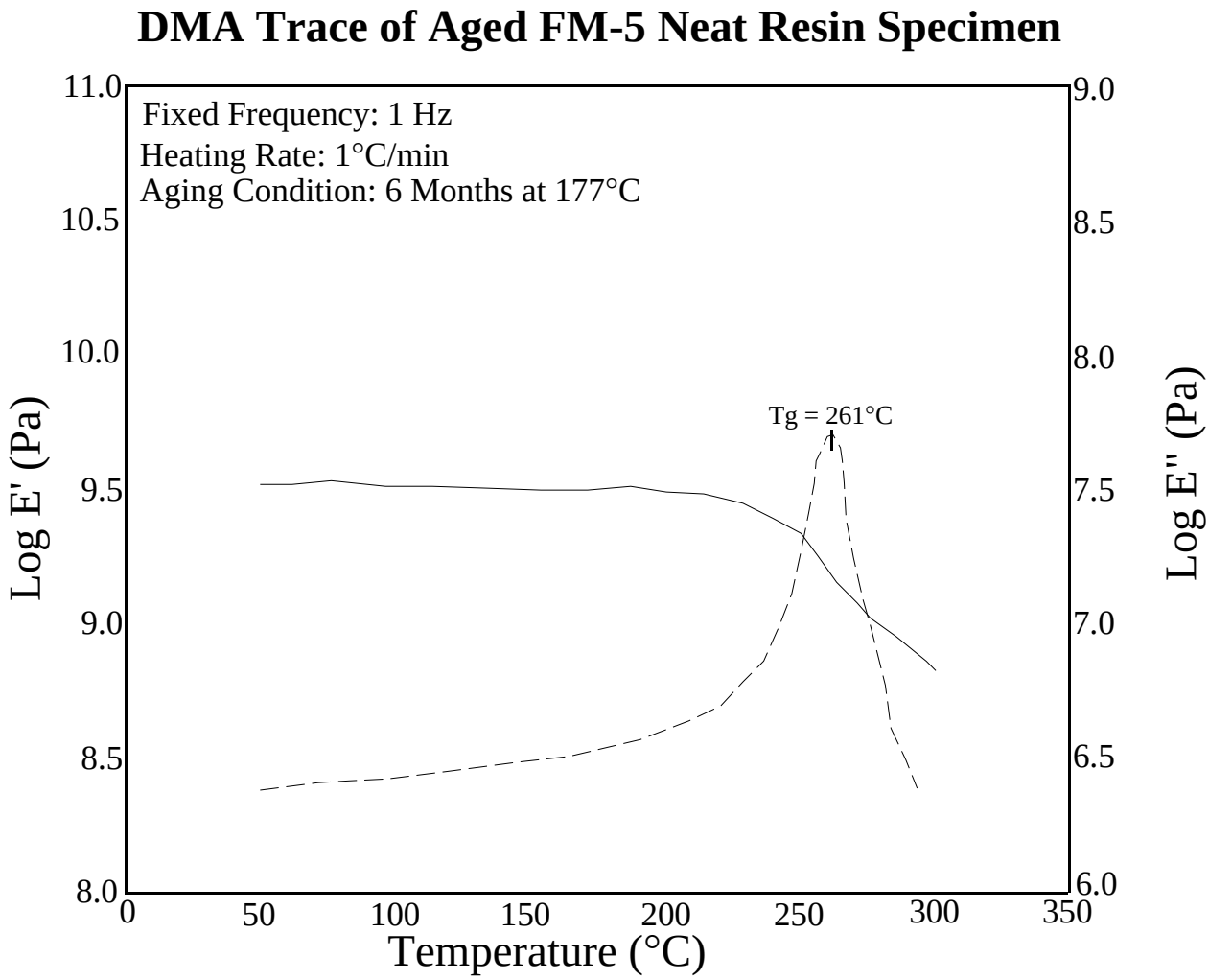

Figure 3.29. DMA characteristics of a FM-5 neat resin specimen aged for 6 months in air at 177°C.

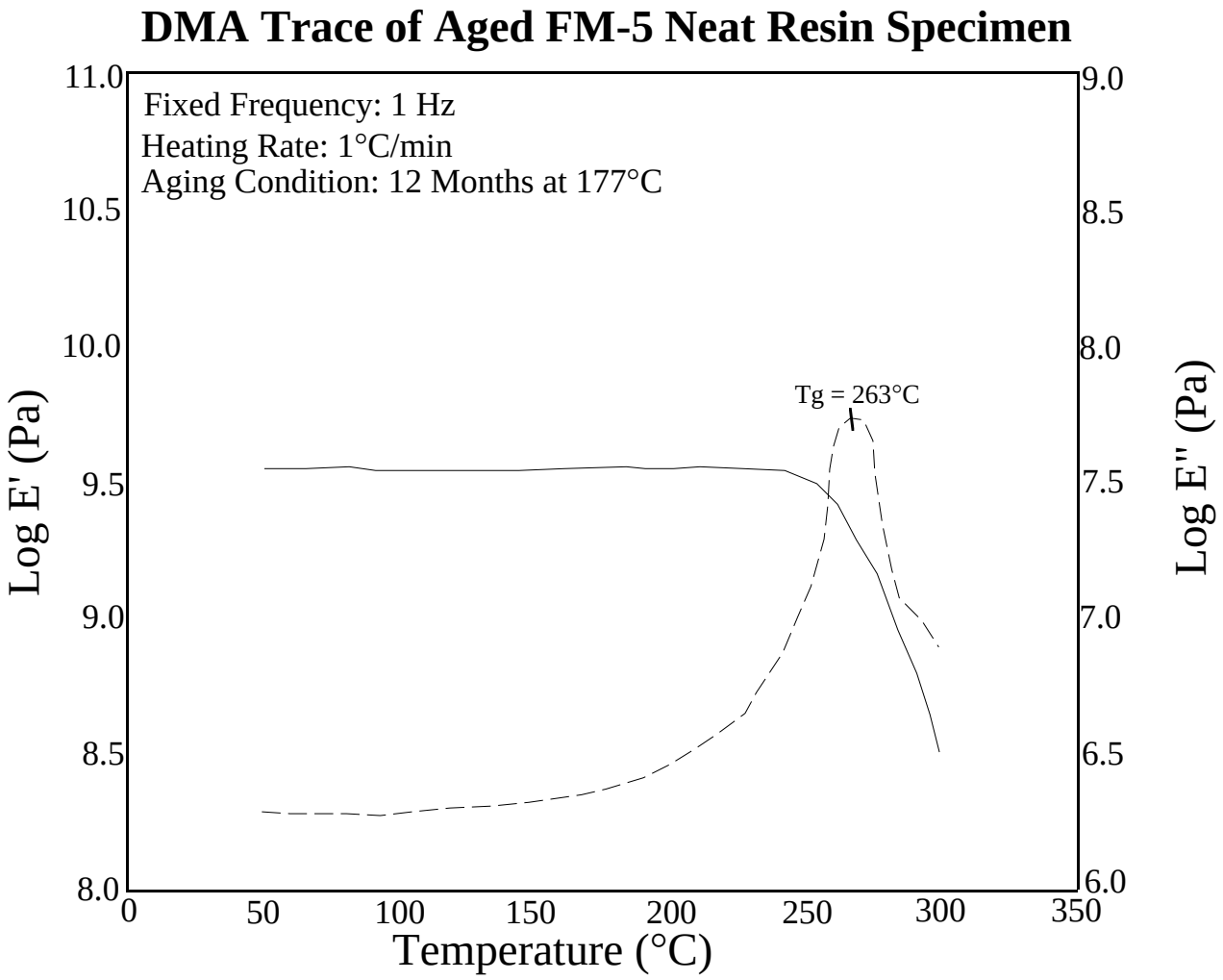

Figure 3.30. DMA characteristics of a FM-5 neat resin specimen aged for 12 months in air at 177°C.

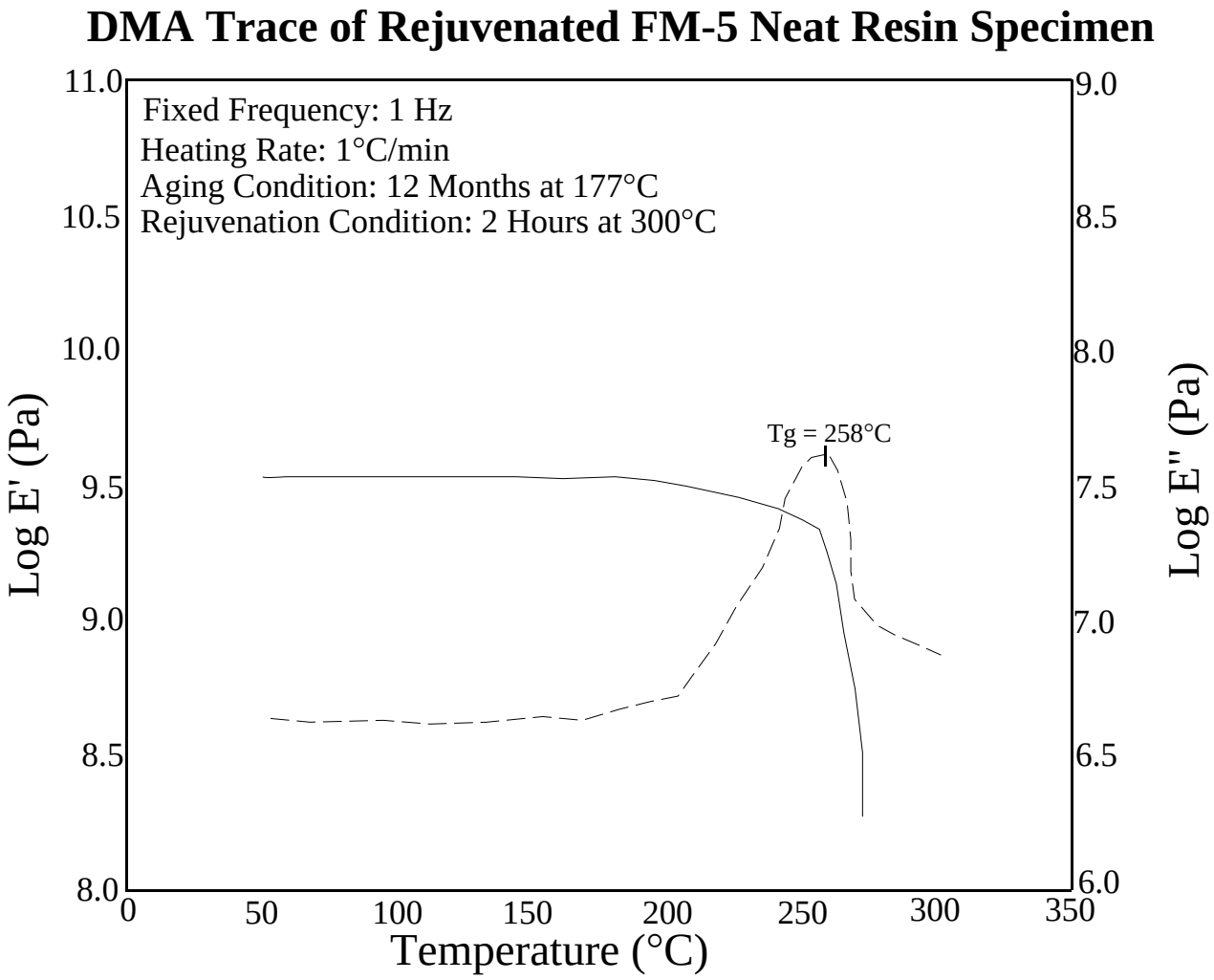

Figure 3.31. DMA characteristics of an aged and rejuvenated FM-5 neat resin specimen. Sample was aged for 12 months in air at 177°C. Rejuvenation condition was 300°C for 2 hours.

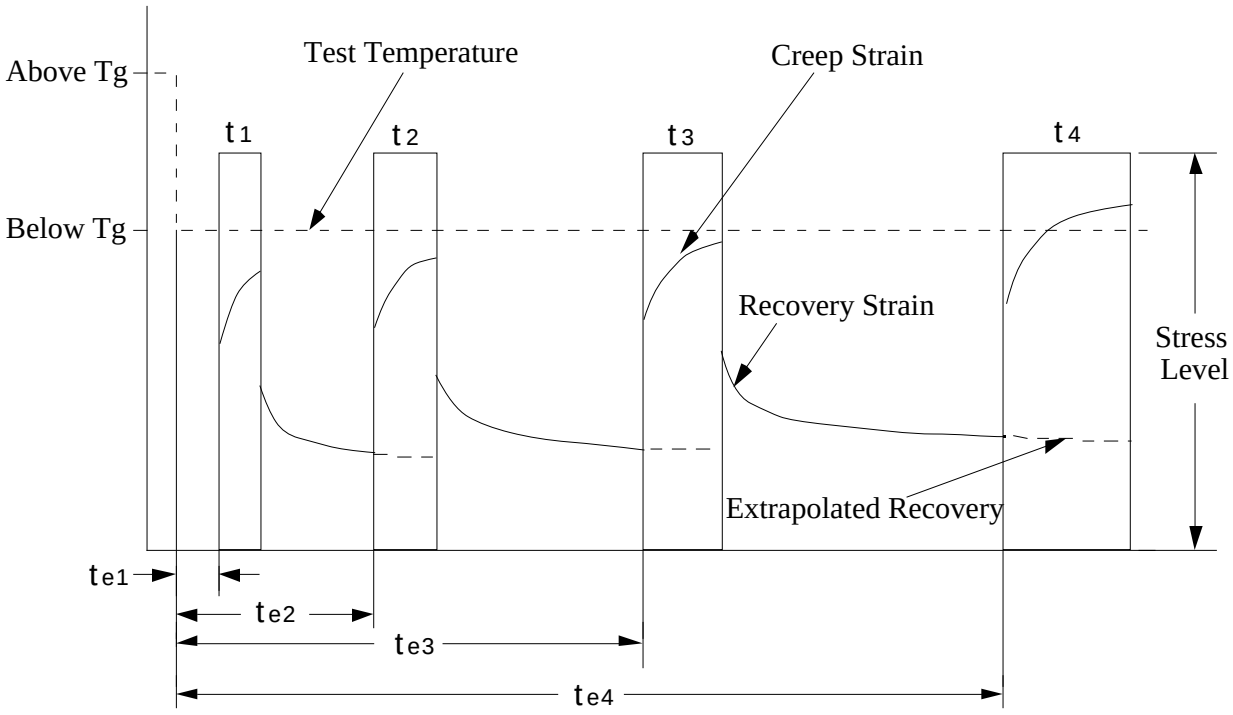

Figure 3.32. Schematic of a sequenced creep test conducted to measure physical aging [14].

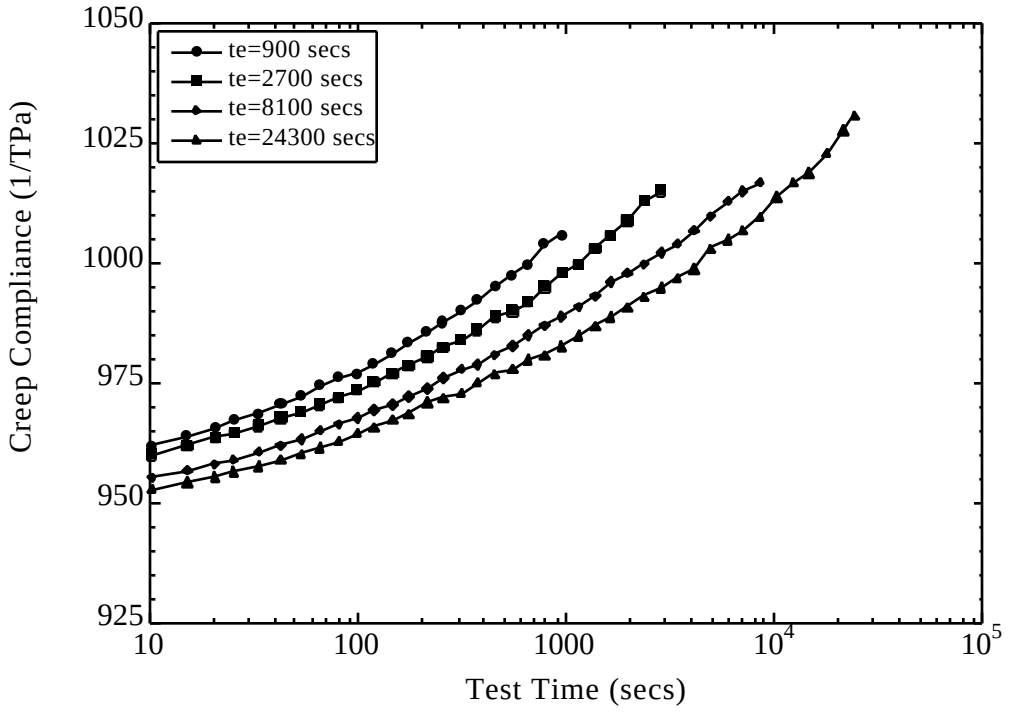

Figure 3.33. Typical creep compliance data for FM-5 neat resin specimen at 150°C.

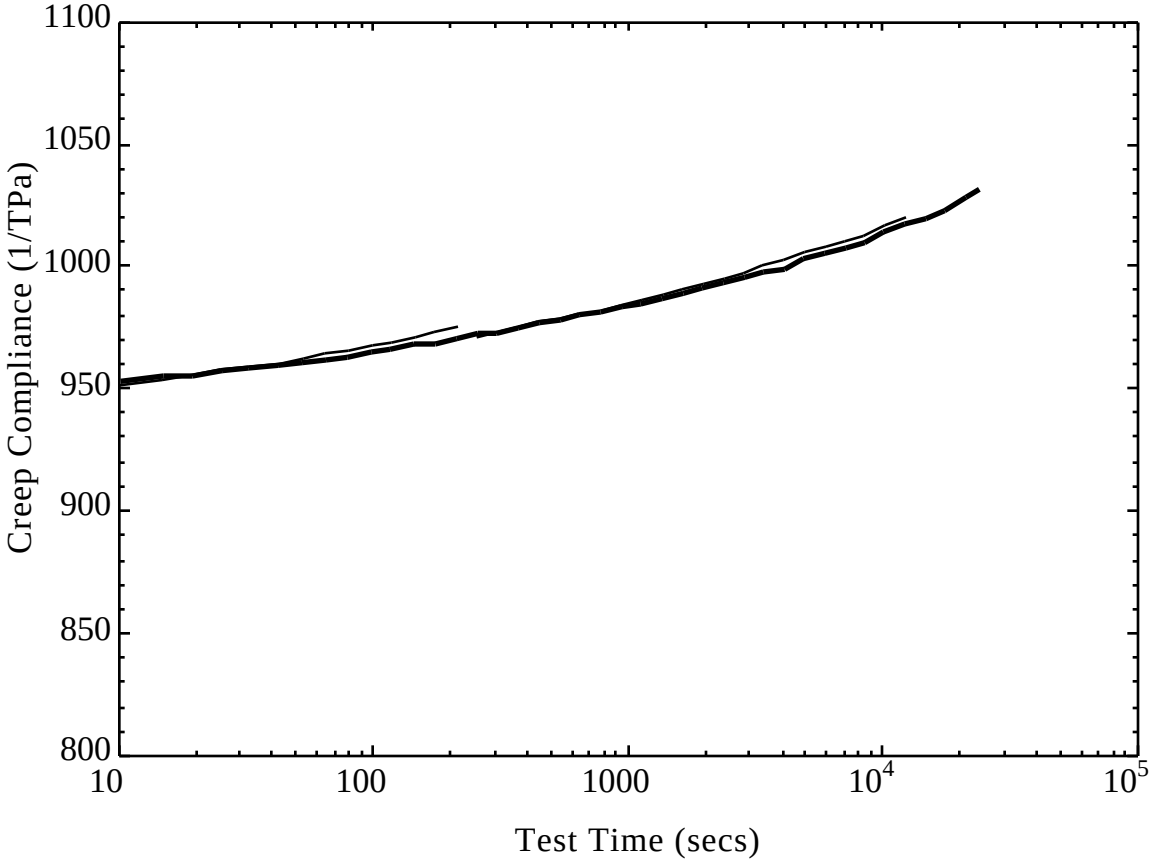

Figure 3.34. Creep compliance master curve for FM-5 resin specimen at 150°C.

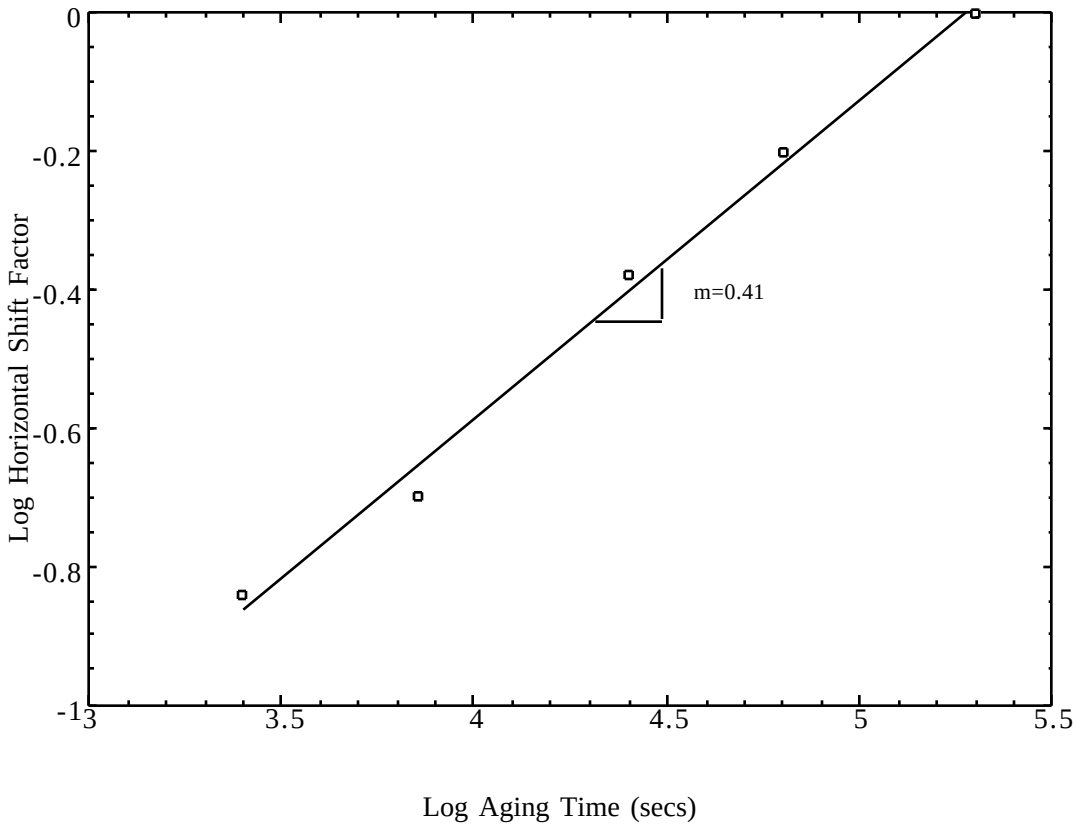

Figure 3.35. Shift rate, μ, determination for FM-5 resin specimen at 150°C.

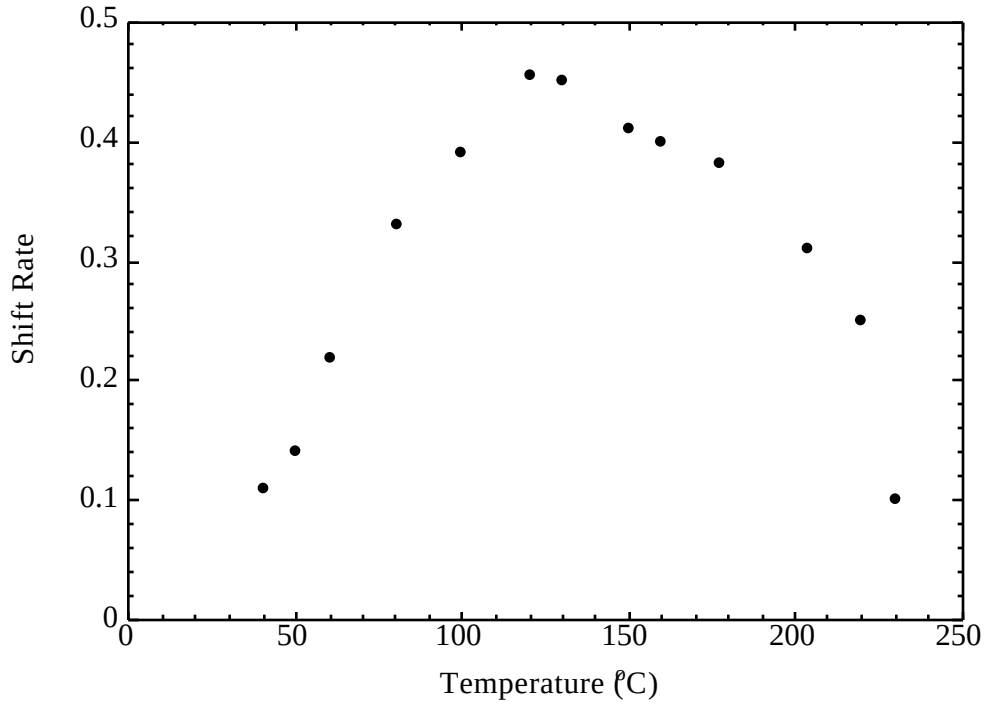

Figure 3.36. Shift rate versus temperature plot for FM-5 neat resin specimens.

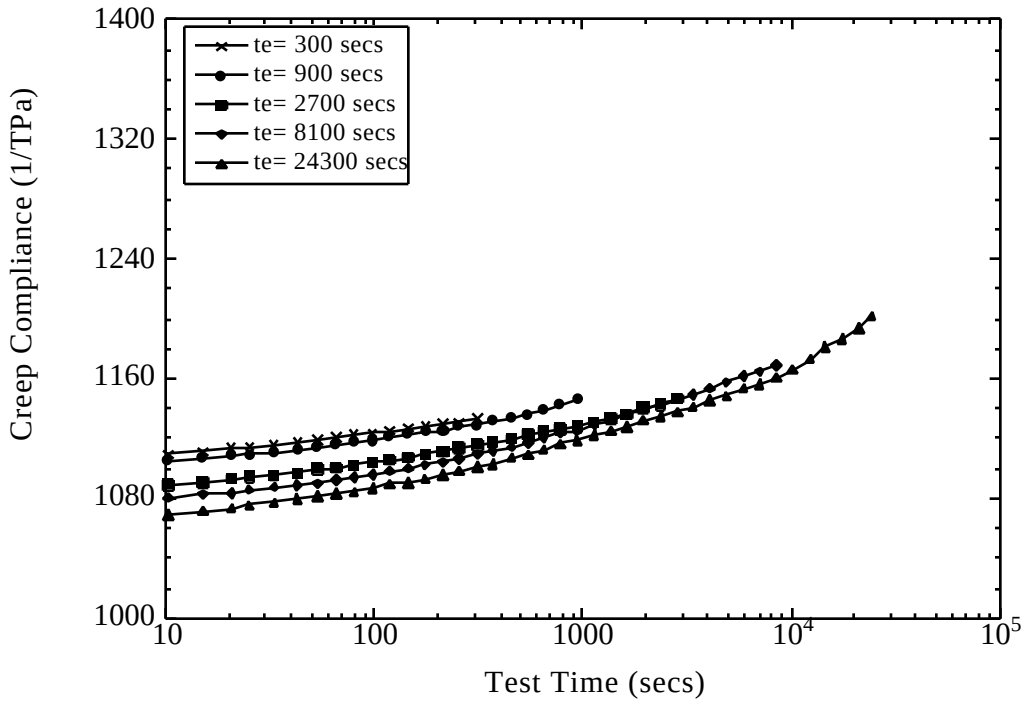

Figure 3.37. Creep compliance data on an as-received FM-5 resin specimen at 177°C.

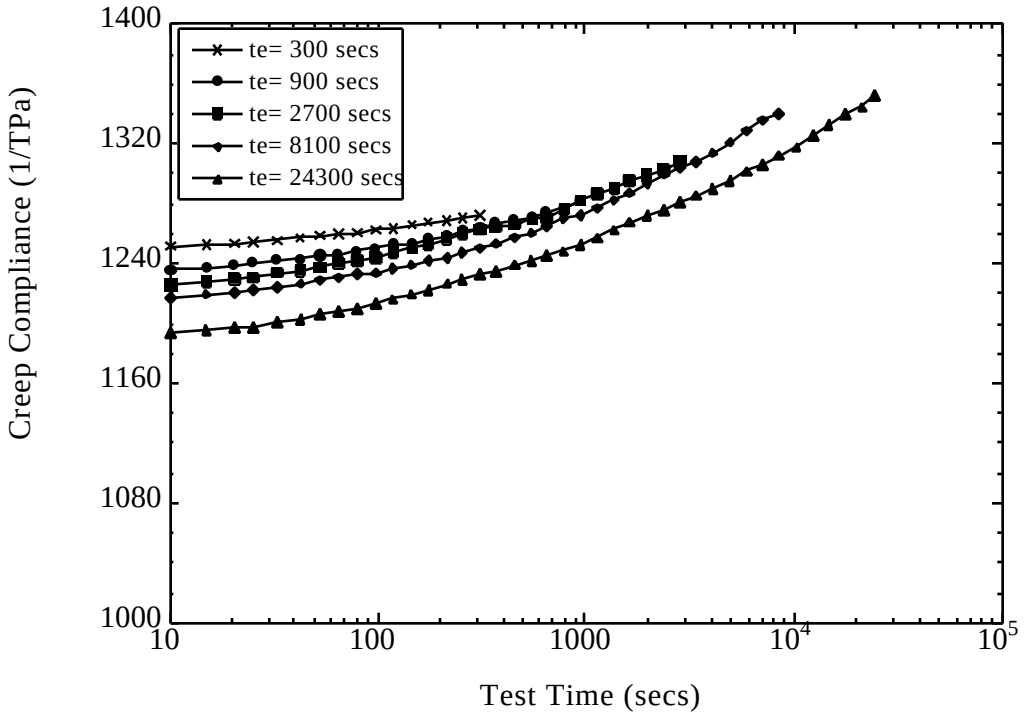

Figure 3.38. Creep compliance data on an aged and rejuvenated FM-5 resin specimen. The sample was aged for 6 months in air at 177°C and rejuvenated at 300°C for 2 hours.

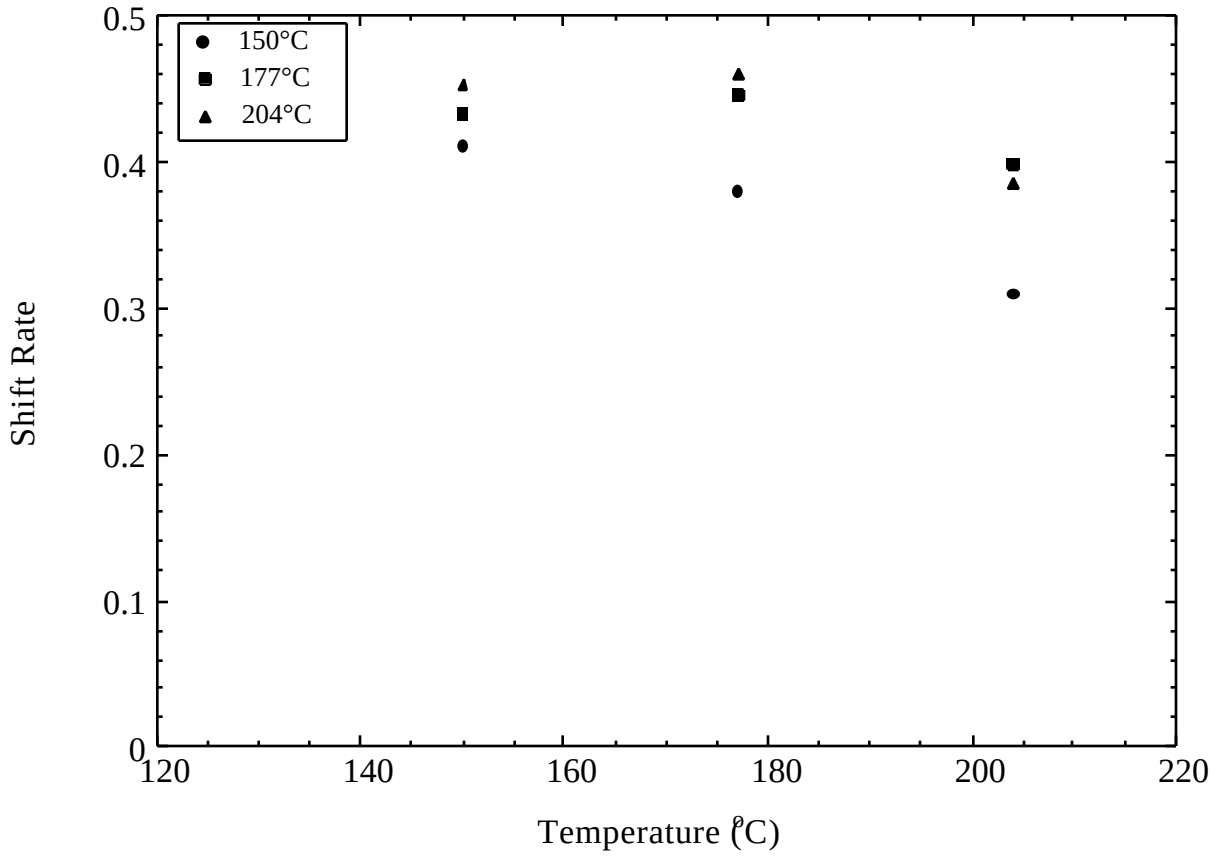

Figure 3.39. Comparison of shift rate data between as-received FM-5 coupons and aged and rejuvenated specimens at test temperatures of 150°C, 177°C, and 204°C. Samples were aged for 6 months in air prior to being rejuvenated at 300°C for 2 hours.

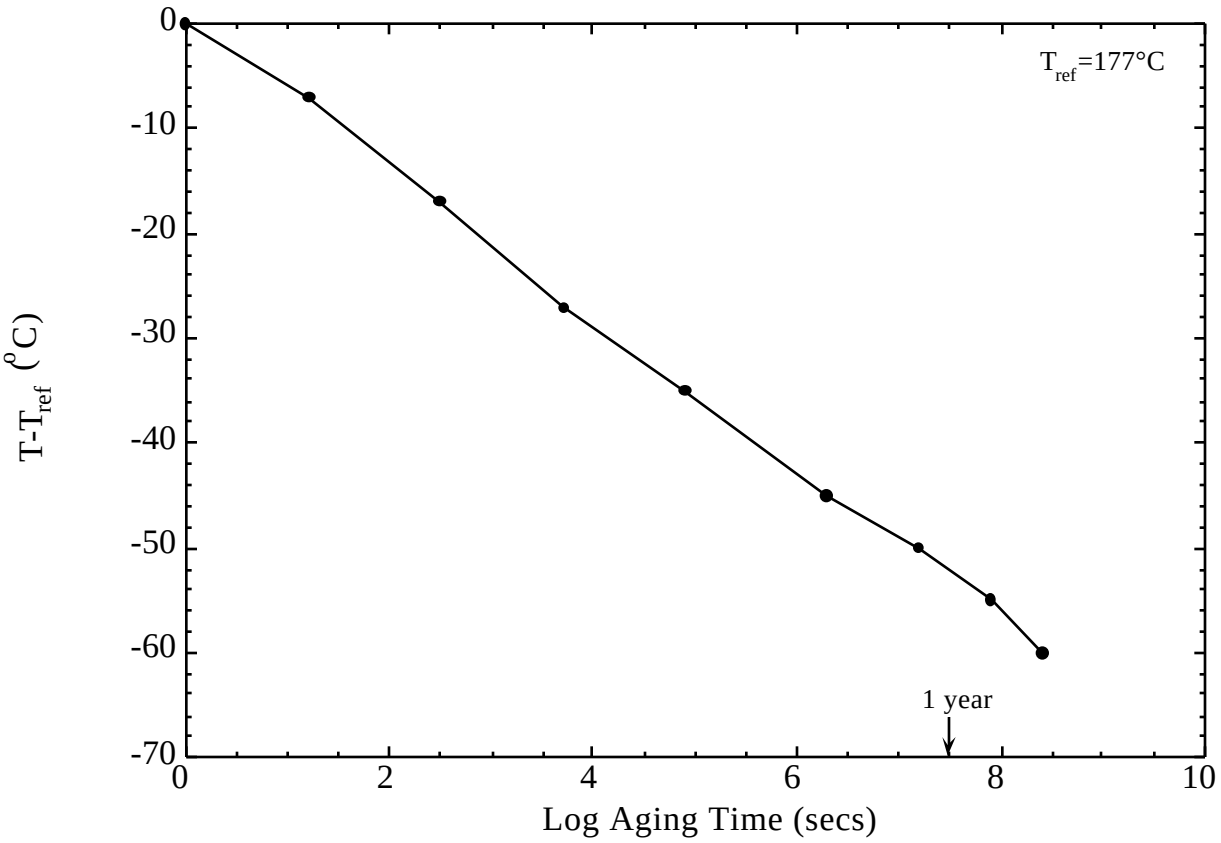

Figure 3.40. Aging time-temperature equivalency plot for FM-5 neat resin specimens.

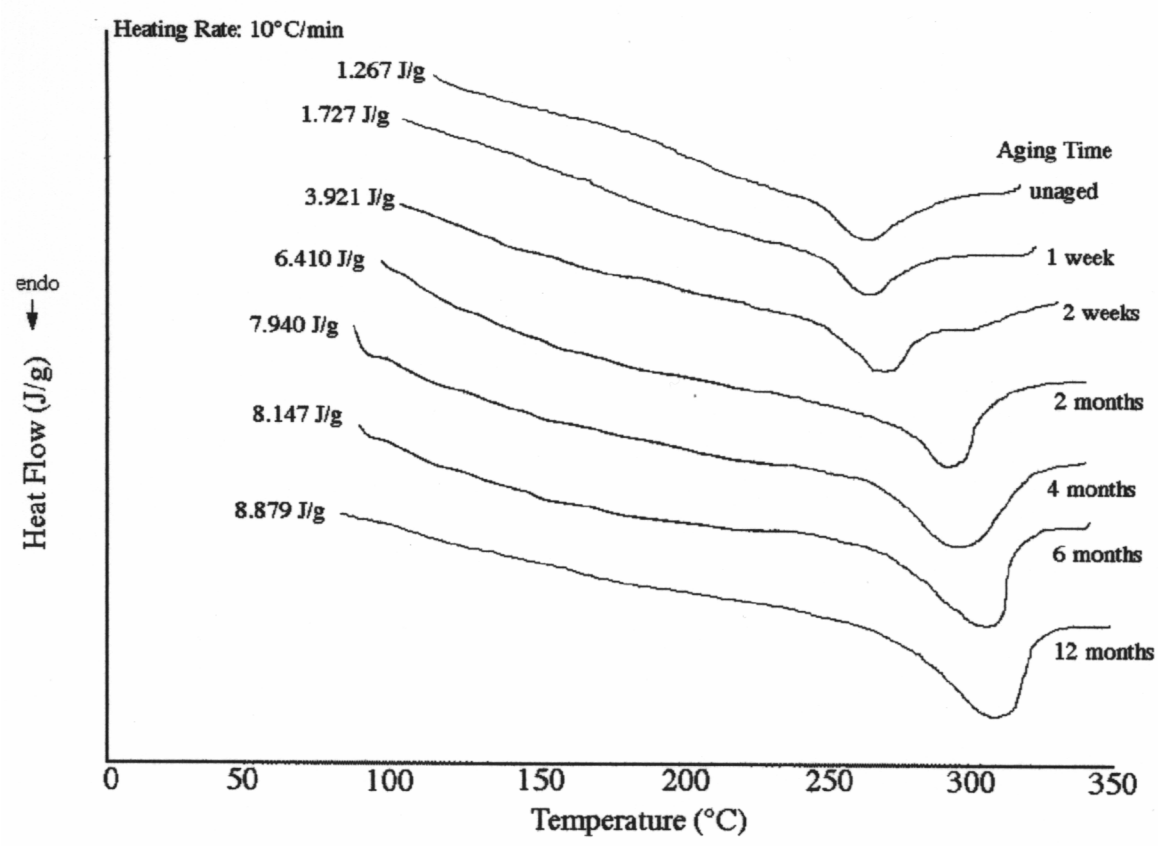

Figure 3.41. DSC data showing the effects of physical aging in FM-5 resin following air aging for 12 months at 204^{o}C.

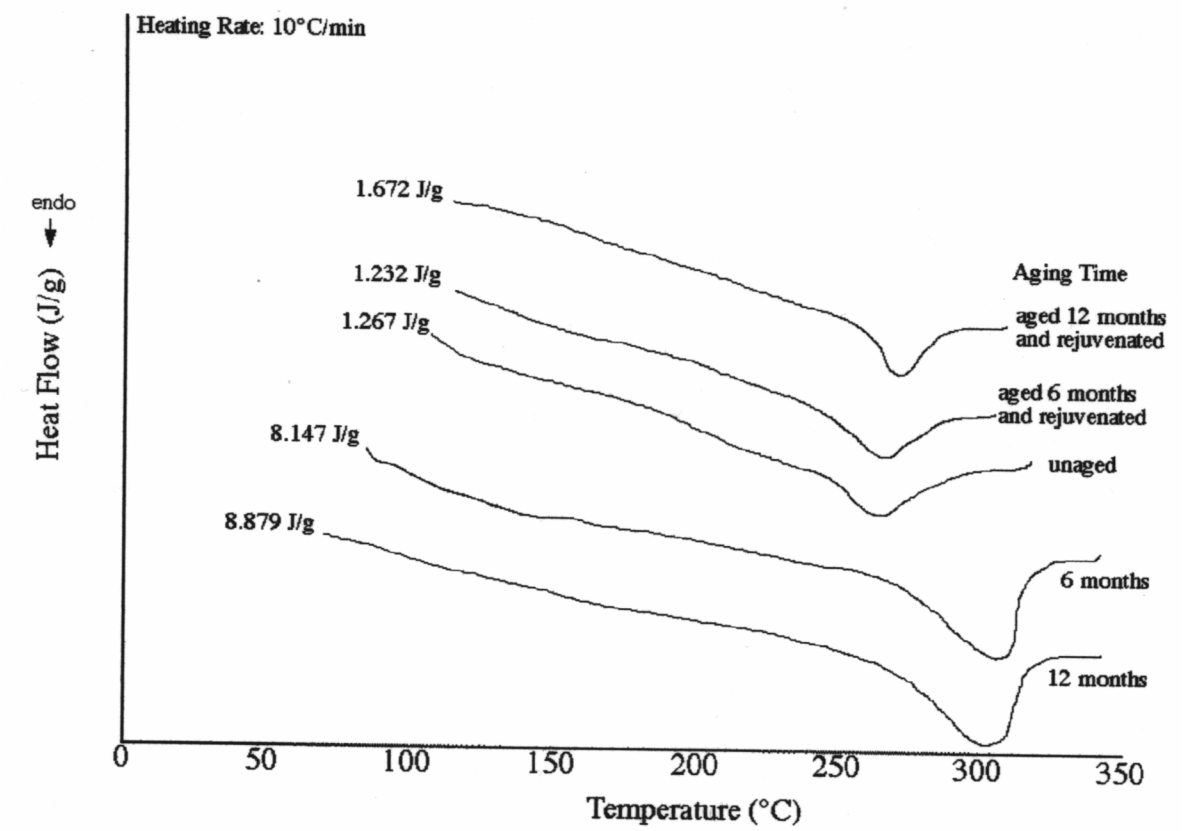

Figure 3.42. DSC data showing the effect of rejuvenation in FM-5 resin following air aging for up to 12 months at 204°C. Rejuvenation condition was 2 hours at 300°C.

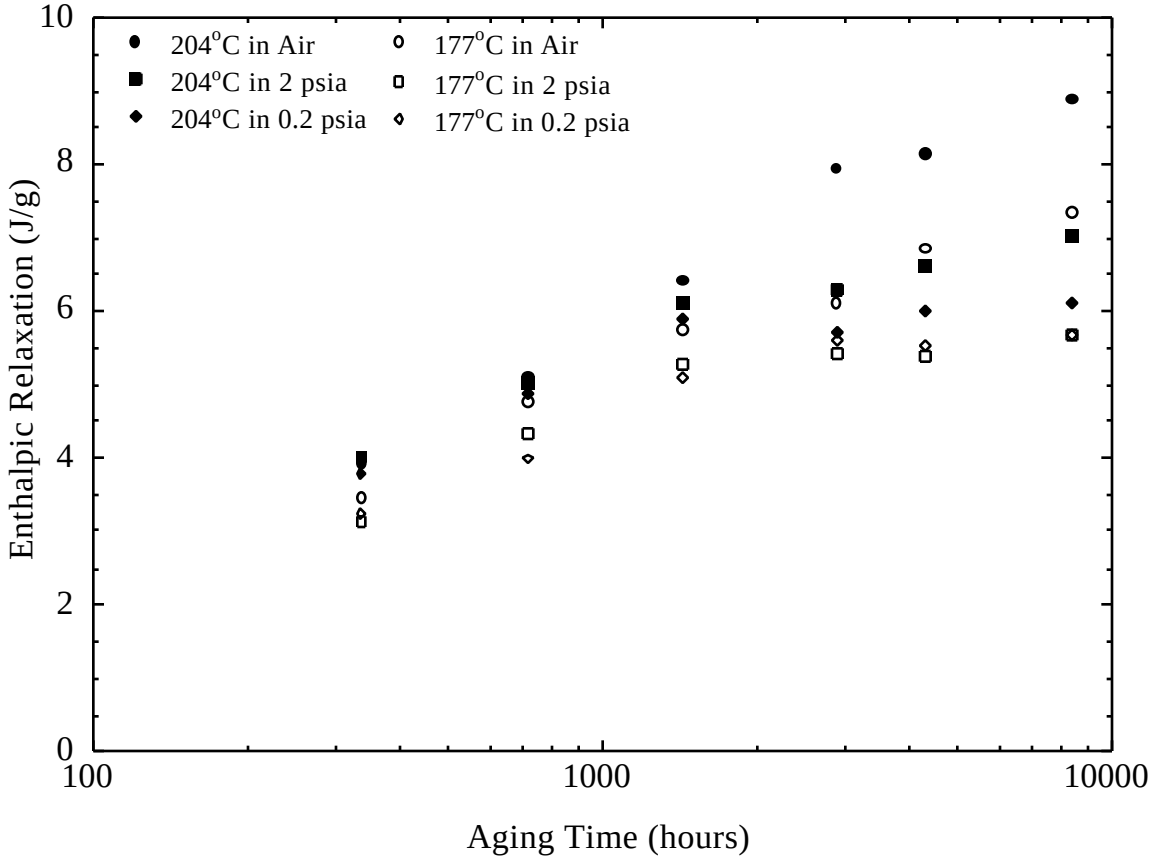

Figure 3.43. Plot of enthalpic relaxation as a function of aging time, temperature and environment for FM-5 resin.

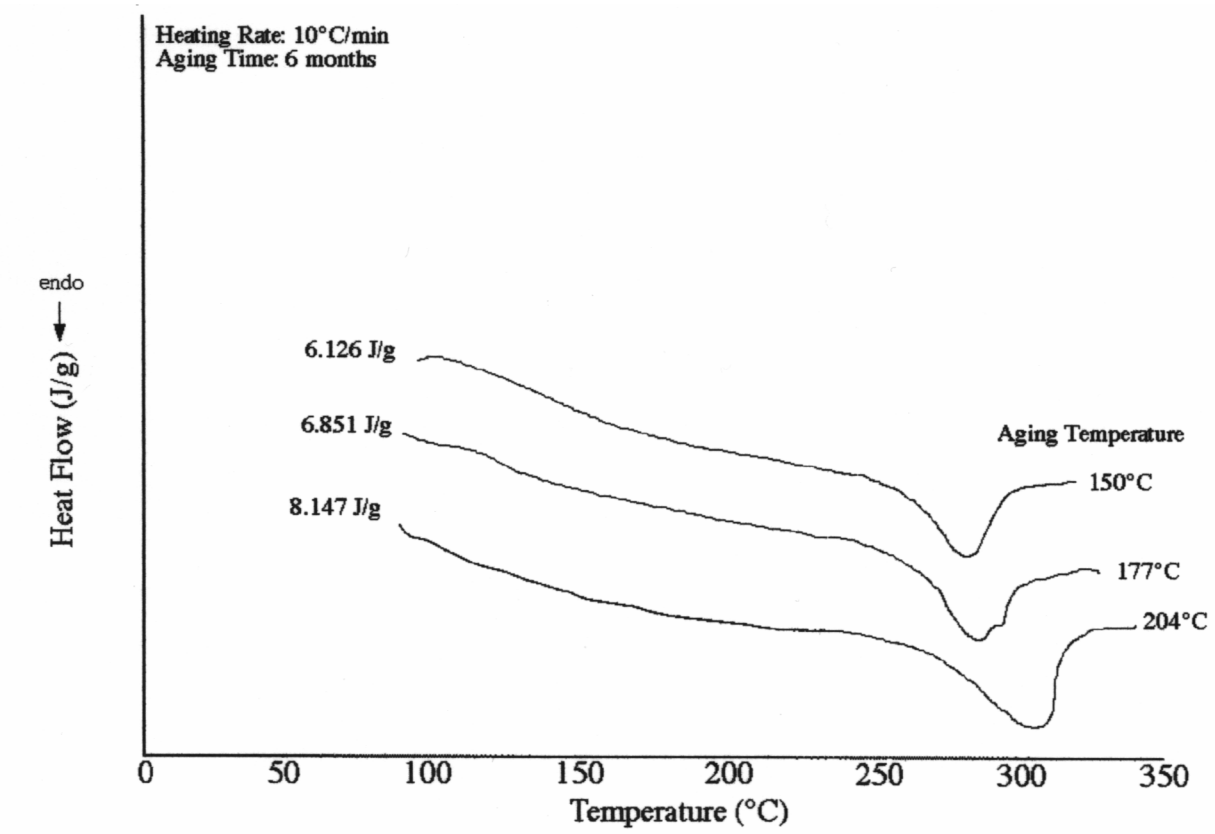

Figure 3.44. DSC traces on FM-5 resin samples aged for 6 months at 150°C, 177°C, and 204°C.

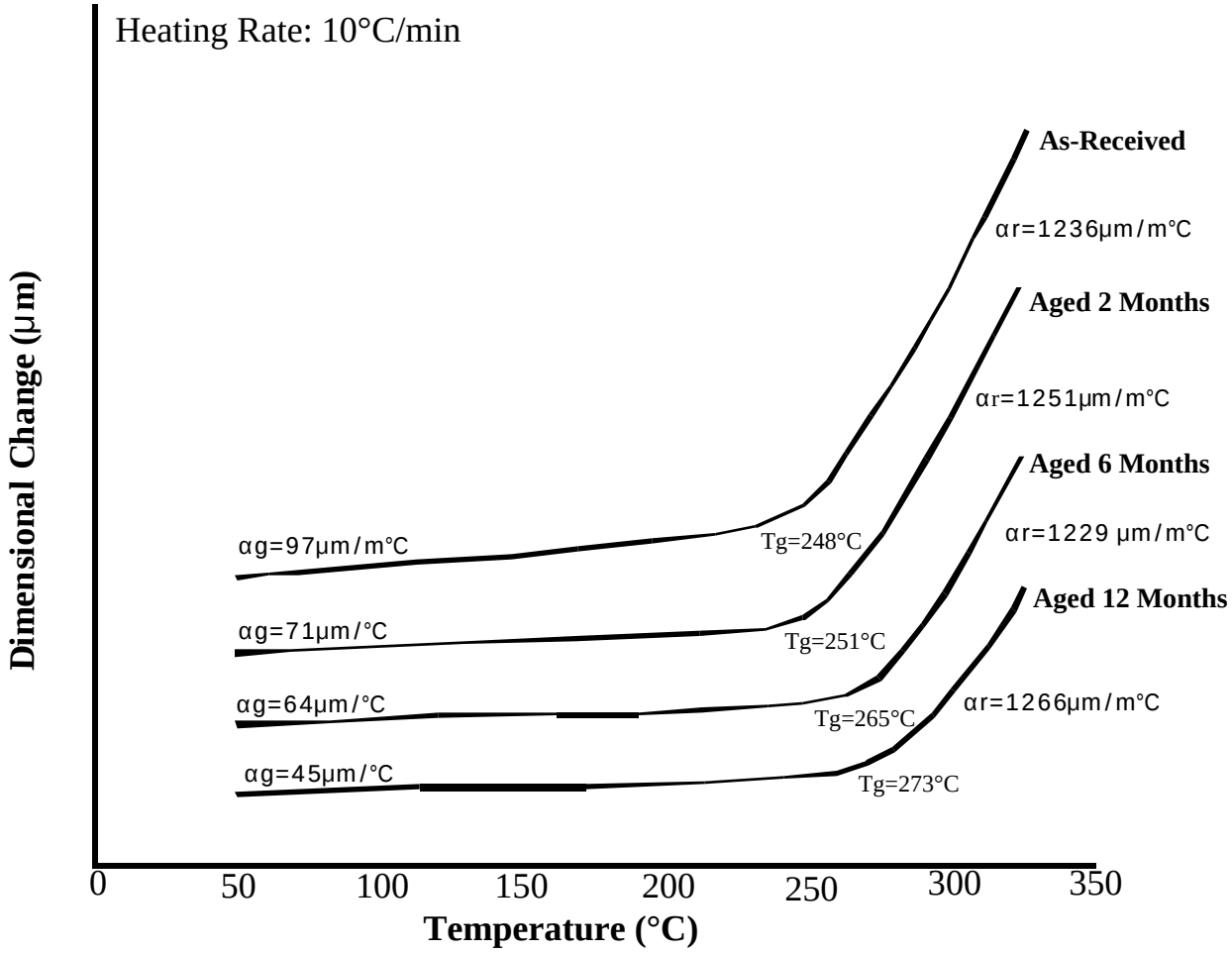

Figure 3.45. TMA traces on FM-5 neat resin samples aged in air for 12 months at 204°C.

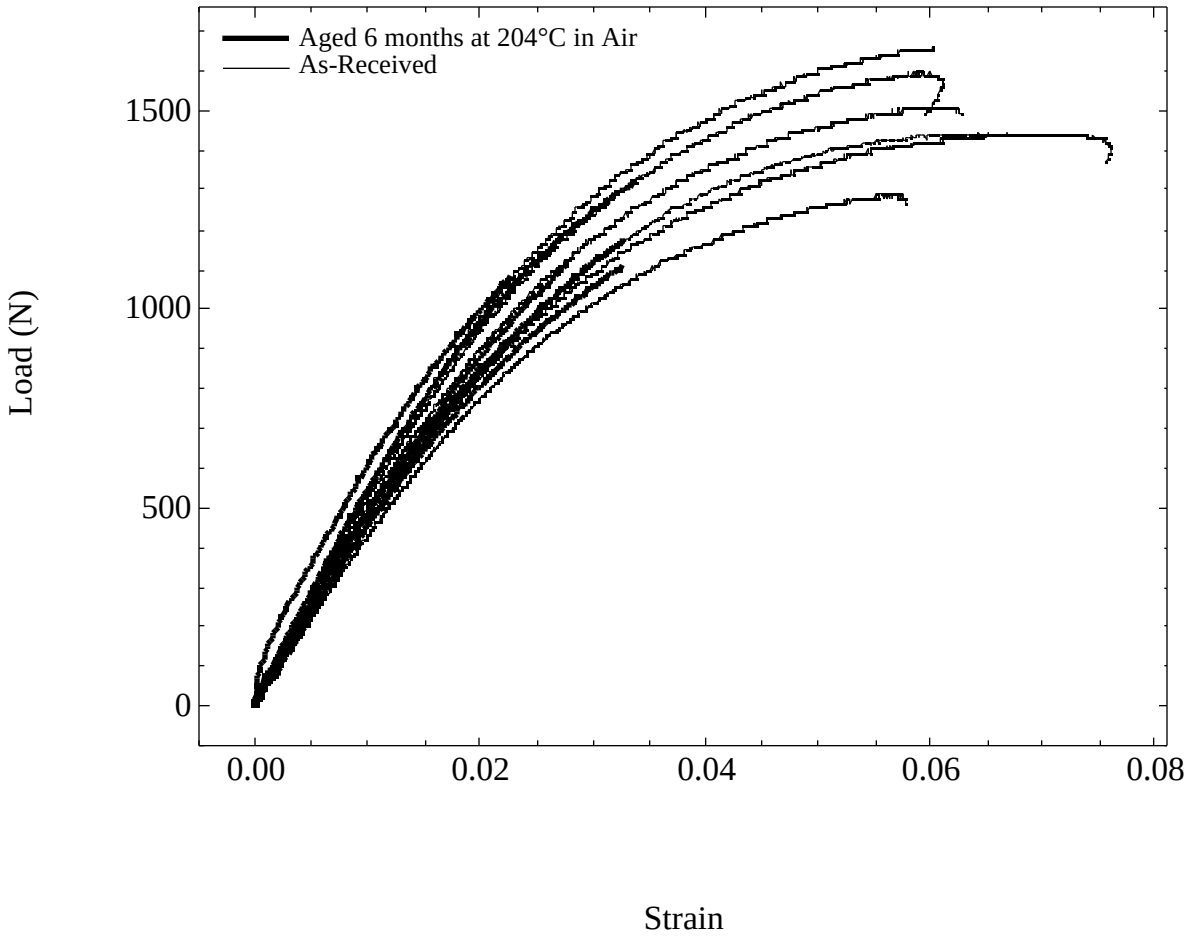

Figure 3.46. Load-Strain curves for FM-5 neat resin samples. Comparison is made between as-received specimens and those aged for 6 months in air at 204°C.

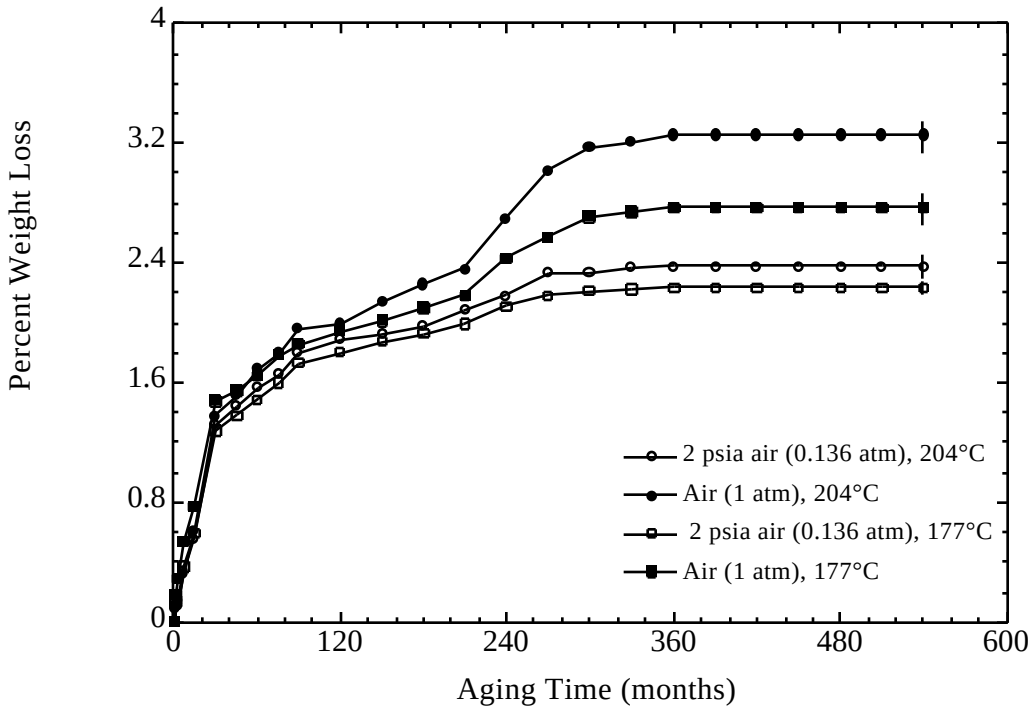

Figure 3.47. Weight loss in FM-5 resin as a function of aging time, temperature and environment.

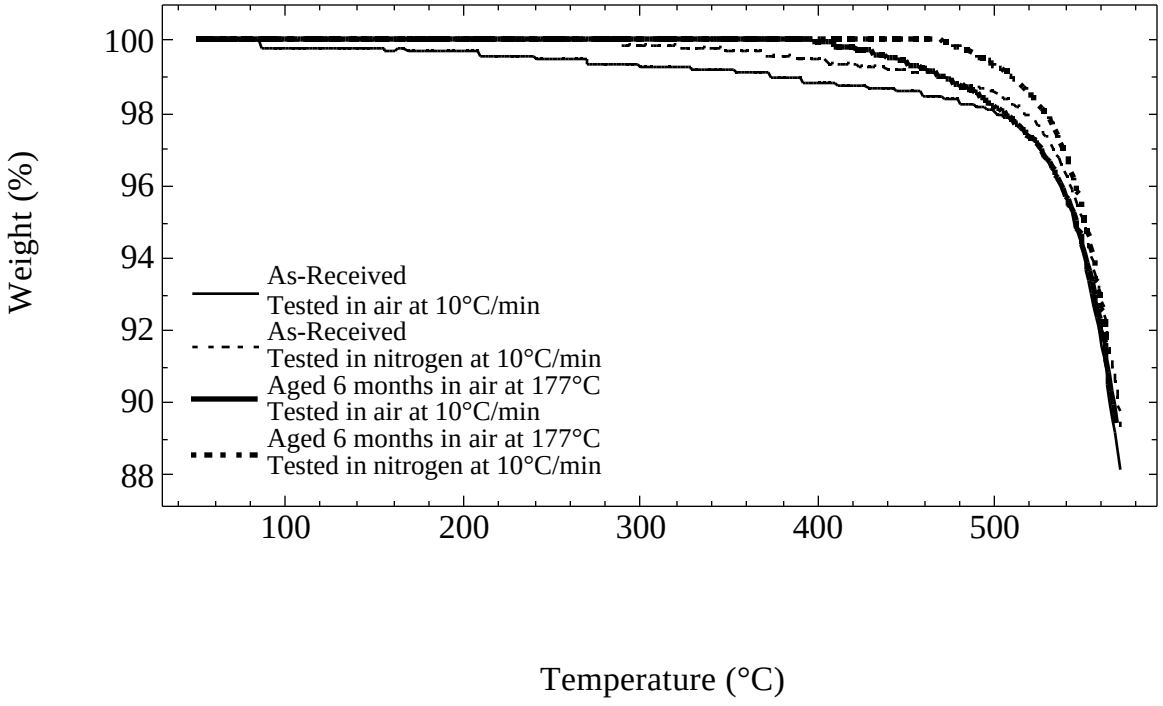

Figure 3.48. TGA plots comparing as-received and aged FM-5 resin specimens. Samples were aged for 6 months in air at 177°C. Testing was performed both in air and nitrogen gas.

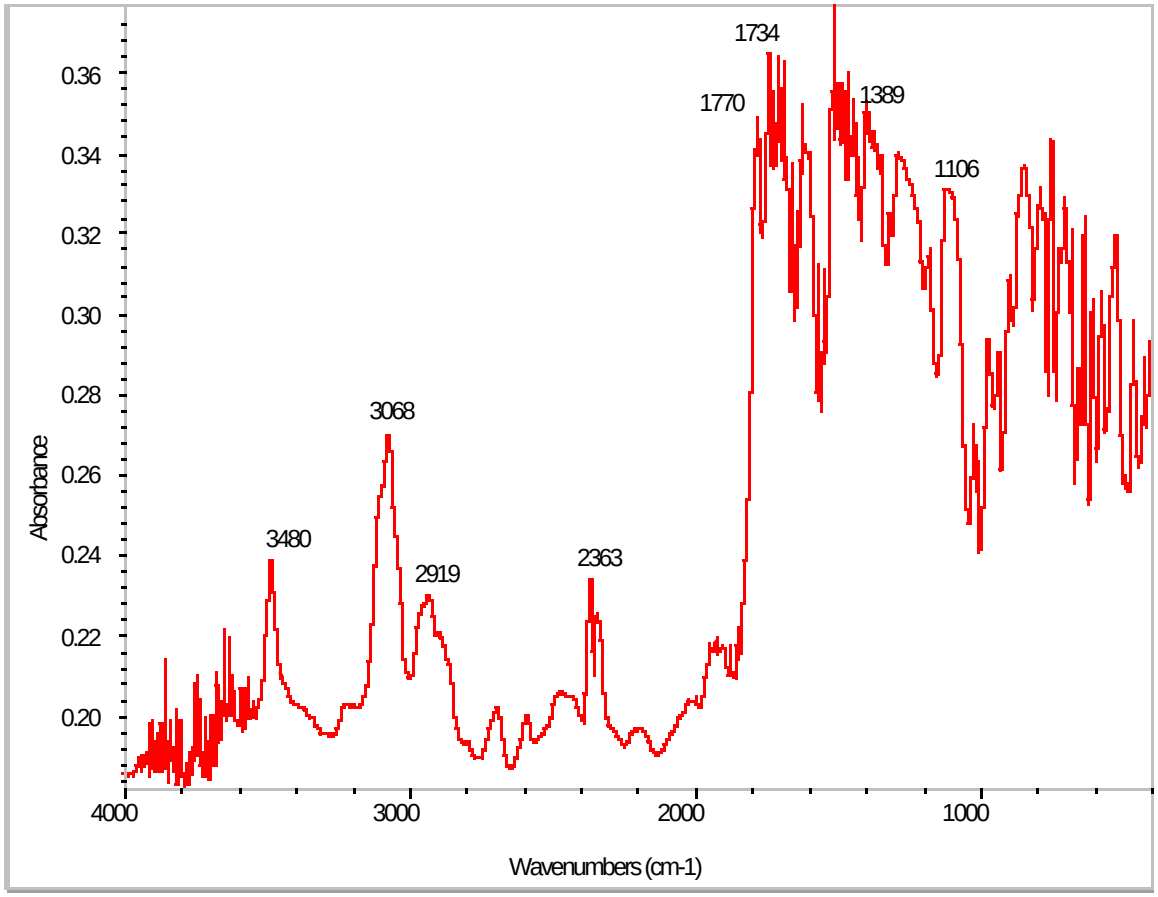

Firgure 3.49. FT-IR spectrum from the dried "residue" material obtained from the Soxhlet extraction testing on neat FM-5 resin that was aged for 12 months in air at 204∞C.

Aging Time	LSS Following Aging at 177°C in Air (psi)	LSS Following Aging at 204°C in Air (psi)
As-Received	7183	7183
1 Week	--	7279
4 Weeks	7080	6510
4 Months	6475	--

Table 3.1. Lap shear test results from Ti-6Al-4V/FM-5 bonds aged in 177°C and 204°C for up to 4 months in ambient atmospheric air [18].

Surface Pretreatment	G_{ARR} (J/m^2) +/-Std. Dev.
Chromic Acid Anodization	1902+/-61 (cohesive failure)
Chromium Oxide Grit Blast	1857+/-39 (cohesive failure)
Alumina Grit Blast	367+/-44 (adhesive failure)
Titanium Dioxide Grit Blast	1167+/-151 (mixed failure)
Silicon Dioxide Grit Blast	433+/-31 (adhesive failure)
Titanium Disilicide Grit Blast	267+/-18 (adhesive failure)
Phenylethynyl trimethyl Silane	202+/-26 (adhesive failure)
Allyl triethoxy Silane	45+/-11 (adhesive failure)

Table 3.2. Summary of wedge test results on Ti-6Al-4V/FM-5 bonds with different surface pretreatments. Bonds were immersed in boiling water for 72 hours.

G_{MAX} for As-received Specimen: 2561 J/m^2

Aging Condition	Drop in Fracture Energy from As-Received Value J/m^2	Loss in Fracture Energy due to Physical Aging J/m^2	Loss in Fracture Energy due to Chemical Aging J/m^2
6 months in air	248	108	140
6 months in 2 psia	174	82	92
6 months in 0.2 psia	160	86	74
12 months in air	718	158	559
12 months in 2 psia	644	395	249
12 months in 0.2 psia	581	423	158
18 months in air	830	71	759
18 months in 2 psia	713	50	663
18 months in 0.2 psia	541	277	264

Rejuvenation condition: 300°C for 2 hours

Table 3.3. Summary of DCB test results showing the individual contributions of physical and chemical aging responsible for the degradation in Ti-6Al-4V/FM-5 bond toughness. Aging carried out for up to 18 months in three different air pressures at 204°C. Numbers reported are G_{MAX} values.

Tg of As-Received Specimen = 251°C (DMA)

(Heating Rate = 1°C/min)

	177°C		**204°C**	
	Aged	**Rejuvenated**	**Aged**	**Rejuvenated**
2 Months	256°C	254°C	266°C	256°C
6 Months	261°C	255°C	269°C	255°C
12 Months	263°C	258°C	270°C	262°C
18 Months	264°C	260°C	272°C	265°C

* Rejuvenation Condition: 300°C for 2 hours

Table 3.4. DMA measurements of changes in T_g of neat FM-5 resin samples following aging and rejuvenation.

Tg of As-Received Specimen = 250°C (DSC)

(Heating Rate = 10°C/min)

	177°C		**204°C**	
	Aged	**Rejuvenated**	**Aged**	**Rejuvenated**
2 Months	259°C	255°C	269°C	258°C
6 Months	264°C	254°C	272°C	261°C
12 Months	266°C	260°C	271°C	260°C
18 Months	266°C	261°C	273°C	262°C

* Rejuvenation Condition: 300°C for 2 hours

Table 3.5. DSC measurements of changes in T_g of neat FM-5 resin samples following aging and rejuvenation.

(Heating Rate 10°C/min)

Aging Time	177°C			204°C		
	Air	2 psia	0.2 psia	Air	2 psia	0.2 psia
t_e=0	1.212 J/g	1.242 J/g	1.195 J/g	1.267 J/g	1.302 J/g	1.281 J/g
t_e=1 week	1.798 J/g	1.378 J/g	1.414 J/g	1.727 J/g	1.516 J/g	1.662 J/g
t_e=2 weeks	3.445 J/g	3.115 J/g	3.238 J/g	3.921 J/g	4.022 J/g	3.802 J/g
t_e=1 month	4.768 J/g	4.332 J/g	3.981 J/g	5.115 J/g	5.023 J/g	4.876 J/g
t_e=2 months	5.731 J/g	5.271 J/g	5.114 J/g	6.410 J/g	6.117 J/g	5.892 J/g
t_e=4 months	6.113 J/g	5.414 J/g	5.616 J/g	7.940 J/g	6.300 J/g	5.721 J/g
t_e= 6 months	6.851 J/g	5.387 J/g	5.521 J/g	8.147 J/g	6.615 J/g	6.002 J/g
t_e=12 months	7.344 J/g	5.663 J/g	5.678 J/g	8.879 J/g	7.013 J/g	6.114 J/g

Table 3.6. Changes in enthalpic relaxation, ΔH, of FM-5 resin samples as a function of aging time, temperature, and environment.

Testing Rate 1 mm/min

Aging Condition	**Failure Load, N (Std. Dev.)**	**Failure Strain (Std. Dev.)**
As-Received	1356 (121)	0.0603 (0.0027)
3 months in air at 177°C	1416 (106)	0.0585 (0.0051)
6 months in air at 177°C	1126 (80)	0.0355 (0.0033)
6 months in 2 psia at 177°C	1380 (62)	0.0412 (0.0042)
3 months in air at 204°C	1202 (72)	0.0478 (0.0064)
6 months in air at 204°C	1075 (58)	0.0304 (0.0022)

Table 3.7. Tensile stress-strain results on FM-5 neat resin samples as a function of aging time, temperature, and environment.

(Extraction Solvent: NMP)

Aging Condition	177°C, % Gel Fraction	204°C, % Gel Fraction
As-Received	98.1%	98.1%
2 months in air	97%	96%
6 months in air	96%	93%
12 months in air	94%	90.6%
6 months in 2 psia	97.2%	96.6%
12 months in 2 psia	96.5%	95%

Table 3.8. Soxhlet extraction results on FM-5 neat resin as a function of aging time, temperature, and environment. Tests were performed in NMP at elevated temperature.

(Extraction Solvent: NMP)

Aging Condition	177°C, % Gel Fraction	204°C, % Gel Fraction
As-Received	99%	99%
2 months in air	98.7%	98.8%
6 months in air	97.4%	97%
12 months in air	96.2%	94.7%
6 months in 2 psia	98.5%	98.4%
12 months in 2 psia	98%	97.1%

Table 3.9. Soxhlet extraction results on FM-5 neat resin as a function of aging time, temperature, and environment. Tests were performed in NMP at room temperature.

Sample	%C	%O	%N	%Si	%Ti	%Al
Cured FM-5	64.4	24.6	3.2	7.8	--	--
Initial Region-AFS	68.4	22.2	3.4	5.9	0.2	nd
Initial Region-MFS	69.6	21.2	3.7	5.5	nd	nd
Forced Region-AFS	75.9	17.2	5.2	1.7	nd	nd
Forced Region-MFS	56.6	31.1	4.0	3.2	4.2	0.9

MFS-metal failure surface; AFS-adhesive failure surface; nd-not detected (<0.1)

Table 3.10. Atomic concentrations for initial and forced failure regions of a wedge specimen aged for 14,400 hours at 204°C in air. Comparison is made with fully cured scrimmed FM-5 adhesive.

Sample	%C	%O	%N	%Si	%Ti	%Al
Cured FM-5	64.4	24.6	3.2	7.8	--	--
14400 hours at 204°C air (MFS)	56.6	31.1	4.0	3.2	4.2	0.9
10800 hours at 204°C 2 psia (MFS)	68.1	23.1	4.2	3.5	1.1	nd
10800 hours at 204°C 0.2 psi (MFS)	74.0	16.6	4.6	4.0	1.0	nd

MFS-metal failure surface; nd-not detected (<0.1)

Table 3.11. Atomic concentrations for initial and forced failure regions of a wedge specimen aged for over 10,000 hours at 204°C in different air pressures. Comparison is made with fully cured scrimmed FM-5 adhesive.

Sample	%C	%O	%N	%Si	%Ti	%Cl
Cured FM-5	64.4	24.6	3.2	7.8	nd	nd
177°C, MFS	67.5	23.3	4.7	3.6	0.9	nd
177°C, AFS	72.5	20.0	4.5	3.0	nd	nd
204°C, MFS	63.7	27.4	3.4	1.6	2.6	1.3
204°C, AFS	75.0	18.3	5.4	0.9	nd	0.4

MFS-metal failure surface; AFS-adhesive failure surface; nd-not detected (<0.1)

Table 3.12. Atomic concentrations for the "interfacial" and cohesive failure regions of DCB specimens aged for 12 months in air at 177°C and 204°C. Comparison is made with fully cured scrimmed FM-5 adhesive.

Sample	%C	%O	%N	%Si	%Ti	%Al
DCB cohesive failure-Side 1	72.9	18.4	4.9	3.6	0.1	0.3
DCB cohesive failure-Side 2	73.4	18.0	5.1	3.2	0.0	0.3
Residue from Soxhlet Extract	75.1	17.2	4.9	2.8	--	--

Side 1 and Side 2 are arbitrarily labeled

Table 3.13. Atomic concentrations from the "residual" material dried from the Soxhlet extraction solution. Comparison is made with a cohesively failed DCB specimen.

Band Assignments	LaRC PETI-5 Wave Number (cm-1)
imide CO in-phase	1777
imide CO out-of-phase	1737
imide CNC axial stretch	1383
imide CNC transverse stretch	1106
imide CNC out-of-phase bending	741
OH stretches of carboxylic acid	3068
=NH	3480
-CH	2919
$C0_2$	2363

Table 3.14. Selected band assignments for diffuse reflectance spectra for LaRC PETI-5 polyimide [32].

4.0 Solvent Effects on High Temperature Polyimides and Their Bonded Joints

4.0 Abstract

Environmental stress crazing/cracking (ESCR/C) of adhesives under organic solvent exposure is a subject of great practical importance to adhesive end-users, especially dealing with structural applications. In the past, the mechanical properties of several adhesive systems have been shown to degrade considerably after both prolonged and momentary exposure to solvents under a state of stress. It is therefore essential to study the solvent resistance of any adhesive system to organic solvents that may come in contact with the adhesive during its service life. The adhesive systems used in this study were: FM-5 a thermosetting polyimide developed by Cytec Engineered Materials, Inc., VT Ultem thermosetting polyimide, developed by Prof. McGrath's laboratory at Virginia Tech, and REGULUS^{TM}, a thermoplastic polyimide produced by Mitsui Toatsu.

Initially, dog bone samples (0.5 mm thick) of the FM-5 and REGULUS^{TM} resin systems were prepared, according to ASTM Standard D638-91a, and these soaked in the solvents to obtain equilibrium solvent mass uptake curves. The solvents used in the study included acetone, methyl ethyl ketone (MEK), ethylene glycol. The equilibrated samples were then tested in a miniature tensile testing machine (Minimat), to obtain stress-strain characteristics. In all cases moduli, strains to failure, and yield stresses were computed, and comparisons made with unexposed control specimens. Secondly, samples equilibrated in the solvents were held in a vacuum environment at 150^{o}C which is below the glass transition temperature of the adhesives to desorb the solvent, and these were then tested on the Minimat to obtain residual properties.

To study the durability of bonded joints under solvent exposure, Ti-6Al-4V/adhesive bonds were prepared and wedge tests were performed on them for periods up to several days in solvent baths. Based on the measured crack lengths, the strain energy release rate due to solvent induced environmental stress cracking (G_{ESC}) was computed as a function of crack growth rate.

The G_{ESC} measurements help quantify the durability of the bonded joints on exposure to the various solvents, and further help in ranking the adhesives in terms of solvent resistance.

4.1 Introduction

Environmental stress cracking (ESC) of polymers is a failure phenomenon of great practical significance and first noted in polyethylene in the 1950s [1]. Since the 1970s, researchers [2-4] found that many thermoplastic adhesives and polymers, mechanically loaded and immersed in certain kinds of fluids, undergo failure by crazing or cracking. The loads required for the failure of specimens exposed to solvents are significantly less than those required for failure in air. Failures like these are called environmental stress crazing (ESCR) and environmental stress cracking (ESC). The mechanisms for ESC/CR are not fully understood to date, however, several reasons for this phenomena have been suggested by researchers who have worked in this area. Some of the most common reasons suggested for ESC behavior are plasticization of polymer material [2], solubility parameter differences between polymer and solvent [5], hydrogen bonding [6], reduced crystallinity [7], and residual stresses [8]. Parvatareddy, et. a.l [9] showed that high performance composites exhibited ESC when exposed to common organic solvents used in the aircraft industry. Recent studies by Dillard, et. al. [10] and Clifton [11] showed that even high performance polyimide adhesives may be sensitive to organic solvents and aircraft fluids. In light of the observations made by Dillard, et. al. [10], it is essential to study the solvent sensitivity of high performance structural adhesives in context to the solvents which may come into contact with the adhesive and/or joint during the service life.

In the present study the phenomenon of ESC is investigated in three high performance adhesives, FM-5, VT Ultem, and REGULUS^{TM}, and their adhesively bonded joints. The solvents used in this research included acetone, methyl ethyl ketone (MEK), toluene, jet fuel, hydraulic fluid, and ethylene glycol. The FM-5 adhesive system is being currently investigated to study its feasibility for application in a future supersonic civil transport aircraft. Thus, this

study is of relevance to the aircraft industry because some of the solvents used in this study are currently used as degreasers and paint strippers in the aircraft industry [12].

4.2 Experimental

4.2.1 Materials

The FM-5 adhesive is based on a polyimide originally developed at NASA Langley Research Center (LaRC PETI-5) [13] and then modified and supplied by Cytec Engineered Materials, Inc., Havre de Grace, Maryland. The molecular weight of the adhesive used in this study was 5000 g/mole. The adhesive was supplied in two forms; as polymer film supported on a woven fiberglass cloth and as an unsupported film. The supported film contained 85% polymer by weight. This supported film also contained approximately 4% by weight of the solvent N-methyl-2-pyrrolidinone (NMP). The supported film was used to bond titanium adherends to conduct wedge tests. The unsupported film had less than 0.5 % by weight of the solvent and was used to conduct the solvent uptake and desorption tests and the tensile tests. The adhesive was cured at a temperature of 250^{o}C for 30 minutes, followed by a hold for 60 minutes at 350^{o}C while maintaining a curing pressure of 75 psi (0.518 Mpa). The glass transition temperature, T_g, of the cured adhesive was approximately 250^{o}C.

VT (Virginia Tech) Ultem [14] , is a thermosetting polyimide in the same class as the LaRC PETI-5 polymer. This polymer was synthesized at Virginia Tech under the guidance of Prof. McGrath in the Chemistry Department. The molecular weight of the VT Ultem material used in this study was 3000 g/mole. The VT Ultem material was also supplied as a scrimmed adhesive film with approximately 85% polymer by weight. The bonding procedure used for making wedge specimens with the VT Ultem is as follows: 250°C for 30 minutes under no pressure, followed by a hold for 90 minutes at 380°C while maintaining a pressure of 75 psi (0.518 Mpa). The T_g of the cured adhesive was around 240°C.

REGULUS^{TM} is a thermoplastic polyimide produced by Mitsui Toatsu Chemicals, Inc., Japan. For this study, the REGULUS^{TM} adhesive was supplied by the Boeing Company. The adhesive was bonded to titanium metal for conducting the wedge tests using the following cure cycle: 2 hours hold at 150^{o}C under contact pressure, followed by a 10 minute cure at 400^{o}C under a pressure of 300 psi. The T_g of the adhesive was reported to be 250°C.

The adherends used in the study were cut from Ti-6Al-4V plates, having dimensions of 200 x 25 x 3.175 mm, and supplied by President Titanium Company, Hanson, MA. The adherends were surface pretreated with chromic acid anodization (CAA) before bonding with the adhesive.

4.2.2 Solvent Uptake and Desorption

Solvent uptake tests were performed on unsupported neat FM-5 and REGULUS^{TM} resin. Dog bone specimens of the neat resin, 0.5 mm thick, were prepared in accordance with ASTM D638M-91a [15]. The solvents used in the study included acetone, MEK, toluene, jet fuel, ethylene glycol, hydraulic fluid, and water. Ten dog bone specimens of each resin were immersed in each of the solvents and the samples periodically weighed to obtain equilibrium solvent mass uptake data. Data was collected on the specimens in excess of 1200 hours. Following saturation of the various solvents in the adhesive specimens, five equilibrated specimens from each solvent were held in a vacuum environment at 150^{o}C for 60 minutes, to desorb the solvent.

4.2.3 Minimat Tensile Testing

The solvent saturated and redried specimens were tested in a miniature tensile testing machine according to ASTM D638M-91a [15] to obtain stress-strain characteristics. In all cases, moduli, strains to failure, and yield stresses were computed, and comparisons made with unexposed control specimens.

4.2.4 Wedge and DCB Testing

To study the durability of bonded joints under solvent exposure, Ti-6Al-4V/adhesive wedge specimens were prepared and tests performed for several hours in solvent baths. Based on the measured crack lengths, the strain energy release rate due to environmental stress cracking (G_{ESC}) was computed as a function of crack growth rate [16]. The G_{ESC} measurements help to quantify the durability of the bonded joints on exposure to the various solvents, and further help in ranking the solvent resistance of the adhesive. Five wedge specimens were exposed to each of the solvents and the results reported in a later section are average values from the five tests. Anodized Ti-6Al-4V/FM-5 DCB specimens were also prepared and these specimens soaked in several solvents (2 specimens per solvent) for one month. Following the soak period, the samples were tested in accordance with the procedure described in section 2.8.3.

4.3 Results and Discussion

4.3.1 Solvent Uptake and Desorption

Figure 4.1 shows equilibrium solvent mass uptake curves for dog bone specimens of neat FM-5 resin. Ten specimens each were exposed to seven different solvents for over 1200 hours. The highest solvent uptake occured in MEK (~6%). Jet fuel and toluene had similar uptakes (~4%). Acetone was next with around 3% uptake, followed by hydraulic fluid, ethylene glycol, and water (~1%). Following the solvent uptake tests, 5 of the specimens from each solvent were dried in a vacuum oven at 150^{o}C for 60 minutes. The results from the desorption study are summarized in Figure 4.2. As seen in this figure, all the other specimens lost most of the solvent they had absorbed, except for samples soaked in toluene which retained around 1.5% by weight of the solvent.

Figure 4.3 shows the solvent uptake data for REGULUS^{TM} films exposed to the same solvents as the FM-5 resin. For this adhesive material the highest solvent uptake was seen in

acetone (~1.5%) followed closely by toluene and MEK, and the least in water and hydraulic fluid. Upon drying, all the films lost most of the absorbed solvent, while those saturated in toluene retained around 0.1% by weight of the solvent (see Figure 4.4). The drying procedure used was similar to that described for the FM-5 system in that the specimens (5 out of the 10 saturated specimens per solvent) were dried in a vacuum oven at 150°C for 60 minutes.

4.3.2 Tensile Test Results

Following the desorption tests, all specimens, both saturated with the solvents and redried, were tested in a tensile testing machine. The stress-strain curves obtained from these tensile tests for the FM-5 specimens are summarized in Figure 4.5. Samples saturated with acetone, MEK, and toluene were plasticized, as evidenced by the lower yield stresses and the higher strains to failure. However, on drying the specimens, irrespective of the solvent to which the samples were exposed, all the stress-strain curves resembled that obtained for the as-received specimen. This finding indicates that there may be minimal residual effects of the solvents on the FM-5 resin. Further, the FM-5 resin system appears to be considerably solvent resistant, compared to for example, the polymers tested in References 7 and 8. The results for the REGULUS^{TM} resin system are summarized in Figure 4.6. Samples saturated with toluene and jet fuel were plasticized, yielding very high strain-to-failure values. However, similar to the results obtained for the FM-5 resin, upon drying of the REGULUS^{TM} specimens and retesting, all the stress-strain curves approached the stress-strain characteristics obtained on an as-received specimen. This shows that, upon proper drying out of the adhesive material after solvent exposure, there is very little residual effect of the various solvents on the REGULUS^{TM} polyimide.

4.3.3 Wedge and DCB Test Results

To study the effect of solvent exposure on adhesive bond durability, Ti-6Al-4V/adhesive bonded specimens treated with CAA were immersed in solvents for periods up to 168 hours. Five specimens each were immersed per solvent and crack length data collected as a function of exposure time. Results from these wedge tests obtained on the Ti-6Al-4V/FM-5 system are summarized in Figures 4.7 and 4.8. Data shown are average values obtained from the 5 test specimens per solvent. As can be seen from Figure 4.7, the longest crack growth was obtained from samples immersed in boiling water, while the least was seen in the samples immersed in room temperature water. The rest of the solvents had a certain ranking in terms of the crack length obtained following exposure of the bonded joint. In terms of ascending durability, as can be seen from the arrest fracture energy values (Figure 4.8) the ranking order was: acetone, MEK, toluene, jet fuel, ethylene glycol, hydraulic fluid, and room temperature water. The crack growth showed mixed-mode failure characteristics in the boiling water, while it was cohesive in the rest of the solvents. Figure 4.9 summarizes the DCB test results obtained on the Ti-6Al-4V/FM-5 bonds after the bonded specimens were soaked in different solvents for 1 month and tested. The data shown are an average from 2 specimens per solvent condition. While jet fuel and hydraulic fluid have no effect on the mode I fracture toughness, a 10-15% drop in fracture toughness was noted in MEK, acetone and toluene solvents. This drop in toughness is rather small considering that the bonded samples were submerged in the solvents for a month. Further, It must be noted that it is highly unlikely that the adhesive bonds would be submerged in acetone, MEK or toluene, for a 1 month period during actual service. Also, it is encouraging to note that there was no drop in toughness following the continued exposures to jet fuel and hydraulic fluid. There is a greater probability that the above two solvents may come into contact with a bonded aircraft structure for a prolonged period of time during service.

Figure 4.10 summarizes the results obtained from wedge tests conducted on CAA Ti-6Al-4V/REGULUS^{TM} bonds following the interaction of the bonded joints with different solvents over a 162 hour period. While boiling water showed the least durability based on the arrest

energy release rates that were calculated, the best durability was seen in the samples immersed in hydraulic fluid. The arrest fracture energies for this bonded system were considerably lower than the Ti-6Al-4V/FM-5 bonded system over a similar exposure period to exactly the same solvents. Trends similar to those observed with the titanium/REGULUS^{TM} bonds, were seen in the CAA Ti-6Al-4V/VT Ultem bonded specimens. These results are summarized in Figure 4.11.

4.4 Summary and Conclusions

This study was undertaken to gain an understanding of the important issue of solvent sensitivity and environmental stress cracking in the FM-5 adhesive and its titanium bonded joints. The Ti-6Al-4V/FM-5 adhesive bonded system is currently being evaluated for application in a future supersonic aircraft application. It is common knowledge that adhesives used in aerospace structures often come into contact with organic solvents and aircraft fluids during their service life. Past studies with high performance polymers have shown them to be susceptible to organic solvents under load, therefore making it imperative to study the behavior of the titanium/FM-5 bonds in certain organic solvents and aircraft fluids. As a part of this study, the performance of the FM-5 adhesive in different solvents was also compared and contrasted with two other polyimide adhesives, VT Ultem and REGULUS^{TM}.

Tensile tests conducted on neat FM-5 specimens, both saturated with solvent and re-dried, showed no cracking or crazing of the polymer. Under the saturated condition, some of the solvents appeared to have a plasticization effect on the polymer. However, upon drying of these specimens, they behaved in a normal fashion similar to the as-received samples. To study the interaction of the solvent and stress on the bonded joints, wedge tests were conducted on the titanium/FM-5 system. The wedged bonds were submerged in different solvents for a week and crack measurements taken over this period of time. These crack length measurements helped rank the different solvents in terms of their detrimental effect to the bonded system. If carried out for longer periods of time, this test could serve as a very good durability test for any adhesive

bonded system exposed to different solvents. As well, the arrest fracture energies that can be calculated from this test can prove useful for design purposes.

The one notable conclusion that can be drawn from this study is that the FM-5 adhesive material is fairly resistant to the solvents that were used in research. This augurs well for the future application of this adhesive on aircraft structures. It must also be mentioned here that the VT Ultem and REGULUS^{TM} adhesives were chemically resistant to the solvents used in this study. The one difference between the FM-5 and REGULUS^{TM} resins in terms of performance was that the arrest fracture energies obtained from the wedge tests on the REGULUS^{TM} bonds were considerably lower than the FM-5 material.

4.5 References

1. J. B. Howard, *Engineering Design for Plastics*, Reinhold, New York (1964)

2. R. P. Kambour, *J. Polym. Sci.: Macromolecular Review*. **7**, 1-154 (1973)

3. A. N. Gent, *J. Mater. Sci.* **5**, 925-932 (1970)

4. E. H. Andrews, L. Bevan, *Polymer* **13**, 337-346 (1972)

5. G. A. Bernier, R. P. Kambour, *Macromolecules* **1**, 393-400 (1968)

6. P. I. Vincent, S. Raha, *Polymer* **13**, 283-292 (1972)

7. J. N. Hay, D. J. Kemmish, *Polymer* **29**, 613-620 (1988)

8. A. J. Hsieh, J. J. Vanselow, *Advanced Composites and Processing Technology: Proc. of the Sym.* ASME Winter Meeting, Chicago, Il, 13-17 (1988)

9. H. Parvatareddy, C. A. Heithoff, A. P. Clifton, D. A. Dillard, R. G. Kander, *ASTM STP 1274*, 56-68 (1996)

10. D. A. Dillard, P. R. McDaniels, and J. A. Hinkley, *J. Mater. Sci. Lett.* **12**, 1258 (1993)

11. A. P. Clifton, M.S. Thesis, Virginia Polytechnic Institute and State University, Blacksburg, VA (1996)

12. T. J. Reinhart, *Bonded Repair of Aircraft Structures*, Ch. 2, A. A. Baker and R. Jones (Ed.), Martinus Nijhoff Publishers, 19-30 (1988)

13. J. G. Smith, and P. M. Hergenrother, *Polymer Pre-prints* **35**, 353-355 (1994)

14. B. Tan, V. Vasudevan, Y. J. Lee, S. Gardner, R. M. Davis, T. Bullions, A. C. Loos, H. Parvatareddy, D. A. Dillard, J. E. McGrath, J. Cella, *J. Polym. Sci: Part A: Polym. Chem.* **35**, 2943-2954 (1997)

15. ASTM Standard D638M-91a, *Annual Book of ASTM Standards*, Vol. **10.01**, 172-180 (1992)

16. J. Cognard, *J. Adhesion.* **20**, 1-13 (1986)

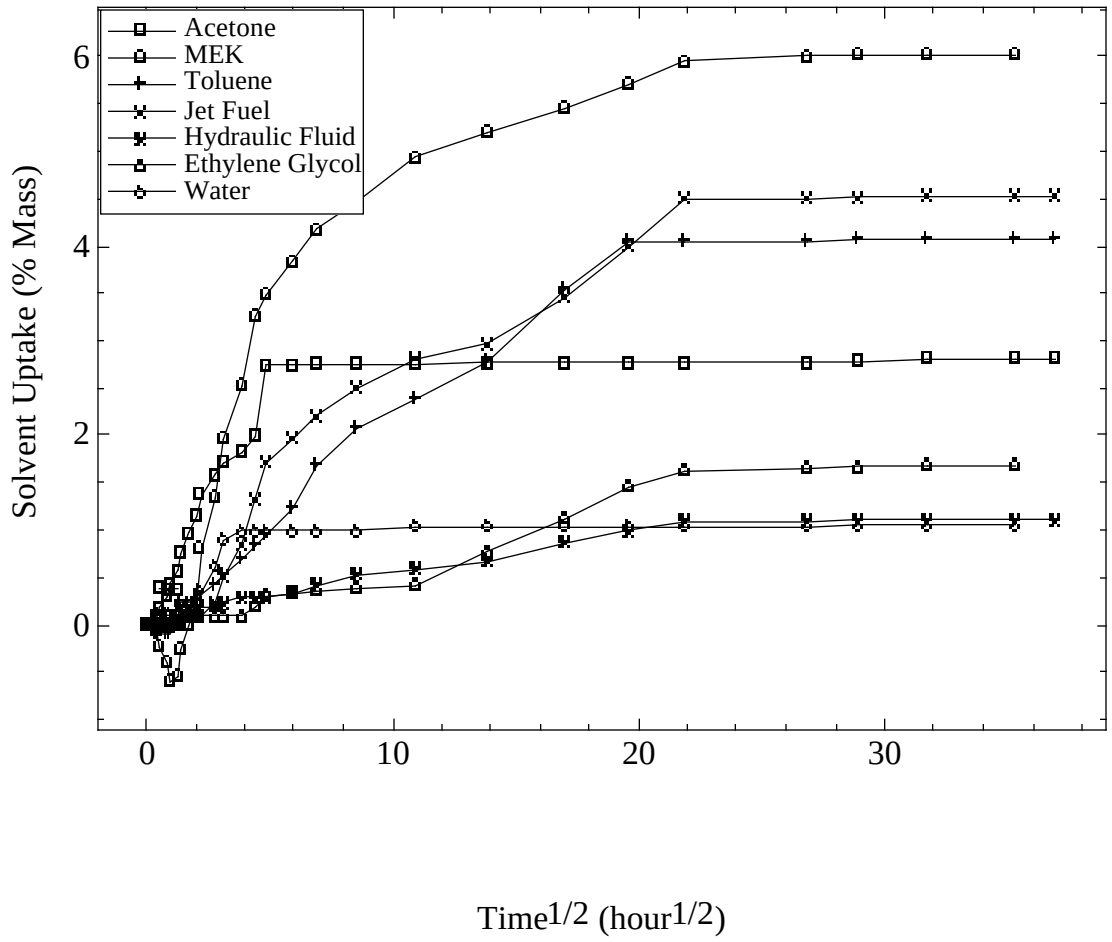

Figure 4.1. Solvent mass uptake curves for FM-5 neat resin specimens.

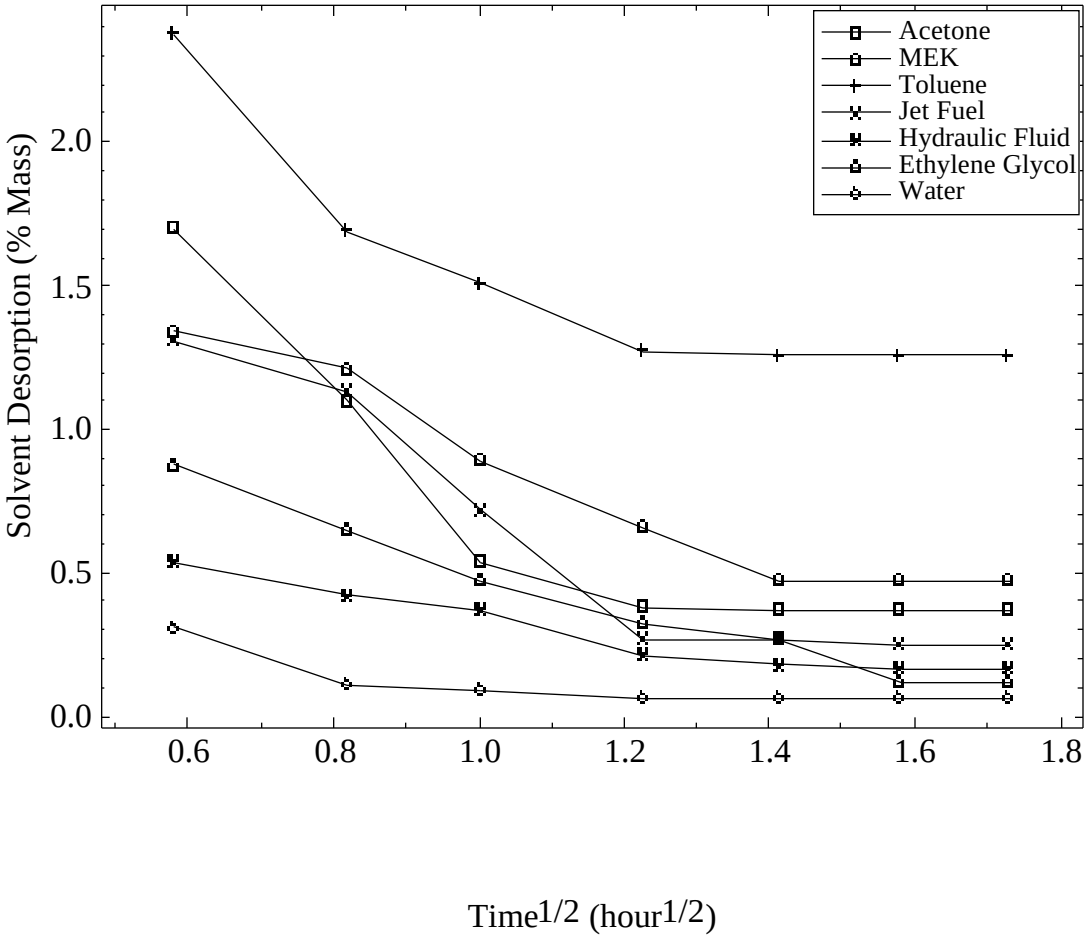

Figure 4.2. Desorption curves for FM-5 neat resin specimens.

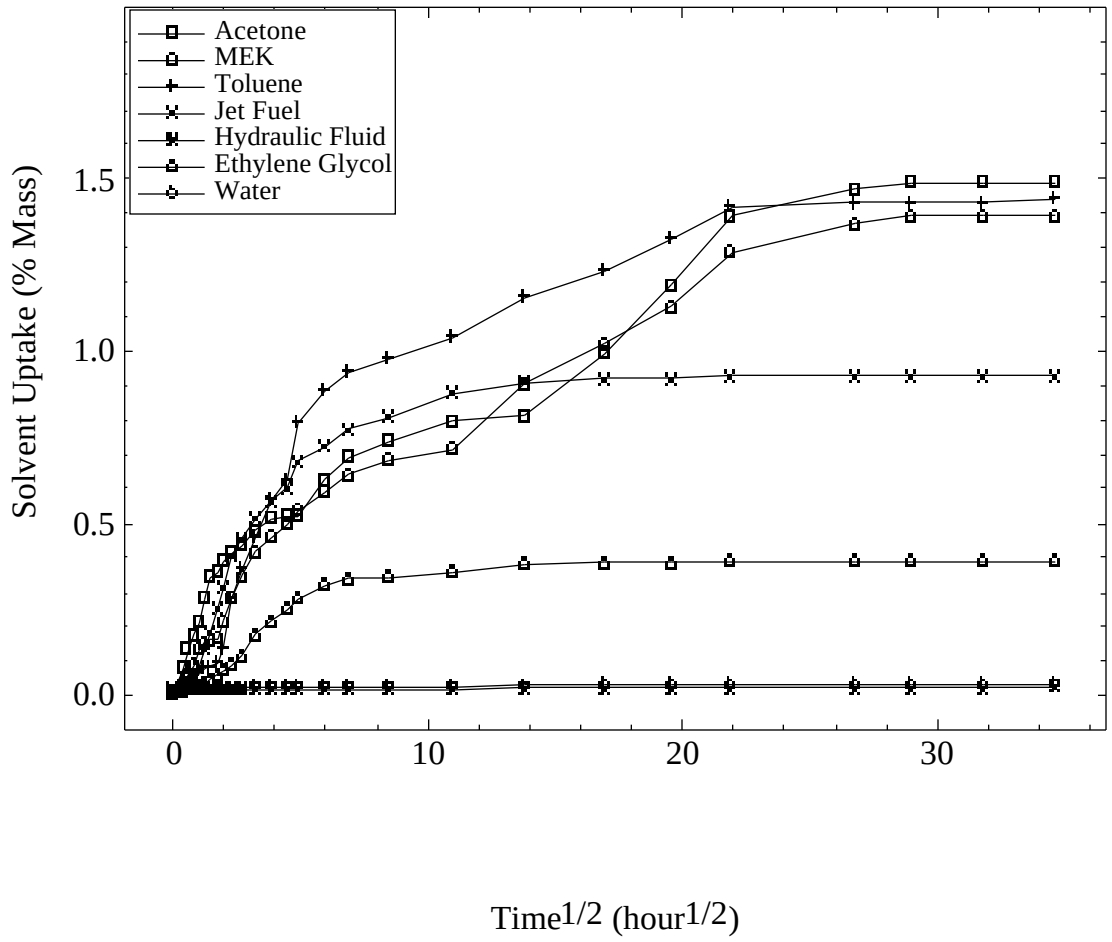

Figure 4.3. Equilibrium solvent mass uptake curves for REGULUS^{TM} neat resin specimens.

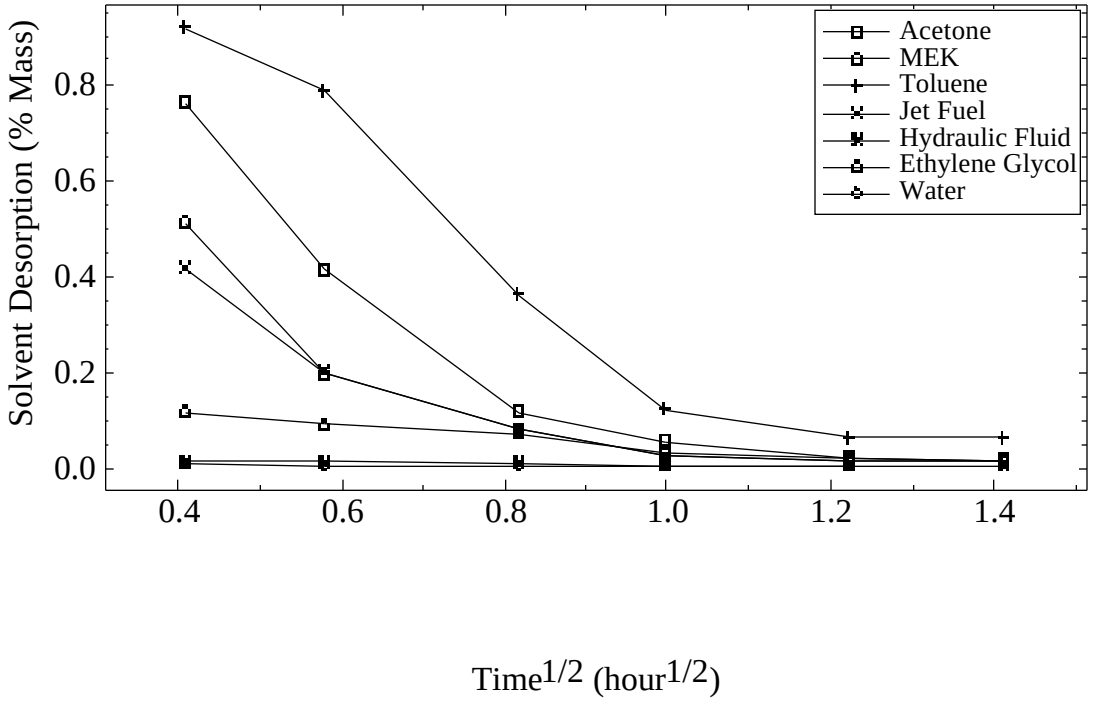

Figure 4.4. Desorption curves for REGULUS™ neat resin specimens.

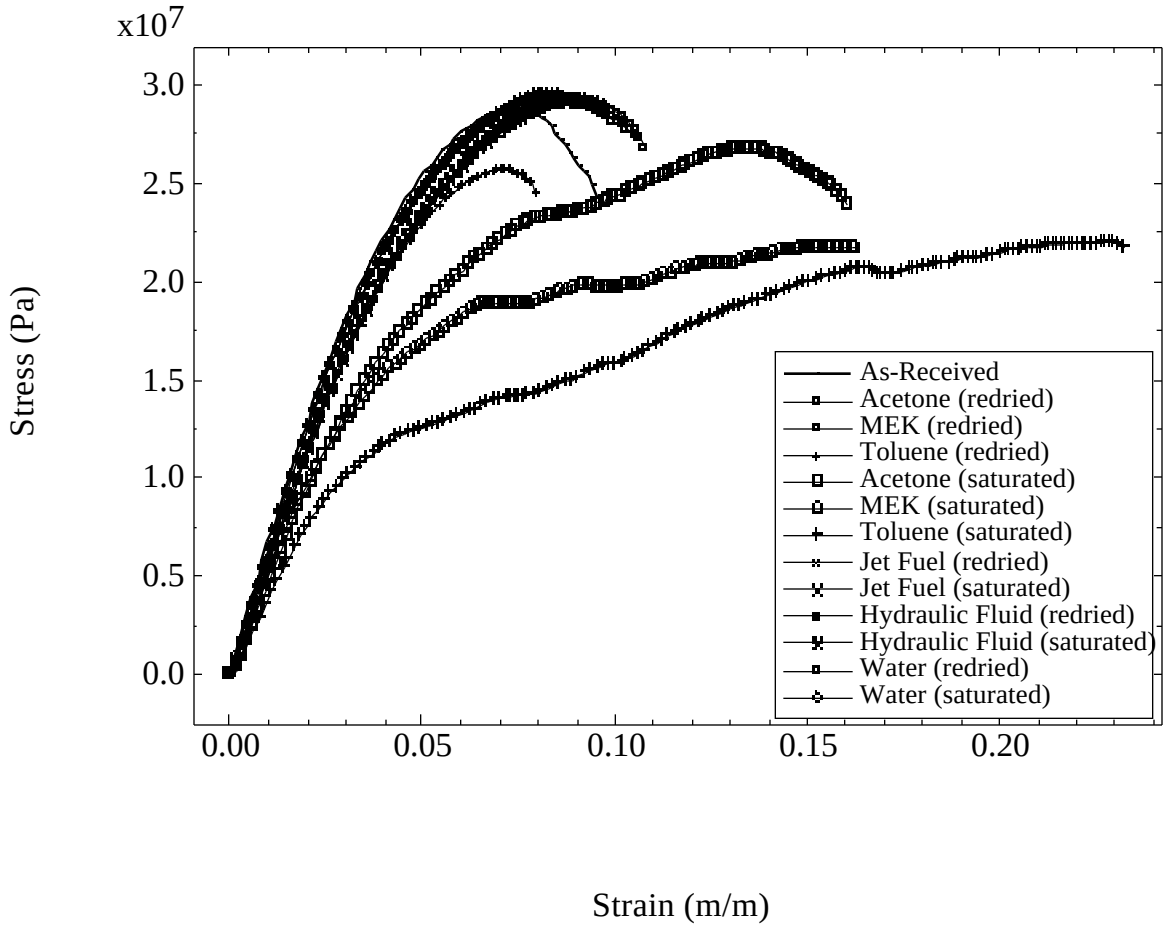

Figure 4.5. Stress-strain curves from solvent saturated and redried FM-5 neat resin specimens.

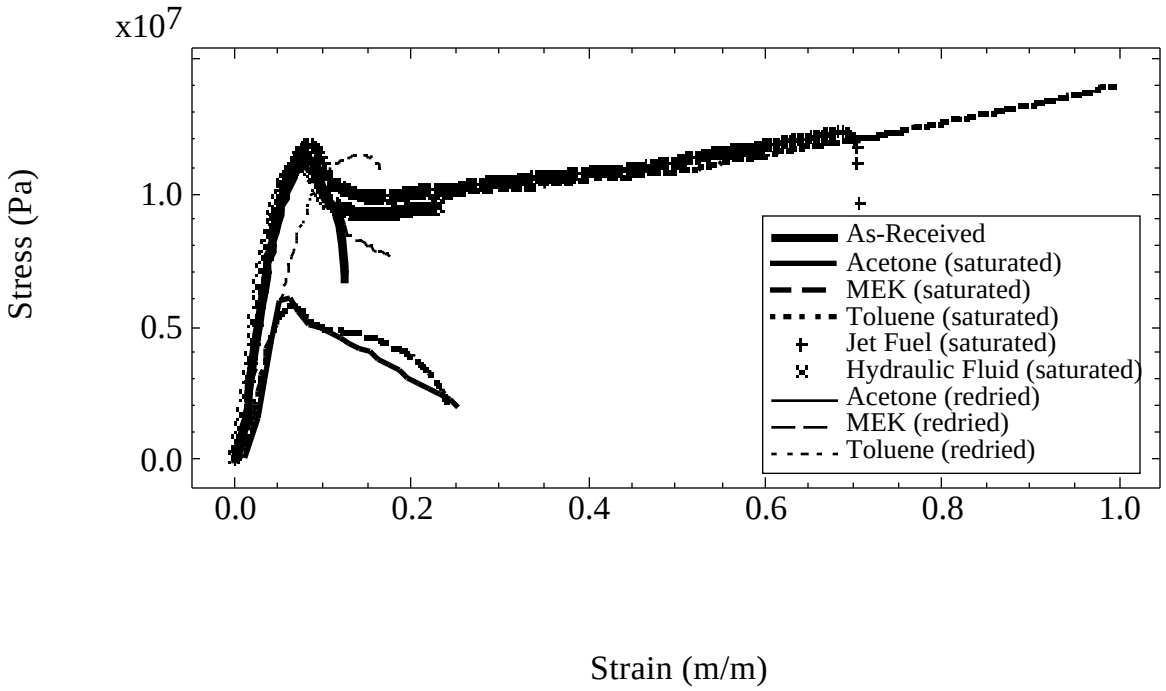

Figure 4.6. Stress-strain curves from solvent saturated and redried REGULUS^{TM} neat resin specimens.

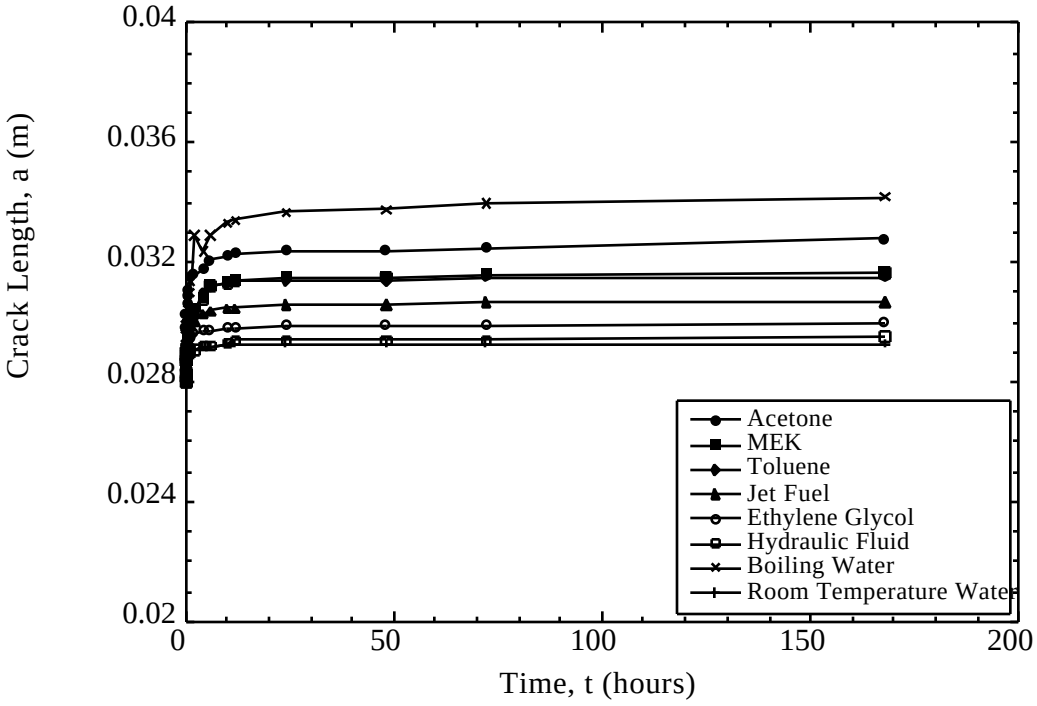

Figure 4.7. Wedge crack length versus exposure time curves for FM-5 neat resin specimens in different solvents. Data were collected for 168 hours.

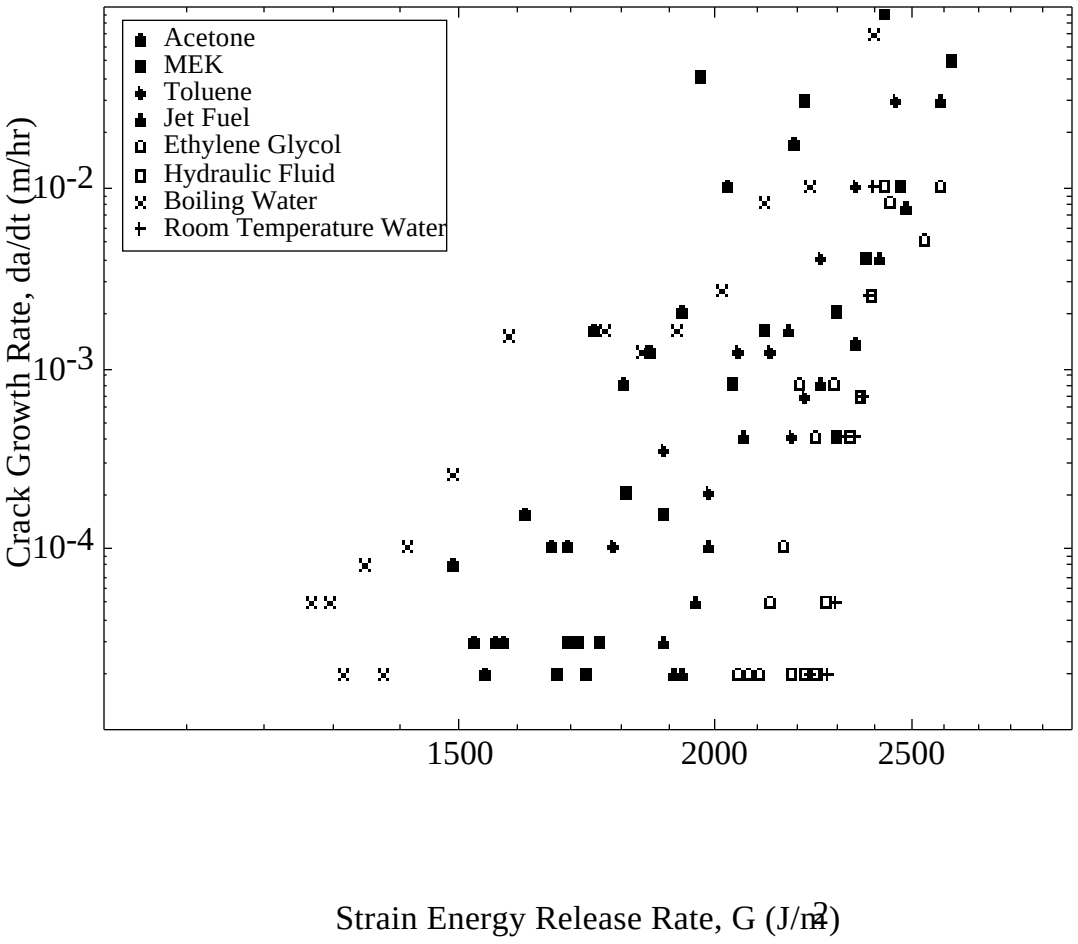

Figure 4.8. Wedge crack growth rate versus fracture energy for FM-5 neat resin specimens exposed to different solvents. Data were collected for 168 hours.

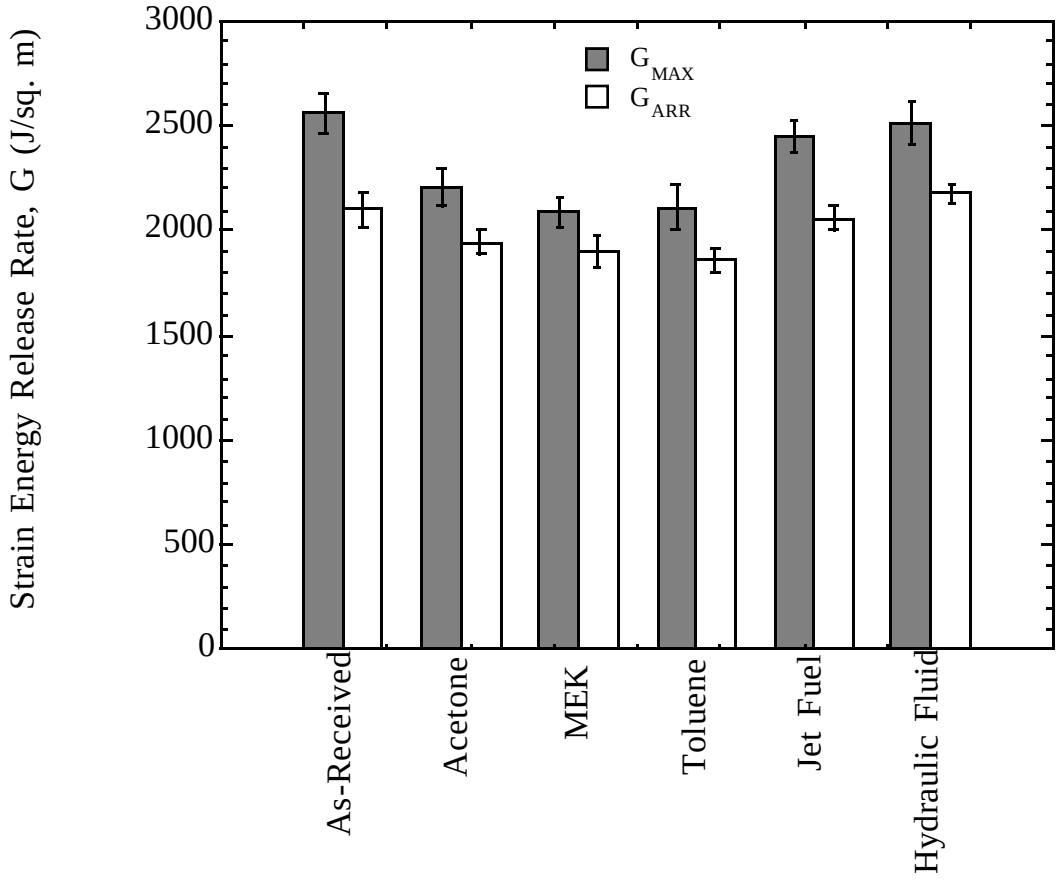

Figure 4.9. DCB test data on anodized titanium/FM-5 bonds immersed in different solvents for 1 month.

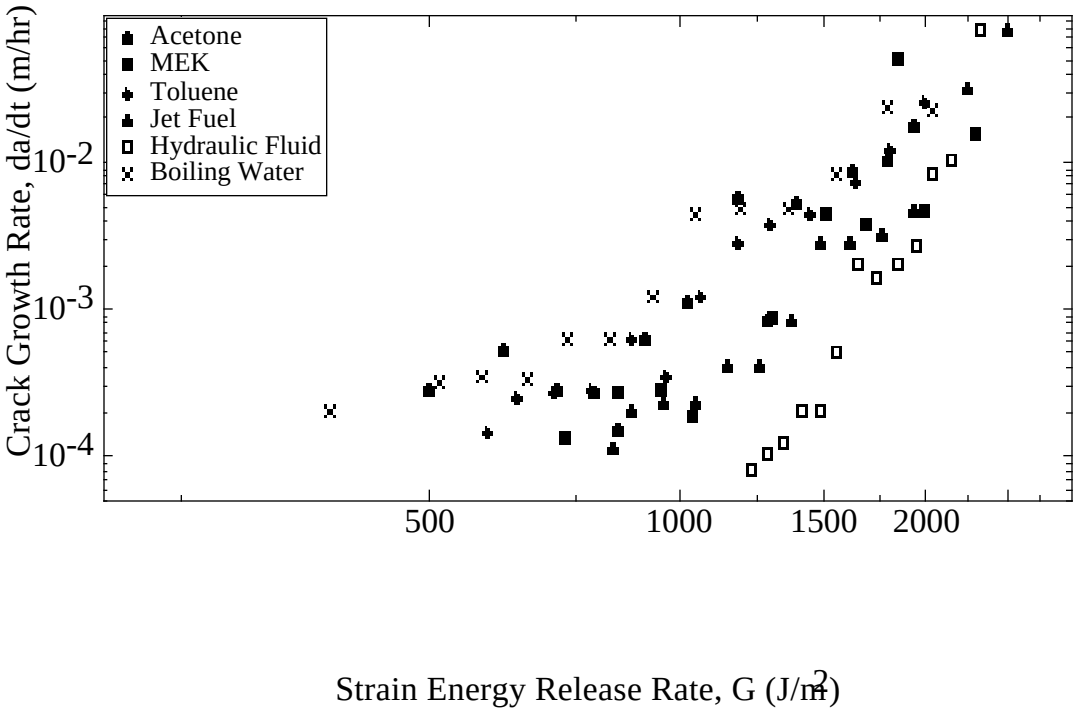

Figure 4.10. Wedge crack growth rate versus fracture energy for REGULUS^{TM} neat resin specimens exposed to different solvents. Data were collected for 168 hours.

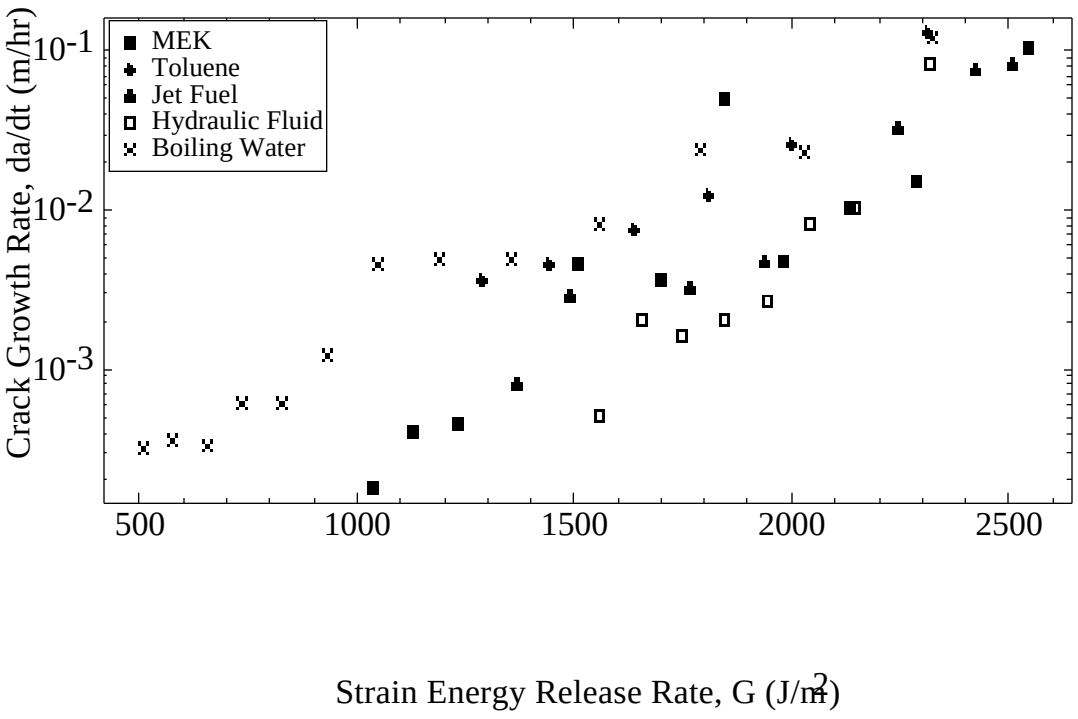

Figure 4.11. Wedge crack growth rate versus fracture energy for VT Ultem neat resin specimens exposed to different solvents. Data were collected for 168 hours.

5.0 Effect of Mode-Mix on Fracture Toughness of Ti-6Al-4V/FM-5 Adhesive Joints

5.0 Abstract

Using fracture tests, the critical strain energy release rate (G_c) of a Ti-6Al-4V/FM-5 adhesive system was evaluated. Pure mode I, pure mode II, and mixed mode (combination of modes I and II) tests were conducted using double cantilever beam (DCB), end notch flexure (ENF), and mixed mode flexure (MMF) geometries. The adherend surfaces were pretreated using chromic acid anodization (CAA) prior to bonding. Interfacial type failures were induced using ENF and MMF specimens as a result of the mode II loading inherent in these tests. Pure mode I loading, as is the case with symmetric DCB specimens, resulted in cohesive failure and fracture energy around 2500 J/m^2, on as-received specimens. The assymetric DCB specimens had fracture energy values around 2000 J/m^2, ENF specimens around 1300 J/m^2, and the MMF specimens close to 1970 J/m$^{2.}$. All the above measurements were made on as-bonded specimens. Titanium/FM-5 bonds supplied by the Boeing Company were then aged in one of three different environments for 2 and 6 months respectively. The environments included: 177°C in air and 2 psia, and 204°C in air. Following the aging, DCB , ENF, and MMF tests were conducted on the specimens. The results showed that aging in all three environments resulted in decreases in fracture energy for the above specimen testing configurations. The biggest drop in G_c of around 20%, was noted in specimens aged for 6 months in air at 204°C. An unusual finding from this study, in sharp contrast to what other researchers have seen on other systems, was that pure mode II fracture energy was significantly lower than mode I fracture energy values. It is believed that crack path selection within the bonded specimens may have played a significant role in causing the lower mode II fracture energies. From the tests conducted, failure envelopes were developed to predict failure energy and type for use in designing structural joints.

5.1 Introduction

For isotropic materials mode I is the lowest fracture energy mode, and cracks typically propagate along a path normal to the direction of maximum principal tensile stress [1]. However, this is not necessarily the case with respect to adhesive joints since crack propagation is often constrained to the adhesive layer, and/or interfaces [1]. Therefore, for the fracture of joints, attention must be given to joint fracture and failure under additional loading modes.

Anderson, et. al. [2] reported from their study with polyurethane/PMMA bonds, that the adhesive fracture energies measured under different loading modes were in the order; modeI<modeII<modeIII. Several studies have been conducted on structural adhesives involving fracture under mode II, combined mode I and II, and mode III loadings (see Figure 5.1 for the three modes of loading). Bascom, et. al. [3], in their study with brittle DGEBA-TEPA adhesive, reported that the mode I fracture energy value was lower than the mode II strain energy release rate. In a study involving a rubber toughened epoxy system, it was reported that the mixed mode G_{I/II_φ} (angle φ increases with increasing mode II loading) values are lower than G_I or G_{II} values, with the latter two fracture energies being approximately equal in magnitude [4]. No apparent explanations were given for the above behavior. In the same study Bascom, et. al. [4] revealed that, apart from the mixed mode fracture energy values being lower than the mode I and mode II fracture toughness values, there existed a maximum in G_{I/II_φ} at $\varphi = 45^o$. A scarf geometry was used in the above study to collect the mixed mode data, and the explanation given for the above observation is that the locus of failure is focused into the interfacial region by the combined stress loading which restrains the development of a large plastic zone at the crack tip. A study by Mall and Kochhar [5] on a commercial rubber toughened adhesive reported that the fracture energy values were very similar for mode I, mode II, and combined mode I and mode II loadings. The only obvious difference between the studies reported in references 4 and 5 besides the adhesive itself, was that while Bascom, et. al. used a scarf joint to obtain mixed mode loading, Mall and Kochhar used a cracked lap shear specimen. Chai [6] studied the effect of bond thickness on G_{Ic}, G_{IIc}, and G_{IIIc} using a brittle and toughened adhesive system. He noted that while G_{IIc} and G_{IIIc}

were essentially of the same magnitude, they were up to 40 times higher than G_{Ic} at common bond thicknesses. Equality in all three toughnesses could only be seen when the results were extrapolated to submicron bond thicknesses. It is however worth noting that the adhesives used by the author in reference 6 were neither scrimmed nor did they contain glass beads for maintaining constant bondline thickness. In a more recent study Leichti and Freda [7] studied the effect of mode I, mode II and mode I-II loading on the fracture toughness of aluminum bonded to FM300 adhesive. The FM300 adhesive was impregnated onto a scrim cloth which was a tricot knit carrier cloth in this case. The authors in reference 7 noted that the mode II fracture toughness measured from ENF tests was 60% higher than the mode I toughness measured from DCB tests. On the other hand, they found that the mixed-mode toughness measured from the MMF test specimens was almost equivalent to the mode I fracture toughness. Ripling, et. al. [8] studied the mode I and mode I-III fracture toughness of aluminum bonded with FM300K adhesive. The FM300K designation indicates that the scrim in this case was an open knit cloth carrier compared to the tricot knit carried used by Leichti and Freda [7]. The authours in reference 8 reported that the mixed-mode toughness of FM300K was twice its mode I fracture toughness. The reason for the difference in results obtained by Ripling, et. al. [8] as compared to Leichti and Freda [7], was that under mode I loading, the open knit carrier separated from the adhesive without being torn itself, while in mode I-III loading, crack growth resulted in a tearing of the cloth, give rise to greater energy dissipation and a higher fracture toughness.

In the present study, critical strain energy release rates (G_c) of the Ti-6Al-4V/FM-5 adhesive bonded system are being evaluated utilizing static loads on symmetric double cantilever beam (DCB), asymmetric DCB, end notch flexure (ENF), and mixed mode flexure (MMF) fracture specimens (see Figure 5.2a-d). The current project is part of a comprehensive study to develop a durable adhesive bonded system for application in the proposed Mach 2.4 high speed civil transport (HSCT) aircraft. Previously, static strength studies on long term aged DCB specimens of the Ti-6Al-4V/FM-5 bonded system have produced cohesive failures (failure within the adhesive layer) [9]. To better investigate the interphase region between the adhesive and the titanium metal substrate, other fracture tests were chosen to induce interfacial failures and

study the energy associated with these failures. As mentioned above, four different fracture tests were performed on the adhesive system producing, in each case, a different mode or mode combination of failure.

5.2 Experimental

5.2.1 Materials

The adhesive used in this study was designated as FM-5, a thermosetting polyimide modified from the original LaRC PETI-5 polymer synthesized at NASA Langley Research Center [10] and supplied by Cytec Engineered Materials Inc., Havre de Grace, Maryland. The adhesive was supplied as a polymer film supported a woven fiberglass scrim cloth containing 85% polymer by weight. The supported film was used to bond titanium adherends to conduct DCB, ENF, and MMF tests.

The adherends used in the study were cut from Ti-6Al-4V plates into bars having dimensions of 200 x 25.4 x 3.175 mm and 200 x 25.4 x 6.350 mm, and purchased from President Titanium Company, Hanson, Massachusetts.

5.2.2 Surface Pretreatment

The samples were prepared, prior to bonding, using a chromic acid anodization (CAA) treatment. First, the titanium adherends were cleaned with acetone and a 3M Scotch-Brite^{TM} pad. After ensuring that most of the surface contaminants were removed, the titanium was then rubbed with #800 crocus cloth. Following this step, the titanium was soaked in Isoprep 177 for 10-15 minutes, followed by a 5 minute bath in boiling water. The samples were subsequently placed in a solution of nitric acid (HNO_3)/hydrofluoric acid (HF) for 1.5-3 minutes followed by a cold deionized water rinse. The anodization was accomplished at 5-6 volts and a current of .20-.40 amps/m^2 for 20 minutes using Ti-6Al-4V plates as cathode. After rinsing in deionized water,

the samples were dried in an oven for 1-1.5 hours at 60°C, and specimens were fabricated within 72 hours of completing the treatment.

5.2.3 Specimen Preparation and Fabrication

Symmetric double cantilever beam and end notch flexure specimens were produced by individually bonding 200 x 25.4 x 3.175 mm or 200 x 25.4 x 6.350 mm plates of pretreated Ti-6Al-4V. Also, plates with thicknesses of 3.175 mm were bonded with 6.350 mm plates for use in the unsymmetric DCB tests. The mixed mode flexure specimens were made by bonding the plates with the same geometry, but a 50 mm length was cut off of one aherend leg after bonding. The supported film was cut to dimensions of 200 x 25 mm and placed between the titanium adherends. The thickness of the adhesive film was found to be 0.5 mm initially and 0.15 mm after bonding. The drop in the thickness of the adhesive layer following the bonding procedure resulted from a "squeezing-out" of the adhesive from the specimen edges during the cure-cycle. This "squeeze-out" would have been considerably reduced if larger panels were bonded together, instead of bonding individual specimens. Irrespective of this adhesive flow problem, which was initially viewed with some concern, there were no noticeable differences in properties within different test specimens made in different batches.

The CAA treated titanium pieces were bonded using the following cure cycle. The adhesive system was initially heated to 250°C at a heating rate of 5°C/min. and held for 30 minutes. The specimens were then heated to 350°C at the previous heating rate and held for 60 minutes under a pressure of 75 psi (0.518 MPa). Following the cure at the high temperature and pressure, the specimens were cooled to room temperature at a rate of 15°C/min. This cure cycle was developed in order to minimize air bubbles and voiding in the specimen bondline. For the aging study, samples were supplied by the Boeing Company. The difference in the samples made at Virginia Tech and Boeing is that while samples at Virginia Tech were individually bonded, those made at Boeing were machined out after bonding a larger panel. Another difference

is that the samples made at Boeing had a primer applied to the titanium metal prior to the bonding.

5.2.4 Specimen Conditioning

Aging in atmospheric air was accomplished in convection type ovens manufactured by Precision Scientific Group, Chicago, Illinois and these were maintained at temperatures of 177^{o}C and 204^{o}C. A vacuum oven (used in conjunction with a vacuum pump) was used to age bonds at 177°C in the reduced air pressure of 2 psia (13.8 KPa).

5.3 Testing

5.3.1 Static DCB Analysis and Testing (Symmetric and Unsymmetric)

The fracture energy of the static symmetric and unsymmetric DCB tests was determined by using equation 5.1 (given below), which was derived using the compliance method with corrections for the crack length offset and adherend stiffness [11-13] and also accounts for crack tip deflections and rotations. The symmetric DCB test is a pure mode I (opening) specimen in comparison to the unsymmetric DCB test which is 92% Mode I and 8% Mode II (G_{II}/G=8%) [14].

$$G = \frac{9\Delta^2 (EI_{eff})}{4B(a + x)^4} \qquad 5.1$$

where,

B: specimen width

a: crack length

x: apparent crack length offset

EI_{eff}: effective flexural rigidity

Δ: specimen's opening displacement at point of load application

The parameters EI_{eff} and x are determined from experimental data according to:

$$EI_{eff} = \frac{2}{3m^3} \quad \text{and} \quad x = \frac{b}{m} \qquad 5.2$$

where the experimental coefficients m and b are the slope and y-intercept, respectively, of the cube root of the measured compliance plotted as a linear function of the crack length. Compliance, C, is obtained by dividing the specimen's crack opening displacement, Δ, by the corresponding load, P, where Δ and P are experimentally measured. Due to the linear relationship of the experimental data, a value of the crack length can be obtained for a given crack opening displacement, Δ, and the load, P, and the strain energy release rate G computed. This procedure is a modification of the ASTM D3433 standard [15].

Static DCB specimens were tested in an Instron machine controlled through its GPIB interface using LabVIEW software developed by National Instruments, Austin, Texas. The specimens were loaded at a crosshead speed of 1 mm/minute. As a specimen was loaded, several events took place which can be clearly seen on a typical load versus deflection plot. For example, when the curve deviates from linearity, the crack had begun to grow and the critical fracture energy, G_{IC}, has been reached. Due to the rate dependent failure of these adhesive systems, the loading value continued to increase. When the load reached a maximum and began to rapidly decrease, the specimen had achieved a maximum loading level, G_{MAX}. Once the maximum loading was detected, the crosshead motion was stopped to allow the crack growth to continue until it approached equilibrium conditions. The criterion used to establish a reasonable arrest loading level was that the value of strain energy release rate decreased by less than 1 J/m^2 per minute. This procedure was used to identify the arrest fracture energy, G_{ARR}. Once crack growth slowed sufficiently, the specimen was unloaded to ensure plastic deformation of the adherends had not occurred. If plastic deformation had occurred, the P-Δ curve would not return to the origin, but instead would intersect the deflection-axis to the right of the origin. Finally, the load-hold-unload procedure was repeated until the specimen failed. It was seen that in all the DCB tests reported, the P-Δ curves did return to the origin indicating that there was no

significant plastic deformation of the adherends. This was also confirmed by observation that there was no permanent curvature in the beams.

5.3.2 ENF Analysis and Testing

The fracture energy of the end notch flexure tests was determined by using equation 5.3, which was derived using the compliance method [7,16,17]. ENF specimens were also tested in an Instron machine controlled through its GPIB interface using LabVIEW software. The test fixture used for this study was a standard three-point bend fixture. Each specimen was loaded at a crosshead speed of 0.5 mm/minute in the elastic range, sliding the specimen in the fixture between loadings to vary the crack length. Load-displacement plots were obtained for crack lengths of 0, 15, 20, 25, 30, 35, and 40 mm (measured from the specimen edge), and a compliance versus crack length curve was plotted for each specimen. The parameter, EI_{eff}, was also determined experimentally for each specimen. Following the determination of the compliance versus crack length curve, the ENF test was performed by loading the specimen in flexure until a crack grows from the root of the starter crack. This crack grows rapidly until it reaches the mid-span of the specimen and arrests at the position of the load nose. By providing a large overhang at the unnotched end, the specimen is shifted over and reloaded to obtained a second, third and fourth fracture energy values.

$$G = \frac{3(a + x)^2 P^2}{64BEI_{eff}} \qquad 5.3$$

where,

a: crack length

B: specimen width

EI_{eff}: effective flexural rigidity

P: load

5.3.3 MMF Analysis and Testing

The fracture energy of the mixed mode flexure tests was determined by using equation 5.4, which was derived using the compliance method [18-20]. MMF specimens were also tested in an Instron machine controlled through its GPIB interface using LabVIEW software, and at a crosshead speed of 0.5 mm/minute. The MMF specimen is similar to the pure Mode II ENF specimen except that at one end, the load is applied to the upper arm only, thus providing crack opening as well as shear. The opening mode contribution to the MMF specimen was calculated using beam theory and was found to be 57% (G_I/G=57%) [18]. The testing of the MMF specimens was carried out similar to the ENF specimens, and a compliance versus crack length calibration curve was plotted for each specimen. The parameter, EI_{eff}, was then determined from the experimental compliance versus crack length plots for each specimen.

$$G = \frac{7(a+x)^2 P^2}{64BEI_{eff}} \qquad 5.4$$

where,

a: crack length

x: crack length correction

B: specimen width

EI_{eff}: effective flexural rigidity

P: load

5.4 Results and Discussion

5.4.1 DCB Results (Symmetric and Unsymmmetric)

The strain energy release rate for as-bonded symmetric DCB (pure mode I) specimens having 3.175 mm thick adherends was: G_{MAX}~2500 J/m^2 and G_{ARR} ~ 2100 J/m^2 (see Figure 5.3) To address a concern that the adherends being used in the testing were not of a sufficient

thickness to prevent yielding, 6.350 mm thick adherend specimens were tested and the results (Figure 5.4) showed the strain energy values of the thicker specimens to be consistent with the values obtained from the 3.175 mm specimens. The failures in the specimens were found to be of a cohesive type, that is, within the adhesive layer, as can be seen from a photograph of the fracture surface shown in Figure 5.5. However, it is to be noted that the actual failure occurred at the interface of the adhesive and the supporting glass cloth.

As previously noted, the combination of 3.175 mm adherends bonded to 6.350 mm adherends produces a mixed mode combination of 92% mode I and 8% mode II. For these specimens the average G_{MAX} was found to be 2000 J/m^2 and G_{ARR} to be around 1800 J/m^2. These results are summarized in Figure 5.6. The observed failure was found to be predominantly cohesive but some small regions of interfacial failure were also seen, upon visual observation.

To study the effect of elevated temperature aging in different air pressure environments, DCB samples supplied by the Boeing Company were aged for periods up to 6 months. The aging environments included; 177°C in air and 2 psia, and 204°C in air. Symmetric DCB tests were conducted following both 2 and 6 months of aging in the above environments. A 5-10% drop in fracture energy was seen over a 6 month aging period, with the biggest drop in fracture energy recorded in samples aged at 204°C in air. These results are summarized in Figure 5.7. The failure in all the aged specimens continued to be cohesive.

5.4.2 ENF Results

The results of the end notch flexure tests (as-received) on symmetric thickness specimens (3.175 mm thick) which produced a pure mode II loading, showed the average maximum strain energy release rate to be 1300 J/m^2, and the average arrest strain energy release rate to be 1180 J/m^2. The results are summarized in Figure 5.8. The failure that resulted upon fracturing the specimens was interfacial, as can be seen from the photograph of a failed sample, shown in Figure 5.9. Visual observations indicated titanium metal on one side with the matching adhesive on the other adherend surface. However, when XPS analysis was performed on the failure surfaces, the

metal failure side (mfs) showed small traces of titanium metal, and constituents that were characteristic of the adhesive material. This was indicative of failure in the adhesive material in near interfacial region, and not in the metal oxide layer. Upon aging the specimens for 6 months at elevated temperature, there was a 20% drop in mode II fracture energy. The average maximum fracture energy from samples aged for 6 months in air at 204°C was 980 J/m^2 (see Figure 5.10). Once again interfacial failures were noted from visual observation of the fracture surfaces. XPS analysis of the failed samples showed both titanium and aluminum concentrations on the metal failure side (mfs) and traces of titanium on the adhesive failure side (afs). These results are compared with those obtained from fully cured scrimmed FM-5 adhesive and summarized in Table 5.1. One conclusion that could be drawn from the above results is that aging tends to move the locus of failure closer to the metal-adhesive interface (that is near to or within the metal oxide layer), and the XPS results on the aged specimens support this claim.

5.4.3 MMF Results

By cutting one adherend leg shorter and using the ENF test setup, a 57% mode I loading is produced. The maximum strain energy release rates from the as-received the mixed mode flexure specimens was found to be approximately 1970 J/m^2, while the average arrest strain energy release rate was found to be 1800 J/m^2. The results for the maximum energy release rate are shown in Figure 5.11. Due to the significant contributions of both Mode I and Mode II to the failure of the specimen, the fracture surface exhibited a mixed-mode failure (Figure 5.12). Upon aging in air at 204°C for 6 months, the average G_{MAX} value from the MMF tests decreased to 1710 J/m^2, as summarized in Figure 5.13. Failure in the aged samples continued to be of a mixed-mode type as noted from visual observation.

5.4.4 Fracture Toughness/Failure Envelopes

Based on the above four tests, failure envelopes were developed for the Ti-6Al-4V/FM-5 adhesive bonded system both prior to and after aging. The envelope for the as-bonded specimens is presented in Figure 5.14. Inside the envelope, there is not enough energy, under static laboratory loading conditions, for the crack to begin propagating and therefore the specimen will not fail. However, if there is energy sufficient to reach the envelope, the crack will be able to propagate through the bond. Along the boundary, the type of failure, that is whether it is interfacial, cohesive, or mixed, can be predicted. Figures 5.15-5.17 show failure envelopes for the samples aged at 177°C and 204°C for both the 2 and 6 month periods. It is seen that the biggest drops in fracture energy (in mode I, mode II, and combination mode I and II loading) are seen at the 204°C aging temperature. These results are quite consistent with the long-term aging DCB test data collected at different temperatures and presented in chapter 3 of this dissertation. If longer term aging data is collected on the bonded system to generate failure envelopes, then these envelopes can serve as useful tools for designing structural joints such as needed in the HSCT.

5.5 Summary and Conclusions

This chapter addresses the important issue of the effect of mode mixity on fracture toughness of Ti-6Al-4V/FM-5 adhesive joints. Although adhesive joints usually fail under mode I (opening mode) loading situations, it is not possible to discount scenarios where mode II loading (shear loading) plays a significant role in the failure process. It was therefore decided to evaluate the performance of the titanium/FM-5 bonds under conditions of pure mode I, pure mode II, and combinations of mode I and II (mixed-mode) loadings. Tests were conducted on as-bonded specimens and also on aged specimens. The aging was conducted in environments that closely mimicked the expected service environment of the HSCT aircraft structure. All the tests were conducted using a beam type of bonded geometry. The advantage to using this geometry was

that the specimen configuration, via very small modifications, could be used to conduct mode I (DCB), mode II (ENF), and mixed-mode (MMF and unsymmetric DCB) fracture tests.

It is a popular notion that when adhesive joints fail, they fail along the path of least resistance, and consume the least energy during this failure process. The results obtained from the titanium/FM-5 system were quite the contrary. The mode I fracture energies were significantly greater than the mode II fracture energy, and this was in sharp contrast to what other researchers had observed studying bonded joints. While cohesive failures occurred in the samples tested in mode I (that is at the adhesive and glass scrim-cloth interface) near-interfacial failures were observed between the metal and the adhesive during mode II loading. One question that immediately comes to mind is, "why is the crack growth occurring within the adhesive layer dissipating greater energy during the mode I tests, when it can occur at the metal-adhesive interface dissipating much lower energy"?. There are no easy answers to this question as the crack growth process in an adhesive bond is a very complicated phenomena, determined by an interaction of the applied stress state and changes in material properties along the bond length. With respect to the titanium/FM-5 system, one can gage the enormity of the problem that is posed by simply listing the several components that actually make up the final adhesive joint. Firstly there are the bulk Ti-6Al-4V metal adherends, then there is the metal oxide layer that is formed due to the CAA surface pretreatment, and finally there is scrimmed FM-5 adhesive that contacts the oxide layer. There are several interface/interphase regions that are formed between the adherends and the adhesive, and the adhesive and its reinforcing glass cloth. Besides the above components, it must also be mentioned that the FM-5 adhesive itself is a very complex entity with its own set of modifiers, additives, and fillers.

Although there are no direct answers to the above question at this point, there is a feeling that several insights into the failure process can be gained from simply studying and understanding the locus of debond propagation or crack path selection. In the mode I tests, failure was cohesive within the adhesive material, however, the fracture energy obtained was highest because the locus of crack propagation was indirect and tortuous. On the other hand, the mode II tests showed interfacial failures and lower fracture energies. The locus of crack

propagation in this case was much more direct and straight. XPS failure analysis of the as-received ENF test specimens showed the failure to occur in the adhesive material very close to the oxide layer. On the other hand, the aged samples showed failure that was occuring within the metal oxide layer. This clearly shows that the dynamics of the loading process, the changes in the material properties along the length and thickness of the bondline, and environmental aging, play a very important role in determining the locus of joint failure, and thereby the calculated fracture energies.

5.6 References

1. A. J. Kinloch, *Adhesion and Adhesives-Science and Technology*, Chapman and Hall, London, 311-313 (1987)

2. G. P. Anderson, K. L. DeVries, M. L. Williams, *J. Colloid Interf. Sci.* **47**, 600 (1974)

3. W. D. Bascom, R. L. Cottington, C. O. Timmons, *Appl. Polymer Sym.* **32**, 165 (1977)

4. W. D. Bascom, R. L. Jones, C. O. Timmons, *Adhesion Science and Technology*, Vol. **9B**, L. H. Lee (Ed.), Plenum Press, New York, 501 (1975)

5. S. Mall, N. K. Kochhar, *Structural Adhesives in Engineering*, Institute of Mechanical Engineering, London, 71 (1984)

6. H. Chai, *ibid.* **37**, 137-148 (1988)

7. K. M. Leichti and T. Freda, *J. Adhesion.* **28**, 145-169 (1989)

8. E. J. Ripling, P. B. Crosley, and W.S. Johnson, *ASTM STP 981*, 163-182 (1988)

9. H. Parvatareddy, J. G. Dillard, J. E. McGrath, and D. A. Dillard, *J. Adhesion Sci. Technol.* in press (1997)

10. J. G. Smith, and P. M. Hergenrother, *Polymer Pre-prints.* **35**, 353-355 (1994)

11. M. D. Rakestraw, M. A. Vrana, D. A. Dillard, J. G. Dillard, and T. C. Ward, *Durability and Damage Tolerance,* AD-Vol. **43**, *ASME WAM,* 65-77 (1994)

12. M. D. Rakestraw, M. W. Taylor, D. A. Dillard, and T. Chang, *J. Adhesion.* **55**, 123-138 (1995)

13. B. Blackman, J. P. Dear, A. J. Kinloch, S. Osiyemi, *J. Mater. Sci. Lett.* **10**, 253-256 (1991)

14. P. D. Mangalgiri, W. S. Johnston, and R. A. Everett, Jr., *J. Adhesion.* **23**, 263-288 (1987)

15. ASTM D3433-93, *Annual Book of ASTM Standards,* **15.06** Adhesives, 218 (1994)

16. A. J. Russell and K. N. Street, *ASTM STP 876*, 349-370 (1985)

17. E. J. Ripling, S. Mostovoy, and H. T. Corten, *J. Adhesion.* **3**, 107-113 (1971)

18. J. R. Reeder and J. H. Crews Jr., *AIAA J.* **28** (7), 1270-1276 (1990)

19. S. Bashyam and B. D. Davidson, *AIAA-96-1419,* 886-896 (1996)

20. A. J. Kinloch, Y. Wang, J. G. Williams, and P. Yayla, *Composite Sci. Technol.* **47**, 225-237 (1993)

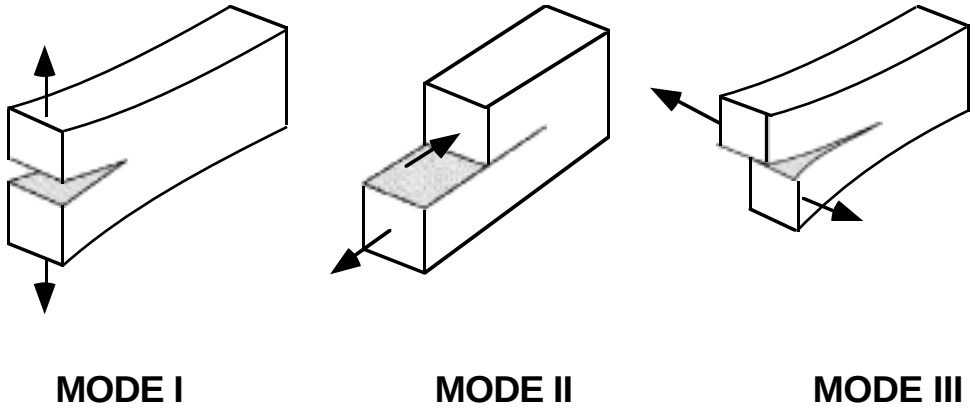

Figure 5.1. Schematic of the three modes of loading. Mode I is opening mode, mode II is shearing mode, and mode III is tearing mode [1].

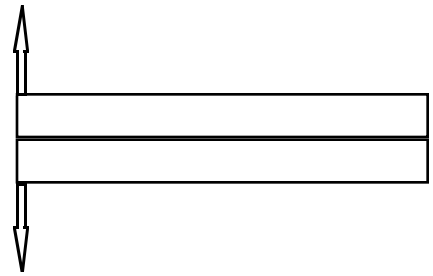

a) Symmetric DCB, Pure Mode I

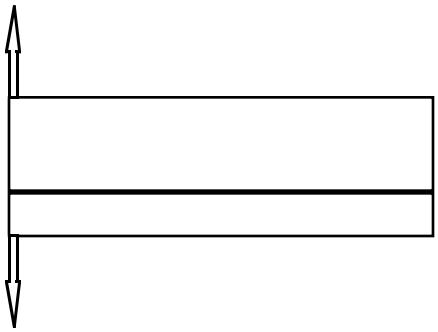

b) Assymmetric DCB, 92% Mode I and 8% Mode II

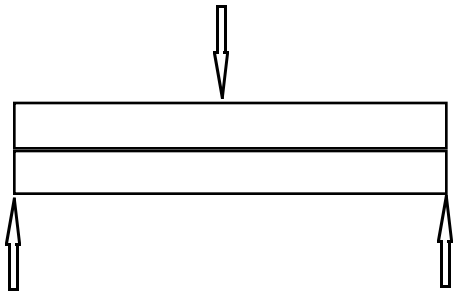

c) End-notched flexure (ENF), Pure Mode II

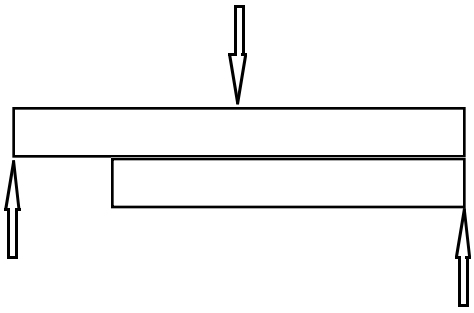

d) Mixed-mode Flexure (MMF), 57% Mode I and 43% Mode II

Figure 5.2. Schematics of symmetric DCB, assymmetric DCB, ENF, and MMF specimen geometries.

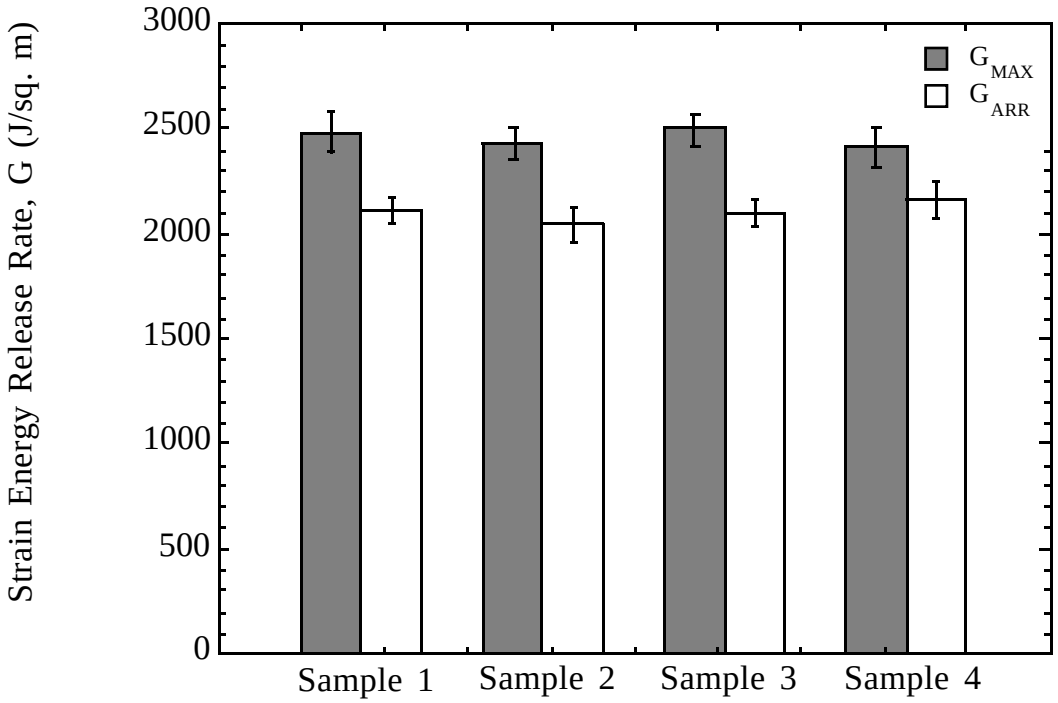

Figure 5.3. Fracture energy for as-bonded symmetric DCB specimens.

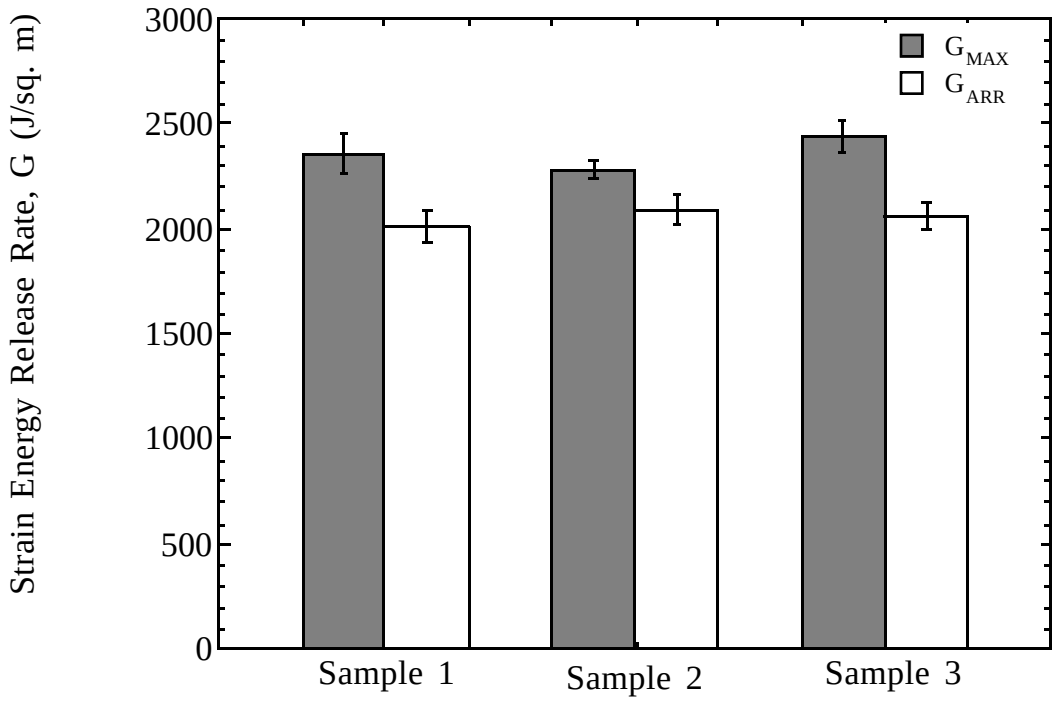

Figure 5.4. Fracture energy for as-bonded symmetric DCB specimens made with 6.350 mm thick adherends.

Figure 5.5. Photograph of the failure surface of a DCB test specimen showing cohesive failure.

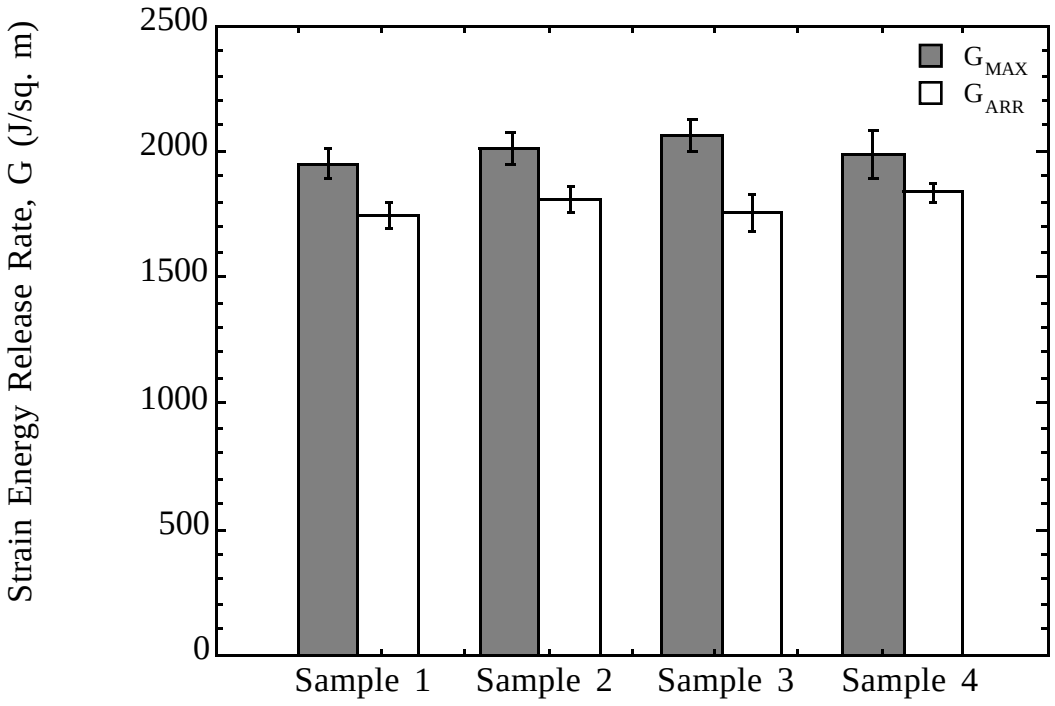

Figure 5.6. Fracture energy for as-bonded unsymmetric DCB specimens.

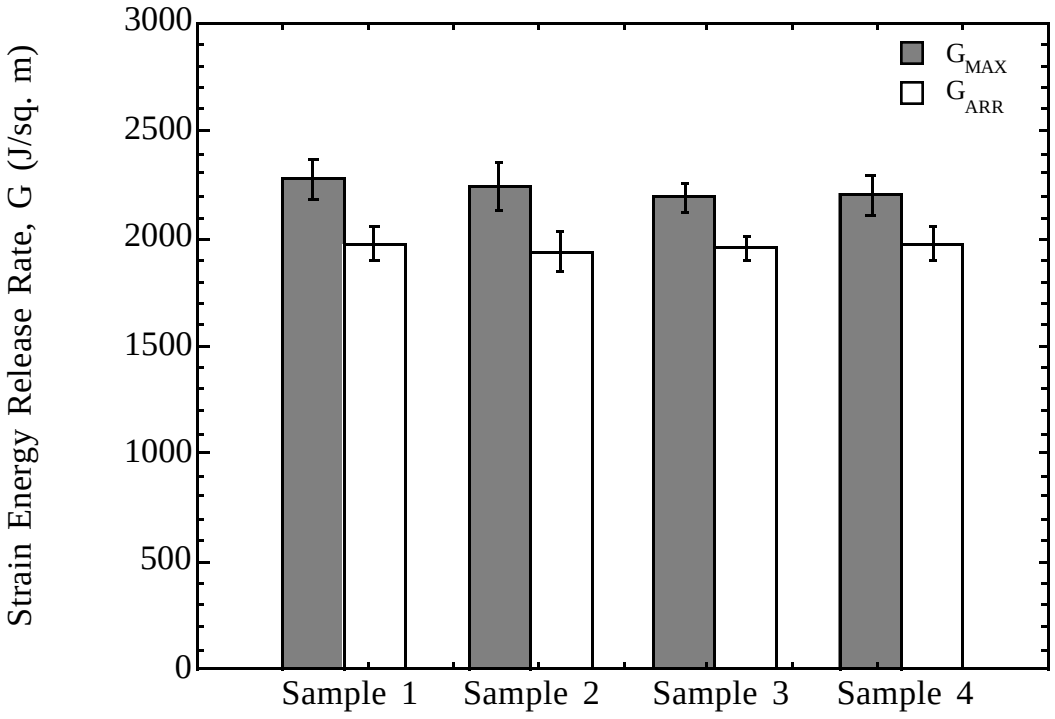

Figure 5.7. Fracture energy for aged symmetric DCB specimens. Samples were aged for 6 months in air at 204°C.

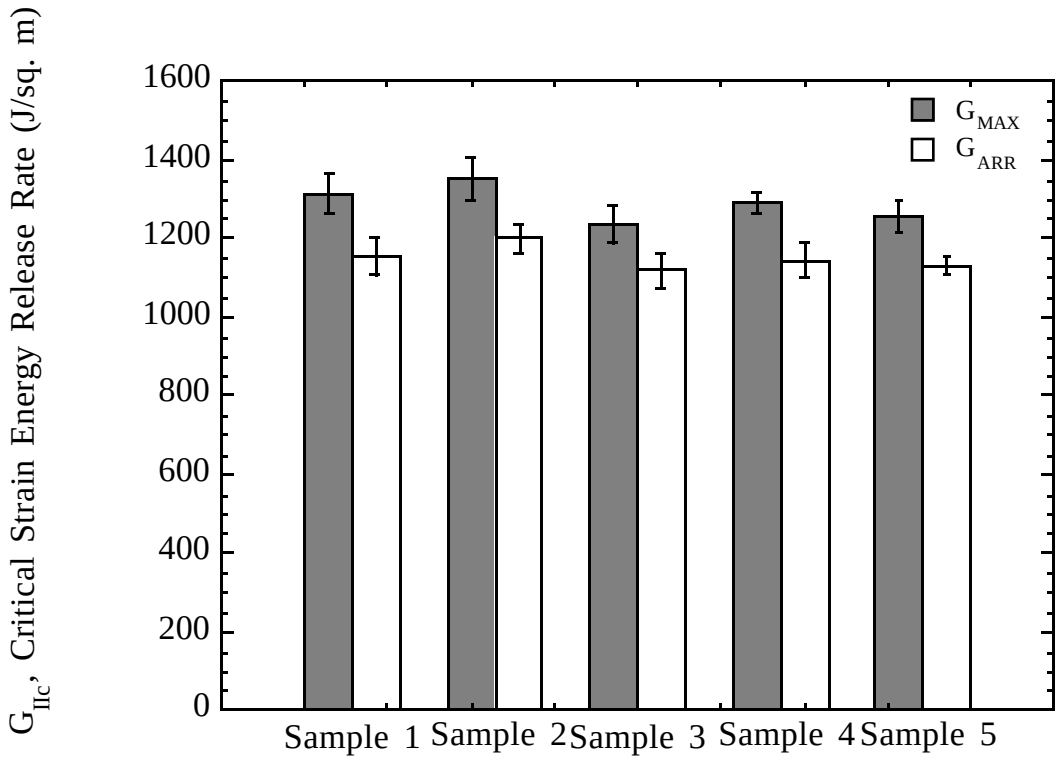

Figure 5.8. Fracture energy of as-received ENF specimens.

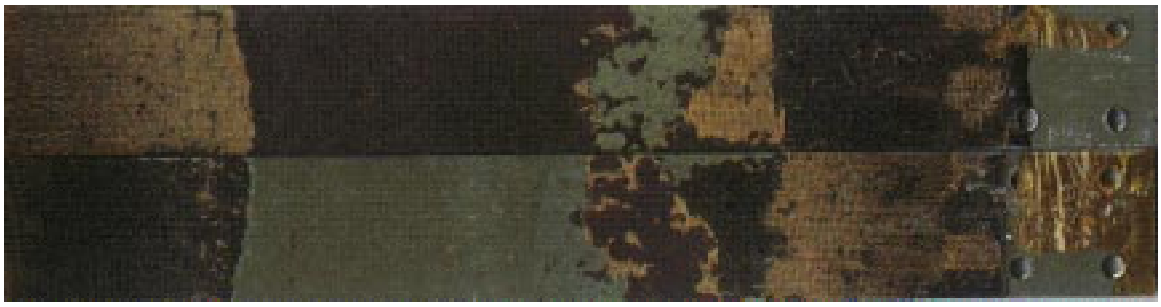

Figure 5.9. Photograph of the failure surface of an ENF test specimen showing interfacial failure.

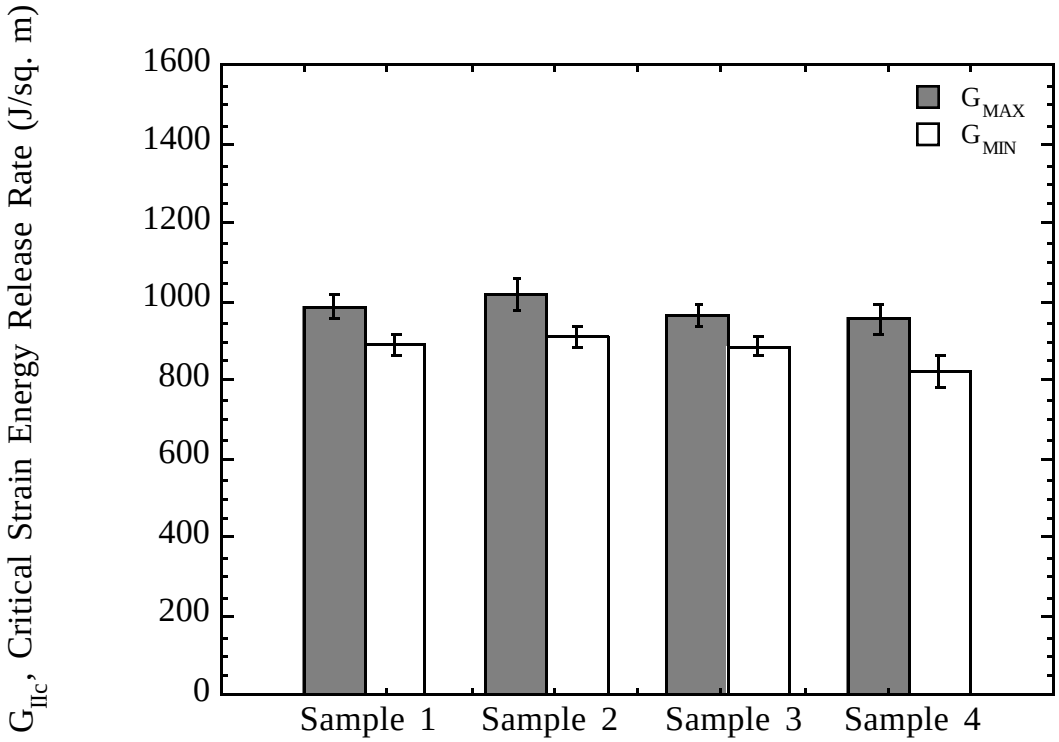

Figure 5.10. Fracture energy for aged ENF specimens. Samples were aged for 6 months in air at 204°C.

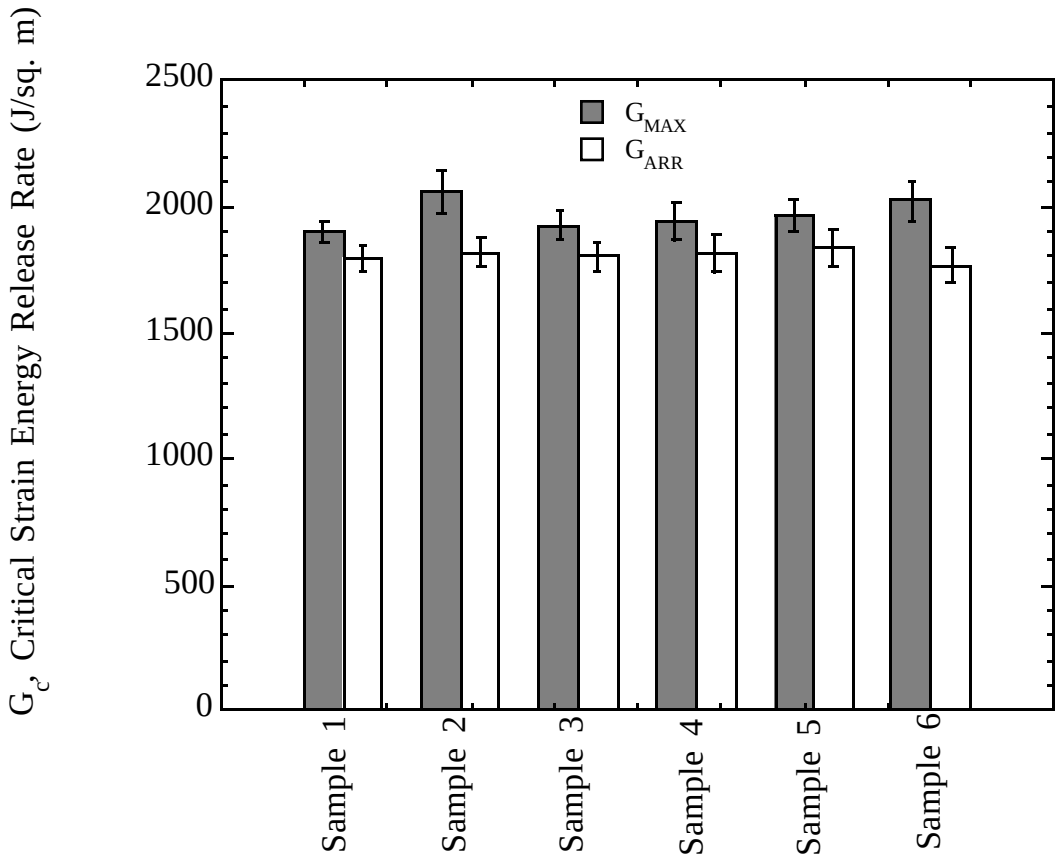

Figure 5.11. Fracture energy for as-bonded MMF specimens.

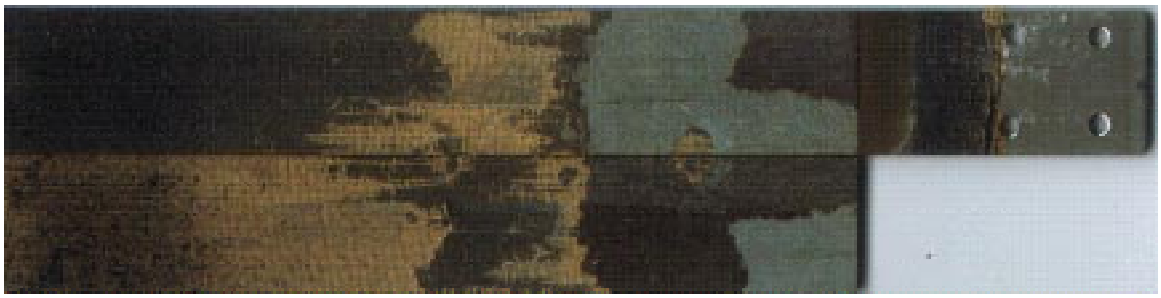

Figure 5.12. Photograph of the failure surface of a MMF test specimen showing mixed-mode failure.

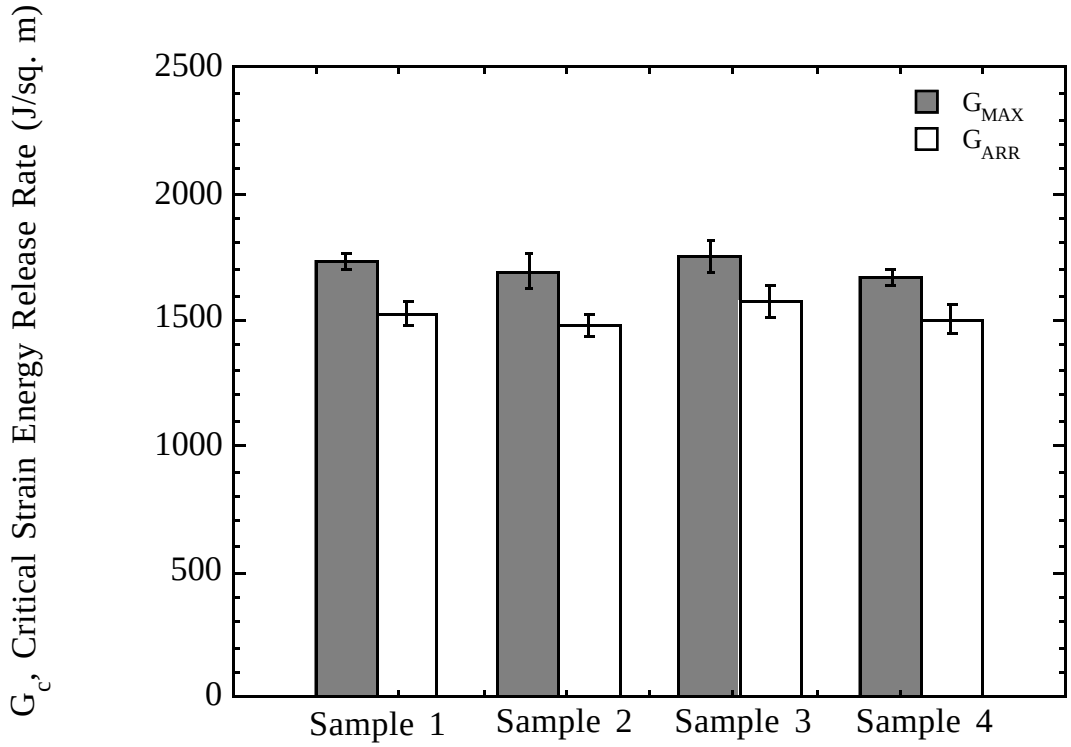

Figure 5.13. Fracture energy for aged MMF specimens. Samples were aged for 6 months in air at 204°C.

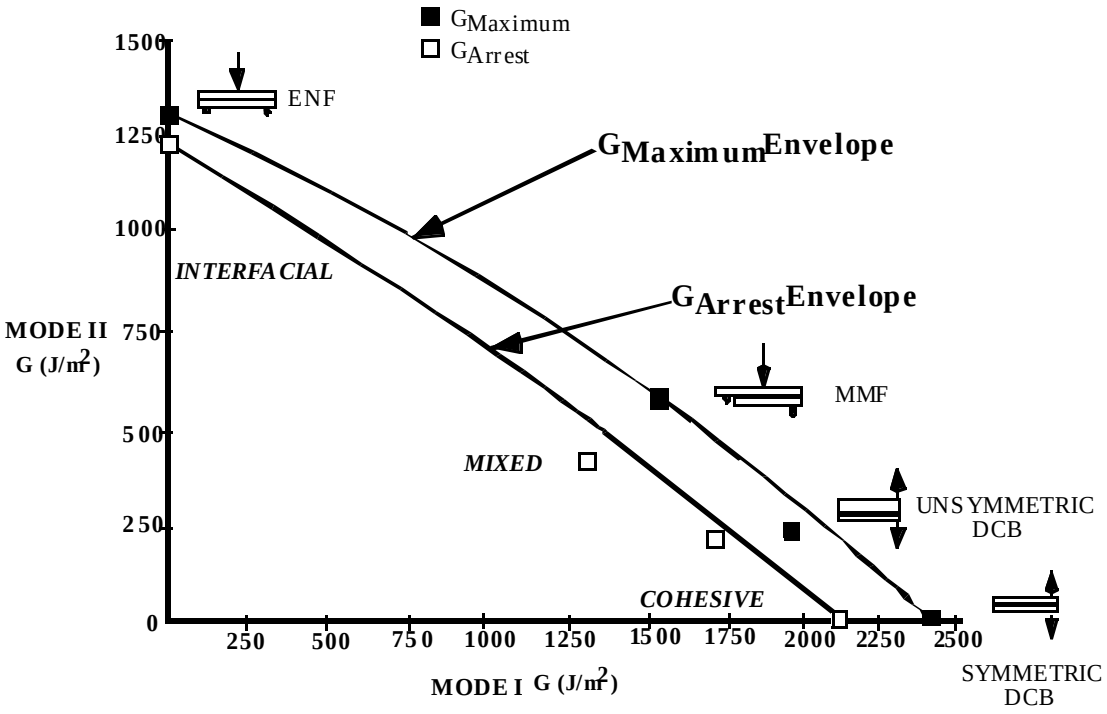

Figure 5.14. Failure envelope for unaged Ti-6Al-4V/FM-5 adhesive bonds.

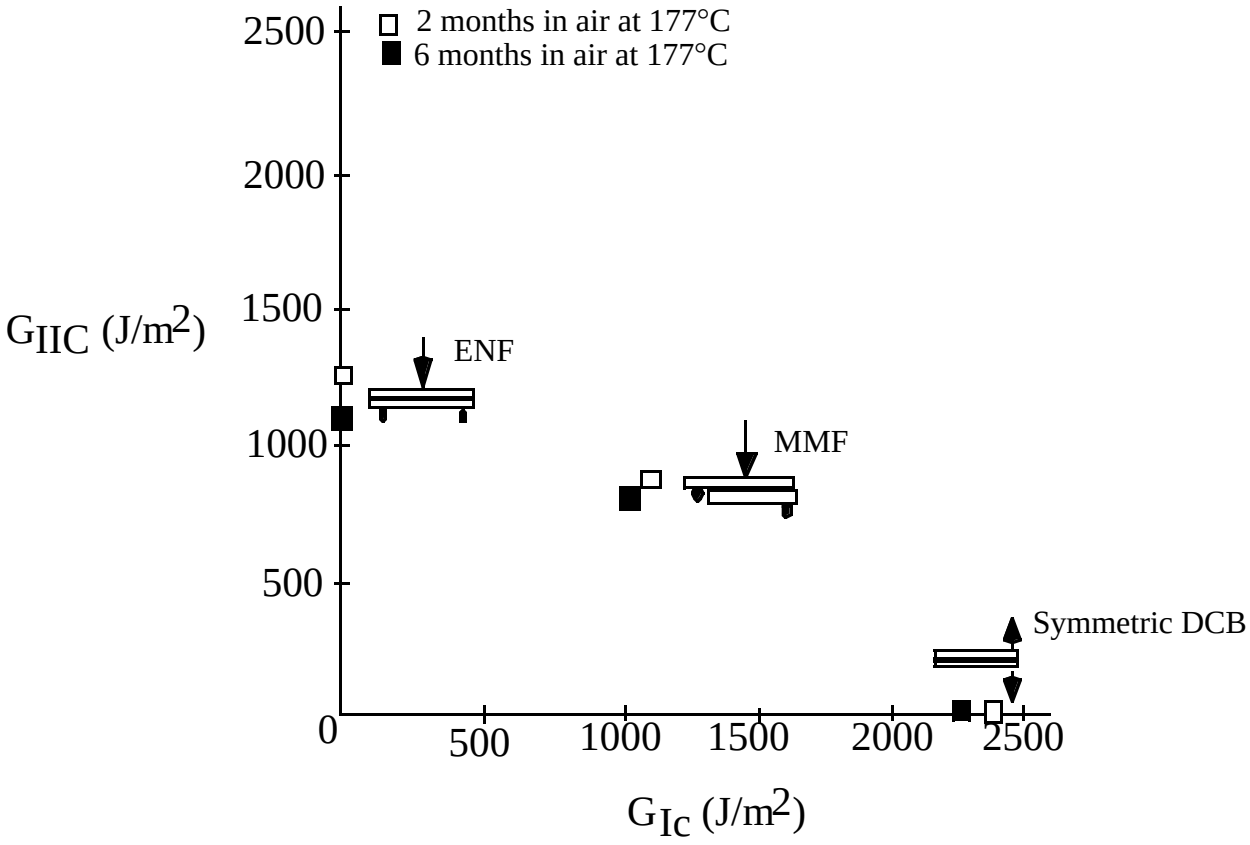

Figure 5.15. Aging failure envelope for Ti-6Al-4V/FM-5 adhesive bonded system. Samples were aged for periods of 2 and 6 months in air at 177°C. Values reported are G_{MAX} values.

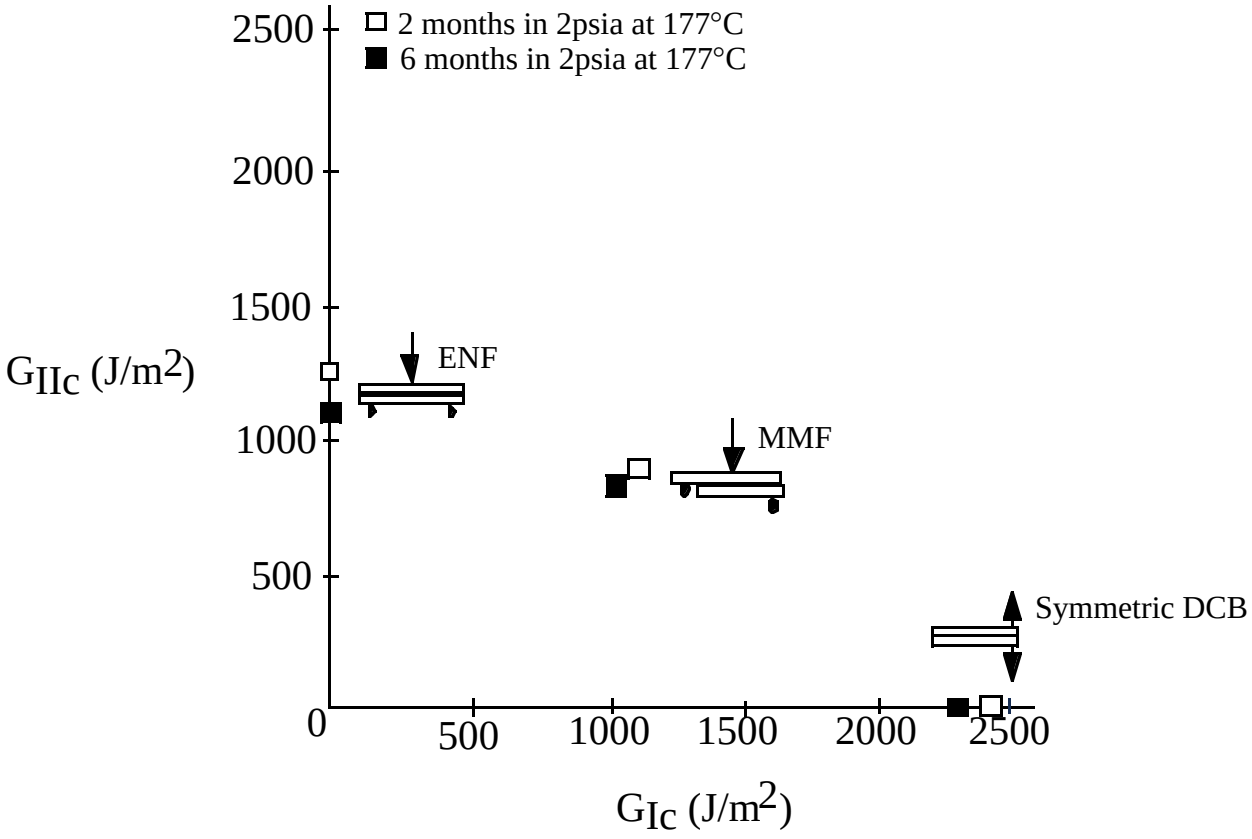

Figure 5.16. Aging failure envelope for Ti-6Al-4V/FM-5 adhesive bonded system. Samples were aged for periods of 2 and 6 months in 2 psia at 177°C. Values reported are G_{MAX} values.

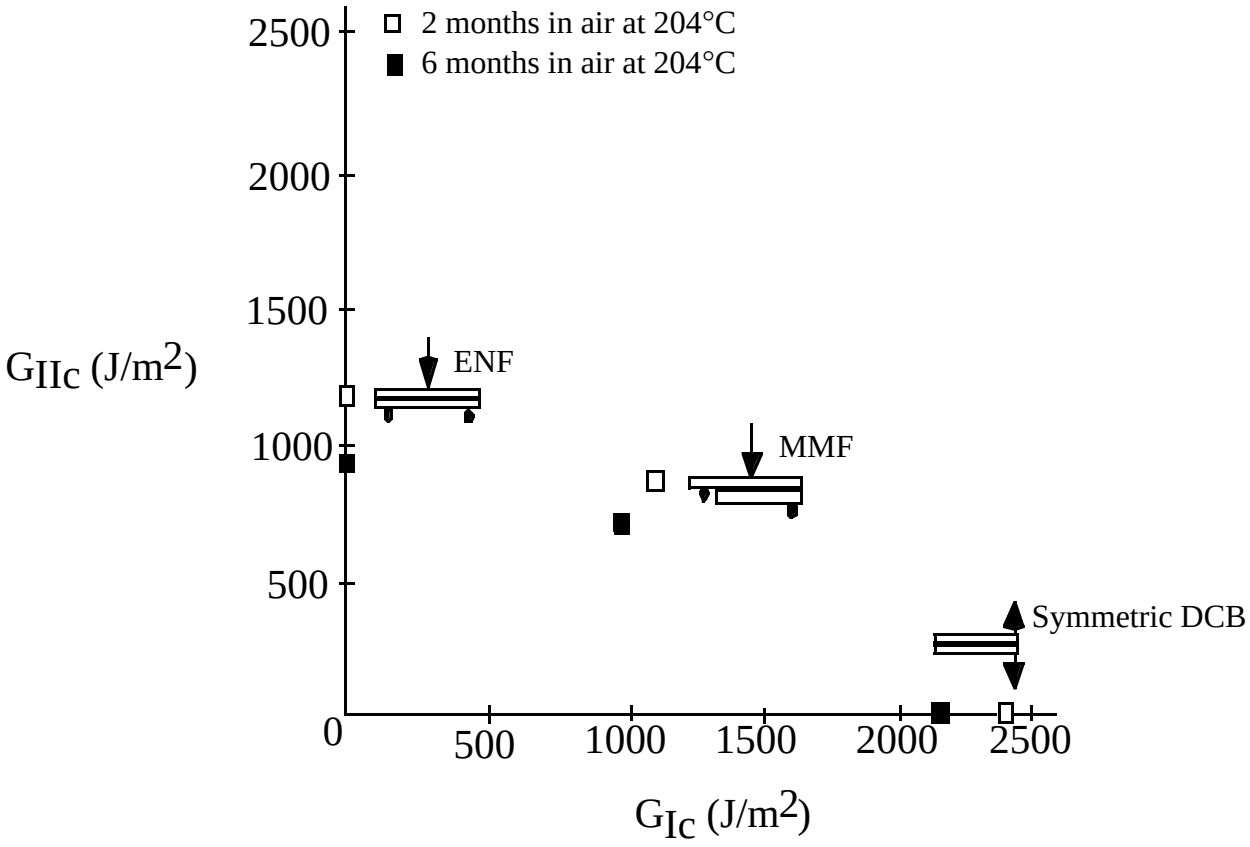

Figure 5.17. Aging failure envelope for Ti-6Al-4V/FM-5 adhesive bonded system. Samples were aged for periods of 2 and 6 months in air at 204°C. Values reported are G_{MAX} values.

Sample	%C	%O	%N	%Si	%Ti	%Al	%Na	%Cl
Cured FM-5	64.4	24.6	3.2	7.8	nd	nd	nd	nd
ENF Sample 204°C, MFS	61.9	25.9	4.5	4.4	2.2	1.0	0.2	nd
ENF Sample 204°C, AFS	70.0	20.8	5.6	3.3	0.1	0.0	0.3	nd

MFS-metal failure surface; AFS-adhesive failure surface; nd-not detected (<0.1)

Table 5.1. Atomic concentrations from the interfacial failure region on an ENF specimen that was aged for 6 months in air at 204°C.

6.0 Closure

As is the case with most research studies, this study has answered some questions, but has raised several others. However, it is the author's belief that a start has been made in the right direction in terms of assessment of adhesive bond durability for high temperature applications. Insights gained from this study are useful for the design engineer, materials engineer, and the synthetic chemist, as well as, can be used to guide future studies in this area. As is often the case, a design engineer must sometimes make decisions about an adhesive or a metal-adhesive bonded joint, long before the materials engineer fully understands the phenomena under question. This is particularly true for phenomena such as physical and chemical aging. Further, the issue is especially complicated for aerospace applications, where material durability has to be assessed over thousands of hours, under different exposure conditions. From this research study, it is quite evident that both physical aging and chemical degradation are taking place in the FM-5 resin. Data collected to date on the Ti-6Al-4V/FM-5 bonded system shows a 32.4% decrease in mode I toughness over 18 months of aging in air at 204°C, and an even more dramatic 69.4% decrease in lap shear strength after 14 months of air aging at 204°C (see Table 6.1). The above statistic would be of definite concern to the design engineer. In light of the above data, suitable modifications should be made to both the adhesive material and the metal-adhesive interface region, prior to prototype design and testing. Unfortunately, the mechanism(s) for chemical aging are not clearly understood to date. Once this is more thoroughly understood by the materials engineer, the synthetic chemist can then be involved to make suitable alterations to the adhesive chemistry to obtain a more durable adhesive.

The following paragraphs detail some salient findings from the *environmental aging study* on the Ti-6Al-4V/FM-5 adhesive bonded system, as well as, some directions for future work.

Based on a 3 day water boil screening test, chromic acid anodization (CAA) was chosen as the control standard pretreatment for the titanium/adhesive bonds in this study. As mentioned in the literature review part of this report, the anodization process results in toxic chromate (Cr VI) waste material, which is environmentally hazardous. The aircraft industry, especially the

high speed civil transport (HSCT) group, would therefore be better served if an alternative durable and environmentally friendly surface pretreatment is developed. Research is underway in this area, and there are some promising alternatives currently being tested both at the Boeing Company and Virginia Tech. XPS characterization of CAA Ti-6Al-4V/FM-5 bonds suggests that the failure is moving towards the metal-adhesive interface with aging. This suggests a weakening of the metal-oxide layer besides other things. The above finding further strengthens the need for the development of a more durable surface preteatment that would improve the adhesion between the titanium metal and the FM-5 adhesive.

Both physical and chemical aging were detected in the FM-5 resin system, using mechanical and materials testing techniques. Physical aging appears to be thermally reversible to some degree, in the FM-5 resin. Chemical degradation of the resin becomes noticeable after several months of aging at elevated temperature. Thermal rejuvenation in conjunction with DCB fracture tests, were used with a moderate degree of success to separate the effects of physical and chemical aging on bond toughness. The greatest reduction in bond toughness was seen at the highest aging temperature (204°C), and the environment with the highest oxygen concentration (14.7 psia). Following aging for several months at elevated temperatures, the DCB failure specimens showed a "picture frame" type failure pattern. This failure pattern was indicative of a failure mechanism that was diffusion-controlled. For future work, the diffusion of oxygen gas into the bonded joints (from the specimen edges) can be calculated based on the permeability of oxygen molecules into a networked polymer structure (e.g. epoxy). Depending on the concentration of oxygen in the aging environment, and the rate at which this oxygen reacts with the polymer, predictions can be made to determine how much time it takes for the oxygen to diffuse across the width of the bonded specimen, and completely degrade the bonded area. Following this, degradation profiles based on oxidation can be generated for the different air pressure environments. Correlations/comparisons can then be made between these theoretical calculations and experimentally observed interfacial failure regions seen on aged specimens. It must be kept in mind that the above calculations would at best show trends that could take place in the bonded joints. This is because of the fact that diffusion-controlled oxidation of the

adhesive material may not be an independent phenomenon, and it could be coupled with several other processes taking place in the bonded joint, as a result of thermal aging.

FM-5 is a proprietary polymer, manufactured and supplied by Cytec Engineered Materials, Inc. after suitable alteration of the original LaRC PETI-5 adhesive. Since the fillers, modifiers, and additives in the FM-5 resin were unknown, it was difficult to pin-point exactly the source or location of chemical degradation in the adhesive material/bonded joints following long-term thermal aging. Two possible mechanisms are oxidative chain-scissioning and hydrolysis. In order to identify the degradation mechanism, a collaborative effort between Cytec Engineered Materials, Inc. and Virginia Tech is proposed. Some of the testing techniques that could be used towards this end are XPS, FT-IR spectroscopy, and TGA mass spectrometry. Upon identification of the degradation mechanism, suitable alterations can be made to the adhesive material to make it more durable under the current exposure conditions. It must be mentioned here that as part of this research effort, XPS and FT-IR spectroscopy was performed on FM-5 adhesive films, both prior to and after aging. The results from this study showed no noticeable differences in the XPS and FT-IR spectra following thermal aging. However, it must be mentioned that there was significant fluorine and silicon contamination on the surface of the films that were tested. It is quite possible that these contaminants masked the effects of chemical degradation in the adhesive resin. In order to study the effects of chemical degradation on the FM-5 resin as a result of thermal aging, the XPS and FT-IR tests should be repeated on samples that have been prepared and aged in a very controlled manner. Presently, FM-5 films are being aged in sealed glass containers under different levels of vacuum. These films will be tested at several aging times in the future, to study the chemical/thermal degradation of the FM-5 resin, as well as, to possibly identify the mechanism(s) of degradation. One additional advantage to identifying the degradation mechanism is the possibility of using accelerated aging techniques to study bond durability. If “the” specific degradation mechanism can be accelerated by aging the bonds at higher temperatures, e.g: 220°C, this would greatly minimize the exposure times. A word of caution, however, in doing this study is that care should be taken to accelerate the right

mechanism(s) that are responsible for the degradation in the first place. This may not be a trivial problem.

One early criticism of mode I fracture test specimens (DCB and wedge), was that they are not very discriminating of the titanium/FM-5 bonds at short aging times. This was a valid criticism as can be gaged by the fact that failure in most DCB joints was cohesive (at glass scrim cloth/adhesive interface) up to 6 months of aging, while mixed-mode failure was seen following 12 and 18 months of aging. With a view to better interrogate the interface between the titanium metal and the FM-5 adhesive, the ENF test specimen was introduced into the testing program. The ENF specimen provided failures that were either near-interfacial (on as-bonded specimens) or within the metal-oxide layer (following moderate aging of the bonds). Table 6.1 summarizes the results obtained upon aging and testing of CAA titanium/FM-5 bonds, using the DCB, ENF, MMF, and SLS test specimen geometries. In each case comparison is made to either the fracture toughness or lap shear strength of an as-bonded specimen. The aging condition chosen for this comparison is ambient atmospheric air at 204°C. After 6 months of aging under the above mentioned environment, a 9.7% decrease in bond toughness was seen from the DCB specimen geometry, 24.6% from the ENF specimen geometry, and 13.2% from the MMF specimen geometry. On the other hand, after only 2.5 months in the above environment, a 31.4% drop in strength was seen from the SLS specimen geometry. Two conclusions can be drawn from the above study. Firstly, in future aging studies involving the titanium/FM-5 bonded system, it is beneficial to use a fracture test specimen that has a mode-mixity (greater mode II component as compared to mode I component may be preferred). Such a specimen would drive the failure towards the metal-adhesive interface and enable a better understanding of the "adhesion" process. Secondly, it is still viable to pursue SLS tests as screening tests for adhesive joints. Although this specimen has several drawbacks, it is simple to make and test, and continues to provide some useful information regarding the failure process and failure mechanism in adhesive joints.

Following several months of aging at elevated temperatures, mixed-mode failure (combination of interfacial and cohesive)was observed in the DCB specimens. XPS analysis of the interfacial failure regions revealed a thin layer of adhesive present on the metal oxide layer.

There are no definitive answers to date as to why the locus of failure moves towards the interface following aging. Some current theories are degradation/instability of the metal oxide layer, and preferential migration of lower molecular weight species in the adhesive material towards the interface region during the bonding process. A more thorough study must be conducted to understand this phenomena. One possibility involves the use of an atomic force microscope (AFM) (in tapping mode) to study the changes in the material properties across the thickness of the bondline, with aging.

The HSCT aircraft is expected to see a range of temperatures going from -54°C during subsonic flight to around 177°C during supersonic flight. There is a distinct possibility of the aircraft structure picking up moisture when it is landed, and as the aircraft takes-off and goes from subsonic to supersonic speeds, this moisture would undergo a freeze-thaw-evaporation cycle. In order to mimic this behavior, cyclical environmental/temperature exposure of the Ti-6Al-4V/FM-5 bonds should be explored, under both static and fatigue loading conditions. Tests conducted in this manner would provide much more useful durability information as they are closer to reality, than testing conducted under static environmental conditions alone.

The following paragraph lists the findings from the *solvent sensitivity study* on the titanium/polyimide bonded systems, as well as, suggests some possibilities for future work.

The FM-5, VT Ultem, and REGULUS^{TM} resin systems displayed good resistance to common organic solvents and aircraft fluids. There was no evidence of solvent induced stress cracking or crazing in the three adhesive resins, although some solvents did accelerate debonding in wedge specimens. Wedge tests conducted by immersing the specimens in different solvents, helped rank the exposed solvents in terms of crack growth rate characteristics. One possibilities for future work involves fatigue testing of solvent-exposed adhesive bonds. Solvent induced stress cracking requires a synergism between solvent and externally applied load. A second possibility for extending work in this area involves the construction of a test fixture and chamber (compatible with a universal loading frame), that would enable the testing of both neat resin specimens and bonded joints in either tension or bending, while fully immersed under solvent.

The following paragraph lists the findings from the *mode-mixity study* on the Ti-6Al-4V/FM-5 adhesive bonded system, and suggests possibilities for future work in this area.

ENF and MMF testing procedures induced interfacial failures in the bonded system, as opposed to cohesive failures with pure mode I DCB tests. The largest decrease in fracture energy over a 6 month aging period was seen in the ENF test specimens. Pure mode II fracture energy was found to be significantly lower than mode I energy release rate, in contrast to what several researchers have observed with other bonded systems. Although no definitive conclusions were reached to explain the above behavior, there is reason to believe that both the glass scrim-cloth support and the presence of residual solvent play a significant role in influencing the mode I and mode II fracture toughness results. For future work, it is proposed to conduct tests with bonds made from loosely-woven scrim adhesive and unscrimmed adhesive to compare with the present results. It is felt that the concentration of solvent would be greatly minimized in the loosely-woven scrim adhesive and the unscrimmed adhesive material. This would therefore help eliminate one important variable that plays a significant role in determining the obtained fracture toughness value. It is also proposed to complement the above testing with spectroscopic and microscopic analysis, to document crack growth/path profiles. This would help gain a better insight as to why mode II fracture energies are lower than mode I fracture energy.

Aging Condition	DCB (J/m^2)	ENF (J/m^2)	MMF (J/m^2)	SLS* (psi)
As-bonded	2561	1300	1969	7102
Aged 2.5 months	--	--	--	4870 (31.4%)
Aged 6 months	2313 (9.7%)	980 (24.6%)	1710 (13.2%)	--
Aged 8 months	--	--	--	3020 (57.5%)
Aged 12 months	1783 (30.4%)	--	--	--
Aged 14 months	--	--	--	2176 (69.4%)
Aged 18 months	1731 (32.4%)	--	--	--

* data provided by Kevin Pate (Boeing Company)

Table 6.1. Comparison of DCB, ENF, MMF, and SLS data on CAA Ti-6Al-4V/FM-5 bonds that were aged in ambient atmospheric air at 204°C. Specimens were aged for periods up to 18 months. The numbers in parantheses indicate the % drop in toughness or strength from the as-received value.

Appendix A

Study of Ti-6Al-4V/FM-5 Bonds with Different Scrim Options

FM-5 adhesive samples containing no scrim, a sized glass scrim (standard), and a graphite cloth scrim are currently being evaluated (to study comparative durability) using wedge and static DCB tests. The DCB tests on as-bonded samples showed that the unsupported FM-5 adhesive bonds had fracture energy values in the range of 600 J/m^2, the graphite-scrimmed FM-5 adhesive bonds around 1000 J/m^2, and the standard glass-scrimmed FM-5 adhesive bonds around 1650 J/m^2. This shows that the glass-scrimmed adhesive possesses the best durability in testing thus far, followed by the graphite-scrimmed adhesive, and the non-scrimmed adhesive in that order. The crack propagation in all the above samples is cohesive, within the adhesive layer.

Wedge crack length data was collected on the adhesive bonds with the different scrim options. Samples were conditioned in atmospheric air at 204^oC. Following 12 months of aging at the above environment, the summary of wedge results is as follows: The magnitude of the arrest strain energy release rate varies in the manner standard > graphite > no scrim. The specific values (J/m^2) are: standard, 1500; graphite, 950; and no scrim, 525 (Figure A.1). The values determined should be directly related to the strength of the scrim-adhesive interaction since failure occurred at the scrim-adhesive interface for specimens containing scrim. On the other hand, the value for the no scrim specimens reflects the cohesive strength of the adhesive, since failure in the adhesive was noted (see Figure A.2). The rate of crack growth as a function of strain energy release rate for the glass-scrimmed adhesive revealed that the strain energy release rate is of the order of 1400-1600 J/m^2 for crack growth rates in the range 10^{-5} to 10^{-3} m/hr. The corresponding strain energy release rates, over the 10^{-5} to 10^{-3} m/hr crack growth rate region, are for graphite, 900 to 1100 J/m^2, and for the non-scrimmed specimen the values are 400 to 600 J/m^2 (Figure A.3).

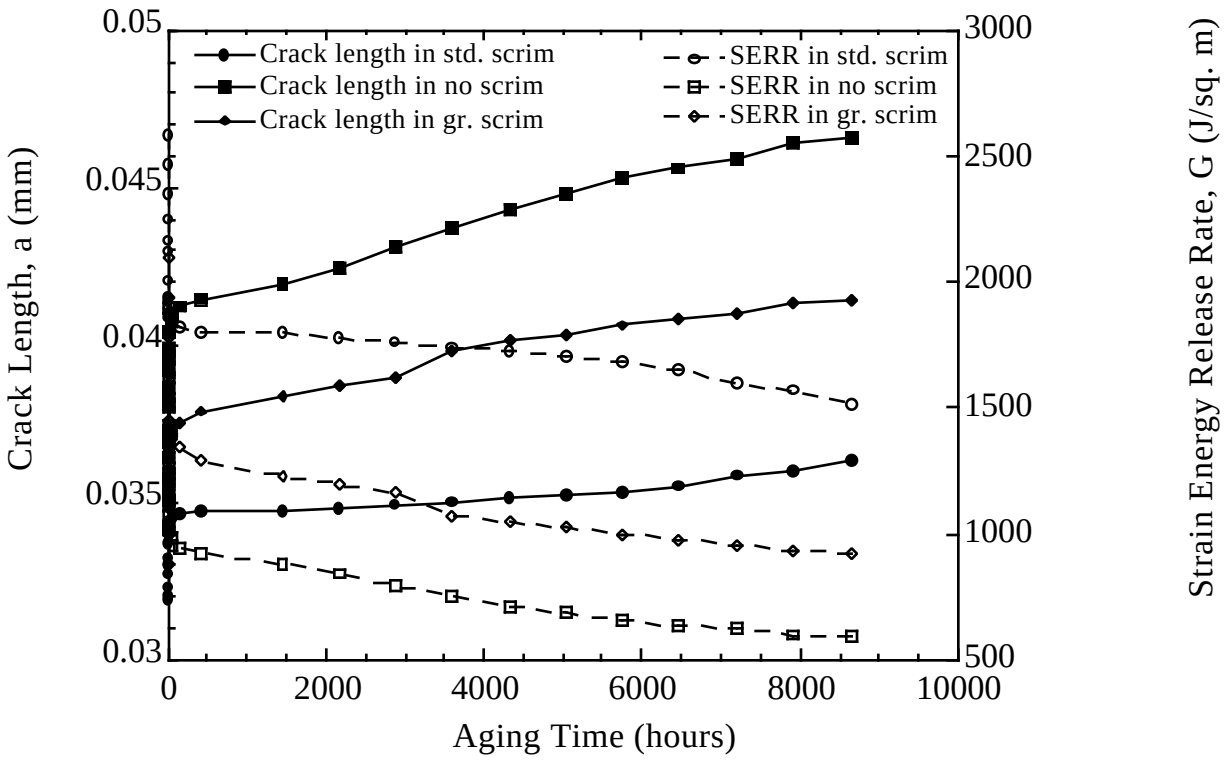

Figure A.1. Wedge crack length and fracture energy data as a function of aging time for titanium/FM-5 bonds with different scrim options. Samples were aged for 12 months in air at 204°C.

No Scrim Graphite Scrim Standard Glass Scrim

Figure A.2. Photograph showing the fracture surfaces of titanium/FM-5 bonds with different scrim options.

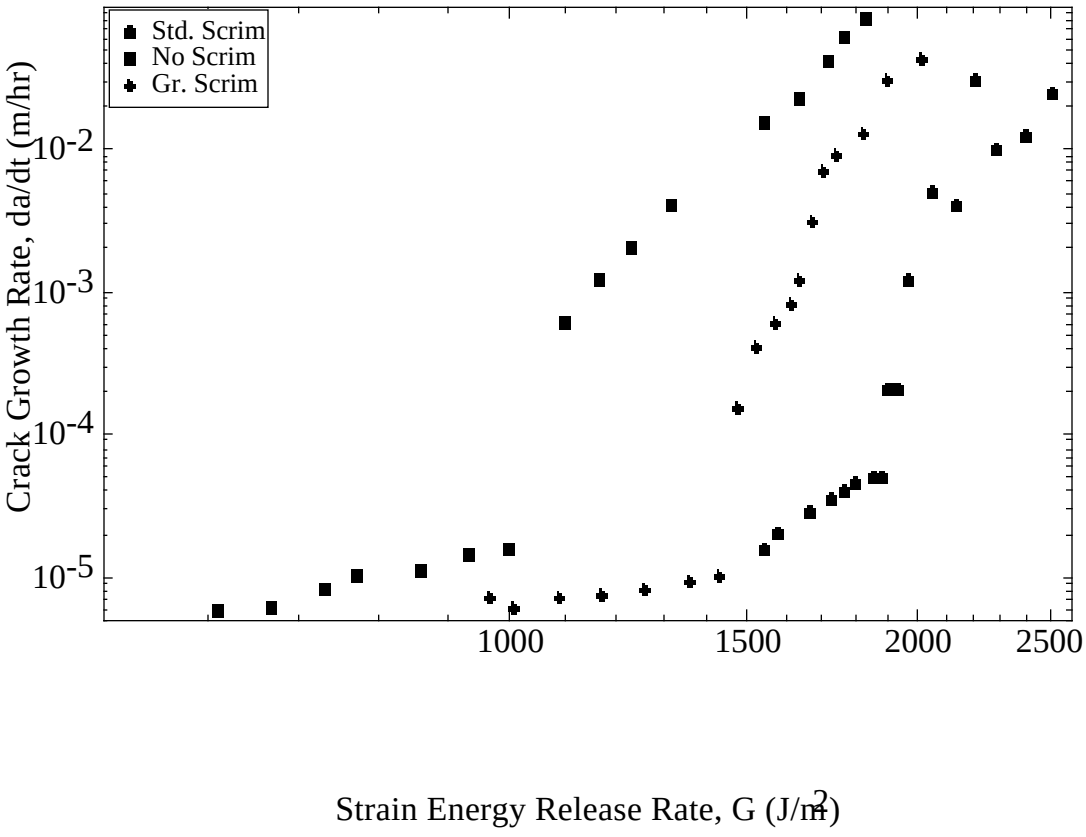

Figure A.3. Wedge crack growth rate versus fracture energy for titanium/FM-5 bonds with different scrim options. Bonds were aged for 12 months in air at 204°C.

Appendix B

Study of Ti-6Al-4V/FM-5 Adhesive Bond Toughness as a Function of the Variations in the Bonding/Manufacturing Procedure

Ti-6Al-4V/FM-5 bonded specimens from 5 different panels were supplied by the Boeing Company (February 1997) for conducting fracture tests. The 5 panels were designated as 4-1, 4-2, DCB4, DCB1, and GM2. It was noted that there were differences in the processing conditions as well as in the materials used in manufacturing the above panels. Panels 4-1, 4-2, and DCB4 were made using the same process and materials (standard glass scrimmed FM-5 adhesive was used in the bonding) and it was indicated that the middle of the panels showed significant porosity compared to the sample edges. Panel DCB1 was cured with a thick caul plate on the panel and was noted as having less porosity than the above panels. DCB1 was bonded using the standard glass scrimmed FM-5 adhesive. Panel GM2 was bonded with a version of FM-5 adhesive which had a non-woven glass mat scrim. It was noted that the specimens made from this panel had significantly less porosity and thinner bondlines.

It was decided to test at least 3-4 specimens per panel using both pure mode I and pure mode II loadings, to study the changes in properties with processing/material differences. Figure B.1 shows a typical outlay of a panel. Several specimens were machined out from each panel, with dimensions of 200 x 25 mm in length and width. In the subsequent Figures B.2-B.6 summarizing the results, it must be mentioned that sample#1, #2 or #8 refer to specimens typically from the edge of a particular panel, sample#5 or #6 the middle of a panel, and sample#4 or #7 off-center of a particular panel.

Figure B.2 summarizes the results obtained on panel 4-1. It is seen from the figure that 3 specimens were tested overall, that is two edge specimens and one at the center of the panel. Each sample was tested part way under pure mode I loading (DCB) before switching to a pure mode II loading (ENF). The maximum and arrest strain energy release rate values were calculated for each loading condition. It was seen that the DCB fracture energy values were higher on the

edge specimens and lower by about 15% on the center specimen designated as sample#5. The failure in all the three samples under mode I loading was found to be cohesive, that is at the adhesive and glass scrim cloth interface. Similar trends were found from the ENF testing of these samples, although the differences in fracture energy between the edge specimens and the center specimen was considerably lower. The failure in all the three samples tested under pure mode II loading was also cohesive, but the locus of failure was not at the adhesive/glass scrim interface but in the adhesive layer above the titanium metal and below the glass scrim cloth. The mode II fracture energy values were around 1800 J/m^2 as opposed to around 2500 J/m^2 obtained under pure mode I loading. The one significant conclusion we can draw from these results is that while we are essentially measuring an adhesive fracture toughness under mode II loading, we are obtaining a "composite" toughness under pure mode I loading due to the crack extending along the adhesive/glass scrim cloth interface. It also appears that while the porosity affects the mode I results (going from panel edges to the interior), it does not have much bearing on the mode II results. Trends similar to those seen on panel 4-1 were also found on specimens from panels 4-2 and DCB4 as shown in Figures B.3 and B.4.

Figure B.5 summarizes results obtained on specimens from panel DCB1. Upon manufacturing, panel DCB1 showed less porosity compared to the above panels, and this is reflected in the results. Samples tested from the panel edges and interior showed similar fracture energy values, under both modes of loading. The locus of fracture under mode I was at the adhesive/glass scrim cloth interface, and under mode II, at the interface beween the metal and adhesive.

Figure B.6 summarizes the results obtained on specimens from panel GM2. This panel as mentioned above was bonded with a version of FM-5 adhesive which had a non-woven glass mat scrim. The DCB results showed no variation in fracture toughness values from specimens taken from the panel edges and panel interior. From the tests, mode I fracture energy values around 1800 J/m^2 were obtained. The failure under pure mode I loading was cohesive in the adhesive material. One conclusion that can be drawn from this test and the tests on the previous four panels is as follows; fracture toughness values of around 1800 J/m^2 were obtained under

mode II loading of panels 4-1, 4-2, DCB4, DCB1, and under mode I loading of panel GM2. This suggests that the locus of failure in the above tests is essentially the same (within the adhesive material), and we are measuring a fracture toughness of the FM-5 adhesive. Mode II results from panel GM2 resulted in fracture toughness values around 1500 J/m^2.

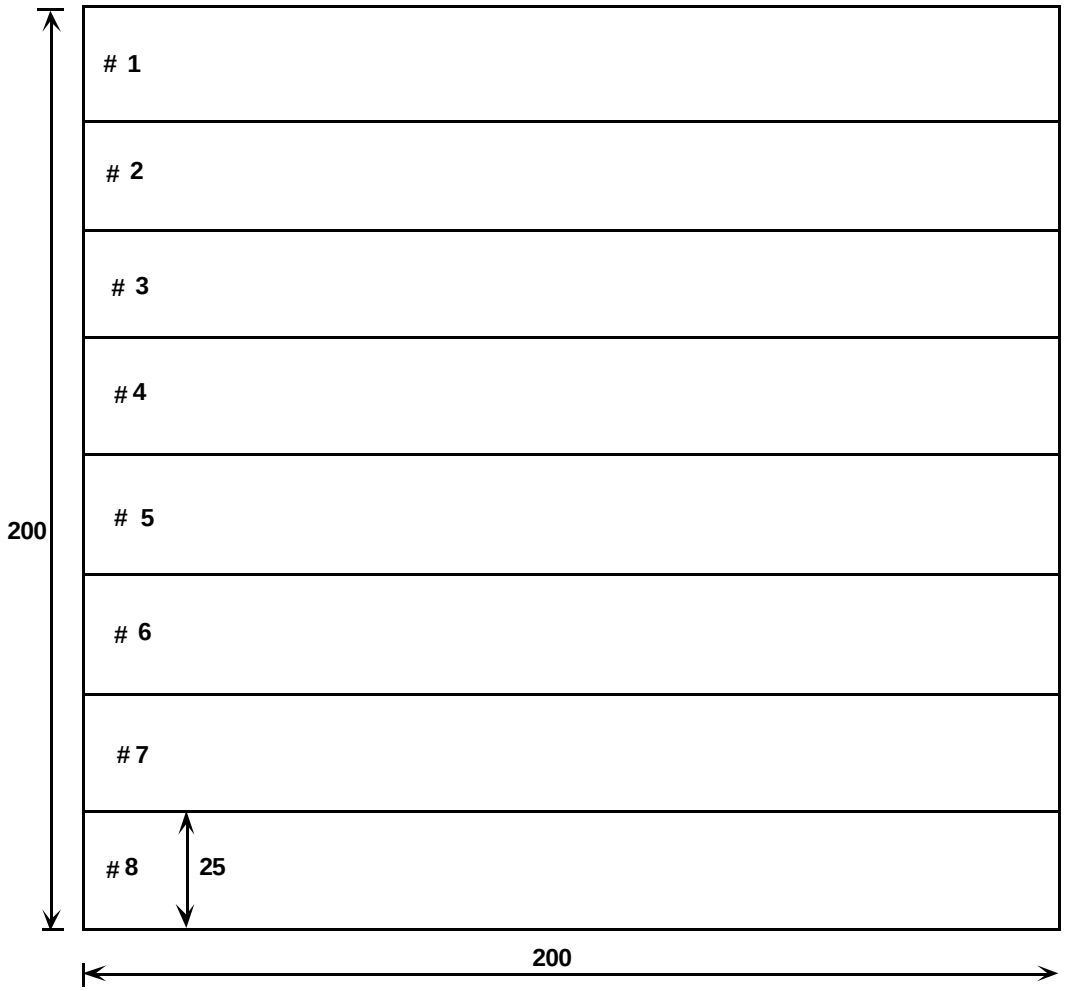

Figure B.1. Typical layout of a bonded panel from which DCB specimens are machined. Dimensions are in millimeters.

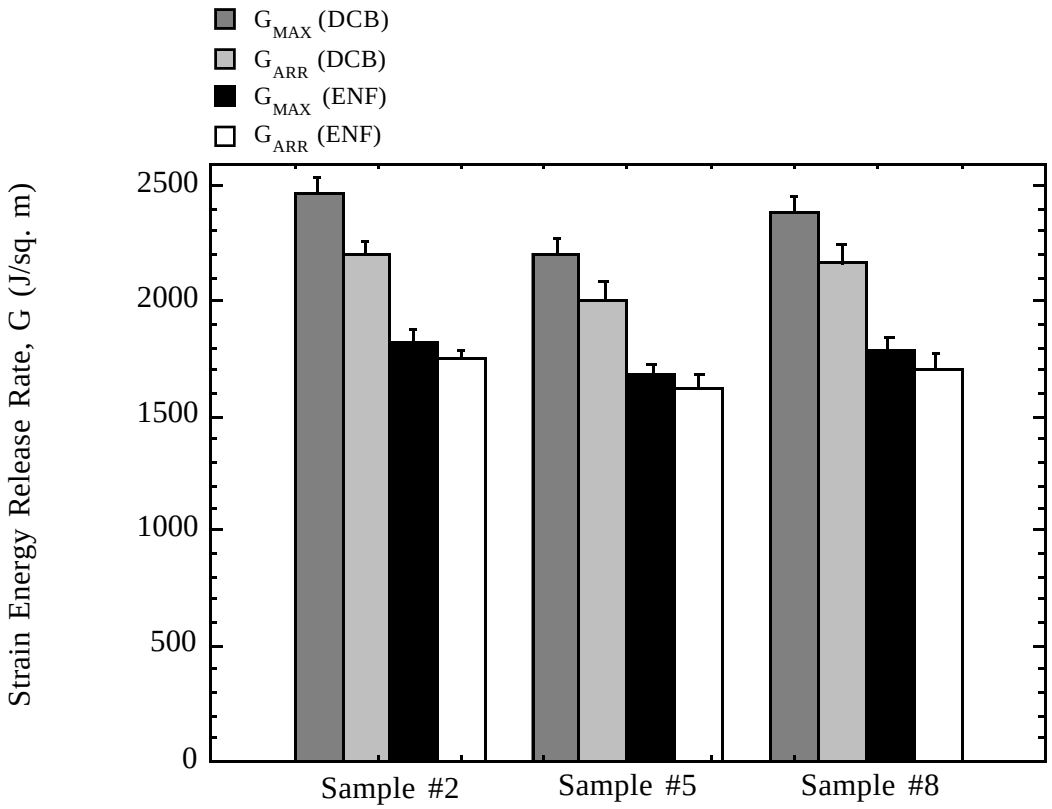

Figure B.2. DCB and ENF results from panel designated as 4-1.

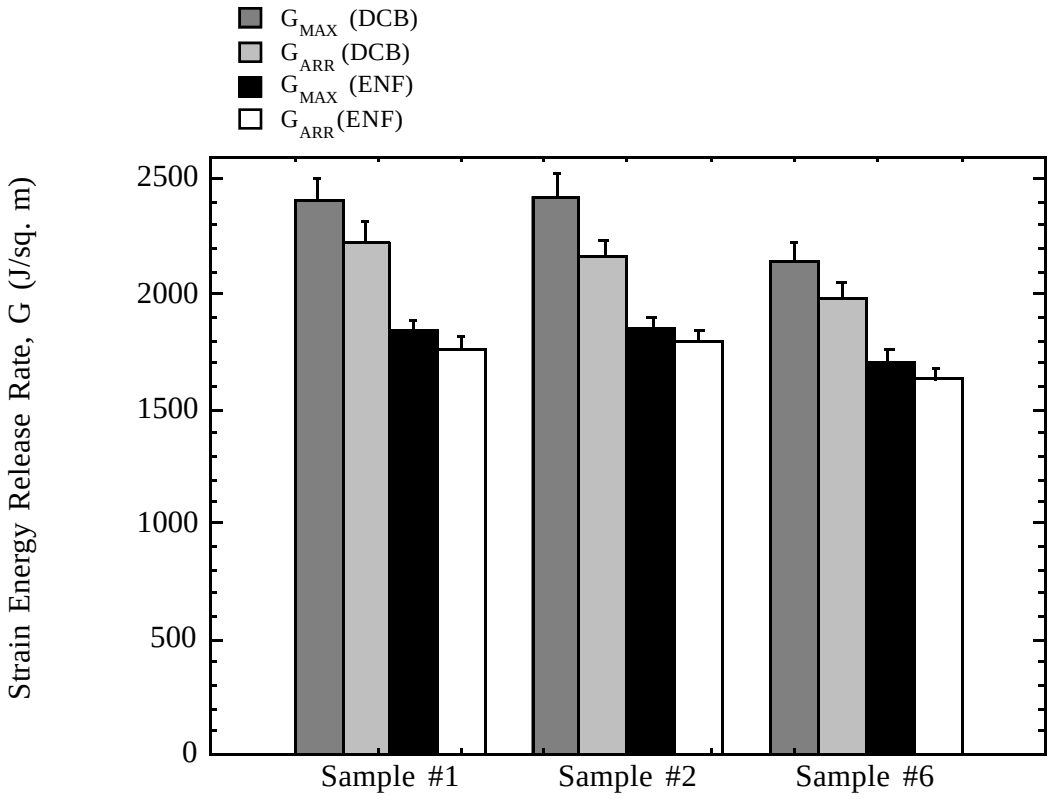

Figure B.3. DCB and ENF results from panel designated as 4-2.

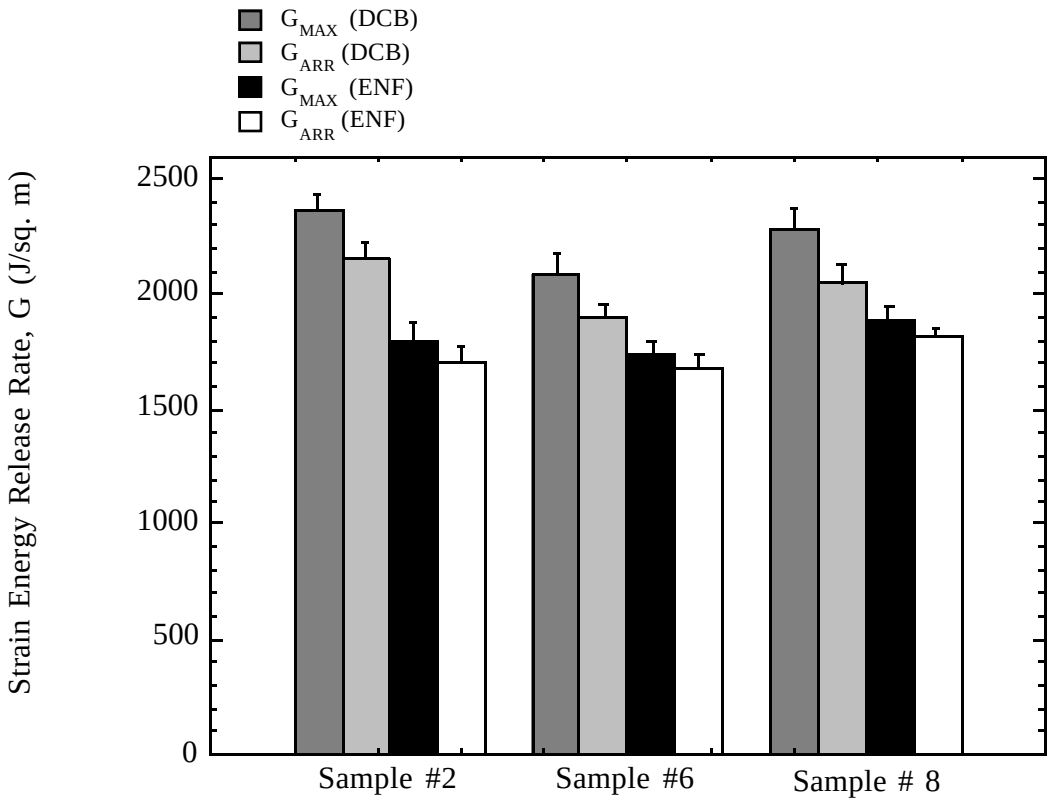

Figure B.4. DCB and ENF results from panel designated as DCB4.

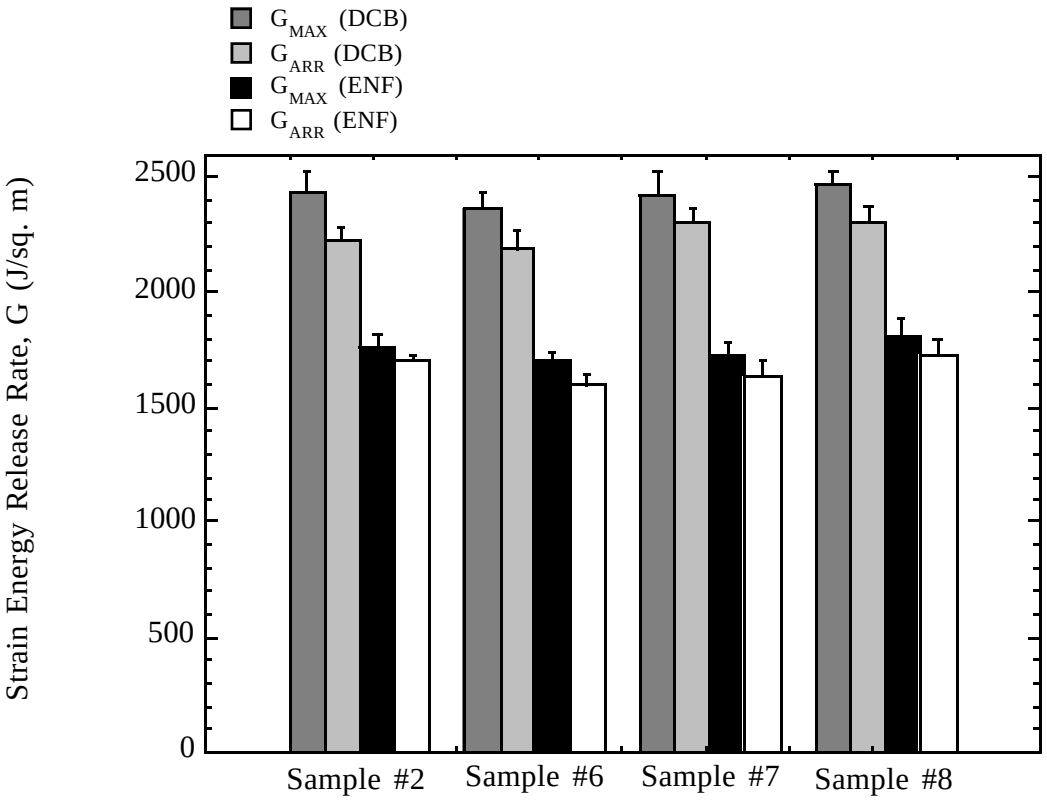

Figure B.5. DCB and ENF results from panel designated as DCB1.

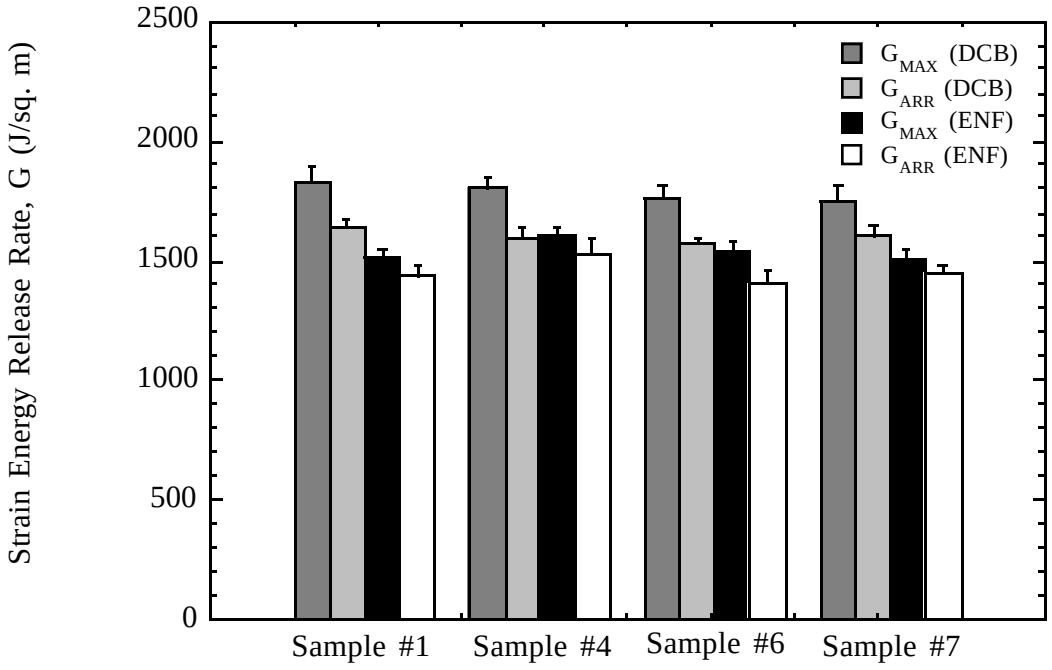

Figure B.6. DCB and ENF results from panel designated as GM2.

Vita

Hari Parvatareddy, son of Dr. P. Ramachandra Reddy and Mrs. P. Vijayalakshmi, was born on November 6, 1968, in Hyderabad, India. Upon graduating from high school (The Hyderabad Public School, Begumpet, Hyderabad), he joined the Mechanical Engineering program at Osmania University, Hyderabad. He graduated with his Bachelor of Engineering degree (B.E) in Mechanical Engineering in June, 1991. He then moved to Blacksburg, Virginia in August 1991, where he enrolled in the Engineering Science and Mechanics Department for a Masters' degree. He completed his Master of Science (M.S) degree requirements in April, 1994, working under Prof. David A. Dillard. He then enrolled in the doctoral program in Materials Engineering Science (MESc), continiung to work under the guidance of Prof. David A. Dillard. He completed his doctoral degree requirements in November, 1997. Upon graduation, he will move to Midland, Michigan where he will start working for The Dow Chemical Company, in their Materials Sciences Laboratory.